600382094

FINAL EVALUATION OF URBAN-SCALE PHOTOCHEMICAL AIR QUALITY SIMULATION MODELS

by

Kenneth L. Schere and Jack H. Shreffler
Meteorology and Assessment Division
Environmental Sciences Research Laboratory
Research Triangle Park, North Carolina 27711

ENVIRONMENTAL SCIENCES RESEARCH LABORATORY
OFFICE OF RESEARCH AND DEVELOPMENT
U.S. ENVIRONMENTAL PROTECTION AGENCY
RESEARCH TRIANGLE PARK, NORTH CAROLINA 27711

DISCLAIMER

This report has been reviewed by the Environmental Sciences Research Laboratory, U.S. Environmental Protection Agency, and approved for publication. Mention of trade names or commerical products does not constitute endorsement or recommendation for use.

AFFILIATION

Dr. Shreffler and Mr. Schere are on assignment to the Meteorology and Assessment Division, Environmental Sciences Research Laboratory, from the National Oceanic and Atmospheric Administration, U.S. Department of Commerce.

ABSTRACT

The research study discussed here is a continuation of previous work whose goal was to determine the accuracy of several selected urban photochemical air quality simulation models using data from the Regional Air Pollution Study in St. Louis. The report summarizing the initial work on this project discussed four models and used a sample of 10 days for testing. This work continues testing on three of the models with an increased sample size of 20 days.

The models evaluated here are: The Photochemical Box Model (PBM) developed in-house by EPA, The Lagrangian Photochemical Model (LPM) developed by Environmental Research and Technology, Inc., and The Urban Airshed Model (UAM) developed by Systems Applications, Inc. Emphasis in this report is directed at the ability of the models to reproduce the maximum 1-hour ozone concentrations observed on 20 days selected from nearly 2 years of data. The PBM, LPM, and UAM have been evaluated using statistical methods and graphical techniques and all show potential as air quality management tools.

The standard deviation of the differences between observed ozone maxima and predicted concentrations at the same place and time ranged from 0.04 to 0.06 ppm for maxima of 0.16 to 0.26 ppm. This measure of uncertainty should be recognized by decision-makers using these models in regulatory and planning processes.

This report covers a period from March 1981 to February 1982.

CONTENTS

Abstract iii
Figures vi
Tables ix

1. Introduction 1
2. Conclusions and Recommendations 5
3. The Data Set 8
4. Photochemical Box Model 12
   Overview 12
   Results 13
   Conclusions 21
5. Lagrangian Photochemical Model 39
   Introduction 39
   Method 39
   Results 43
   Conclusions 46
6. Urban Airshed Model 63
   Introduction 63
   Results 65
   Conclusions 74

References 93
Appendices

A. PBM - Time series for remaining test days 95
B. PBM - Summary of statistical results 126
C. LPM - Time series for remaining test days 132
D. UAM - RS and RO plots for remaining test days 179
E. UAM - Contour plots for remaining test days 228
F. UAM - Summary of statistical results 237

FIGURES

Number		Page
1	Map of the St. Louis area	11
2	Schematic drawing of the PBM domain	23
3	Map of the PBM domain	24
4	PBM simulation results for Day 142 of 1975	25
5	PBM simulation results for Day 178 of 1975	27
6	PBM simulation results for Day 207 of 1975	29
7	PBM simulation results for Day 212 of 1976	31
8	PBM simulation results for Day 275 of 1976	33
9	PBM frequency histograms for all data	35
10	PBM residual vs. obs. conc. plots for all data	37
11	LPM simulation results for Day 231 of 1975	48
12	LPM simulation results for Day 251 of 1975	51
13	LPM simulation results for Day 226 of 1976	54
14	LPM simulation results for Day 237 of 1976	57
15	LPM simulation results for Day 275 of 1976	60
16	Schematic drawing of the UAM domain	76
17	UAM simulation results for CO on Day 142 of 1975	77
18	UAM simulation results for NO_2 on Day 142 of 1975	78
19	UAM simulation results for O_3 on Day 142 of 1975	79
20	UAM contours of max. O_3 field on Day 142 of 1975	80
21	UAM simulation results for CO on Day 207 of 1975	81
22	UAM simulation results for NO_2 on Day 207 of 1975	82
23	UAM simulation results for O_3 on Day 207 of 1975	83
24	UAM contours of max. O_3 field on Day 207 of 1975	84
25	UAM simulation results for CO on Day 195 of 1976	85
26	UAM simulation results for NO_2 on Day 195 of 1976	86
27	UAM simulation results for O_3 on Day 195 of 1976	87
28	UAM contours of max. O_3 field on Day 195 of 1976	88
29	UAM simulation results for CO on Day 275 of 1976	89
30	UAM simulation results for NO_2 on Day 275 of 1976	90
31	UAM simulation results for O_3 on Day 275 of 1976	91
32	UAM contours of max. O_3 field on Day 275 of 1976	92
A-1	PBM simulation results for Day 182 of 1975	96
A-2	PBM simulation results for Day 183 of 1975	98
A-3	PBM simulation results for Day 184 of 1975	100
A-4	PBM simulation results for Day 209 of 1975	102
A-5	PBM simulation results for Day 221 of 1975	104
A-6	PBM simulation results for Day 230 of 1975	106
A-7	PBM simulation results for Day 231 of 1975	108
A-8	PBM simulation results for Day 251 of 1975	110
A-9	PBM simulation results for Day 159 of 1976	112

A-10 PBM simulation results for Day 160 of 1976 114
A-11 PBM simulation results for Day 195 of 1976 116
A-12 PBM simulation results for Day 211 of 1976 118
A-13 PBM simulation results for Day 225 of 1976 120
A-14 PBM simulation results for Day 226 of 1976 122
A-15 PBM simulation results for Day 237 of 1976 124
C-1 LPM simulation results for Day 142 of 1975 134
C-2 LPM simulation results for Day 178 of 1975 137
C-3 LPM simulation results for Day 182 of 1975 140
C-4 LPM simulation results for Day 183 of 1975 143
C-5 LPM simulation results for Day 184 of 1975 146
C-6 LPM simulation results for Day 207 of 1975 149
C-7 LPM simulation results for Day 209 of 1975 152
C-8 LPM simulation results for Day 221 of 1975 155
C-9 LPM simulation results for Day 230 of 1975 158
C-10 LPM simulation results for Day 159 of 1976 161
C-11 LPM simulation results for Day 160 of 1976 164
C-12 LPM simulation results for Day 195 of 1976 167
C-13 LPM simulation results for Day 211 of 1976 170
C-14 LPM simulation results for Day 212 of 1976 173
C-15 LPM simulation results for Day 225 of 1976 176
D-1 UAM simulation results for CO on Day 178 of 1975 180
D-2 UAM simulation results for NO_2 on Day 178 of 1975 181
D-3 UAM simulation results for O_3 on Day 178 of 1975 182
D-4 UAM simulation results for CO on Day 182 of 1975 183
D-5 UAM simulation results for NO_2 on Day 182 of 1975 184
D-6 UAM simulation results for O_3 on Day 182 of 1975 185
D-7 UAM simulation results for CO on Day 183 of 1975 186
D-8 UAM simulation results for NO_2 on Day 183 of 1975 187
D-9 UAM simulation results for O_3 on Day 183 of 1975 188
D-10 UAM simulation results for CO on Day 184 of 1975 189
D-11 UAM simulation results for NO_2 on Day 184 of 1975 190
D-12 UAM simulation results for O_3 on Day 184 of 1975 191
D-13 UAM simulation results for CO on Day 209 of 1975 192
D-14 UAM simulation results for NO_2 on Day 209 of 1975 193
D-15 UAM simulation results for O_3 on Day 209 of 1975 194
D-16 UAM simulation results for CO on Day 221 of 1975 195
D-17 UAM simulation results for NO_2 on Day 221 of 1975 196
D-18 UAM simulation results for O_3 on Day 221 of 1975 197
D-19 UAM simulation results for CO on Day 230 of 1975 198
D-20 UAM simulation results for NO_2 on Day 230 of 1975 199
D-21 UAM simulation results for O_3 on Day 230 of 1975 200
D-22 UAM simulation results for CO on Day 231 of 1975 201
D-23 UAM simulation results for NO_2 on Day 231 of 1975 202
D-24 UAM simulation results for O_3 on Day 231 of 1975 203
D-25 UAM simulation results for CO on Day 251 of 1975 204
D-26 UAM simulation results for NO_2 on Day 251 of 1975 205
D-27 UAM simulation results for O_3 on Day 251 of 1975 206
D-28 UAM simulation results for CO on Day 159 of 1976 207
D-29 UAM simulation results for NO_2 on Day 159 of 1976 208
D-30 UAM simulation results for O_3 on Day 159 of 1976 209

D-31 UAM simulation results for CO on Day 160 of 1976 210
D-32 UAM simulation results for NO_2 on Day 160 of 1976 211
D-33 UAM simulation results for O_3 on Day 160 of 1976 212
D-34 UAM simulation results for CO on Day 211 of 1976 213
D-35 UAM simulation results for NO_2 on Day 211 of 1976 214
D-36 UAM simulation results for O_3 on Day 211 of 1976 215
D-37 UAM simulation results for CO on Day 212 of 1976 216
D-38 UAM simulation results for NO_2 on Day 212 of 1976 217
D-39 UAM simulation results for O_3 on Day 212 of 1976 218
D-40 UAM simulation results for CO on Day 225 of 1976 219
D-41 UAM simulation results for NO_2 on Day 225 of 1976 220
D-42 UAM simulation results for O_3 on Day 225 of 1976 221
D-43 UAM simulation results for CO on Day 226 of 1976 222
D-44 UAM simulation results for NO_2 on Day 226 of 1976 223
D-45 UAM simulation results for O_3 on Day 226 of 1976 224
D-46 UAM simulation results for CO on Day 237 of 1976 225
D-47 UAM simulation results for NO_2 on Day 237 of 1976 226
D-48 UAM simulation results for O_3 on Day 237 of 1976 227
E-1 UAM contours of max. O_3 field on Day 178 of 1975 229
E-2 UAM contours of max. O_3 field on Day 182 of 1975 229
E-3 UAM contours of max. O_3 field on Day 183 of 1975 230
E-4 UAM contours of max. O_3 field on Day 184 of 1975 230
E-5 UAM contours of max. O_3 field on Day 209 of 1975 231
E-6 UAM contours of max. O_3 field on Day 221 of 1975 231
E-7 UAM contours of max. O_3 field on Day 230 of 1975 232
E-8 UAM contours of max. O_3 field on Day 231 of 1975 232
E-9 UAM contours of max. O_3 field on Day 251 of 1975 233
E-10 UAM contours of max. O_3 field on Day 159 of 1976 233
E-11 UAM contours of max. O_3 field on Day 160 of 1976 234
E-12 UAM contours of max. O_3 field on Day 211 of 1976 234
E-13 UAM contours of max. O_3 field on Day 212 of 1976 235
E-14 UAM contours of max. O_3 field on Day 225 of 1976 235
E-15 UAM contours of max. O_3 field on Day 226 of 1976 236
E-16 UAM contours of max. O_3 field on Day 237 of 1976 236

TABLES

Number		Page
1	Summary of Meteorological Conditions on 20 Test Days	10
2	Predicted and Observed O_3 Maxima for the PBM	20
3	Initial Pollutant Concentrations Assigned in the LPM	42
4	Predicted and Observed O_3 Maxima for the LPM	47
5	Predicted and Observed O_3 Maxima for the UAM	71
6	O_3 Regression Statistics for the UAM	73
B-1	Summary of Model Performance Statistics from the PBM	128
C-1	Temporal Correlation Coefficients for the LPM	133
F-1	Summary of Mean Concentration Statistics from the UAM	238
F-2	Summary of Analysis of Trends Data from the UAM	243
F-3	Summary of Concentration Maxima Statistics from the UAM	246

SECTION 1

INTRODUCTION

This report covers a final evaluation of selected urban scale photochemical models which could be applied in regulatory situations. A report (hereinafter referred to as Report I) on a preliminary evaluation was prepared by Shreffler and Schere (1982). In the interest of brevity, material in Report I is not repeated here unnecessarily. Referenced documentation on the models and Report I are essential to fully understand the procedures used in the simulations.

The Regional Air Pollution Study (RAPS) was conducted in the St. Louis region over the period 1974-1977 (Schiermeier, 1978). RAPS was designed to provide a comprehensive data set for the testing and evaluation of numerical air quality simulation models on an urban scale. While the RAPS field measurements were in progress EPA surveyed the available, state-of-the-art, photochemical air quality simulation models, and selected 3 for evaluation. Under contract, the builders adapted their models to the RAPS data base and were supplied 3 days of data for test simulations. In addition, there was a need to look at a simple box-model approach which was not embodied in an existing model. A box model was therefore constructed by EPA.

The following models were investigated in the evaluation program.

Photochemical Box Model (PBM) - a single cell Eulerian model constructed by EPA.

Lagrangian Photochemical Model (LPM) - a multi-level parcel model developed by Environmental Research and Technology, Inc.

Livermore Regional Air Quality Model (LIRAQ) - a single-level Eulerian grid model developed by Lawrence Livermore Laboratory.

Urban Airshed Model (UAM) - a multi-level, Eulerian grid model developed by Systems Applications, Inc.

LIRAQ, described by MacCracken et al. (1978), was dropped from the evalution because of a series of technical and logistics problems detailed in Report I. LIRAQ was unable to produce significant ozone levels for St. Louis, but no specific, correctable error could be identified. Aside from the technical problems with the model, which are unresolved and unevaluated, LIRAQ did not seem well suited as a general-use model easily transferable to new locales. No conclusions can be made from this effort about the use of LIRAQ by specialized user groups at specific locales.

Some of the other conclusions reached from the preliminary work described in Report I are that (a) the PBM performs best in near-stagnation conditions, (b) the LPM needs modification of the fixed-box formulation for the air parcel and (c) the UAM tends to consistently underpredict ozone. It was also generally found that the variability between specific 1-hour predicted and observed concentrations at a particular location tends to be substantial.

The PBM, LPM and UAM were again tested extensively for this study and corrections of obvious errors or deficiencies were made. However, no effort was made to adjust or tune the model predictions to observed concentration values. The prevailing philosophy behind the evaluation effort was to use the models in an off-the-shelf mode, much as they eventually would be applied by a user in a regulatory situation. However, great care was taken in preparation of data sets and model executions. Although model assumptions vary, effort was made to use data in similar manners in all models. Data preparation and actual execution of the models was accomplished solely by the authors at EPA. The goal of the evaluation was to provide a fair and objective determination of the accuracy of a set of photochemical models when tested in an operational mode against a comprehensive urban data base.

Photochemical air quality models are designed to predict ozone concentrations and thereby provide a means to assess beforehand the effects of changing emission levels in an urban area. Emission changes may result from addition of

new sources or controls on existing sources designed to reach ozone levels defined by the National Ambient Air Quality Standards (NAAQS). In either case, knowledge of the effects of emissions changes would allow prudent economic decisions on plant siting or control equipment use. The numerical air quality model synthesizes knowledge about the emissions, transport and transformation of pollutants into a workable computational framework, but the central problem is how to be reasonably certain that the model is correct in its projections.

The only reasonable method of determining accuracy is to test the model against an extensive observational data base. Providing such a data base was the purpose behind the RAPS. Since the level of the ozone maximum for each day is of paramount importance relative to the NAAQS, the comparison between its observed value and the model prediction at the same time and place would be of central interest. The method of evaluation consists of selecting a set of test days, executing model simulations and computing residual concentrations (observed-predicted). The specific outcome of the evaluation is a presentation of information on residuals under the given circumstances. Conclusions about model acceptability require further assumptions and judgements.

The residual reflects a composite effect of input errors, input uncertainties and model errors. Errors, if not compensating, will tend to produce a non-zero average residual over many cases. If the average residual is nearly zero, we might be willing to accept that the model is appropriately formulated for predicting absolute levels of high ozone in the area where the observations were taken. The case-by-case variation could be ascribed to uncertainties in the input. The acceptance of the model for absolute prediction leads rather naturally to accepting that it will respond to emissions changes in the same manner as the real-world system. Finally, we are likely to conclude that the model is transferrable to another location, provided the meteorological and chemical modules are judged sufficiently flexible to adapt to the new conditions. This line of reasoning underlies the decision-making process attendant to model use.

This report details the performance of 3 completed models using the RAPS data base. Input information and model components were carefully checked

before proceeding. Effort was directed at ascertaining that individual modules were doing what they were purported to do, but not to evaluate their accuracy separately. Improvements are perhaps possible in some of the modules, but this is left to the future. This report indicates the accuracy of the finished models used in an operational mode with the best information available at present.

SECTION 2

CONCLUSIONS AND RECOMMENDATIONS

This report presents the second, and final, evaluation of urban-scale photochemical air quality simulation models by EPA's Meteorology and Assessment Division. The 3 models included in the analysis span a wide range in complexity and sophistication but are all based on numerical solutions to mass-conservative equations. They are selected from the general categories of box, trajectory (Lagrangian) and grid (Eulerian) models. The first evaluation, described in Report I, gave detailed results from the model runs on 10 days selected for simulation from the RAPS data base. The sample size for this evaluation is 20 days; an additional 10 days were combined with the original sample. Some changes in the model algorithms, including the data preprocessors, from the time of the original testing on the 10-day sample made it necessary to perform the original simulations over. Emphasis in the model performance evaluations is placed on ozone, although results for other pollutant species are also discussed. Conclusions on the performance of specific models did not change appreciably from those listed in Report I although our confidence in them has increased because of the consistency in results obtained from both studies.

The PBM predictions for maximum O_3 for the average of the monitoring stations within the model domain were generally on the high side. The average O_3 residual implied a 23% overprediction over all test days. However for the 5 stagnation-type days where the maximum observed O_3 occurred within the PBM domain, the average overprediction of 8% was considerably better than for the entire sample. Only a slight tendency towards overprediction was indicated for the LPM. The biases of the residuals were relatively small, 11% of the average observations at Level-1 and only 2.5% at Level-3. The standard deviations of the LPM residuals were the highest among the three models tested, but nearly halved from the initial tests described in Report I. The large variance in the residuals might be expected since the LPM generates a prediction which likely is the most specific to a particular place and time. Model predictions

for maximum O_3 by the UAM in a specific sense (at the same time and location as the observed maximum) were consistently low for all evaluations with an average 32% underprediction over the sample. Originally it was thought that spurious numerical diffusion in the advection component of the model was responsible for the low UAM predictions. However the underprediction problem still persisted after the original advection algorithm was replaced with one containing much less inherent numerical diffusion. If the time and location of the model predictions are not constrained to be the same as those for the maximum observed O_3, the average model bias for the 20 days implied a 4% overprediction. This excellent agreement might suggest that the uncertainty in specifying a wind field for a grid model like the UAM could lead to large apparent errors in the model results.

The choice of which particular model to use in a specific application involves not only the accuracy of the model but also the resources required to operate it. The models tested here have resource requirements correlated with their level of complexity. In terms of man-months needed to set up a single day simulation and computer time expended (minutes of CPU on a UNIVAC 1100/82) the approximate requirements are:

PBM ---------- 0.15 man-month ---------- 1 minute CPU
LPM ---------- 0.20 man-month ---------- 10 minutes CPU
UAM ---------- 0.50 man-month ---------- 110 minutes CPU

The 3 models discussed in this report have all shown themselves to be acceptable tools for analysis of urban ozone air quality. The specific configuration of an application along with the quantity and quality of related data and resources available to the user must all be considered in the final selection of a model. For an indication of average O_3 air quality in an urban area under stagnation conditions or as a screening method for a more complex model the PBM is appropriate. The choice of a trajectory model, such as the LPM, or a grid model, like the UAM, might well be decided by resource requirements or by the number of proposed simulations. In any event, the user of any of these models must have a strong scientific background and exercise extreme care in implementing the air quality simulations. For an air quality analyst making regulatory decisions based, in part, on model results it should be

understood that substantial variability can exist between a single 1-hour predicted and observed concentration at a particular location.

These models are now being made available to EPA's Office of Air Quality Planning and Standards for further statistical and sensitivity testing and ultimately for use in their regulatory decision-making process. Because model development is an evolving area of research it is very likely that subsequent "improved" versions of the models tested here will become available. A performance test with benchmark results, as described and tabulated in this report, now exists for future use in urban air quality model comparisons with any subsequent versions of the models.

SECTION 3

THE DATA SET

As an integral part of the RAPS a network of 25 surface stations was established in and around the St. Louis region. These stations, shown in Figure 1, comprise the Regional Air Monitoring System (RAMS). The RAMS stations continually monitored various meteorological variables as well as ambient concentrations of pollutant gases. Schiermeier (1978) provides details on the instrumentation. In addition to the RAMS, upper air balloons were released each hour from urban and rural sites to provide wind profiles for modeling purposes.

An essential element in the data set for an air quality modeling exercise is a complete source emissions inventory for all gaseous and particulate species over the domain of interest. Littman (1979) summarizes the comprehensive data gathering and archiving of the RAPS emissions inventory. The inventory is divided into point source and area source classes with points defined as sources emitting at least 0.01 percent of the total emissions of a pollutant for the whole air quality control region. Line source emissions are included in the area source class. The area source emissions data are subdivided onto a horizontal grid of 1989 cells with variable spatial resolution, dependent upon the emissions source density. Grid resolution varies from 1 km in the more dense areas to 10 km in the sparse areas. The temporal resolution of the emission inventory is one hour. Criteria pollutants included in the inventory are TSP (total suspended particles), SO_2 (sulfur dioxide), NO_x (nitrogen oxides), THC (total hydrocarbons), and CO (carbon monoxide). Furthermore, total hydrocarbons are broken down into the component classes of non-reactives, olefins, paraffins, aldehydes, and aromatics. Examples of the gridded spatial distribution of selected pollutants are shown in Report I.

This report presents the results of model simulations for 20 individual days chosen from the RAPS data base. These days, 11 from 1975 and 9 from 1976, account for some of the higher O_3 measurements observed in the RAPS surface monitoring network. Maximum hour-average single station O_3 values all exceeded 0.16 ppm on the 20 days. Table 1 lists the basic characteristics of the days: wind speed and direction, temperature, and solar radiation computed as averages over 0700-1359 CST. Also listed are the maximum mixing heights for each day as determined from the upper air sounding data. Higher O_3 levels generally occur when a prevailing high atmospheric pressure system exists over the area with little associated cloud cover, and represent the situations conducive to production of O_3 from locally generated precursor emissions. Both the dates and Julian day numbers for the 20 days are listed in Table 1 and either form may be used throughout this report to reference a particular day.

TABLE 1. A SUMMARY OF WIND SPEED (WS), WIND DIRECTION (WD), TEMPERATURE, SOLAR RADIATION (ALL WAVELENGTHS), AND MAXIMUM AFTERNOON MIXING HEIGHT (MH) FOR THE 20 DAYS EXAMINED.*

Date	Day (Julian)	WS (m/s)	WD (deg)	Temp (°C)	Solar (ly/min)	Max MH (m)
5/22/75	142	1.1	224	29	1.12	1504
6/27/75	178	0.4	245	29	0.96	1822
7/01/75	182	1.4	70	29	0.99	2606
7/02/75	183	1.4	15	30	0.92	2488
7/03/75	184	1.8	324	30	0.85	1875
7/26/75	207	1.0	139	26	0.98	1477
7/28/75	209	2.0	18	30	0.98	1909
8/09/75	221	0.4	88	26	0.98	1195
8/18/75	230	1.6	167	27	0.96	1488
8/19/75	231	1.3	168	28	0.95	1052
9/08/75	251	1.8	181	25	0.89	1797
6/07/76	159	1.0	129	25	1.06	1972
6/08/76	160	1.3	284	27	1.01	1772
7/13/76	195	2.3	145	28	1.02	1853
7/29/76	211	0.3	251	26	0.53	1706
7/30/76	212	1.7	205	30	0.82	1304
8/12/76	225	2.3	253	29	0.70	730
8/13/76	226	1.1	273	30	0.86	1427
8/24/76	237	1.3	110	28	0.82	2124
10/01/76	275	0.6	222	22	0.78	527

*Meteorological variables (except MH) are network averages over the period 0700-1359 CST.

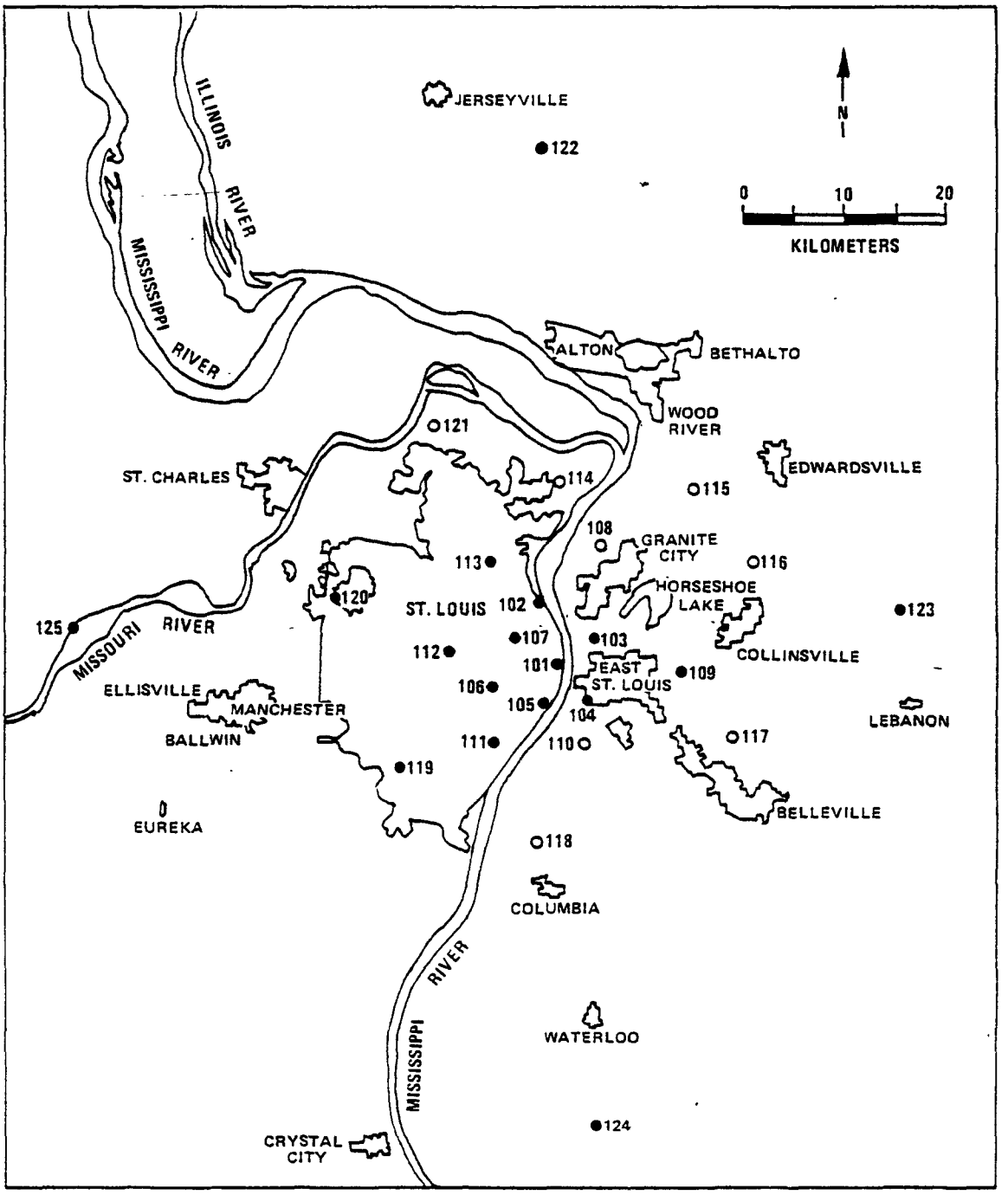

Figure 1. The St. Louis area with locations of the RAPS surface stations.

SECTION 4

PHOTOCHEMICAL BOX MODEL

INTRODUCTION

The Photochemical Box Model (PBM), a single cell Eulerian air quality simulation model, simulates the transport and chemical transformation of air pollutants in smog-prone urban atmospheres. The model's domain is set in a variable volume, well-mixed reacting cell where the physical and chemical processes responsible for O_3 generation by HC and NO_x precursors are mathematically created. These processes include the transport and dispersion of pollutant species through the cell, the injection of primary precursor species by emission sources, and the chemical transformation of the reactive species into intermediate and secondary products. They are schematically illustrated in Figure 2.

To apply the model to the St. Louis RAPS data base, the horizontal length scale of the cell was set at 20 km and the vertical scale was time dependent, proportional to the depth of the mixed layer. The model domain was chosen such that it included most major emission sources on either side of the Mississippi River. Source emissions were assumed to be distributed uniformly across the surface face of the cell. Twelve of the RAMS surface monitoring stations as well as one upper air sounding location were located within the cell boundaries. This configuration of the model domain is illustrated in Figure 3.

The steps involved in the method for performing a PBM simulation are described in the first evaluation report by Shreffler and Schere (1982), Report I. There are 3 data preprocessors that must be exercised prior to the model simulation itself. They access the RAPS data base and retrieve the appropriate parameters required by the PBM.

The framework of the model itself has not changed from the time of Report I to the present. There was a change made, however, in the method of choosing the upwind HC boundary condition for the model. Originally, if the HC data were invalid from the chosen upwind monitoring locations at a particular hour an alternate algorithm for obtaining these data was invoked. It was a ratio technique based on the average non-methane hydrocarbon (NMHC) to CO fraction over the model simulation period. In this way the boundary condition for HC could be obtained indirectly from the more reliable CO observations. It was found however, that this method occasionally gave spuriously large HC values at the upwind boundary. In a simulation with significant advection through the model domain this had the potential for creating an overly reactive mix of photochemical pollutant species in the box that would lead to an overprediction of O_3. In the simulations presented here, if a particular HC background concentration was invalid, a value of 0.05 ppmC for NMHC was substituted. This is a low-level background value for this quantity that borders on the threshold limits of the monitoring instrumentation. In practice this change caused only small differences in most of the simulation results, although in some cases it had a noticeable effect. Background concentrations of species other than O_3 were generally very small, while those of O_3 were often a significant fraction of the total O_3 burden in the model domain.

PBM simulations were conducted for each of the 20 test days listed in Table 1, including a repetition of the original 10 days described in Report I. Although results for O_3 predictions on all days are summarized, detailed descriptions are presented for only 5 days. Simulation results for pollutants CO, NO_2, and O_3 for Julian days 142, 178, and 207 of 1975 and 212 and 275 of 1976 are emphasized.

RESULTS

Among the 20 selected days for model simulations from the RAPS data base are 5 in which the maximum observed afternoon O_3 concentration occurred within the PBM domain. These were days when stagnation conditions existed with light and variable winds near the surface. Very little of the primary emissions moved out of the modeled area. During this type of episode, a single

cell box model would be appropriate for air quality simulation, since most of the pollutant mass stays within the model domain. On the other modeled days, the maximum O_3 level occurred farther downwind, outside of the PBM's boundaries. Simulations were also conducted on these days even though maximum O_3 measurements within the model domain were somewhat lower than those downwind.

Results are described in detail for those 5 days where the maximum observed O_3 concentration occurred within the model domain. Report I highlighted 2 of these days as well as a case of stronger advection. The latter case was used to demonstrate the 'inertia' effect of numerical box models that can lead to problems where large temporal concentration gradients exist. The interested reader is referred to the earlier report for details.

The PBM simulated concentrations represent spatial averages over the volume of the box. The appropriate observed concentration with which to compare predictions is the average over all 12 monitoring sites within the box. For the 5 days detailed here this concentration for O_3 exceeded the 1-hour National Ambient Air Quality Standard (NAAQS) of 0.12 ppm at least once during each simulation period. These observed average concentrations are represented by the open circles in the concentration time series described below. The observed range of concentration values among the 12 sites within the PBM domain is another feature to consider. The highest and lowest measurements are described by the dashed lines in the time series. A coarse measure of model performance is made by observing whether the PBM predicted concentrations (shown as solid lines), fall within the range of observed concentrations (between the dashed lines) and preferably as close as possible to the average observed concentrations (shown as circles).

The first simulation day considered is Day 142-75. Synoptic meteorological features on this day included an expansive high-pressure system centered over western Virginia with a general windflow from the southwest in the mid-Mississippi Valley area. Wind speeds in St. Louis, however, were light and on the order of 1.0 m s^{-1}. Skies were completely clear. The maximum afternoon hour-average O_3 measurement occurred at noon at site 101 in downtown St. Louis. According to the convention for time referencing employed here, the 1200 hour-average refers to the average concentration from 1200 to 1300 h.

Figure 4a shows the time series for CO on Day 142. The model predictions fall within the 'envelope' of observed concentrations and actually track the average observed values quite well. Carbon monoxide is included in the model evaluation analysis because it reacts very slowly in the atmosphere and may be considered virtually inert for the time scales discussed here. As such, any problems with the emissions or the advective and dispersive portions of the PBM would be reflected in the CO predictions, whereas the complex chemical interactions of a more reactive pollutant could mask problems with transport or emissions.

Figure 4b shows the time series for NO_2 on the same day. These model predictions are consistently greater than the average observations throughout the simulation but generally fall within the concentration envelope. Figure 4c displays the O_3 time series. PBM predictions track the average observations through mid-morning and then diverge near noon when observed O_3 levels begin to decrease while the predictions peak one hour later at 1300 CST. The model-predicted peak O_3 concentration reached 0.148 ppm compared with the average observed peak of 0.137 ppm, an 8% overprediction. This is somewhat better than the 28% overprediction cited in Report I for Day 142. The model predictions fall mostly within the concentration envelope except for the last few hours of the simulation. Background concentrations of O_3 on Day 142 were on the order of 0.06 ppm.

The synoptic-scale meteorological features on Day 178-75 show the eastern third of the U.S. covered by a large high-pressure system. Wind speeds were light and directions variable near the surface as well as at upper levels of the atmosphere. In St. Louis surface winds were generally less than 1.0 m s^{-1}. Skies were hazy most of the day with few clouds reported. Solar insolation levels were high throughout the simulation period. The maximum hour-average O_3 measurement occurred at site 112 in the western part of the model domain at 1400 CST. Background concentrations of O_3 on Day 178 were approximately 0.08 ppm.

The time series for CO on this day is presented in Figure 5a. The PBM underpredicts CO consistently throughout the period although most predictions

do fall within the concentration envelope. The most serious underpredictions occur in the earliest hours of simulation where the differences observed among the stations themselves are greatest. The large departures at the upper edge of the concentration envelope at that time illustrate this. These high values tend to bias the average within the model domain to the high side.

The NO_2 time series in Figure 5b shows the predictions to match the observations throughout the period except for the observed peak at 0700 CST. A phenomenon may be occurring here similar to that which biased the CO peak toward higher values. Nitrogen dioxide, however, is predominantly a secondary pollutant and should therefore not demonstrate fluctuations as large as a primary pollutant like CO. Predicted values for O_3 for Day 178 are seen in Figure 5c. They lag behind the observations during the morning hours and peak two hours later in the afternoon. The rapid morning rise of the O_3 observations may be due to a rather large entrainment rate of O_3 aloft. If the assumed rate of rise of the mixed layer in the PBM is too slow for this particular day the predictions would tend to lag the observations as they do here. The model-predicted peak of 0.173 ppm was 8.8% greater than the observed value of 0.159 ppm. This is an improvement over the 38% overprediction indicated in Report I.

On Day 207-75 a high-pressure system had settled into the northeastern quarter of the U.S. after moving rapidly southeast from the western Canadian provinces. Winds in the St. Louis area quickly dropped to near calm following a frontal passage the previous day. Skies were clear throughout the day. The maximum hour-average observed O_3 concentration occurred at site 113 at 1400 CST, in the northwestern portion of the PBM domain. The background value of O_3 on this day was generally about 0.07 ppm.

Model predictions of CO shown in Figure 6a agree quite well with observations for Day 207. Again there are several large positive anomalies along the upper edge of the CO observed concentration envelope, similar to those occurrences on other modeled days. In Figure 6b the model-predicted NO_2 concentrations peak at the same hour and follow the same trend as the observations in the time series shown, although the predicted values are consistently greater

than those observed throughout the simulation period. With one exception they remain within the NO_2 observed concentration envelope.

Model-predicted O_3 values on Day 207 rise more rapidly than the observations would suggest in Figure 6c. The average observed O_3 peak is a sharp one occurring at 1400 CST at 0.140 ppm, while the predicted peak is more plateau-like with a high point at 1500 CST of 0.145 ppm, a 3.6% overprediction. Possible reasons for the model's more rapid generation of O_3 during the morning hours include an excessive entrainment rate from aloft or an overly reactive assumption concerning the mix of organic hydrocarbon species on this day.

A weak stationary front separating 2 similar zones of high pressure was situated near St. Louis on Day 212-76. The front was aligned mostly in an east-west direction and had drifted north of the area during the previous day enabling the southern-most air mass to dominate. Winds at St. Louis were mostly from the south and southwest at speeds of 1-2 m s^{-1} during the simulation period. A layer of high clouds persisted throughout much of the day and decreased the available insolation by 10 to 20%. The maximum hour-average O_3 measurement occurred at noon at site 108, located in the northeastern corner of the model domain. The background O_3 concentration on this day was 0.10 ppm.

The time series for model-predicted concentrations of CO and NO_2 for Day 212 are shown in Figures 7a and b, respectively. In both cases the predictions track the observations well through most of the period except for the early hours when the peak observed concentration is underpredicted. The O_3 time series in Figure 7c shows good agreement between domain-averaged observations and model predictions. The model-predicted concentrations rise more quickly in the early hours and decline more slowly in the later hours of the simulation than the observations. The average observed O_3 peak occurred at noon at 0.127 ppm and the maximum estimated concentration was 0.121 ppm at 1400 CST, a 4.7% underprediction. It appears that less than 20% of the observed O_3 was produced locally on Day 212 in St. Louis since the background levels were only slightly less than the highest afternoon values.

Day 275-76 is considered to be the most extreme case of stagnation during the 1975-76 RAPS project. The synoptic meteorological conditions revealed a high-pressure region over the Texas-Arkansas area with northwest flow aloft over St. Louis. Near the surface however, winds were very light and variable in direction with little transport through the area. Skies were clear all day and a strong subsidence inversion over the city held the mixed depth to a maximum of just over 500 m above ground during the afternoon. The greatest hour-average O_3 measurement occurred at site 102, just north of downtown, at 1400 CST. Background O_3 levels on Day 275 were approximately 0.06 ppm.

The time series for CO on this day is presented in Figure 8a. Overall concentration levels substantially exceed those on the other modeling days presented here. Report I discusses the implications of attempting to apply the PBM to periods of extreme atmospheric stability as occurred at the very beginning and end of the simulation period on Day 275. The net effect is a substantial underprediction of the peak observed concentration during the stable period. This can be seen in the CO time series. Both NO_2 and O_3 concentration levels, seen in Figures 8b and c, are also considerably greater than those on the other days. The model-predicted NO_2 concentrations follow the average observed concentrations well and show slightly smoother temporal gradients than those observed. Simulated O_3 concentrations also display a trend similar to observed O_3. The afternoon predictions actually track the upper boundary of the concentration envelope better than they track the average observed concentrations. The estimated O_3 maximum is 0.223 ppm at 1500 CST, while the average observed peak is 0.183 ppm at 1400 CST, a 21.9 percent overprediction; nearly the same as that in Report I for Day 275.

Model performance on these 5 days indicates the PBM can simulate the average urban air quality for selected pollutants in relatively stagnant conditions. The weakest performance seems to be with the primary pollutant CO because of the non-homogeneous character of its emission and dispersal. While the areas of maximum observed O_3 on the remaining 15 days listed in Table 1 did not occur within the PBM domain the model was exercised for these days as well in order to provide a consistent statistical summary with the other models discussed in this report. In the tables and figures that follow data from model performance on all 20 days are included.

One significant aspect of photochemical transformation omitted from these discussions on PBM simulation of an urban atmosphere is the presence of volatile organic compounds, or hydrocarbons (HC), in the smog mixture. While the chemical kinetic mechanism in the PBM does account for HC interactions with other reactive species, a discussion of the details of the mechanism is beyond the scope of this paper.

Table 2 summarizes the O_3 maxima predicted and PBM domain-average observed maximum concentrations and an elementary statistical analysis of the results for all 20 modeled days. The "specific" model predictions correspond to the same hour as the observed maximum, and the "independent" predictions represent the peak at any hour of the simulation. The specific and independent predictions may not coincide, indicating a phase lag between observed and predicted O_3 peaks. This lag often appears when the maximum observed O_3 within the model domain occurs before noon. Statistics on the residual concentration, ΔC, have been computed for both the specific and independent predictions. Both the average signed residual and absolute residual, and standard deviation are presented for the analyses. The average residual is negative in both the specific and independent cases, indicating an overprediction of O_3, although the specific value is one-half the independent value. The values of the average absolute residuals are both different from the average signed residuals. This implies that there were underpredictions as well as overpredictions among the individual days. The magnitude of the standard deviation (s.d.) is slightly greater than the average residual. The discrepancy on Day 251 accounts for a large portion of the s.d. The average value of the model's overprediction for O_3 over all 20 days is 23%, compared to the 31% overprediction for the original 10 days cited in Report I. It should be noted that the average value of the overprediction over the 5 days where the maximum measured O_3 occurred within the PBM domain is 7.5%, considerably less than that for the full set of days.

Although the analysis in Table 2 summarizes one aspect of model performance, it is clearly not a complete picture of the accuracy or precision of the PBM. To more fully appreciate PBM performance, the model can be viewed from a broader statistical perspective. Figure 9 presents frequency histograms (RS)

TABLE 2. A SUMMARY OF PREDICTED AND OBSERVED O_3 MAXIMA FOR THE PBM

Julian date[a]	Hour (CST)	Observed at 4-meters (ppm)	PBM Predicted Specific (ppm)	PBM Predicted Independent (ppm)
142 (1975)	12	0.137	0.125	0.148
178	14	0.159	0.162	0.173
182	13	0.094	0.128	0.140
183	13	0.115	0.070	0.097
184	13	0.114	0.182	0.182
207	14	0.140	0.144	0.145
209	10	0.108	0.087	0.122
221	13	0.132	0.125	0.125
230	13	0.072	0.096	0.119
231	10	0.084	0.059	0.101
251	15	0.084	0.205	0.205
159 (1976)	13	0.125	0.203	0.210
160	14	0.162	0.166	0.170
195	15	0.151	0.132	0.137
211	15	0.094	0.084	0.088
212	12	0.127	0.114	0.121
225	12	0.111	0.088	0.092
226	15	0.144	0.171	0.171
237	11	0.115	0.132	0.156
275	14	0.183	0.216	0.223

[a]Twenty days selected from 1975 and 1976.

For the data displayed above:

ΔC = Obs - Specific

$\overline{\Delta C} = -0.012$

s.d.(ΔC) = 0.039

$\overline{|\Delta C|} = 0.029$

ΔC = Obs - Independent

$\overline{\Delta C} = -0.024$

s.d.(ΔC) = 0.036

$\overline{|\Delta C|} = 0.031$

of CO, NO_2 and O_3 residual concentrations, the observed minus predicted model results, over all test days. An ideal distribution would be narrow with a peak at the 0.0 residual. The 3 histograms shown display a range of distributions. The RS for CO is skewed toward the underpredictive side while O_3 is skewed toward the overpredictive. The nitrogen dioxide RS is more symmetric than the others but does contain a few outliers on the underpredictive side. All 3 distributions show a peak at or very near 0.0.

A plot of the residuals versus observed concentrations (RO) should indicate whether a bias in the predictions displays any trend with the magnitude of the measured concentrations. Figure 10 shows RO plots for the same species as presented in Figure 9. For CO and NO_2 there appears to be a trend toward greater underprediction with higher ambient concentrations. The trend is more clear with CO. Ozone however, displays no particular trend with observed concentration, but the PBM generally overpredicts ambient values above 0.05 ppm.

The PBM has been exercised on a variety of days taken from the RAPS data base. Prevailing meteorological conditions occurring some of the days may not have been compatible with the environment for optimum model results. Using the PBM in a regulatory capacity could be restricted to worst case stagnation conditions where the model seems to perform best. Time series for pollutant species on test days other than those discussed here are displayed in Appendix A. Also, tabulated model performance statistics for data on mean concentrations, analysis of trends, and concentration maxima from the PBM are provided in Appendix B.

CONCLUSIONS

A thorough evaluation of the performance of the PBM has been completed. This analysis is a major portion of the documentation of the model's abilities for air quality simulation. Evidence shows that the model is a useful tool in assessing urban air quality for photochemically reactive pollutants, especially in stagnation conditions. The PBM is relatively simple to use and its data requirements are far less stringent than most other numerical air quality simulation models. Areas of further study that may be pursued include:

(1) the hysteresis problem during advection conditions, discussed in Report I;

(2) the relationship between the average O_3 concentration observed within the model domain and the maximum O_3 level observed at a single station;

(3) the continued testing and refinement of the chemical kinetic mechanism within the PBM;

(4) model sensitivity to variations in selected parameters such as initial and boundary concentrations, initial cell depth, emissions, wind speed and solar radiation.

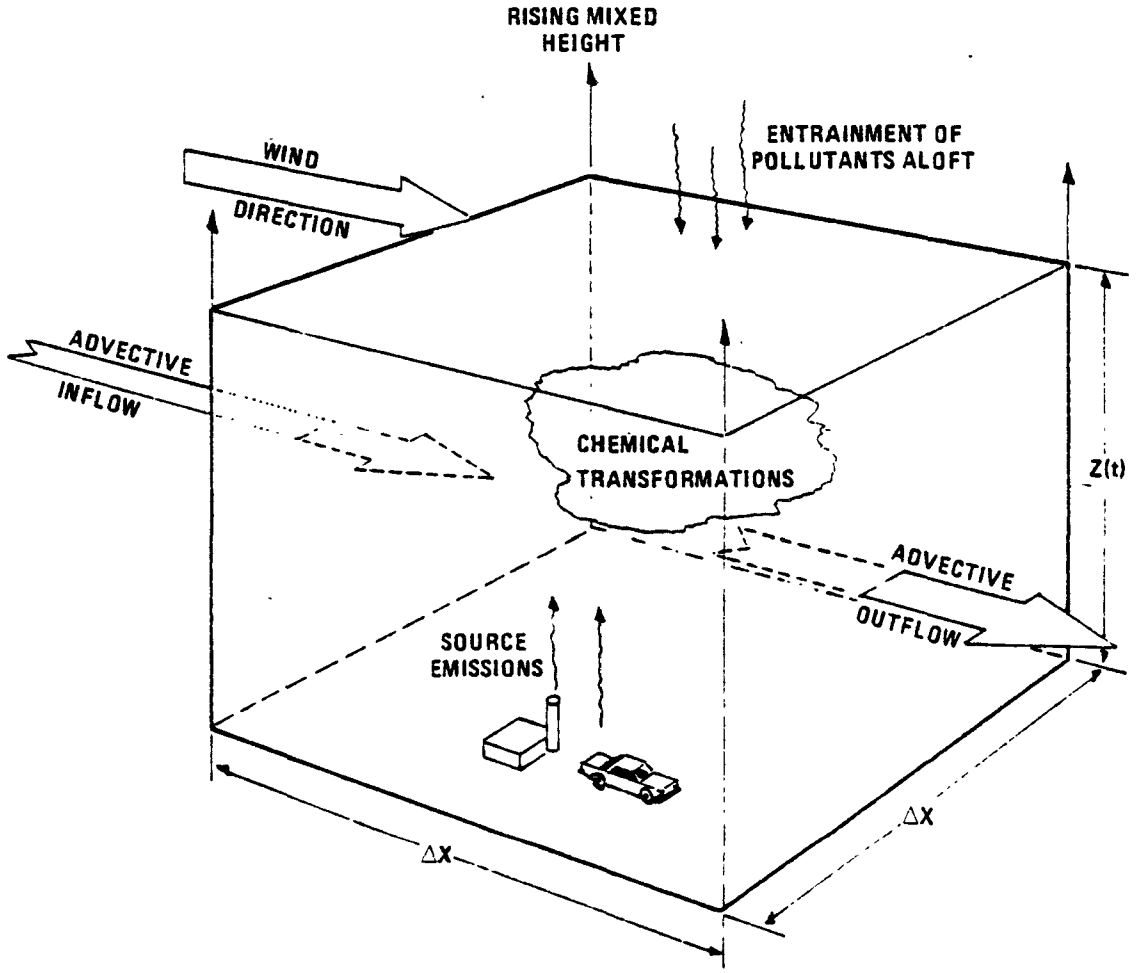

Figure 2. Schematic drawing of the PBM domain.

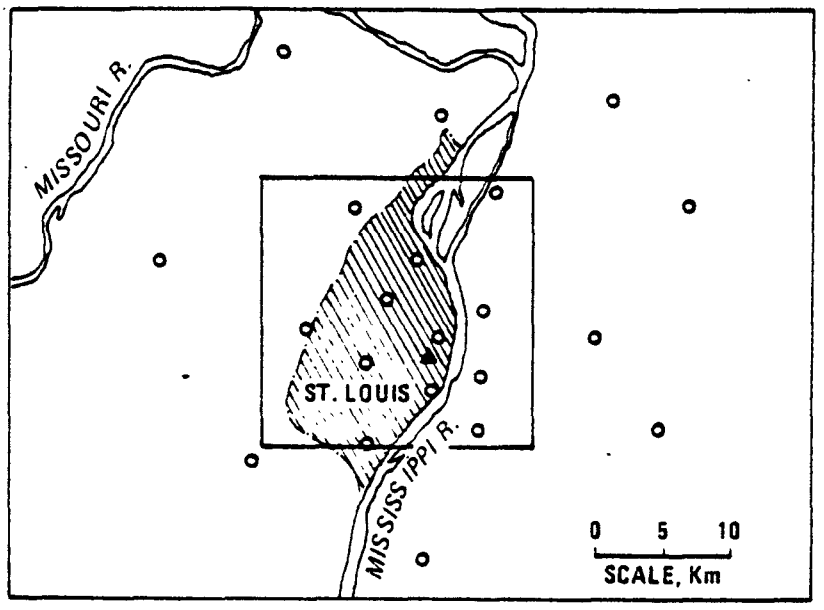

Figure 3. Map of St. Louis area depicting extent of PBM modeling domain (boxed area), city of St. Louis (shaded area), RAPS monitoring stations (circles), and radiosonde ascent site (triangle).

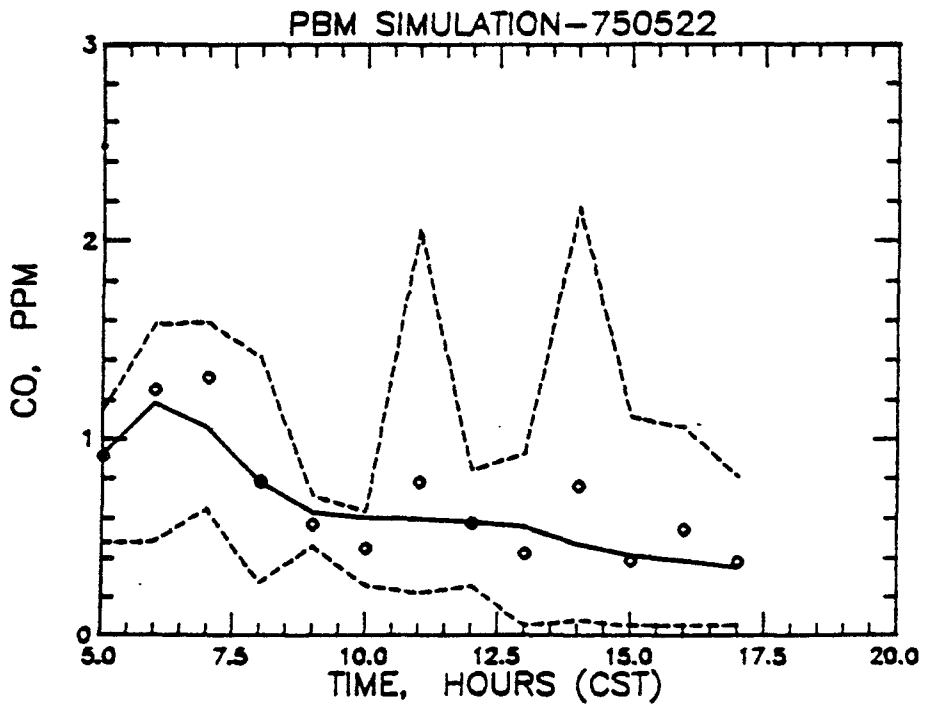

Figure 4a. PBM simulation results for Day 142 of 1975. Time series of average observed (circles), range of observed (dashed lines), and model-simulated (solid line) hour-average concentrations of CO.

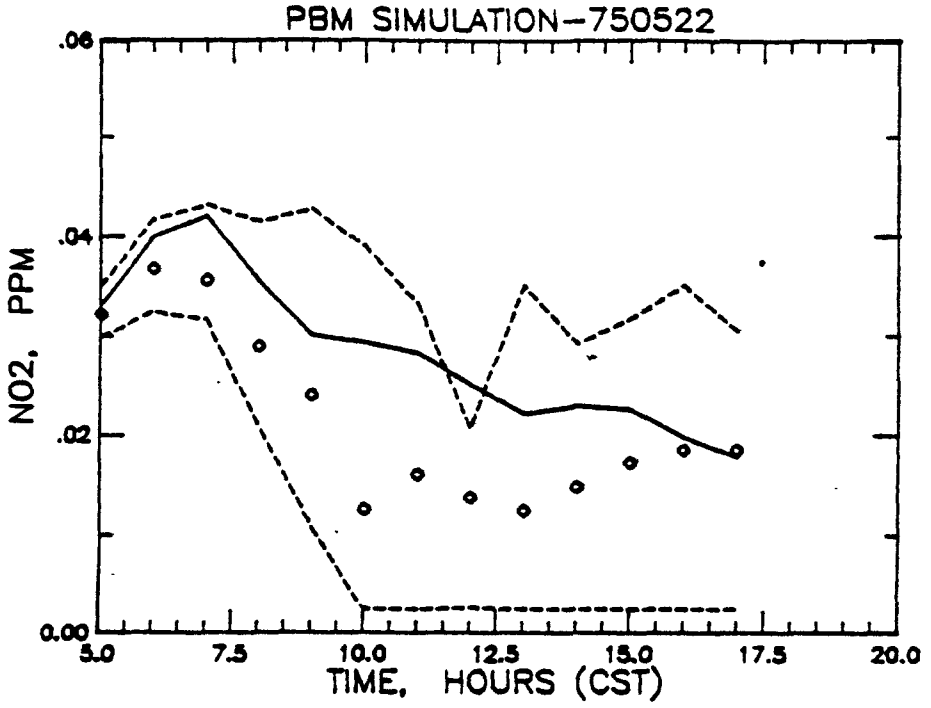

Figure 4b. PBM simulation results for NO_2 - Day 142 of 1975. Keys to figure described in 4a.

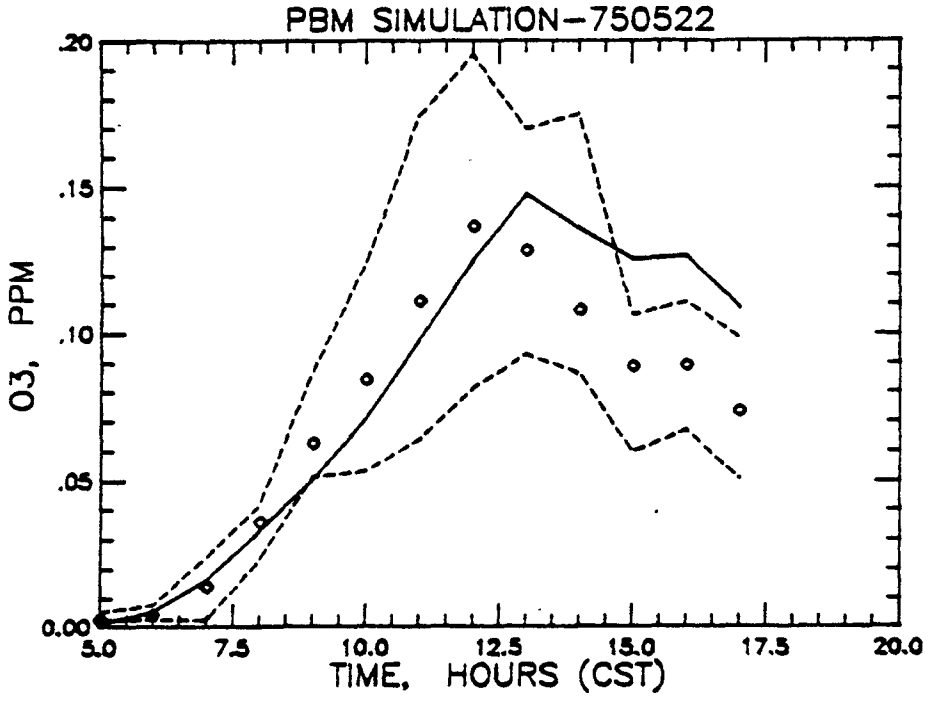

Figure 4c. PBM simulation results for O_3 - Day 142 of 1975. Keys to figure described in 4a.

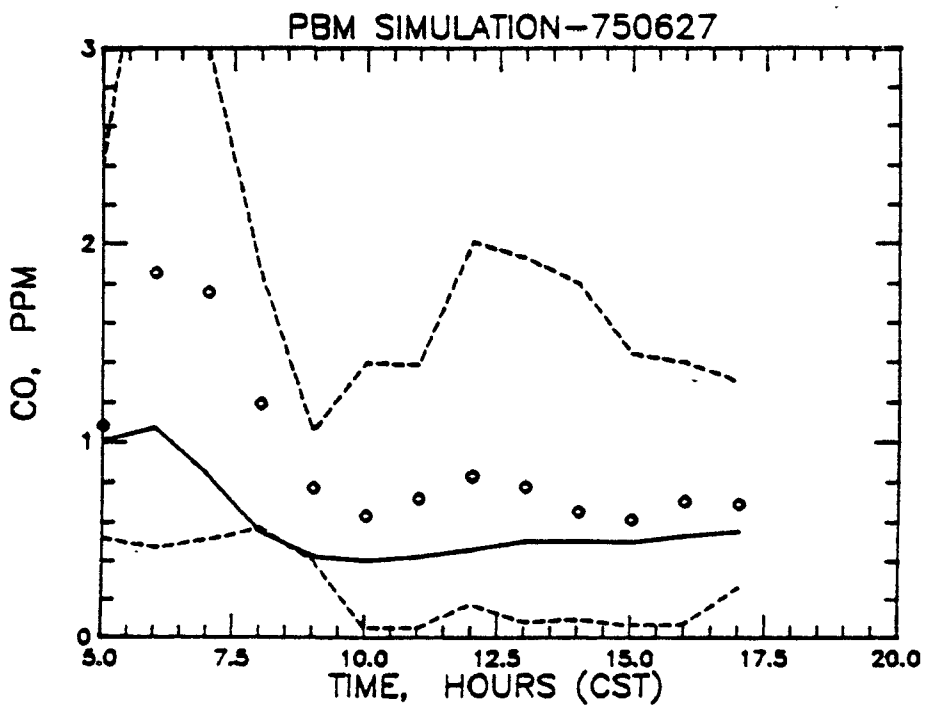

Figure 5a. PBM simulation results for Day 178 of 1975. Time series of average observed (circles), range of observed (dashed lines), and model-simulated (solid line) hour-average concentrations of CO.

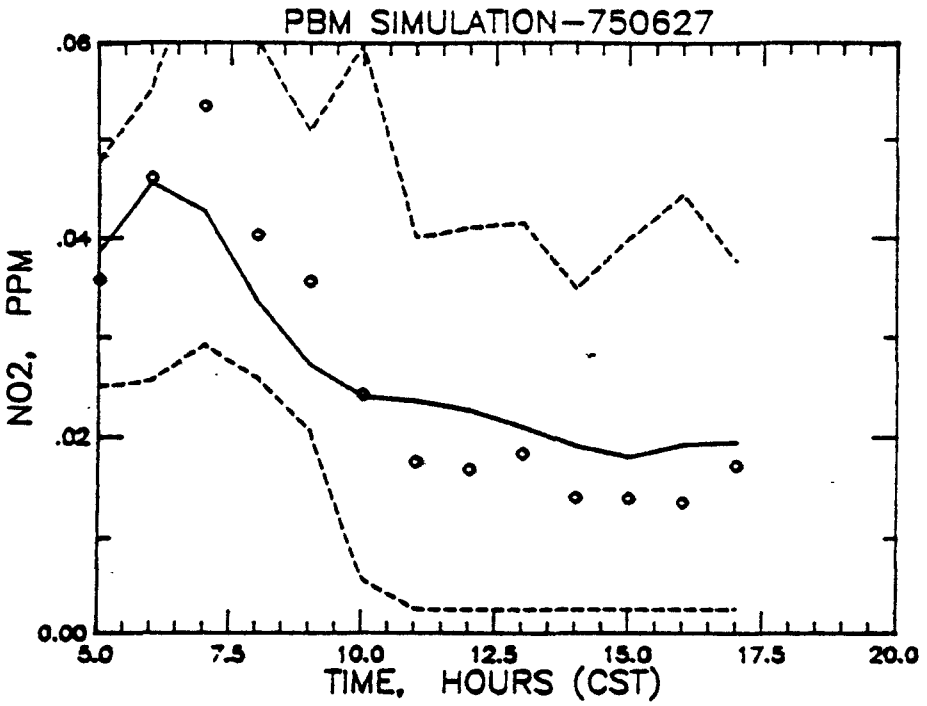

Figure 5b. PBM simulation results for NO_2 - Day 178 of 1975. Keys to figure described in 5a.

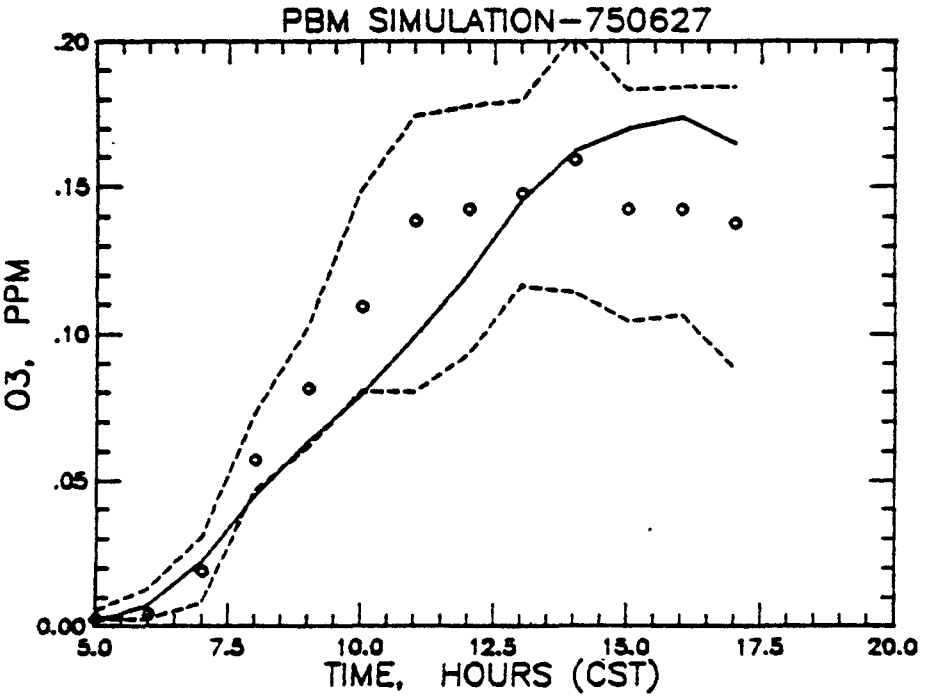

Figure 5c. PBM simulation results for O_3 - Day 178 of 1975. Keys to figure described in 5a.

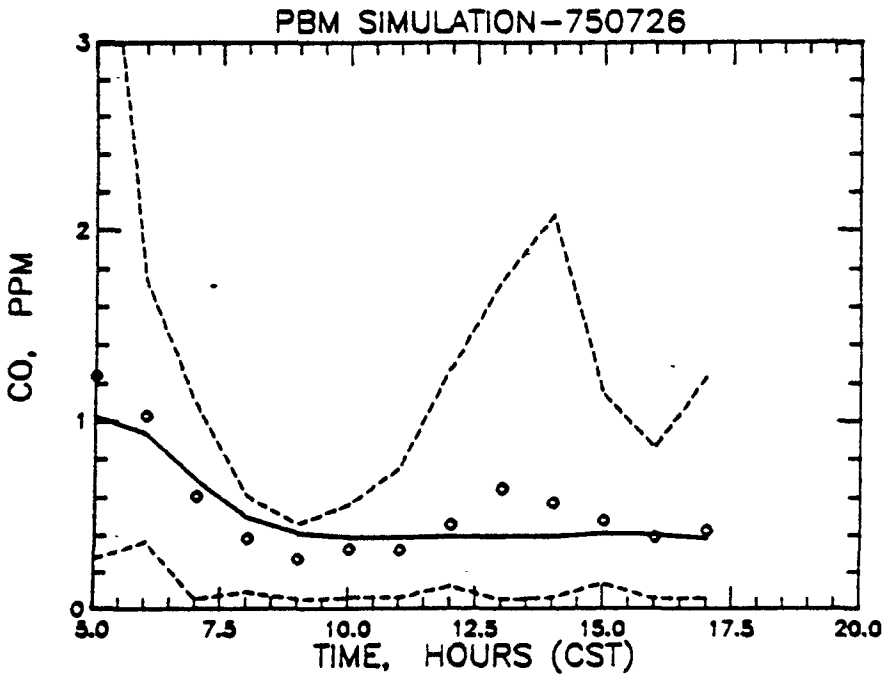

Figure 6a. PBM simulation results for Day 207 of 1975. Time series of average observed (circles), range of observed (dashed lines), and model-simulated (solid line) hour-average concentrations of CO.

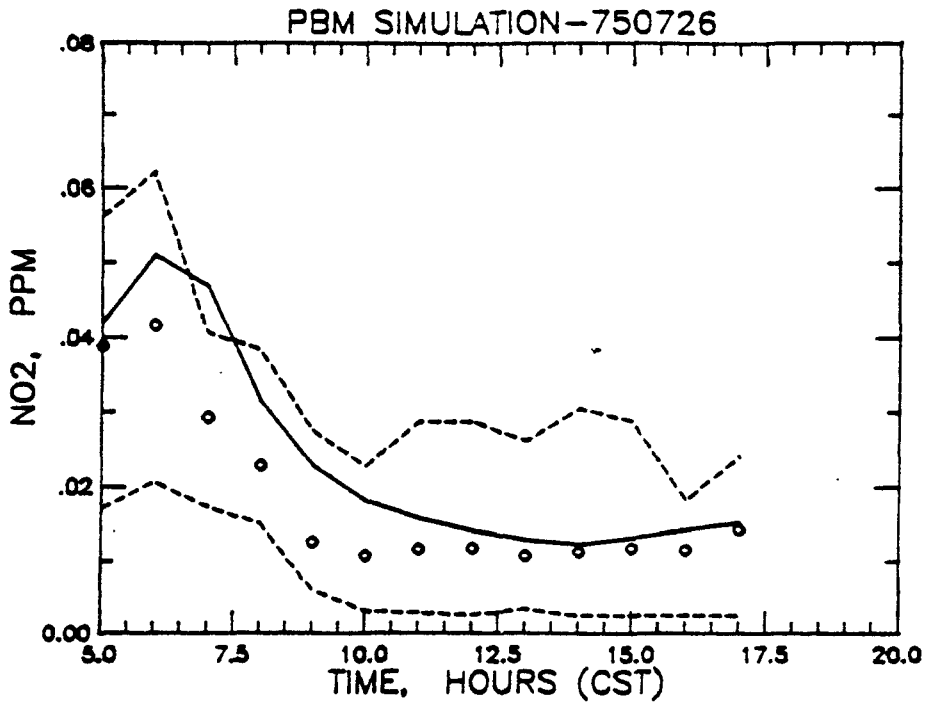

Figure 6b. PBM simulation results for NO_2 - Day 207 of 1975. Keys to figure described in 6a.

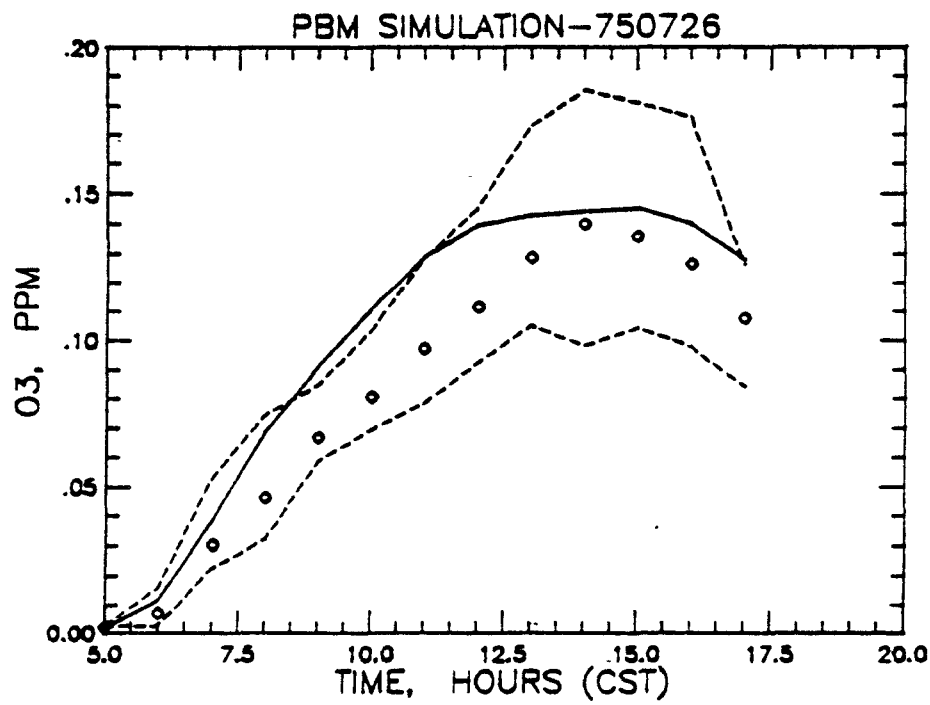

Figure 6c. PBM simulation results for O_3 - Day 207 of 1975. Keys to figure described in 6a.

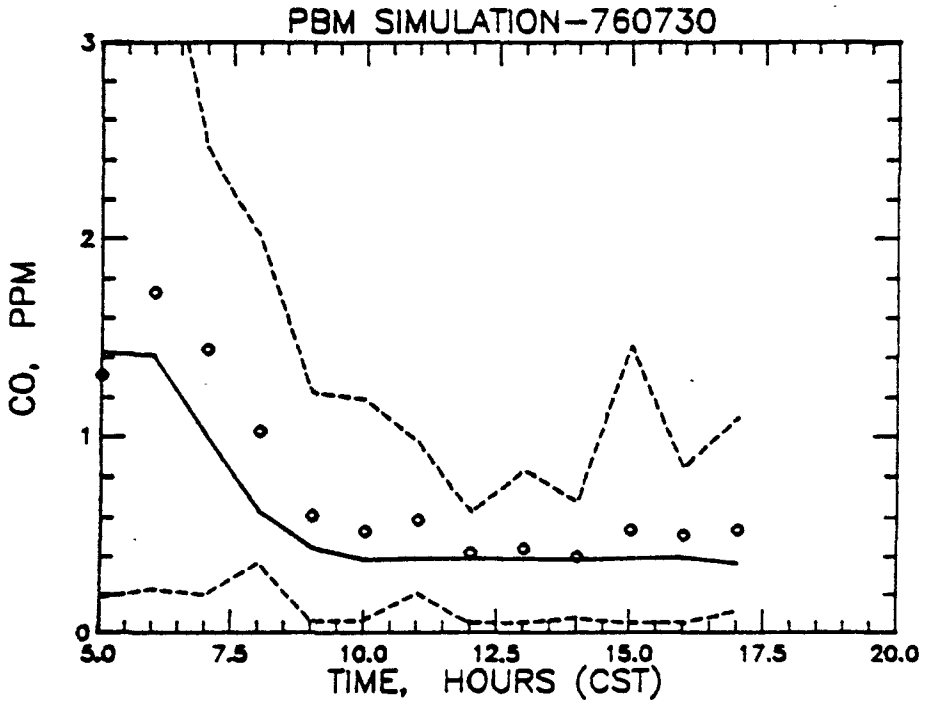

Figure 7a. PBM simulation results for Day 212 of 1976. Time series of average observed (circles), range of observed (dashed lines), and model-simulated (solid line) hour-average concentrations of CO.

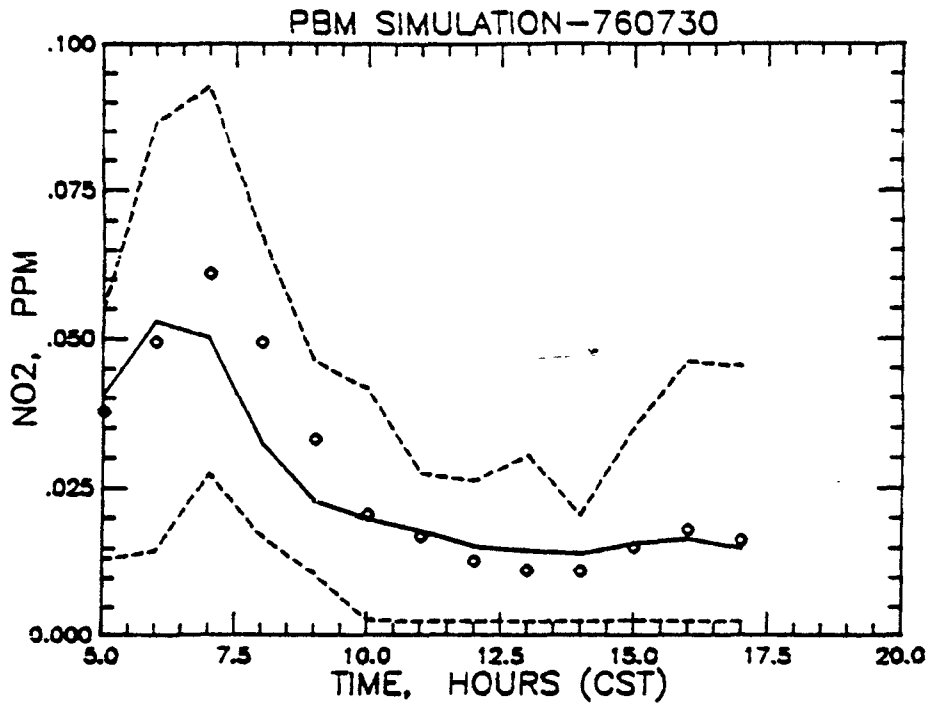

Figure 7b. PBM simulation results for NO_2 - Day 212 of 1976. Keys to figure described in 7a.

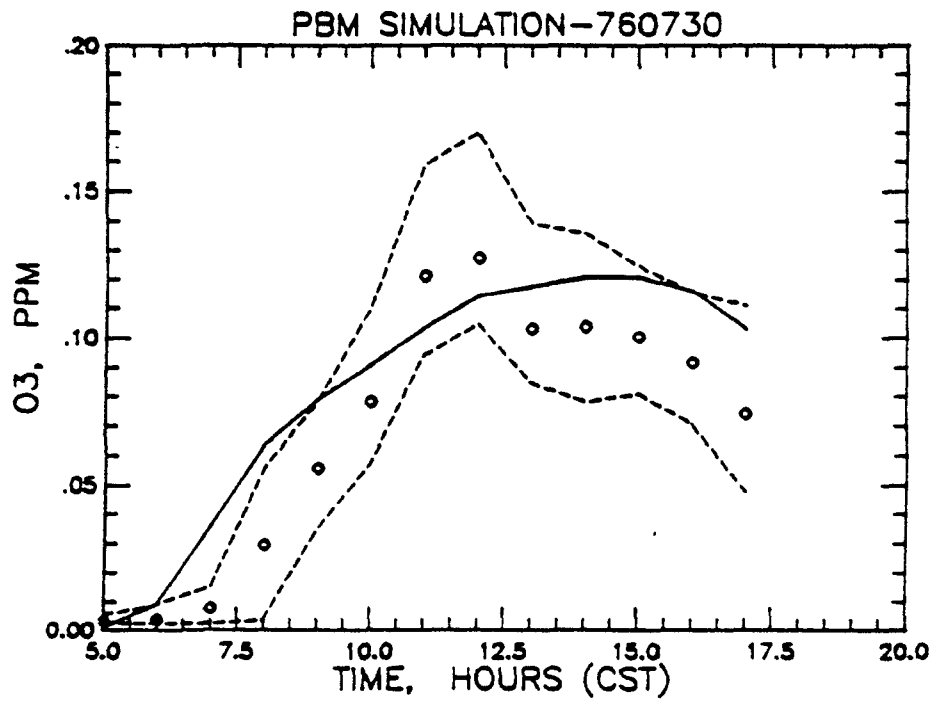

Figure 7c. PBM simulation results for O_3 - Day 212 of 1976. Keys to figure described in 7a.

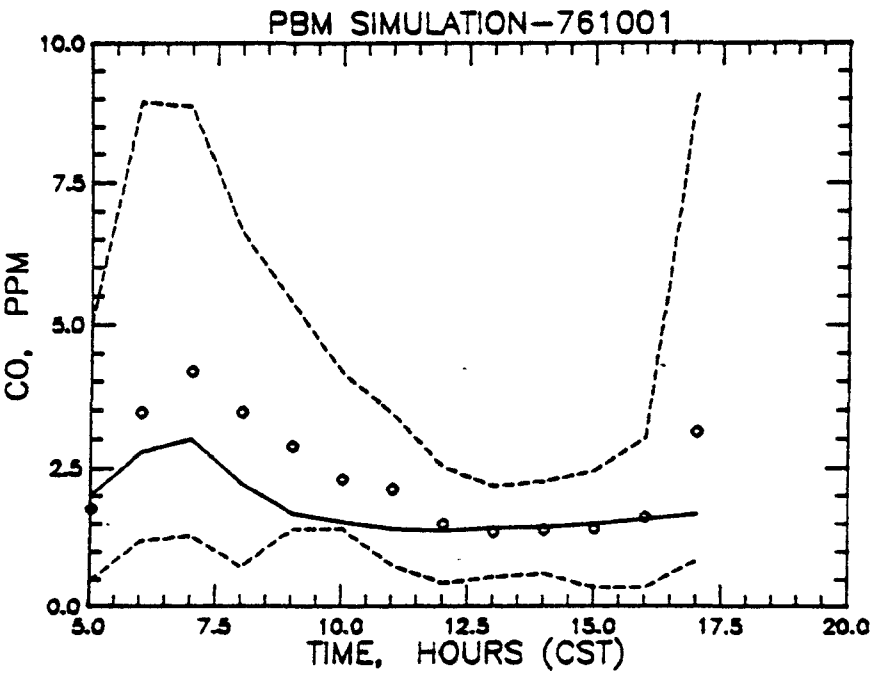

Figure 8a. PBM simulation results for Day 275 of 1976. Time series of average observed (circles), range of observed (dashed lines), and model-simulated (solid line) hour-average concentrations of CO.

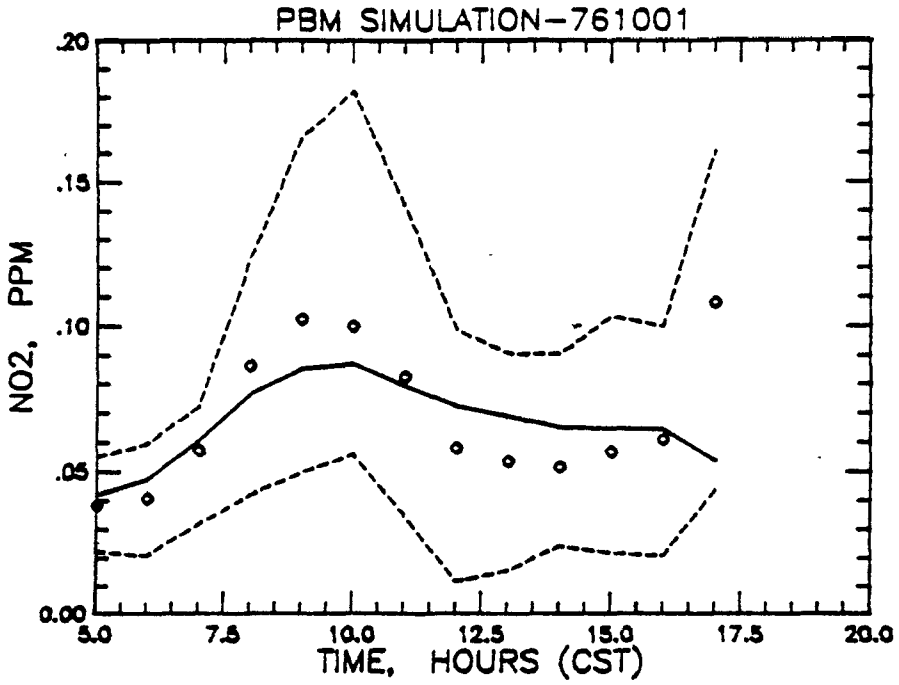

Figure 8b. PBM simulation results for NO_2 - Day 275 of 1976. Keys to figure described in 8a.

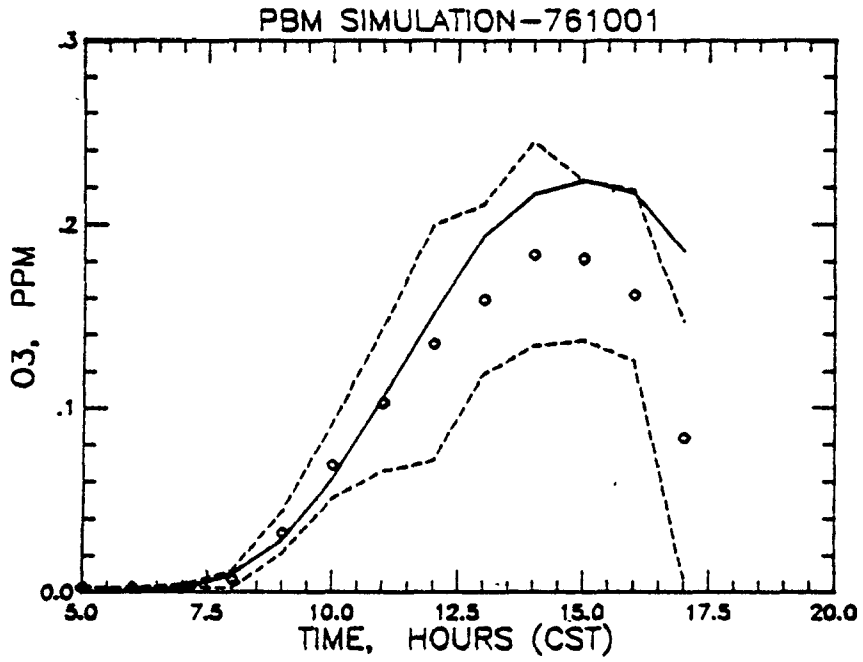

Figure 8c. PBM simulation results for O_3 - Day 275 of 1976. Keys to figure described in 8a.

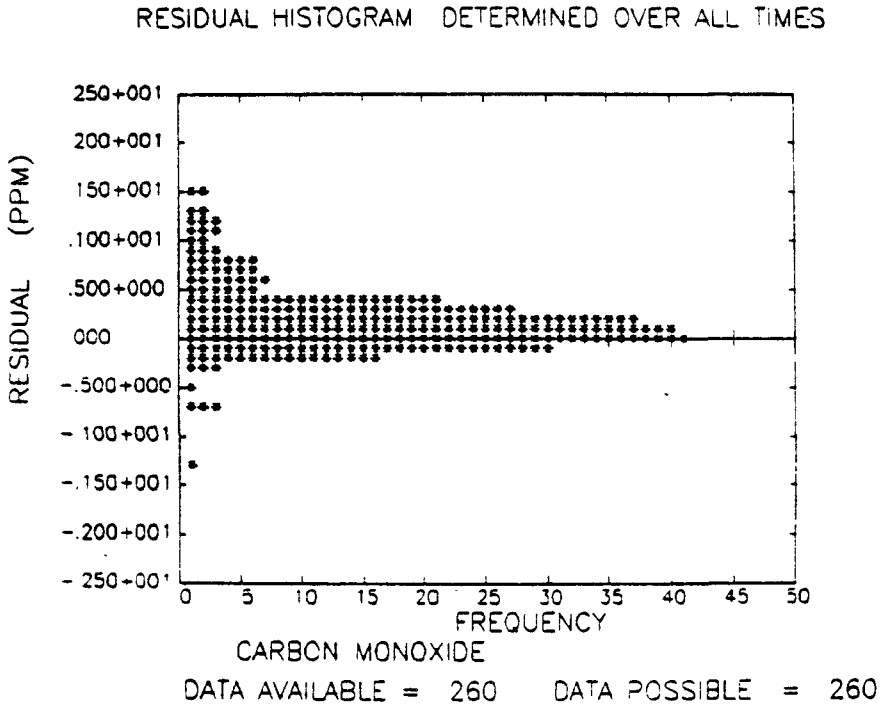

Figure 9a. Residual histogram from the PBM simulation results for all 20 test days for CO.

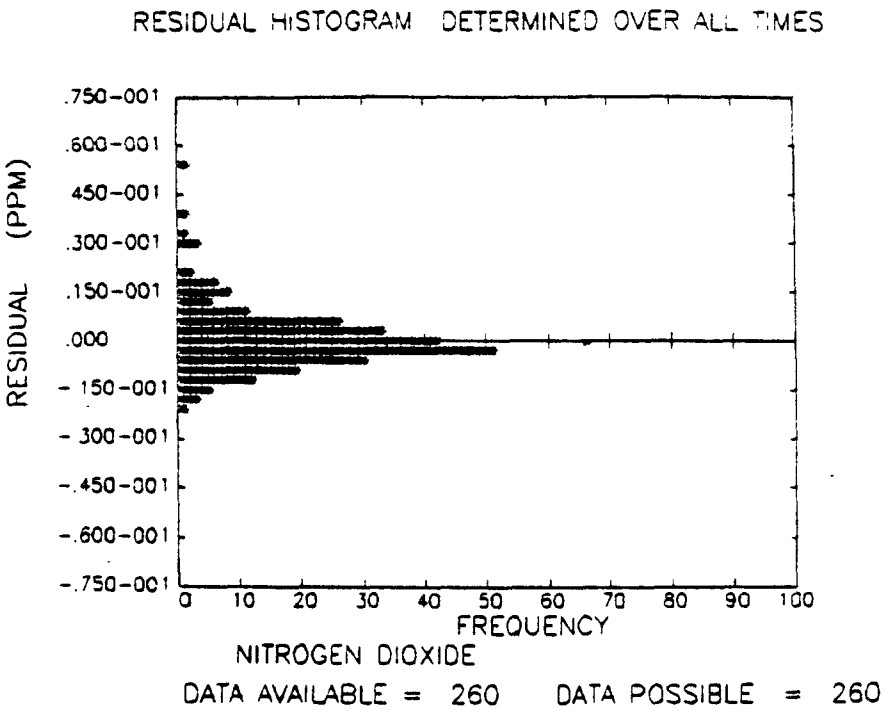

Figure 9b. Residual histogram from the PBM simulation results for all 20 test days for NO_2.

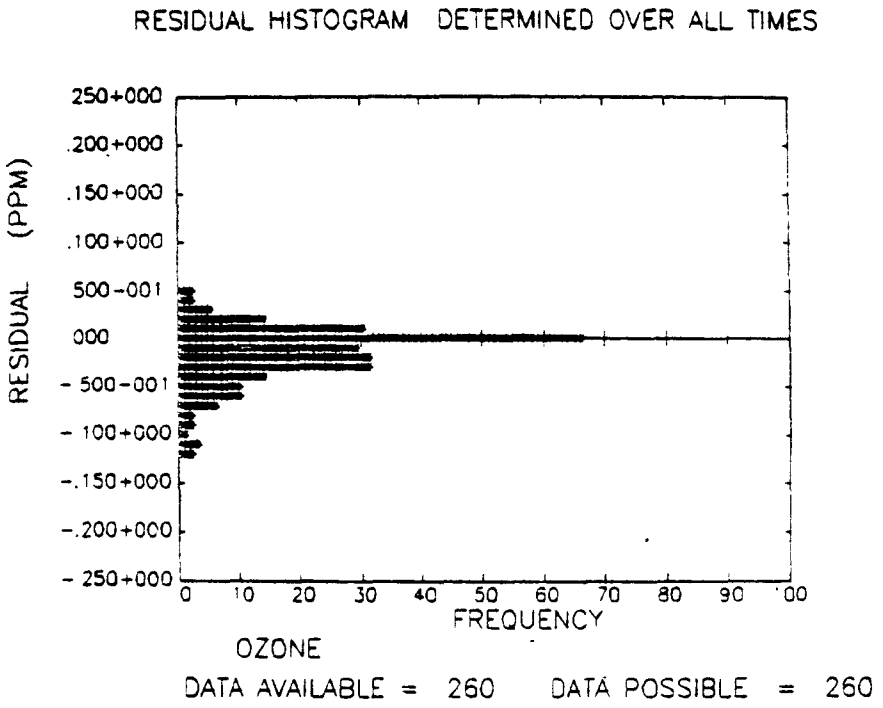

Figure 9c. Residual histogram from the PBM simulation results for all 20 test days for O_3.

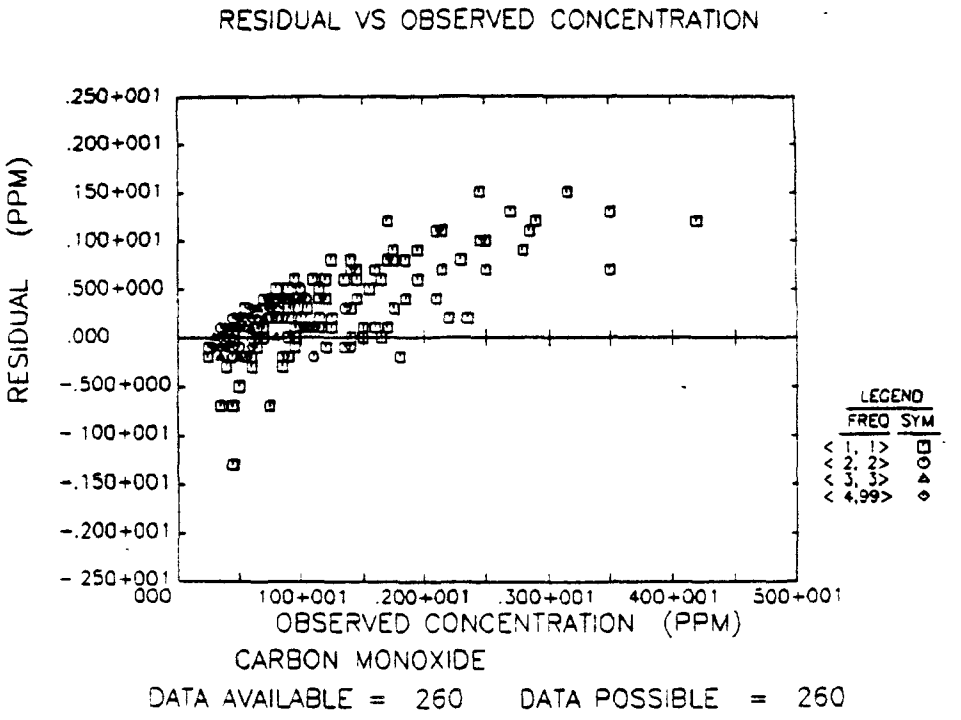

Figure 10a. Residual vs. observed plot from the PBM simulation results for all 20 test days for CO.

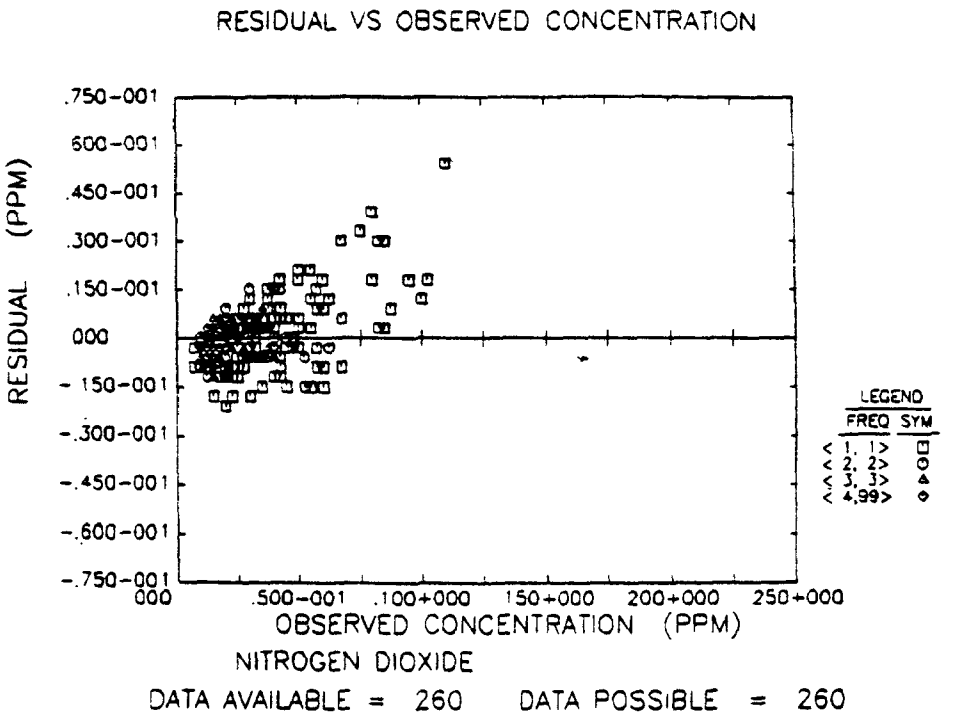

Figure 10b. Residual vs. observed plot from the PBM simulation results for all 20 test days for NO_2.

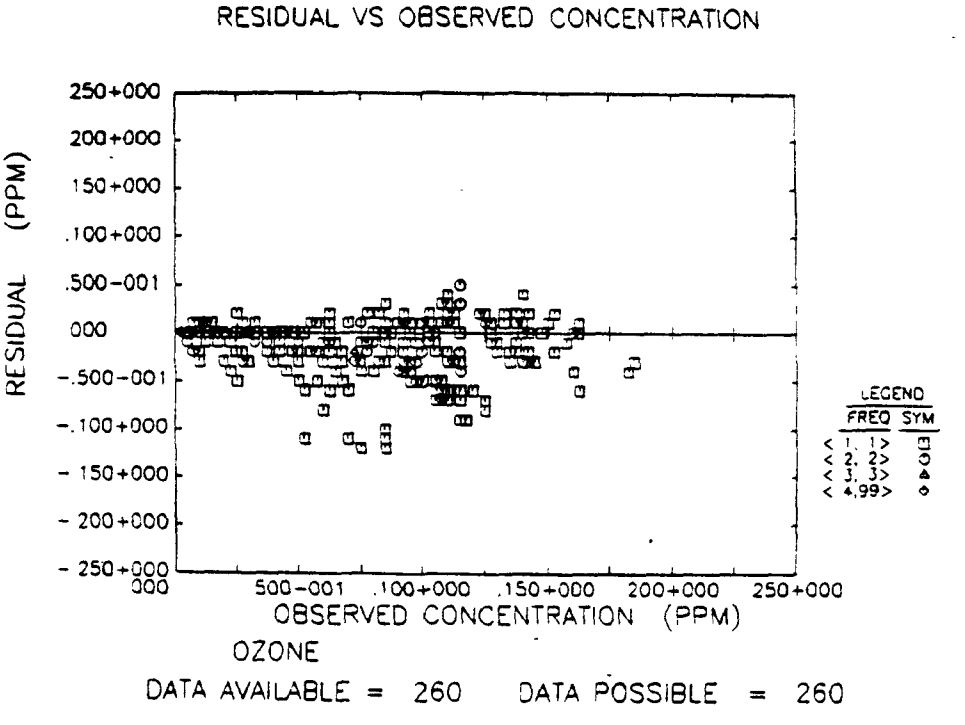

Figure 10c. Residual vs. observed plot from the PBM simulation results for all 20 test days for O_3.

SECTION 5

LAGRANGIAN PHOTOCHEMICAL MODEL

OVERVIEW

The Lagrangian Photochemical Model (LPM) was developed by Environmental Research and Technology, Inc. (ERT) and adapted under contract with EPA for use with the RAPS data base. (The LPM is essentially identical to the general-use model named ELSTAR). The LPM envisions a portion of the atmosphere as an identifiable parcel which can be tracked from early morning to late afternoon. As the parcel moves over the various emissions sources, pollutants are assimilated, vertically mixed, and subjected to photochemical reactions in the presence of solar radiation. The LPM is attractive relative to grid models in that it is fairly simple to execute and uses a moderate amount of computer time. On the other hand, the LPM calculates concentrations only within a parcel and not over a complete spatial field.

Previously, LPM simulations were conducted for 10 days from RAPS and documented in Report I. Findings from that study pointed to the need for lateral diffusion to be included for the parcel and indicated the importance of initial conditions to the final ozone predictions. Based on those findings, the model has been modified to include a Gaussian-type lateral spread of the parcel. Furthermore, the manner in which the initial condition profiles of NO, NO_2 and HC are loaded has been modified from the original recommended method. A series of simulations over 20 days (including the original 10) has been executed, and results are summarized in this section of the report. Meteorological characteristics of the test days are listed in Table 1.

METHOD

The LPM is executed using a series of program modules. They are METMOD, EMMOD and KEMOD, sequentially performing calculations on meteorology and air quality, emissions and photochemistry. The input and running procedures

described by Lurmann et al. (1979) have been generally followed, with some modifications as discussed in Report I. In addition, running procedures for the expanding Lagrangian parcel were established and the method of setting initial concentration profiles was altered. As done previously, the parcel start position was set so it would arrive at the station observing the maximum 1-h ozone value for the day.

Following the initial 10 simulations, attention was focused on the results for Day 251 where the ozone prediction was a factor of 2 higher than the maximum observed concentration. This single case was important in the summary results since the large residual (observed minus predicted) accounted for a substantial portion of the standard deviation of the residuals over the 10 days. Based on early morning surface concentrations, the parcel on Day 251 was initially loaded with very high reactive hydrocarbon (RHC) concentrations, and parametric analysis indicated that the initial loading was totally responsible for the prediction exceeding the observation. Accepting the initial condition formulation, the concept of a fixed parcel size within the LPM seemed a likely contributor to the over-prediction. It seemed more reasonable that, as a parcel leaves the central, high-emissions areas, it should expand so as to simulate lateral diffusion. The net effect would be to decrease concentrations of precursors and, ultimately, ozone. Therefore, under contract to EPA, Lurmann (1980, 1981) implemented an expanding parcel scheme in the LPM. The rate of expansion was based on Gaussian plume σ_y values. The meteorological preprocessor, METMOD, now produces a parcel-width schedule in addition to other outputs. The METMOD input allows the user to specify a proportionality constant for the σ_y expansion and to choose a time when the expansion begins. To maintain an objective evaluation the proportionality constant was taken as 1, and the parcel started expanding at 0800 CST for all simulations. The expansion rate was controlled by an internally computed stability class, but generally parcel widths of 7-10 km were achieved by midafternoon (from an original 5 km). The effect on pollutant concentrations was noticeable but not entirely satisfactory. For example, the Day 251 maximum of 0.53 ppm from Report I (Table 4) dropped to 0.37 ppm, and the s.d. (ΔC) over the 10 days dropped from 0.11 ppm to 0.068 ppm. However, in the second set of 10 days, Day 237 of 1976 also had high initial concentrations with resulting over-predic-

tion, so that the s.d. (ΔC) over 20 days was an unacceptably high 0.090 ppm. It was clear that the expanding parcel alone would not solve the problem of substantial overprediction in certain cases.

These results prompted a re-examination of the method used for initalizing the pollutant profiles for HC and NO_x (only surface measurements were available). As originally implemented by ERT, the assumed initial profile showed concentration decreasing to 1/2 the surface observation at the morning mixing height - typically 200 m - and remaining constant at that value up to the parcel top (the afternoon mixing height, typically 1500 m). The flaw in the original scheme is that the assumed total mass above the morning mixing height may be very large if the surface concentration is large. High HC and NO_x initial concentrations are usually the result of accumulation of near-surface emissions during very calm nights. Therefore, it is reasonable that the true vertical extent of the high loading is only up to the morning mixed layer and that more-or-less background levels should exist above. Such a scenario was implemented in the LPM for the final 20 simulations, with the surface, observed concentrations of NO, NO_2 and RHC assumed constant to the lower boundary of Level-3 in the parcel (up to 150-200 m) and assumed to be at the lower default through Levels-4 and 5. The initial concentrations are given in Table 3, along with the defaults assigned in the upper parcel. The method of estimating the individual hydrocarbon class concentrations in ppm based on the reactive hydrocarbon measurement (RHC) in ppmC was revised from the original proposal by ERT (Lurmann et al., 1979). The new method, also used in the first 10 simulations, is:

[Alkanes]	=	0.0786	[RHC]
[Alkenes]	=	0.0328	[RHC]
[Aromatics]	=	0.0248	[RHC]
[Formaldehydes]	=	0.0405	[RHC]
[Other Aldehydes]	=	0.0405	[RHC]

The initial profiles of O_3 were derived by the same method as described in Report I. Initial profiles for CO were derived in a manner similar to that for RHC and NO_x described above. However, the background value for Levels-4

TABLE 3. INITIAL SURFACE CONCENTRATIONS ASSIGNED TO THE PARCEL FOR REACTIVE HYDROCARBON (RHC), NO, CO, O_3, AND INITIAL CONCENTRATIONS ASSIGNED FOR O_3 ALOFT.

Day	RHC (ppm)	NO (ppm)	CO (ppm)	O_3 (ppm)	O_3 Aloft (ppm)
142	0.26	0.03	0.44	0.00[a]	0.06
178	0.19	0.01	0.41	0.00	0.08
182	0.52	0.04	0.73	0.01	0.12
183	0.15	0.01	0.18	0.01	0.12
184	0.39	0.03	0.77	0.01	0.12
207	0.11	0.01	0.27	0.01	0.07
209	0.32	0.02	0.73	0.01	0.08
221	0.14	0.01	0.69	0.02	0.08
230	0.12	0.02	0.50	0.00[a]	0.06
231	0.15	0.01	0.48	0.01	0.06
251	1.28	0.08	2.60	0.00[a]	0.06
159	0.22	0.01	0.86	0.01	0.11
160	0.05[a]	0.01	0.32	0.02	0.11
195	0.05[a]	0.00[a]	0.17	0.03	0.08
211	0.07	0.01	0.13	0.01	0.05
212	0.10	0.01	0.11	0.01	0.11
225	0.05[a]	0.01	0.32	0.04	0.07
226	0.41	0.01	0.97	0.01	0.09
237	1.57	0.06	2.3	0.01	0.11
275	0.70	0.10	2.82	0.01	0.06

[a]Defaults: RHC=0.05, NO=0.0025, O_3=0.0025

and 5 was inadvertently set to a rather high 0.5 ppm. The general effect of this oversight would be to add several tenths of a ppm to the afternoon CO predictions. This should be kept in mind when viewing simulation results, but, since CO has negligible influence on O_3 production, there was little reason to repeat the simulations to adjust for this error.

Expansion of the parcel implies entrainment of surrounding air during a simulation. LPM therefore requires an estimate of the concentrations for side boundary conditions. For RHC, subject to the split given above, the assumed value was 0.063 ppmC. NO and NO_2 were assumed at continental background values. Ozone was set to the observed midday inflow from upwind stations on that day by a procedure described by Shreffler and Evans (1982). This is the same O_3 value given to the upper levels of the parcel in the initial profile and generally varies from 0.06 to 0.12 ppm.

RESULTS

As was done in Report I, the time series results for Days 231, 251, 226 and 275 are presented in this section. In this way the effect of the new initial conditions and parcel expansion can be judged. From the additional set of 10 selected days, Day 237 (1976) time series results are also presented, since high initial loadings of NO_x and HC were observed on that day. Summary statistics are presented on the residual (observed minus predicted) concentrations at the time and position of the observed ozone maxima for all 20 days. Time series for the remaining 15 days and temporal correlation coefficients are presented in Appendix B.

Figure 11a presents a trajectory map for Day 231. This map covers a square 100 km on a side, and only 9 of the stations are shown to avoid cluttering the figure. These stations are (compare Figure 1) 101 in downtown, 122 and 114 to the north, 109 and 123 to the east, 118 and 124 to the south and 120 and 125 to the west. The location of the parcel each hour along the trajectory is indicated. The start position is indicated by "S" and the start time is given above the figure. On Day 231, the parcel starts in a rural locale south of the city. It moves over the high emissions areas at 0800-1100 CST and continues to the northwest. The O_3 maximum was recorded at 1400 CST by station 121.

Figure 11b gives the O_3 concentrations for Day 231. The RAPS observed values are given by a solid line. The model-predicted values at Level-1 (L-1, understood to be the surface) are given by a dotted line, and the Level-3 (L-3, about 300 m in most cases) predictions are given by a dashed line. (The reader is reminded that the time series represent the concentrations within a moving parcel and not at a single point in space).

The results for O_3 do not differ greatly from those for the original test simulation. There is a slight underprediction up to the time of the observed maximum. Beyond that time the prediction greatly exceeds the observation, but, since the parcel is beyond the measurement network, this comparison has little meaning. The predicted NO and NO_2 peaks are diminished somewhat from the original results, reflecting the lower initial loading and parcel expansion. The CO predictions indicate the influx of morning emissions with the L-1 values showing greater peaks. In the afternoon, the model parcel becomes well-mixed, and the decreasing tail reflects the expansion of the parcel (compare with the original test).

The trajectory for Day 251 is given in Figure 12a. The start point is near downtown St. Louis, and initial loading of the parcel with HC and NO is high. Furthermore, winds are very low during the first 4 hours so that the parcel accumulates large quantities of pollutants from emissions. After 1000 CST the parcel moves more rapidly and arrives at station 122 at 1400 CST. The O_3 time series in Figure 12b shows a substantial response to the new initial condition scheme. Ozone shows an initial surge in the morning, but, as the mixed layer rises, the cleaner air aloft is mixed into the system. The predicted peak at 1400 CST is only slightly above the observation. As seen in the original simulation of this day, the L-3 NO, NO_2 and CO predictions do a better job of tracking the observations. The effect of parcel expansion is evident in the tail of the CO predictions.

As seen in Figure 13a, the trajectory for Day 226 moves from the west side of the city to the east, reaching station 109 at 1300 CST. It then turns and moves back into the city towards evening. The O_3 predictions for this simulation must be deemed excellent. They have decreased from those in Report I.

The L-3 predictions for NO, NO_2 and CO are also quite good. As discussed in Report I, the L-1 (surface) predictions of primary pollutants seem to respond in an unrealistic fashion when a new source is abruptly encountered. Use of the L-3 predictions is recommended since they are essentially buffered from the surface sources.

As shown in Figure 14a, the parcel on Day 237 started about 10 km northwest of downtown St. Louis and moved to the west by late afternoon. This day was not treated in Report I, but is highlighted here because it shows the highest RHC and third highest NO initial values over all 20 days. The resulting O_3 predictions show a rapid initial build-up with a dip at time of inversion dissipation. The O_3 predictions are reminiscent of those for Day 251 in this respect. The ozone prediction greatly exceeds the maximum observed. This case again emphasizes the importance of initial conditions. To reiterate, the conditions assume that the average RHC recorded by nearby stations exists through the lower 200 m and over an area 5x5 km (the parcel size). If, for instance, the vertical extent of the RHC accumulation were only to 100 m, the final ozone predictions likely would be much lower. The kind of detailed definition of the initial state needed for precise calculation is unattainable with RAPS data.

The trajectory in Figure 15a indicates that Day 275 was a very calm day. The parcel starts out southwest of the city center and reaches station 102 at 1400 CST. It then moves south and nearly returns to its origin. Two points should be made concerning such calm conditions. First, the trajectory is subject to great uncertainty, and all that is really known is that the air mass was nearly stationary. Second, the LPM point-source module is not designed to function well when the wind speed is so low that the emissions grid (5x5 km) is not traversed in a single hour. The precise impact of this problem is unknown but may be minimal. Ozone predictions are somewhat lower than those in Report I and in better accord with observations. NO, NO_2 and CO_2 predictions are quite similar to those in Report I.

Table 4 presents a summary of the predicted and observed O_3 maxima and a statistical evaluation of the results for the 20 days of the study. The prediction refers to the model prediction at the time and position of the observed O_3 maximum. The residuals, ΔC, are calculated for both the L-1 and L-3 predictions. The average residual for L-1 indicates slight underprediction, while the average residual for L-3 is essentially zero. There would be an inclination to choose the L-3 prediction because of the aforementioned tendency to track the observations more consistently. For both levels, the s.d. (ΔC)'s are identical, and the average absolute deviations are nearly so.

CONCLUSIONS

Compared to results in Report I, the LPM has shown considerable improvement in its predictive capabilities as indicated by reduced s.d. (ΔC). This improvement resulted from implementation of an expanding parcel and changes in the method of loading initial conditions. Both adjustments reduced the gross overpredictions which occurred when initial surface concentrations were high. $\overline{\Delta C}$ has remained encouragingly small throughout the preliminary and final simulations. The variability on a daily basis may arise from input uncertainties (involving winds or initial conditions) rather than underlying model weaknesses.

The LPM has shown promise as an effective tool to understand O_3 production in an urban region. The model is relatively easy to use, inexpensive to execute, and seems immune to various execution errors which tend to arise unexpectedly in complex computations of this sort.

TABLE 4. A SUMMARY OF PREDICTED AND OBSERVED O_3 MAXIMA FROM THE LPM FOR 20 DAYS SELECTED FROM 1975-1976.

Day	Hour	Station	Observed 4-meters (ppm)	LPM Predicted Level-1 (ppm)	LPM Predicted Level-3 (ppm)
142 (1975)	12	101	0.20	0.07	0.13
178	14	112	0.20	0.15	0.31
182	12	125	0.16	0.25	0.24
183	15	124	0.21	0.18	0.18
184	13	118	0.18	0.21	0.22
207	14	113	0.18	0.11	0.13
209	11	118	0.21	0.14	0.15
221	15	121	0.17	0.16	0.16
230	13	121	0.19	0.18	0.17
231	14	121	0.23	0.19	0.19
251	14	122	0.26	0.29	0.30
159 (1976)	15	122	0.20	0.18	0.18
160	16	115	0.22	0.21	0.23
195	15	114	0.22	0.15	0.15
211	15	120	0.16	0.11	0.12
212	12	108	0.17	0.10	0.11
225	13	117	0.17	0.08	0.09
226	13	109	0.23	0.20	0.22
237	11	120	0.18	0.30	0.29
275	14	102	0.24	0.26	0.30

For the data displayed above:

ΔC = Obs minus L-1 Pred

$\overline{\Delta C} = 0.023$

$s.d.(\Delta C) = 0.058$

$\overline{|\Delta C|} = 0.052$

ΔC = Obs minus L-3 Pred

$\overline{\Delta C} = 0.005$

$s.d.(\Delta C) = 0.058$

$\overline{|\Delta C|} = 0.050$

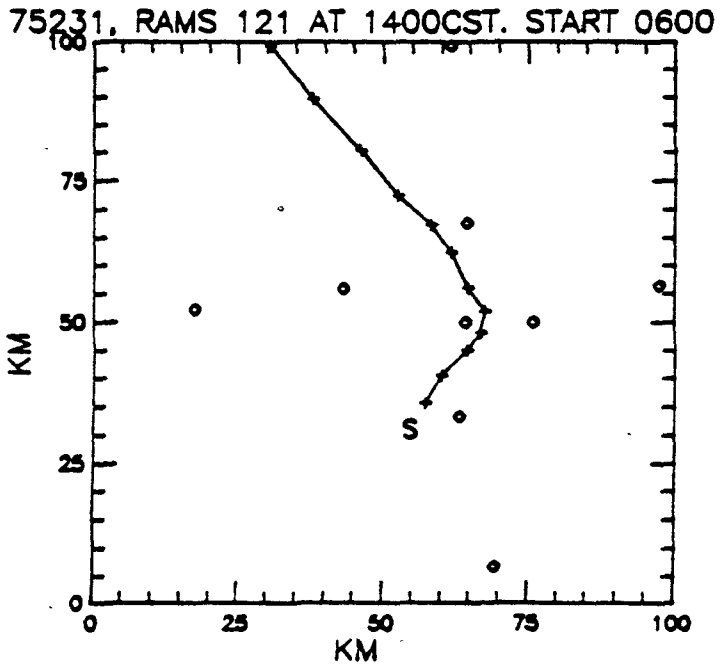

Figure 11a. LPM parcel trajectory for Day 231 of 1975.

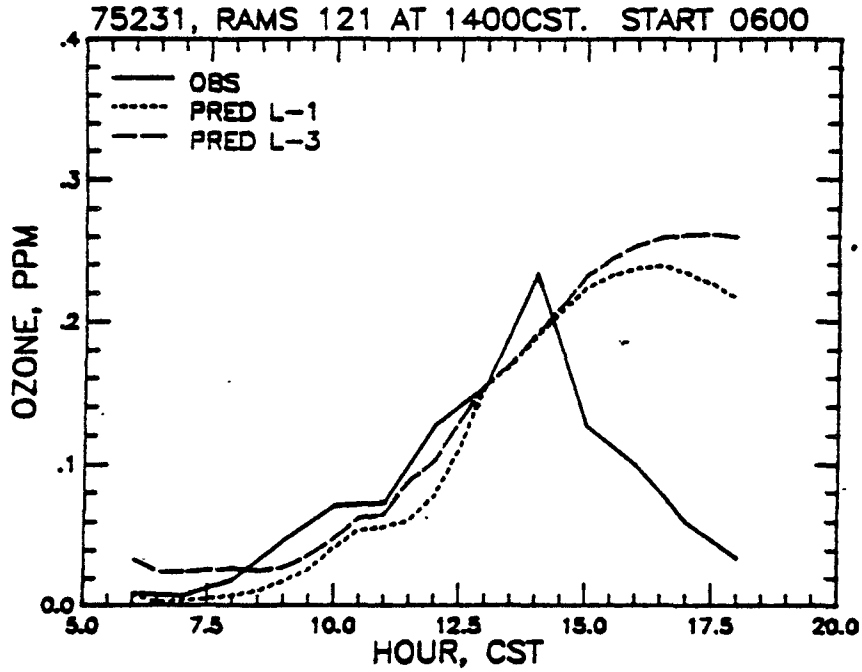

Figure 11b. LPM time series of observed and predicted O_3 hourly concentrations on Day 231 of 1975.

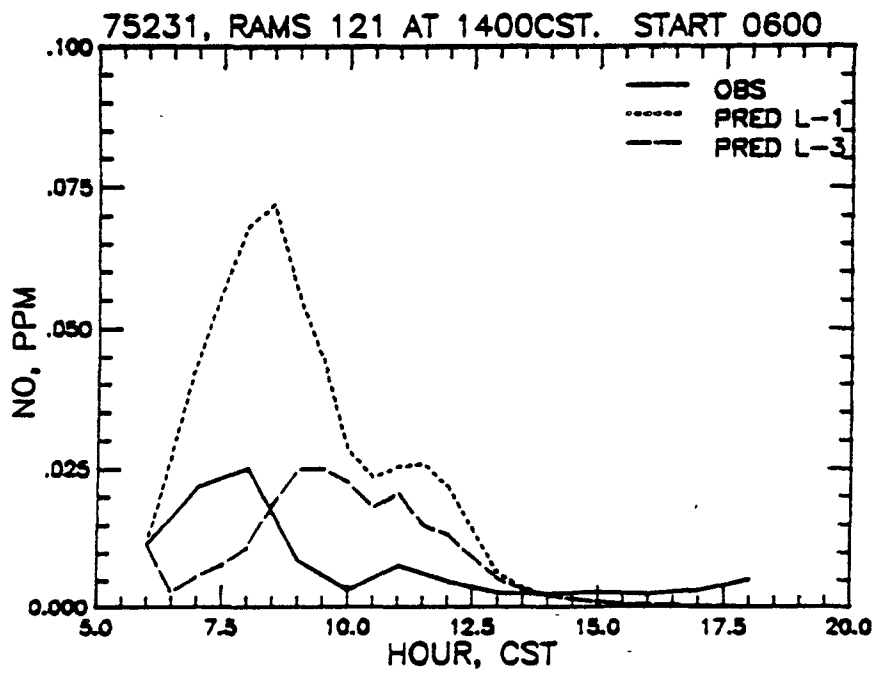

Figure 11c. LPM time series of observed and predicted NO hourly concentrations on Day 231 of 1975.

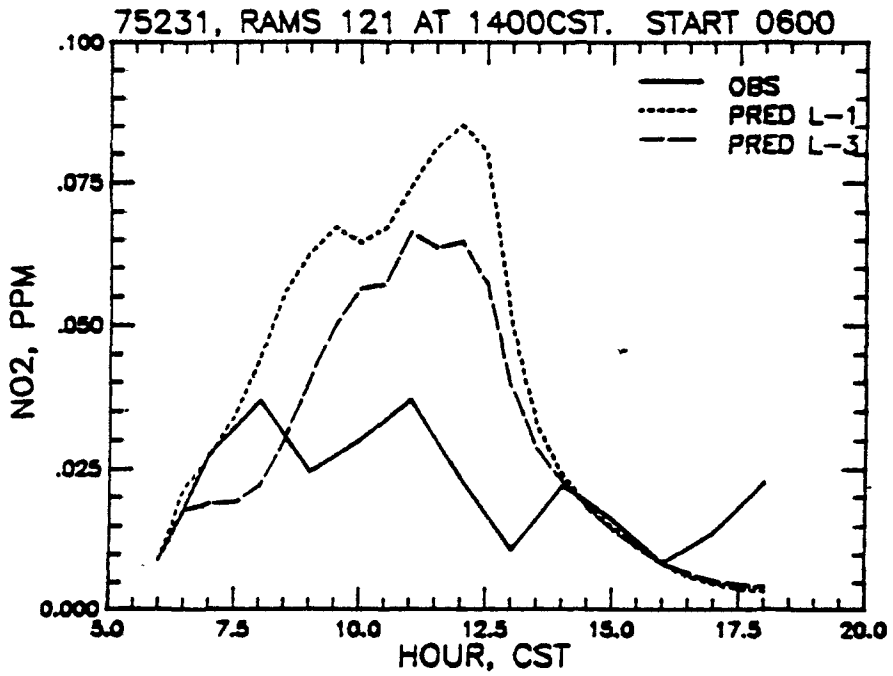

Figure 11d. LPM time series of observed and predicted NO_2 hourly concentrations on Day 231 of 1975.

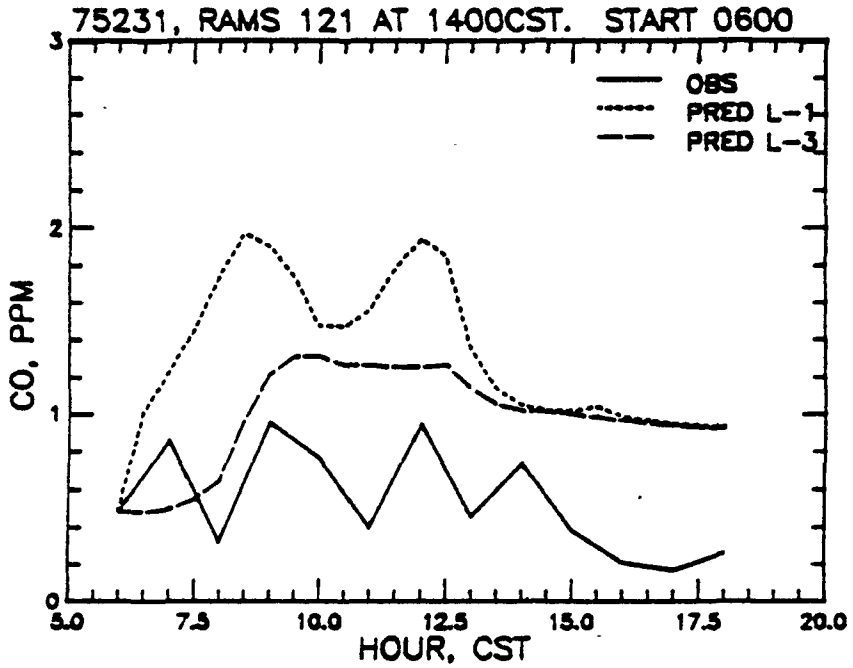

Figure 11e. LPM time series of observed and predicted CO hourly concentrations on Day 231 of 1975.

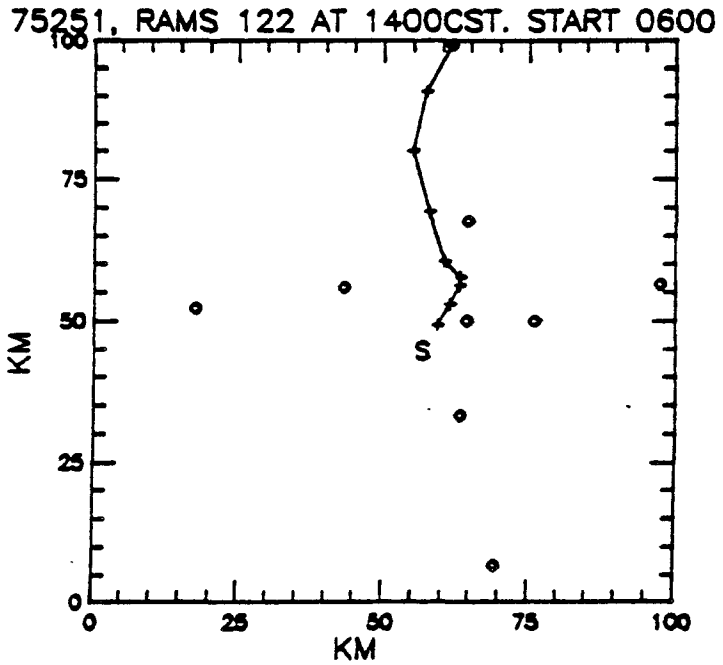

Figure 12a. LPM parcel trajectory for Day 251 of 1975.

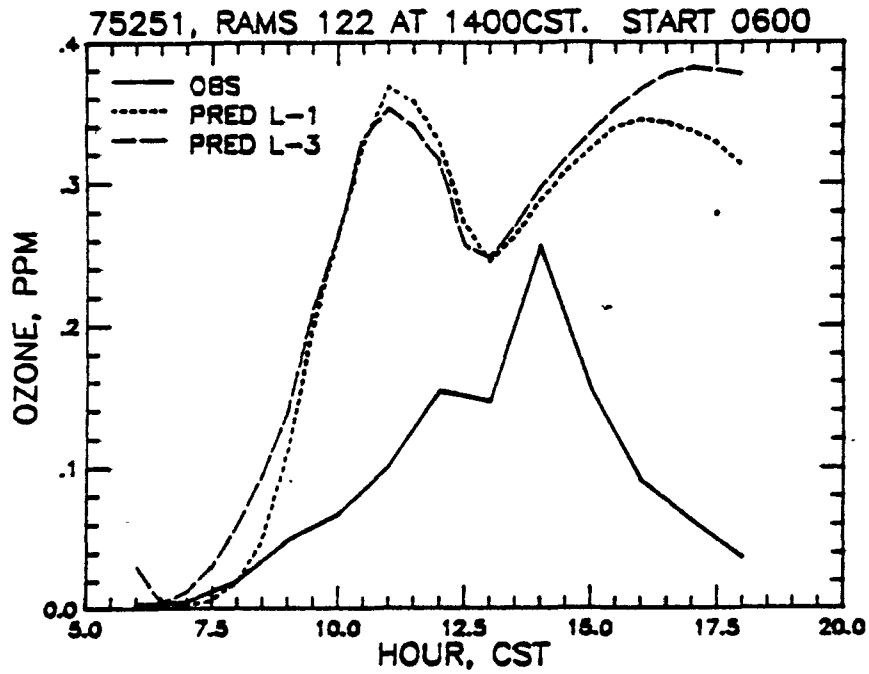

Figure 12b. LPM time series of observed and predicted O_3 hourly concentrations on Day 251 of 1975.

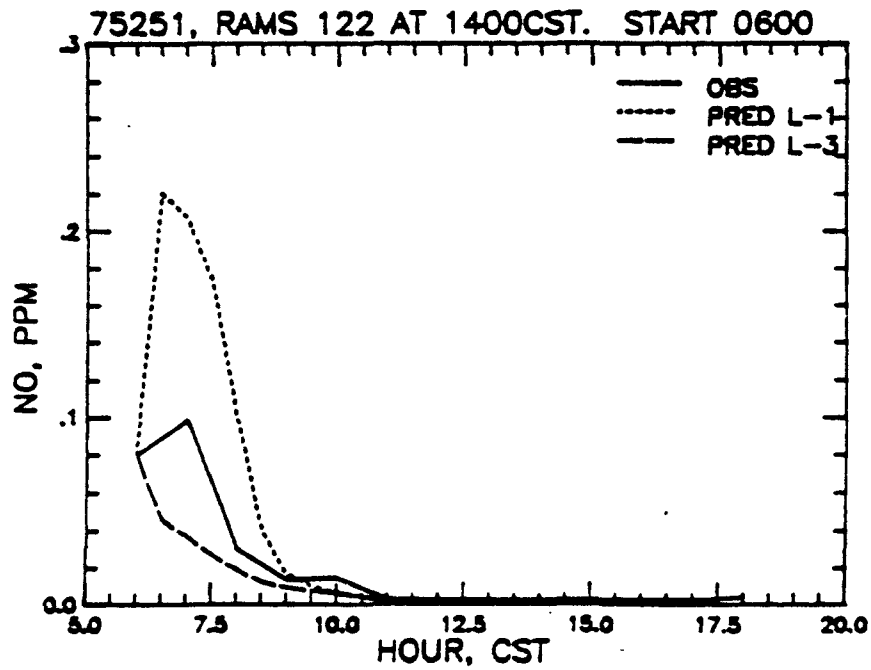

Figure 12c. LPM time series of observed and predicted NO hourly concentrations on Day 251 of 1975.

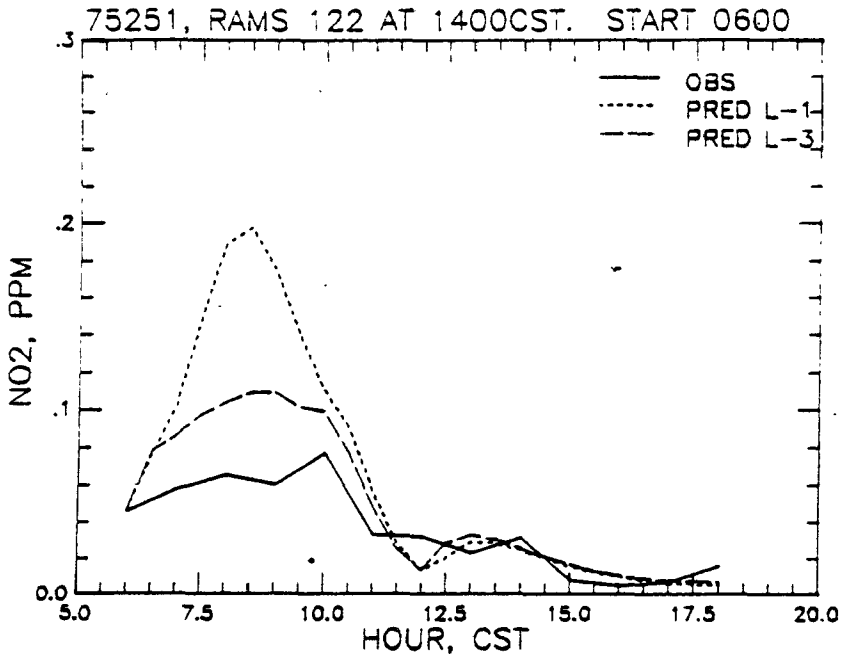

Figure 12d. LPM time series of observed and predicted NO_2 hourly concentrations on Day 251 of 1975.

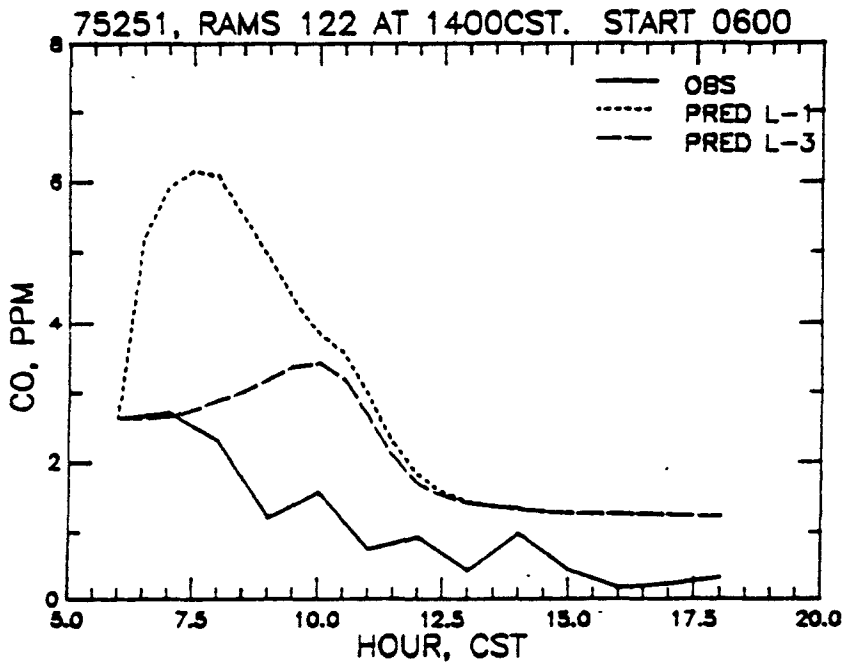

Figure 12e. LPM time series of observed and predicted CO hourly concentrations on Day 251 of 1975.

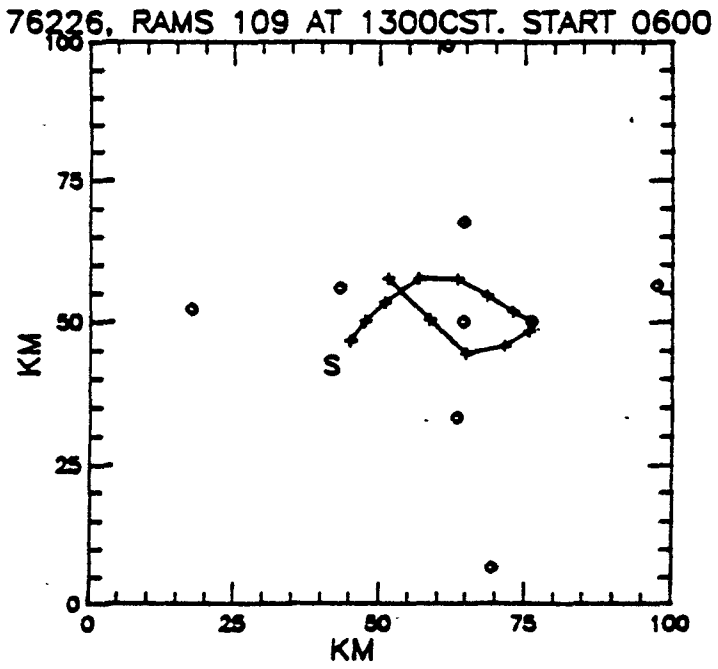

Figure 13a. LPM parcel trajectory for Day 226 of 1976.

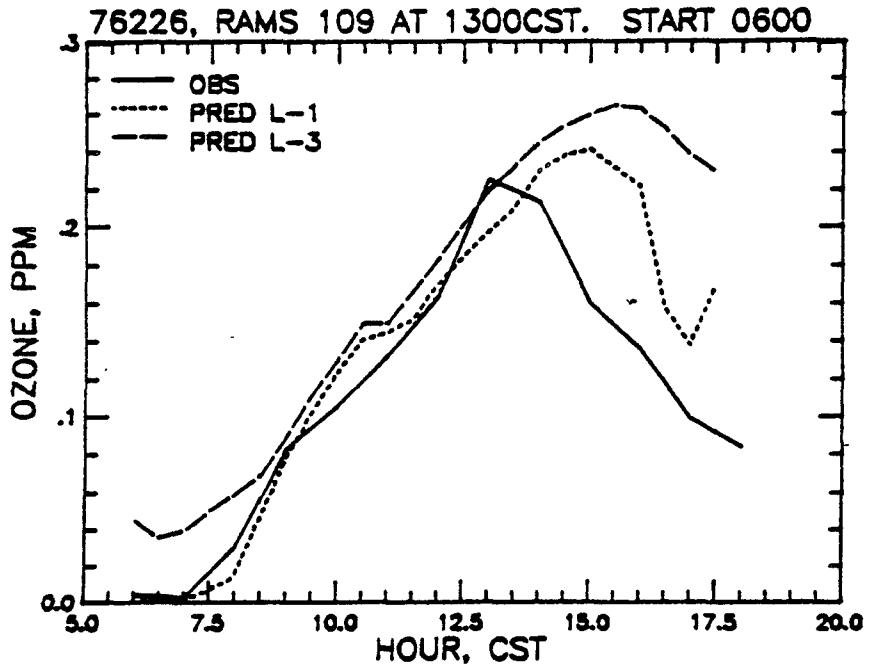

Figure 13b. LPM time series of observed and predicted O_3 hourly concentrations on Day 226 of 1976.

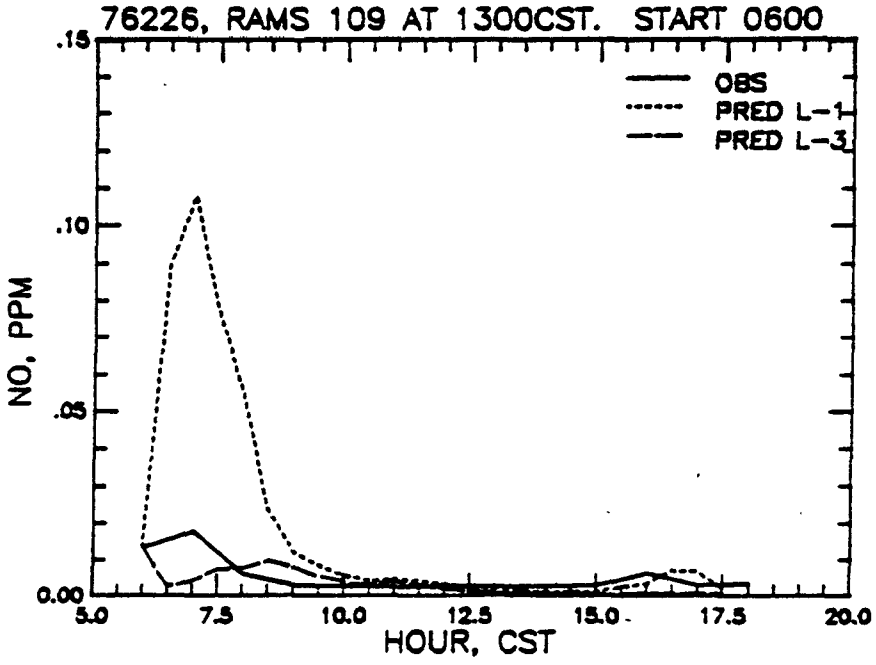

Figure 13c. LPM time series of observed and predicted NO hourly concentrations on Day 226 of 1976.

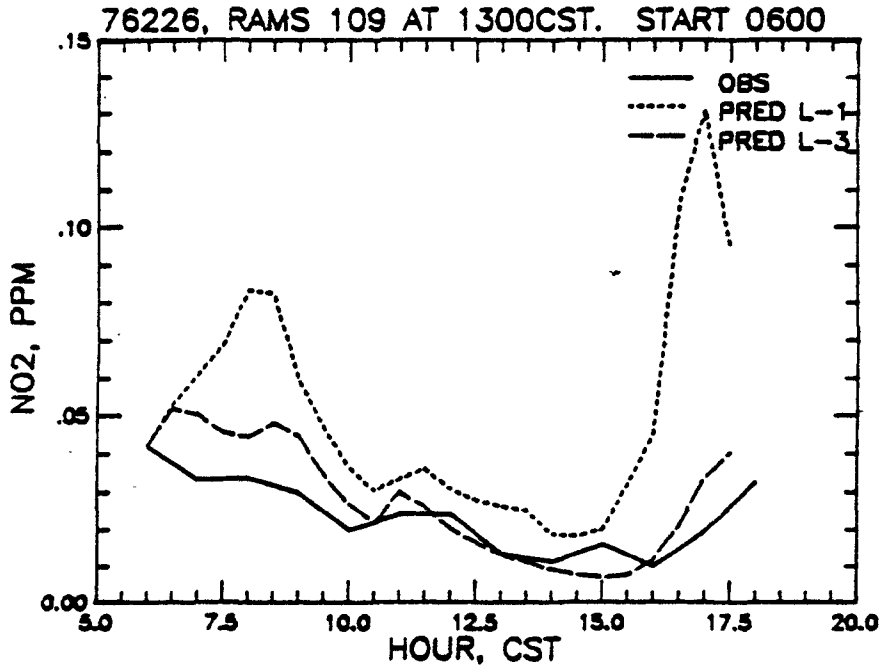

Figure 13d. LPM time series of observed and predicted NO_2 hourly concentrations on Day 226 of 1976.

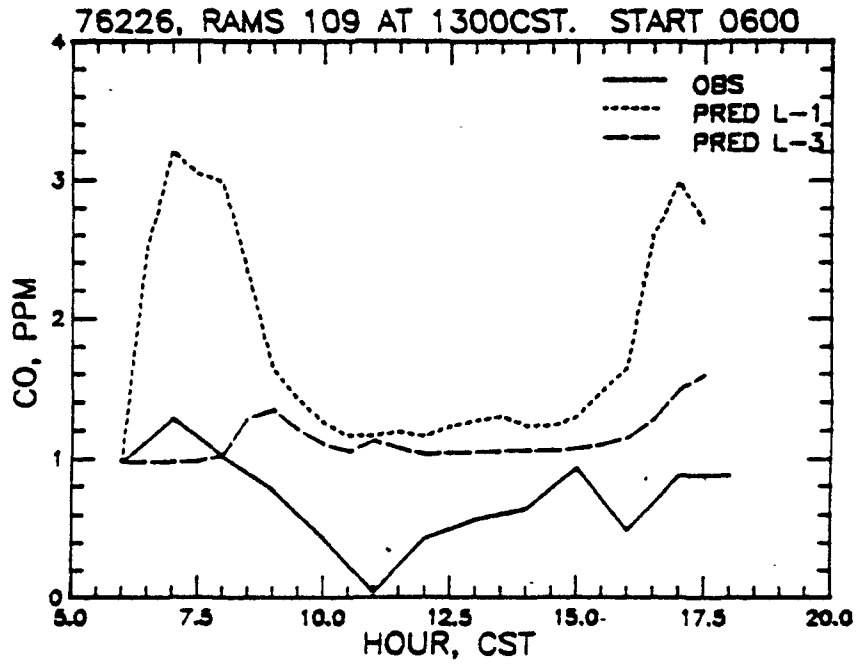

Figure 13e. LPM time series of observed and predicted CO hourly concentrations on Day 226 of 1976.

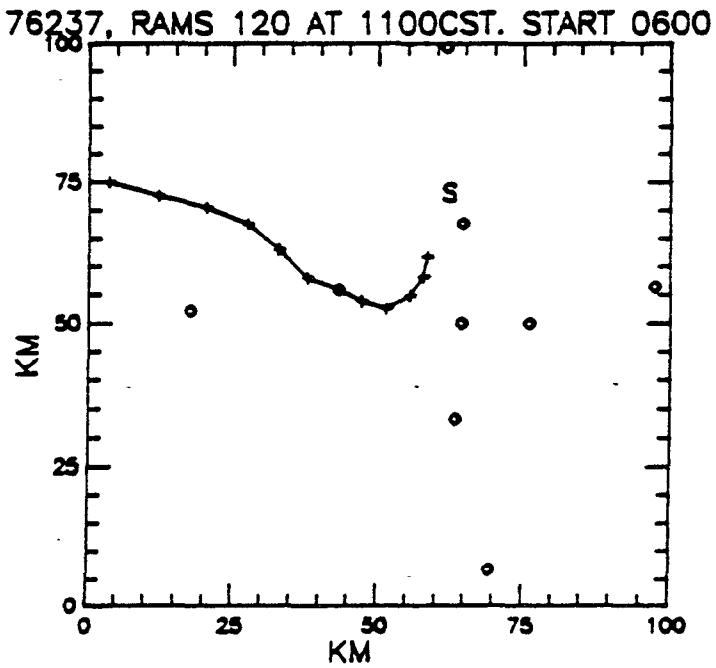

Figure 14a. LPM parcel trajectory for Day 237 of 1976.

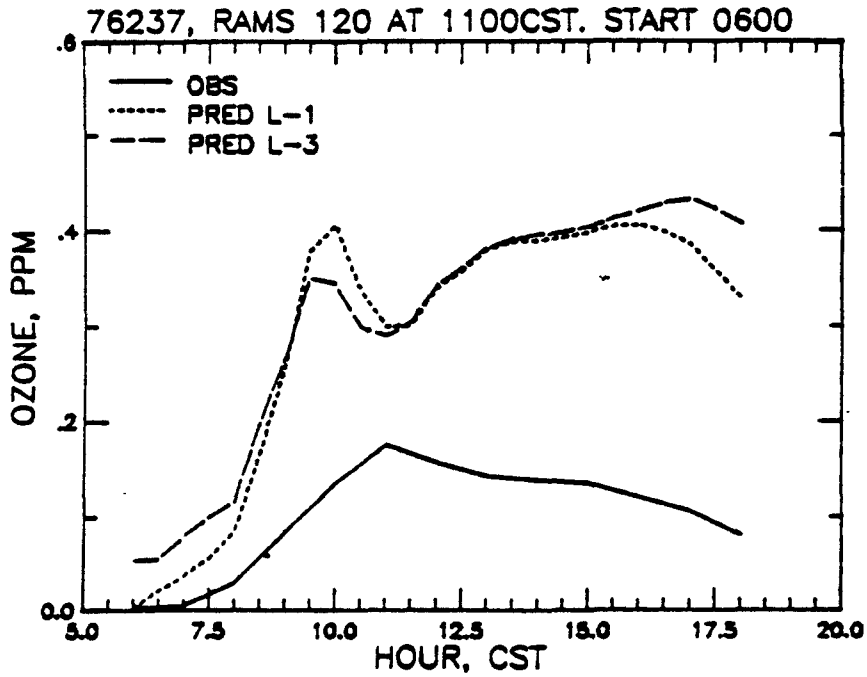

Figure 14b. LPM time series of observed and predicted O_3 hourly concentrations on Day 237 of 1976.

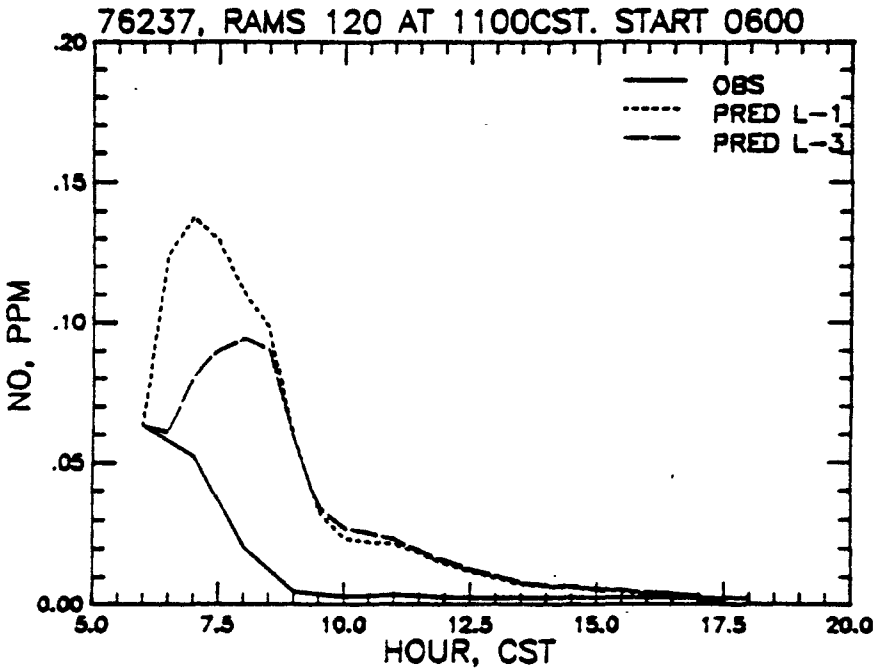

Figure 14c. LPM time series of observed and predicted NO hourly concentrations on Day 237 of 1976.

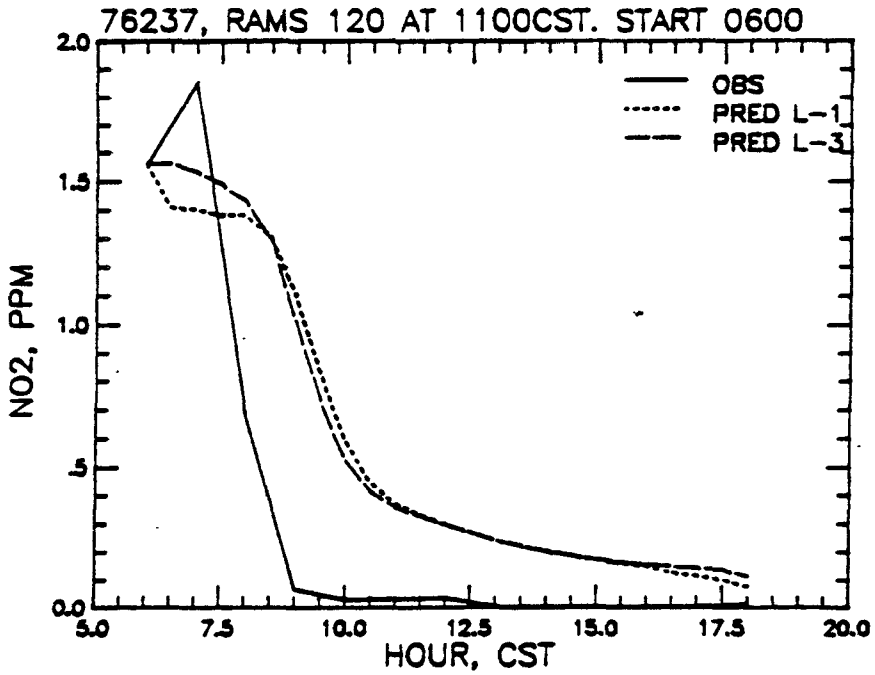

Figure 14d. LPM time series of observed and predicted NO_2 hourly concentrations on Day 237 of 1976.

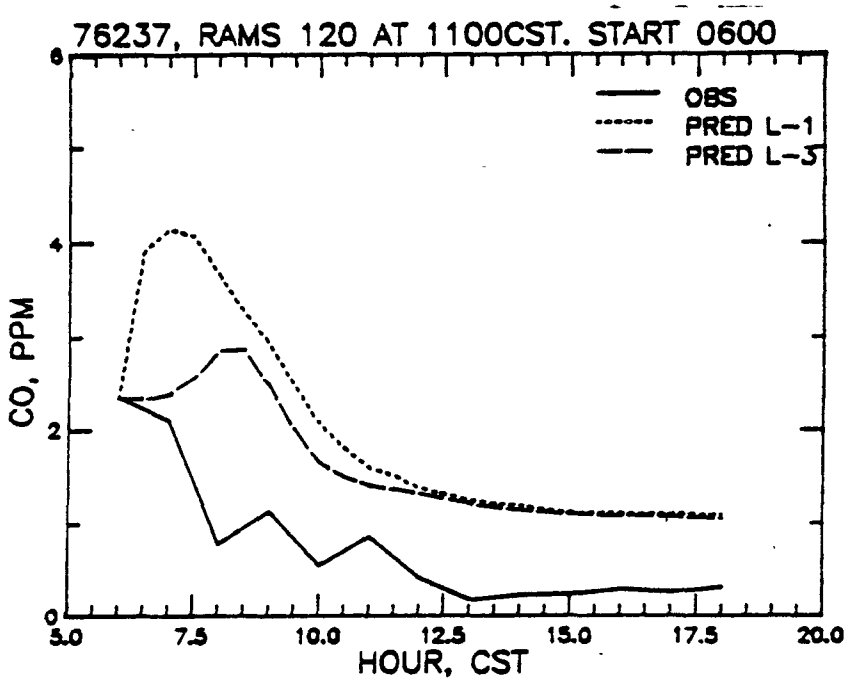

Figure 14e. LPM time series of observed and predicted CO hourly concentrations on Day 237 of 1976.

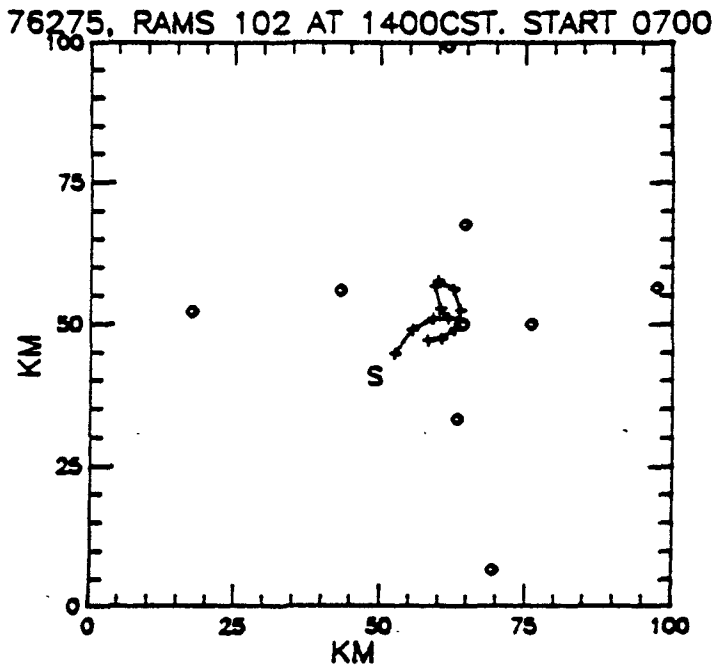

Figure 15a. LPM parcel trajectory for Day 275 of 1976.

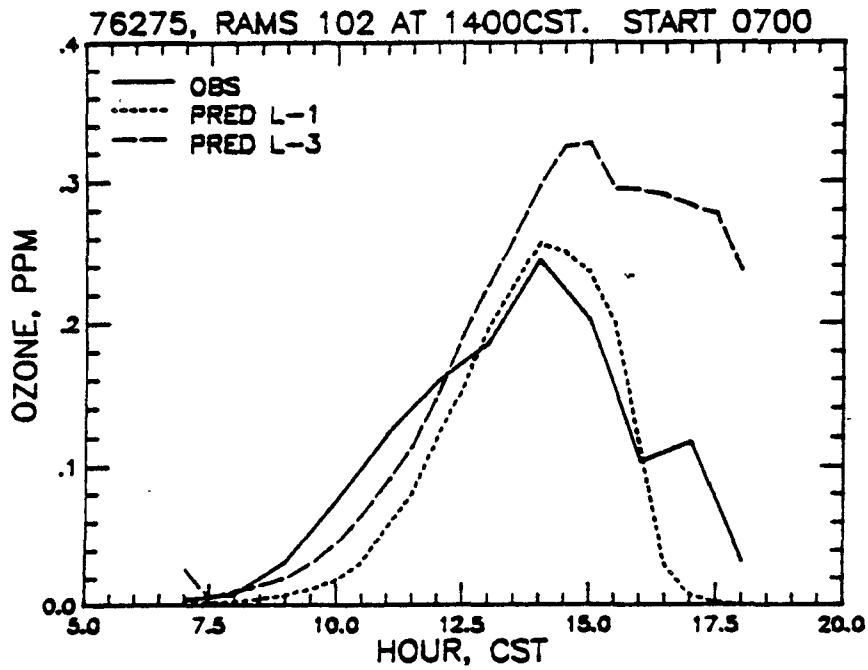

Figure 15b. LPM time series of observed and predicted O_3 hourly concentrations on Day 275 of 1976.

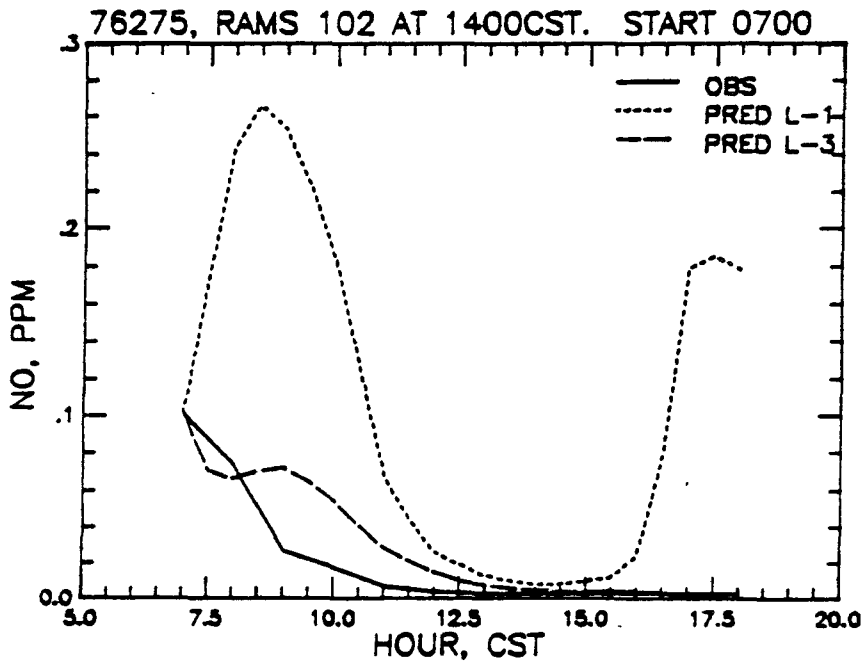

Figure 15c. LPM time series of observed and predicted NO hourly concentrations on Day 275 of 1976.

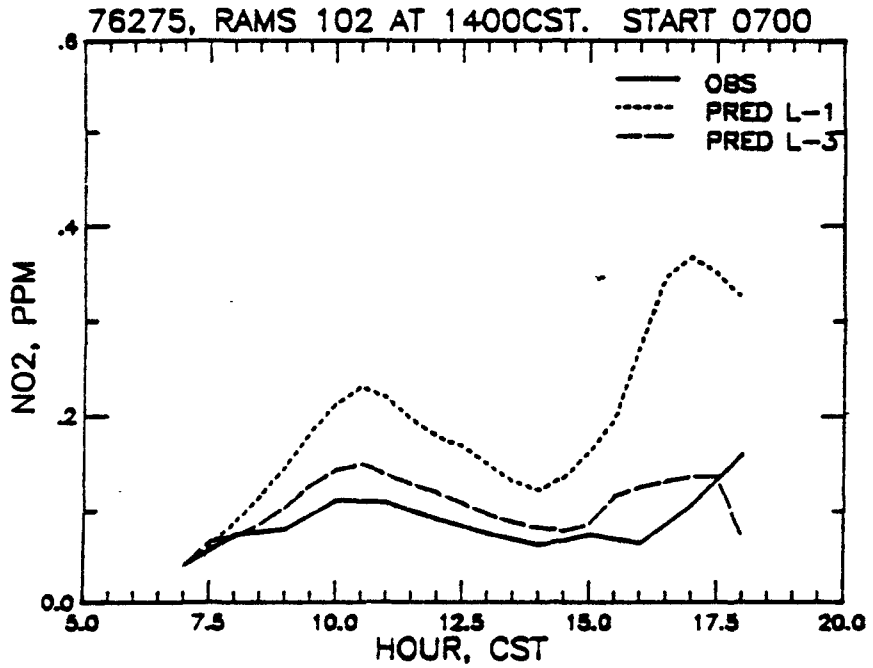

Figure 15d. LPM time series of observed and predicted NO_2 hourly concentrations on Day 275 of 1976.

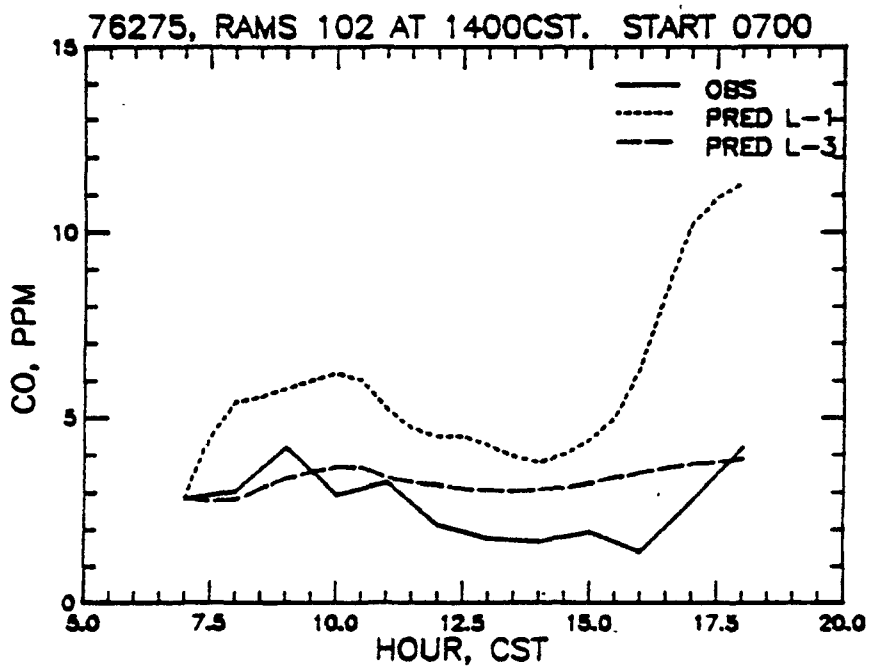

Figure 15e. LPM time series of observed and predicted CO hourly concentrations on Day 275 of 1976.

SECTION 6

URBAN AIRSHED MODEL

INTRODUCTION

The Urban Airshed Model (UAM) is a three-dimensional (3-D), grid-type photochemical air quality simulation model (PAQSM) developed by Systems Applications, Inc. (SAI) of San Rafael, California. The model structure consists of a latticework array of cells, whose total volume represents an urban-scale domain and in which the physical and chemical processes responsible for photochemical smog are mathematically simulated. These include the advection of pollutant species through the modeling domain, the species' entrainment from aloft by a growing mixed layer, diffusion of material from cell to cell, the injection of primary source emissions into the modeled volume, and the chemical transformations of reactive species into intermediate and secondary products. The horizontal dimensions of each cell are constant but cell heights vary throughout a model simulation as mixed layer depth in the UAM changes accordingly.

The area modeled in the St. Louis application was 60 km wide and 80 km long. Individual cells were 4 km on a horizontal side. Vertically, cells totaled 4 layers; the bottom 2 layers simulated the mixed layer and the top 2 represented the region immediately above the mixed layer. The domain of the UAM was centered just west of downtown St. Louis and included the entire metropolitan area. Figure 16 shows a horizontal cross-section of the domain as applied to the RAPS monitoring network. All 25 monitoring station locations are given in relation to the grid pattern. The outer ring contains the boundary cells for the model. Although model simulation does not occur in the boundary cells, they are an important part of the advective transport of the UAM. Four monitoring stations, 122-125, lie outside of the computational domain and are available for determining boundary concentrations. Generally boundary concentrations for all species except O_3 were small, near hemi-

spheric background levels. Ozone levels at the boundary however were sometimes significant compared to those within the model domain. The remaining sites lie within the domain, no 2 residing in the same cell. The 3-D grid model is a sophisticated type of PAQSM and provides both spatially and temporally resolved concentration predictions. Thus, the UAM attempts to estimate the hour-average observed concentration of a pollutant species at each monitoring site within the model domain.

Details of the method for performing a St. Louis simulation with the UAM are described in Report I. There are 12 data preprocessors in the UAM package that must be exercised before the simulation model itself. They access the RAPS data base and retrieve the appropriate parameters required by the UAM. Model simulations begin at 0500 CST and continue through 1700 CST.

The UAM and its preprocessors remain structurally unchanged from the model simulations described in Report I, except for one aspect. An independent test of the numerical advection algorithm was described there and showed that the algorithm in the model at that time produced excess numerical diffusion, a highly undesirable trait for a grid model. A study of the problem revealed that the numerical advection routine in the UAM should be replaced with a sounder method that has the qualities of (1) minimizing the amount of numerical diffusion produced and (2) advecting areas with large concentration gradients such that the gradients are not destroyed. Several advection algorithms were identified and tested as potential candidates for replacing the existing method. The one chosen was a fourth-order version of the multi-dimensional flux-corrected transport algorithms described by Zalesak (1979). This method produced far less numerical diffusion and preserved peak concentration areas better during advection than the algorithm that had resided in the model. An added advantage of the Zalesak algorithm is that the horizontal advection in the model could be performed in one step while the original routine needed a step for each of the x and y directions, another potential source of error. The penalty encountered by changing the numerical advection routine is about a 12% increase in the execution time of the simulation model (on EPA's UNIVAC 1180 computer). The potential for increased accuracy within the model with the new algorithm far outweighs the small increase in overall computational costs.

Model simulations with the revised UAM were conducted for each of the 20 test days listed in Table 1. These test days include the original 10 presented in Report I but are now reflecting the model update described above. Although results for O_3 predictions on all 20 test days are summarized, detailed model results are described for only 4 of these days. Simulation results for the pollutants CO, NO_2 and O_3 on Julian days 142 and 207 of 1975, and 195 and 275 of 1976 are emphasized.

RESULTS

Among the 20 days from the RAPS data base selected for model simulation with the UAM were 4 where the afternoon measured O_3 maximum occurred at one of the monitoring sites located outside the model domain. All other days showed O_3 maxima occurring at sites within the domain. The UAM simulates air quality within each grid cell. Species concentration predictions at particular RAPS monitoring site locations are interpolated from predictions at the closest cells by a distance-weighted (1/r) formula. Detailed simulation results are presented here for 4 of the 20 days modeled, and then summary statistics are given for O_3 alone over all the days.

A UAM simulation provides a wealth of information including the spatial and temporal concentration variations of all modeled species throughout the grid. It is not practical here to display the time series of predicted and observed concentrations for all RAPS sites, even for a few pollutants on a single day of simulation. A more concise method of displaying simulation results is used here. It is based on an analysis of residual concentrations, observed minus predicted, over the 21 RAPS sites within the model domain (Bencala and Seinfeld, 1979). The particular analysis techniques employed here include residual histograms, denoted as "RS", which show the general distribution of residuals for a complete simulation, and the residual vs. observed concentration plot, referred to as the "RO" plot, which demonstrates any trend toward over- or underprediction by the model as a function of observed concentration levels. For a given species on one simulation day, there were 21 sites for each of 13 hours of simulation to account for, or 273 possible data points.

Since this report emphasizes the various models' abilities to estimate O_3 concentrations an additional technique is used for that species to supplement the statistical analysis of the paired observed and predicted data. That technique is the contour plot of observed and predicted O_3 concentrations over the model domain at the hour the maximum O_3 level is observed. These plots reveal the spatial orientation of the peak concentration areas. Visual comparisons can be made that are not dependent on specific paired data. This will help determine if the UAM is predicting the maximum concentration levels well but at incorrect areas of the model domain. It would not be possible to determine this situation from the residual concentration data alone.

The first simulation day discussed is Day 142 of 1975. The synoptic meteorological conditions on this day were described in Section 4. Background O_3 concentrations for Day 142 were 0.06 ppm.

Figure 17a shows the RS for CO on this day. The ideal RS distribution would have a peak at 0.0 ppm and symmetric tails on either side sharply falling off to 0.0 frequency. The figure displays a shape like this except for a bulge in the peak toward overprediction. The RO plot in Figure 17b shows a trend toward underprediction, especially evident in the 3 points corresponding to the highest observed concentrations. Report I discussed the CO underprediction problem for high observed concentrations. The clustering of points in this plot at slightly negative values for very low observed concentrations helps explain the bulge in the RS on the overpredictive side. Both figures are required to provide a total picture of the distribution of the residuals.

The RS for NO_2 is presented in Figure 18a. While the distribution peaks at the 0.0 residual it is slightly skewed toward overpredictions. In the RO plot in Figure 18b the majority of residuals fall to the overpredictive side, but mostly for smaller observed concentrations. At higher concentrations there tend to be more underpredictions. In any case a definite trend would be difficult to discern here for most of the NO_2 residuals fall quite close to 0.0.

Figure 19a displays the RS for O_3 on Day 142. The distribution of residuals here is clearly skewed toward overprediction, with a peak at the 0.0 residual. The RO plot in Figure 19b shows most of the overpredicted concentrations lie in the range of 0.050 to 0.125 ppm observed O_3. At higher observed concentrations no clear trend appears.

The peak hour-average O_3 level observed was 0.195 ppm at site 101 at noon. The model-simulated concentration for the same time and location was 0.116 ppm, a 40.5% underprediction. Figure 20 presents the contours of O_3 concentration for the model-predicted and observed cases for the hour beginning at noon CST. In the model-predicted case the contours have been objectively drawn based on the 300 regularly spaced grid values for the lowest layer of cells in the UAM. For the observed case the contours are based on the 25 irregularly spaced monitoring locations, 4 of which lie outside of the model domain. Here the objective algorithm responsible for generating the contours works best toward the center of the domain where the density of sites, represented in the figure by small crosses, is greatest. The credibility of the contours near the edges is not as high, especially in terms of the extent of the area circumscribed by a given contour. In the figure for Day 142 the maximum concentration areas appear near the center of the domain with magnitudes close to each other. In the model-predicted case the highest valued contour is displaced slightly northwest of the observed maximum area and a relative "valley" has developed in the immediate area of the observed maximum, allowing the large underprediction to occur.

On Day 207-75 a large high-pressure center was located northeast of St. Louis with light winds both at the surface and aloft. Measured wind speeds were generally less than 1.0 m s^{-1} near the surface and directions were variable. Sunny skies prevailed through the duration of the modeling period, although haze persisted during the day. Background O_3 concentrations were approximately 0.07 ppm.

Figure 21a shows the RS for CO on Day 207. The distribution is nearly symmetric about the 0.0 residual with a few outliers on the underpredictive side. The RO plot in Figure 21b reveals these outliers as the residuals

corresponding to the highest observed concentrations. Most CO concentrations on this day were less than 1 ppm. Nitrogen dioxide presents a broader histogram than CO in Figure 22a that is symmetric and centered slightly on the overpredictive side. This bias is probably caused by the great many overpredictions at observed NO_2 concentrations less than 0.02 ppm seen in Figure 22b. Aside from this phenomenon there is no clear trend apparent in the RO plot. The RS for ozone in Figure 23a presents a histogram with the rough outline of a normal distribution but contains periodic gaps throughout. The majority of the predictions are less than the observed concentrations and the RO plot in Figure 23b demonstrates that a definite bias exists toward underpredicting O_3 as observed concentrations increase.

The maximum hour-average O_3 measurement for Day 207 occurred at 1400 CST at site 113, northwest of downtown St. Louis, at 0.185 ppm. The corresponding simulated concentration for this location was 0.141 ppm, a 23.8% underprediction. The contours of observed O_3 concentrations at this hour in Figure 24b reveal a steep gradient aligned from the northwest to the southeast through the city of St. Louis. The predicted concentration field in Figure 24a shows a similar gradient but displaced slightly north and west. The alignment and magnitude of the contours are, in fact, very much alike in the 2 cases. Possible errors in the model's treatment of the wind field, or the generation of the wind field itself, may have contributed to the displacement between the peak areas of predicted and observed concentrations and allowed the apparent underpredictions by the model at the monitoring sites.

The synoptic meteorological situation for Day 195 of 1976 contained an upper air ridge over the center of the country with a warm front northeast of St. Louis. Winds near the surface were from the southeast during the day averaging just over 2.0 m s^{-1}. Skies were mostly clear with occasional high level cloudiness. Background O_3 concentrations were nearly 0.08 ppm.

CO concentrations were low on this day, mostly less than 1 ppm. The RS for CO for Day 195 is presented in Figure 25a. It shows a narrow distribution of residuals peaking slightly on the overpredictive side. In the RO plot in Figure 25b this peak has been translated to the many very low observed concen-

trations often near the detectable limits of the monitoring instruments. At higher concentrations the model tends to underpredict, especially at the 2 distinct data points representing CO hot spots. The NO_2 residual distribution shown in Figure 26a displays a normal symmetric shape about the 0.0 residual. Most of the overpredictions occur at low observed NO_2 concentrations and a trend toward more severe underprediction with increasing observed NO_2 is apparent from the RO plot in Figure 26b. The RS for ozone in Figure 27a is skewed toward underpredictions. Below an observed O_3 level of 0.1 ppm the RO plot in Figure 27b shows little bias in the residuals. Above this level there is a clear trend toward underpredicting at higher observed concentrations. This explains the skewness in the histogram as resulting from the residuals of observations mostly greater than 0.1 ppm.

The highest hour-average O_3 measurement on Day 195 was at site 114 at 1500 CST, north of the city of St. Louis, at 0.223 ppm. The UAM estimated an O_3 concentration of 0.160 ppm at the same time and place, an underprediction of 28.3%. The contours of O_3 predictions and observations for this hour are shown in Figure 28. Agreement in the alignment and location of the contours between the 2 cases is good, although the magnitude of the maximum predicted contour is considerably less than that of the observed. The advection problem discussed in Report I for Day 195 appears to have been corrected here with the substitution of the new advection algorithm.

Day 275 of 1976 is typical of an extreme stagnation episode in St. Louis. The synoptic meteorological conditions on this day were described in Section 4. Background concentrations of O_3 were about 0.06 ppm.

The histogram of residuals for CO is shown in Figure 29a for Day 275. The distribution peaks slightly on the overpredictive side of the 0.0 residual although there is a pronounced skewness toward underpredictions, including several extreme cases. The RO plot in Figure 29b displays the trend toward underprediction of CO at higher observed concentrations. The extreme stability of the atmosphere on the morning of Day 275 is reflected in the highest CO concentrations, on the order of 10 ppm, over twice the level of the observed peak on most of the other modeled days.

The RS for NO_2 in Figure 30a is normally distributed about the 0.0 residual and the RO plot in Figure 30b shows little bias with increasing concentrations for observed NO_2 levels of 0.125 ppm and less. Beyond this point there is evidence of consistent underprediction. The O_3 residual analysis in Figures 31a and b indicates good model performance in the overall predictions for the day. The residual histogram has a broad normal distribution about the 0.0 residual and the RO plot demonstrates no clear trends toward over- or underprediction.

The peak O_3 measurement on Day 275 was 0.244 ppm at site 102, near downtown St. Louis, at 1400 CST. The model prediction for this time and location was 0.220 ppm, a 9.8% underprediction. The contour plots of predicted and observed O_3 concentration for this hour are shown in Figures 32a and b. In both cases the highest concentrations appear near the center of the model domain and are of comparable magnitude. Several pockets of reduced O_3 concentrations appear in the pattern of predicted contours that break up an otherwise consistent pattern with the observations. These appear to be in the vicinity of large NO_x emissions sources that have an exaggerated scavenging effect on nearby O_3 predictions. The observations do not substantiate this effect. The rather simplistic treatment of point source emissions by the UAM is probably a major factor in this problem.

Table 5 summarizes the predicted and observed O_3 maxima and an elementary statistical analysis of the UAM results for all 20 modeled days. The "specific" model predictions correspond to the same location and time as the observed maximum, and the "independent" predictions represent the maximum hour-average O_3 generated by the model in any cell of the lowest grid layer at any time during the simulation. The independent maximum is the greatest surface value the model can produce within its domain. The specific and independent predictions, as seen in Table 5, typically do not coincide. This indicates that the maximum O_3 value produced by the model did not correspond either in space or time, or both, to the maximum value observed in the atmosphere. Statistics on the residual concentration, ΔC, as shown in Table 5, were computed for both the specific and independent predictions. The average residual and standard deviation are also presented for the analysis. Values

TABLE 5. A SUMMARY OF PREDICTED AND OBSERVED O_3 MAXIMA FOR THE UAM

Julian date[a]	Hour (CST)	Station	Observed at 4-meters (ppm)	UAM Predicted Specific (ppm)	UAM Predicted Independent (ppm)
142 (1975)	12	101	0.195	0.116	0.238
178	14	112	0.202	0.156	0.243
182	11	121[b]	0.142	0.083	0.166
183	10	119[b]	0.171	0.154	0.209
184	13	118	0.184	0.132	0.234
207	14	113	0.185	0.141	0.252
209	11	118	0.209	0.128	0.195
221	15	121	0.166	0.118	0.149
230	13	121	0.193	0.095	0.214
231	14	121	0.233	0.133	0.205
251	12	121[b]	0.179	0.146	0.178
159 (1976)	14	114[b]	0.172	0.142	0.312
160	16	115	0.221	0.121	0.190
195	15	114	0.223	0.160	0.174
211	15	120	0.155	0.143	0.169
212	12	108	0.170	0.128	0.155
225	13	117	0.166	0.050	0.073
226	13	109	0.225	0.077	0.124
237	11	120	0.176	0.119	0.203
275	14	102	0.244	0.220	0.246

[a]Twenty days selected from 1975 and 1976.
[b]Overall maximum at 122,123,124, or 125; outside UAM domain.

For the data displayed above:

ΔC = Obs - Specific

$\overline{\Delta C}$ = 0.062

s.d.(ΔC) = 0.035

$\overline{|\Delta C|}$ = 0.062

ΔC = Obs - Independent

$\overline{\Delta C}$ = -0.006

s.d.(ΔC) = 0.053

$\overline{|\Delta C|}$ = 0.041

for the average residual for the specific and independent cases, 0.062 and -0.006 ppm respectively, differ noticeably. The independent predictions show more promise toward maximum O_3 simulation. The average absolute residual is much larger than the average signed residual in the independent case, indicating both over- and underpredictions among the 20 days tested. In the specific case however, the average signed and absolute residuals are identical, signifying that the model has underpredicted consistently over all 20 days. The standard deviations of the specific and independent residuals are 0.035 and 0.053 ppm respectively. The model's average performance for maximum O_3 over all simulations shows a 32.4% underprediction in the specific case and a 4.4% overprediction for the independent.

Table 6 shows a least-squares simple linear regression analysis for all specific O_3 predictions for all simulation hours on each test day at all RAPS sites in the model domain. The correlation coefficient here represents an integrated spatial and temporal measure of model performance. Overall the correlations are quite good. However only 4 of the 20 computed slopes fall between 0.8 and 1.0 with the rest less than 0.8, pointing out that the model generally under-predicts specific simulation results for O_3. Intercepts should ideally be close to 0.0, and 12 of them lie in the range of -0.01 to +0.03 ppm, with the remainder somewhat higher, in the range +0.03 to +0.06 ppm. The sum of squared error term is a relative measure of the variance about the calculated line of regression.

The analyses presented in Tables 5 and 6 are not intended to give a complete picture of UAM performance. Rather, they present 2 aspects of O_3 prediction over a variety of days chosen from the RAPS data base. Ozone on some of the days, such as Day 142, was simulated much better than on others. Using the UAM in a regulatory capacity demands knowledge of the performance potential in specific types of worst-case situations. A summary of other statistical measures of model performance over the 20 test days appears in Appendices D, E and F.

TABLE 6. A SUMMARY OF LEAST SQUARES REGRESSION STATISTICS FOR UAM PREDICTED AND OBSERVED O_3[a]

URBAN AIRSHED MODEL: O_3				
Julian date[b]	Correlation coefficient	Slope	Intercept (ppm)	Sum of squared error (ppm^2)
142-75	0.805	0.887	-0.0057	0.186
178-75	0.864	0.867	0.0183	0.186
182-75	0.875	0.610	0.0263	0.142
183-75	0.864	0.614	0.0284	0.193
184-75	0.726	0.470	0.0436	0.317
207-75	0.927	0.654	0.0373	0.173
209-75	0.759	0.570	0.0347	0.192
221-75	0.795	0.516	0.0433	0.268
230-75	0.819	0.729	0.0059	0.095
231-75	0.814	0.645	0.0176	0.152
251-75	0.821	0.618	0.0232	0.150
159-76	0.859	0.862	0.0021	0.158
160-76	0.937	0.676	0.0464	0.247
195-76	0.947	0.720	0.0296	0.112
211-76	0.833	0.773	0.0010	0.104
212-76	0.912	0.632	0.0244	0.189
225-76	0.753	0.310	0.0504	0.247
226-76	0.796	0.426	0.0574	0.445
237-76	0.687	0.432	0.0581	0.383
275-76	0.844	0.896	-0.0004	0.340

[a]Includes observations and predictions for all times and locations.
[b]Twenty days selected from 1975 and 1976.

CONCLUSIONS

The potential use of a grid-type PAQSM, such as the UAM, clearly is great, although model complexity often makes the solution of problems which arise more difficult. Trouble-shooting and test application exercises have taken place over the past 3 years at EPA after the adaptation of the UAM to St. Louis by SAI. The constituent components of the model have already been investigated and upgraded where necessary. The numerical advection routine was recently replaced by one with less inherent pseudo-diffusion.

The model evaluation discussed here has pointed toward some of the strengths and weaknesses of the UAM. In studying the results for the 3 pollutant species focused on in this report it is clear that while the model typically produces a normal distribution of residuals in a simulation, those estimates corresponding to the highest observed concentrations are often underpredicted. This is especially true of primary species such as CO and NO_2, but has also been indicated in the case of O_3 as well. It is these higher observed concentrations that are of greatest interest from a regulatory perspective. For the case of those species emitted from and affected by emissions from point sources, their simulated performance results may improve with a more physically realistic treatment of point emission sources.

It is quite interesting to note that the average of independent residuals for O_3 maxima over the 20 test days indicates an almost exact match between predictions and observations. Studying the contour maps on the test days reveals that the model usually produces O_3 levels as high or higher than those observed and the contours of predicted and observed often have similar shapes. However, the variance in these residuals of the 20 O_3 maxima is quite large and this is caused, in part, by the different spatial orientations of the predicted and observed contours. Indeed, even the paired predictions and observations typically show poor spatial correlation. This is particularly true for O_3. The spatial alignment of the concentration fields is principally governed through transport in the model. The treatment of winds in the UAM is comparable to most schemes available today for interpolating a wind field across a grid (Schere, 1981). However, even in a relatively simple flow

situation such as St. Louis, problems can arise. An error of only a few degrees in wind direction can lead to gross errors in specific air quality predictions. It will be a major responsibility of any UAM user to substantiate that the wind processor is providing a credible simulation of wind flow in the application area. For complex topographic situations or land-sea interactions within a model domain, a wind field analysis unique to that application may be required.

In summary, the UAM is a powerful tool available for use by the air quality analyst already experienced in working with complex simulation models. Model results should be carefully studied in each application and may not necessarily be used in an absolute sense in any given simulation. An area of future study that may be pursued is model sensitivity to variations in selected parameters, such as initial and boundary conditions, emissions, wind fields and solar radiation.

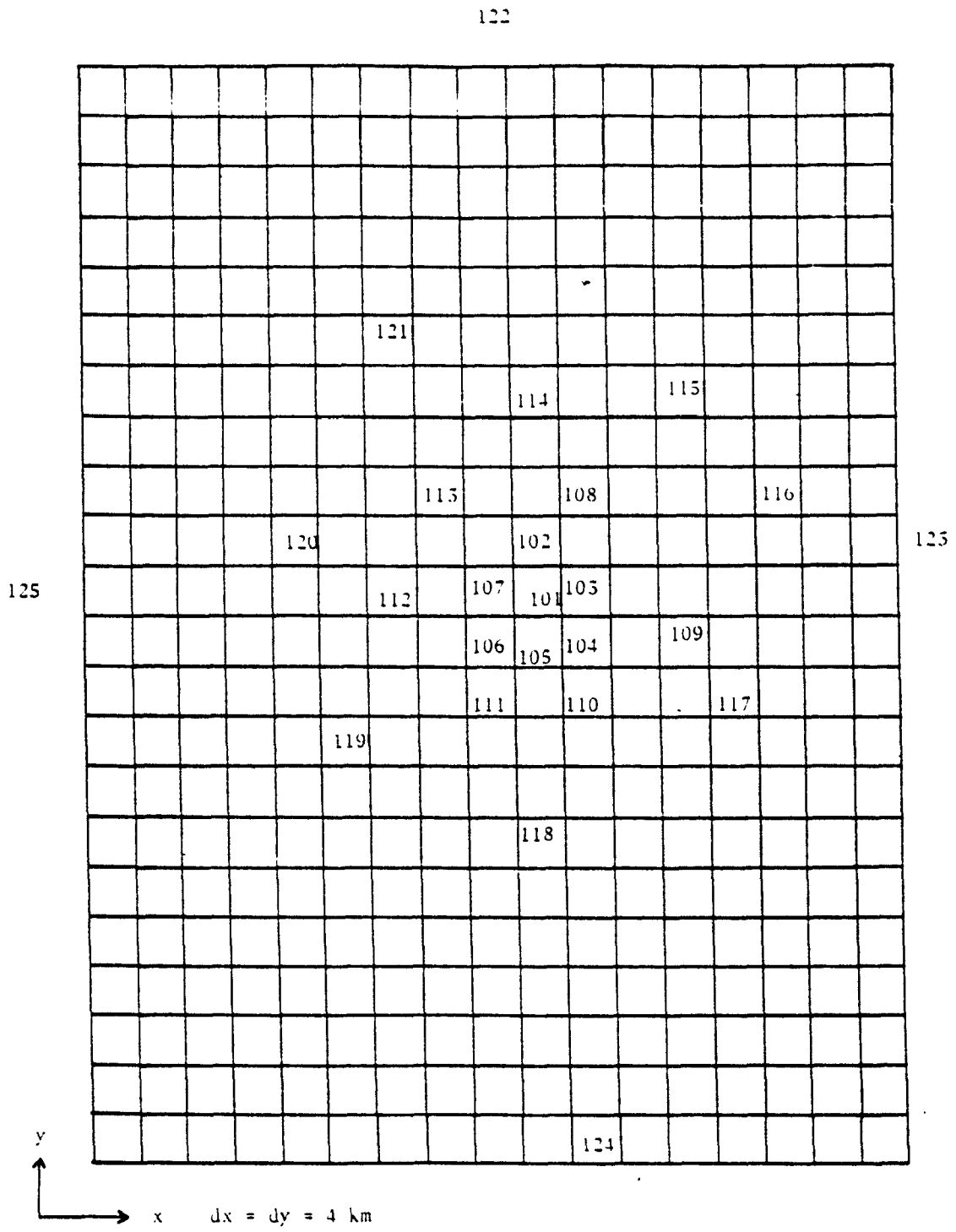

Figure 16. Schematic drawing of horizontal section of UAM domain showing locations of RAPS monitoring sites.

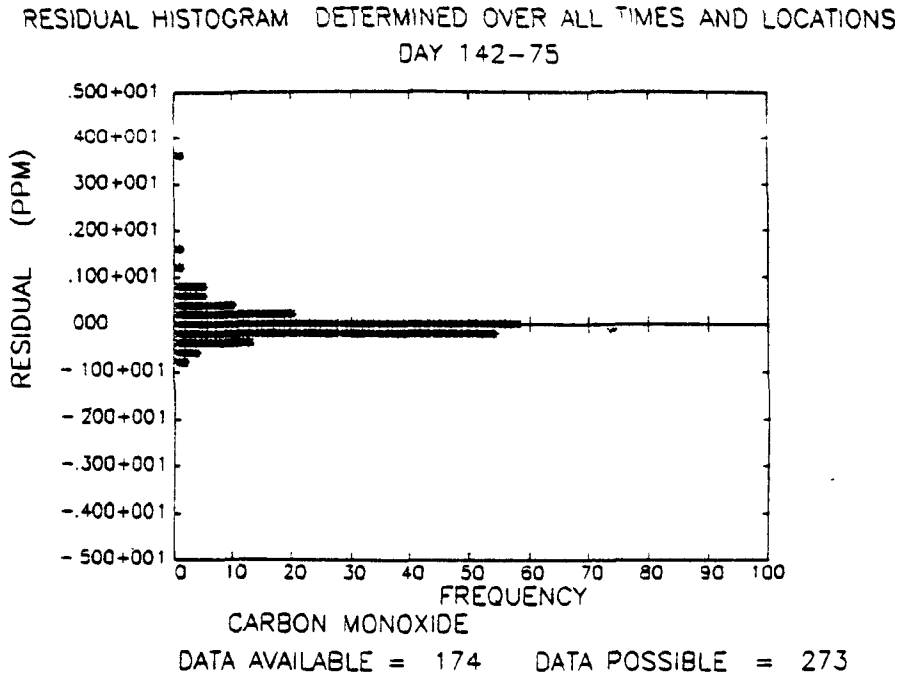

Figure 17a. Residual histogram for CO from the UAM simulation results for Day 142-75.

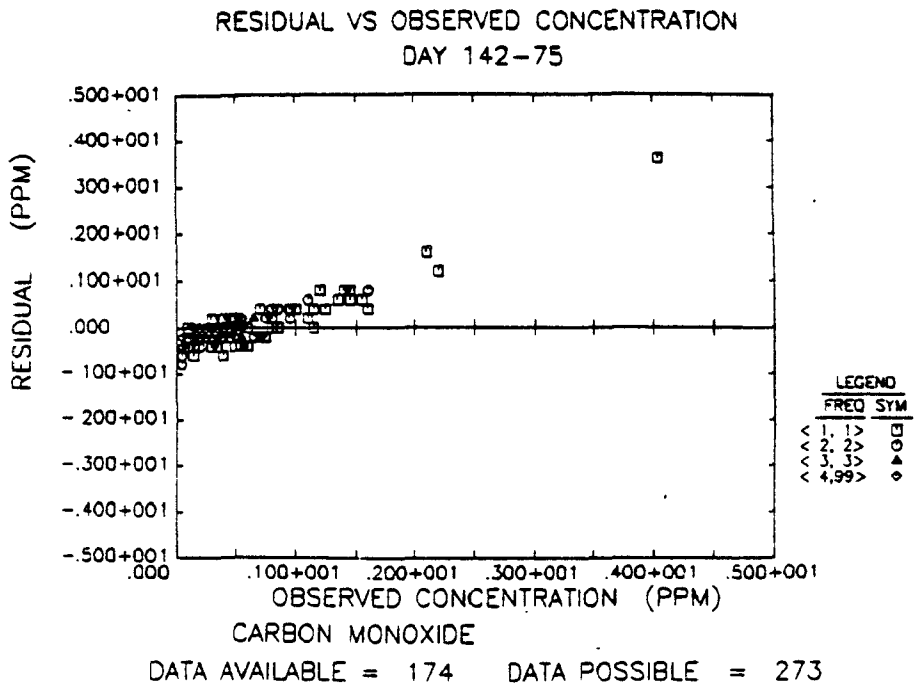

Figure 17b. Residual vs. observed plot for CO from the UAM simulation results for Day 142-75.

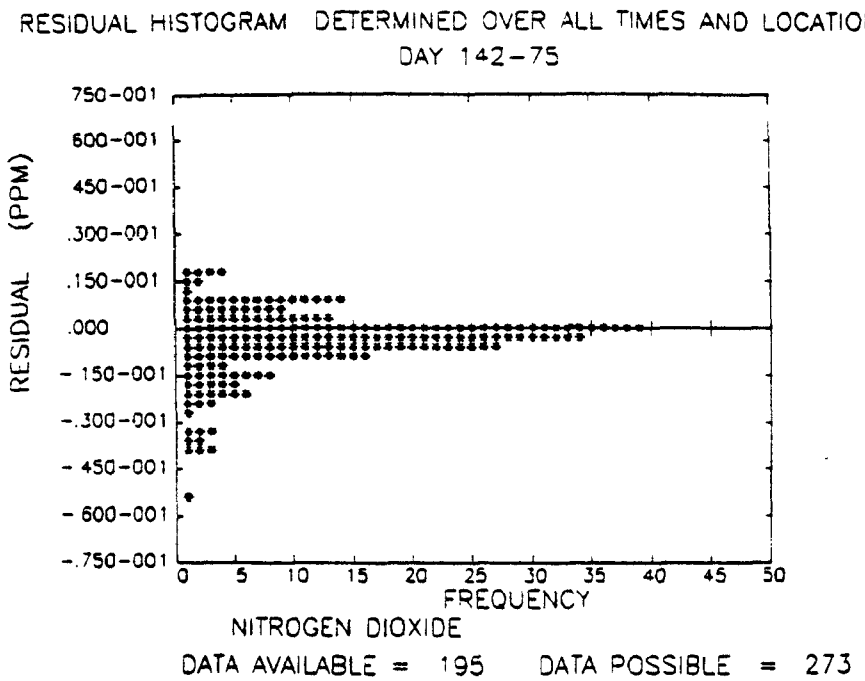

Figure 18a. Residual histogram for NO_2 from the UAM simulation results for Day 142-75.

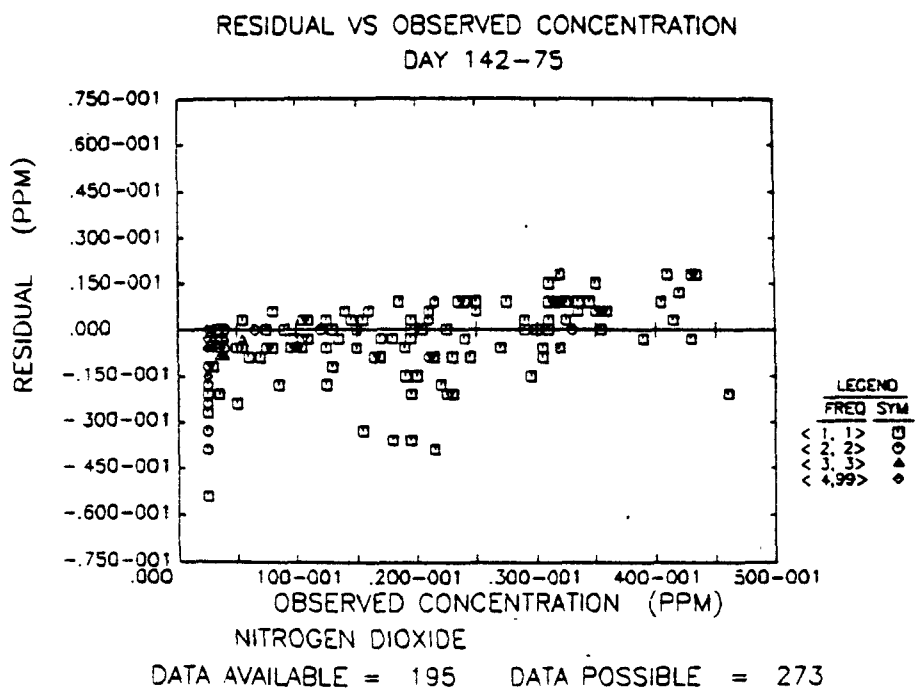

Figure 18b. Residual vs. observed plot for NO_2 from the UAM simulation results for Day 142-75.

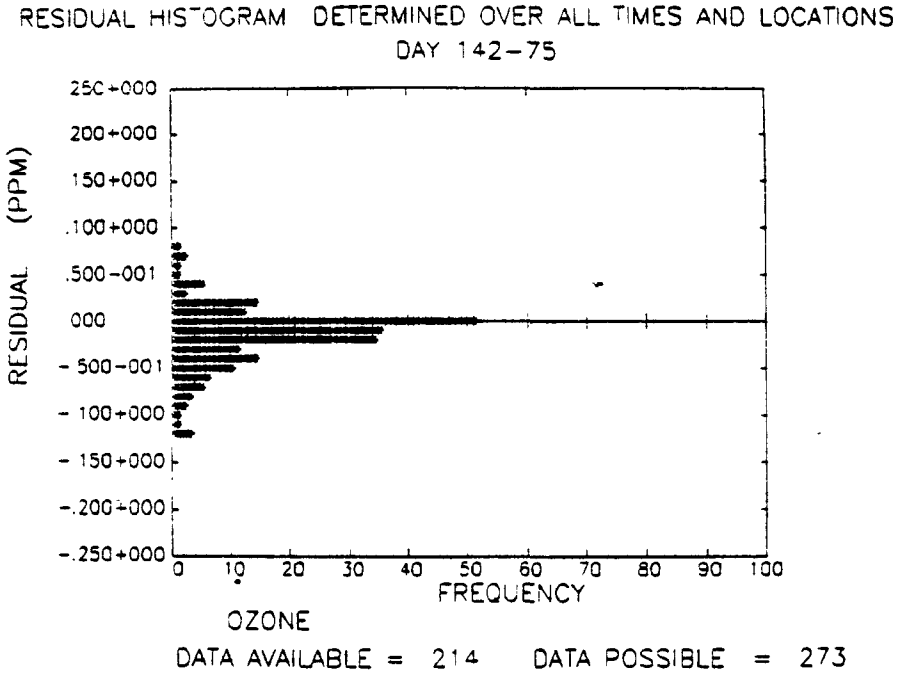

Figure 19a. Residual histogram for O_3 from the UAM simulation results for Day 142-75.

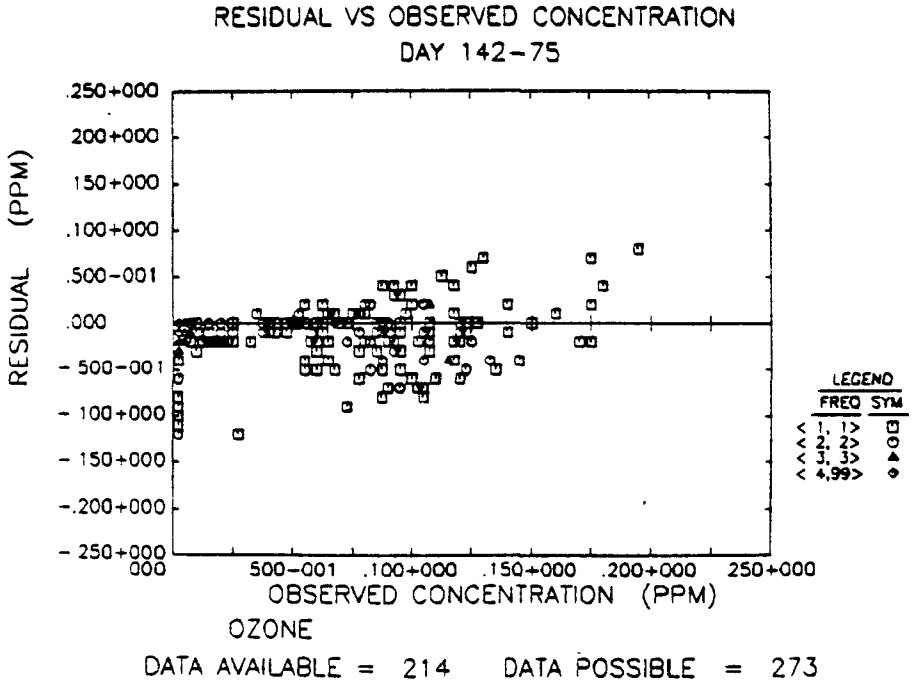

Figure 19b. Residual vs. observed plot for O_3 from the UAM simulation results for Day 142-75.

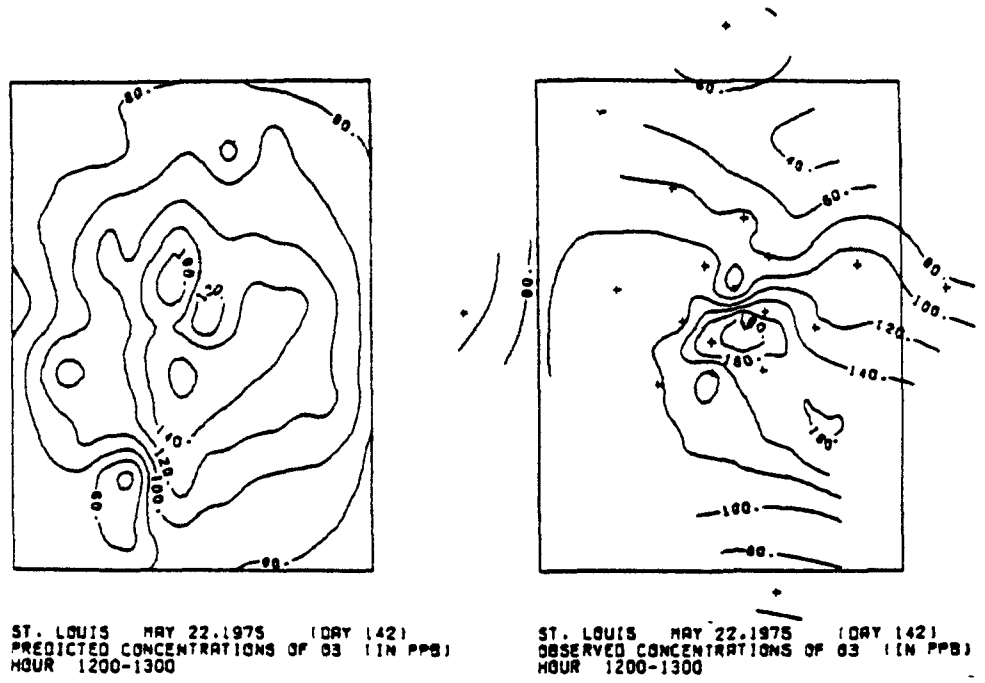

(a) (b)

Figure 20. Contours of (a) predicted and (b) observed fields of O_3 at hour of observed maximum on Day 142-75.

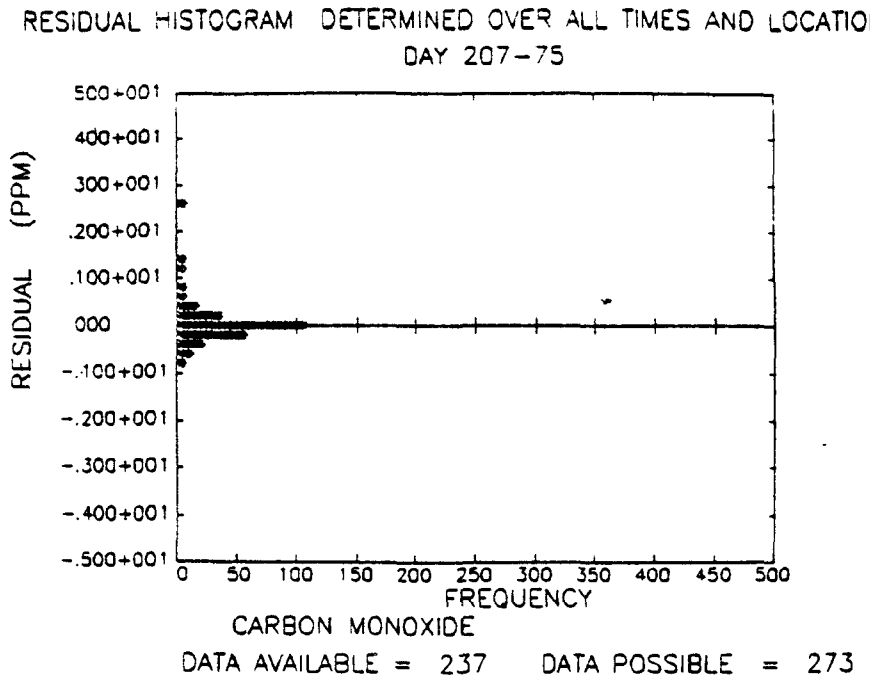

Figure 21a. Residual histogram for CO from the UAM simulation results for Day 207-75.

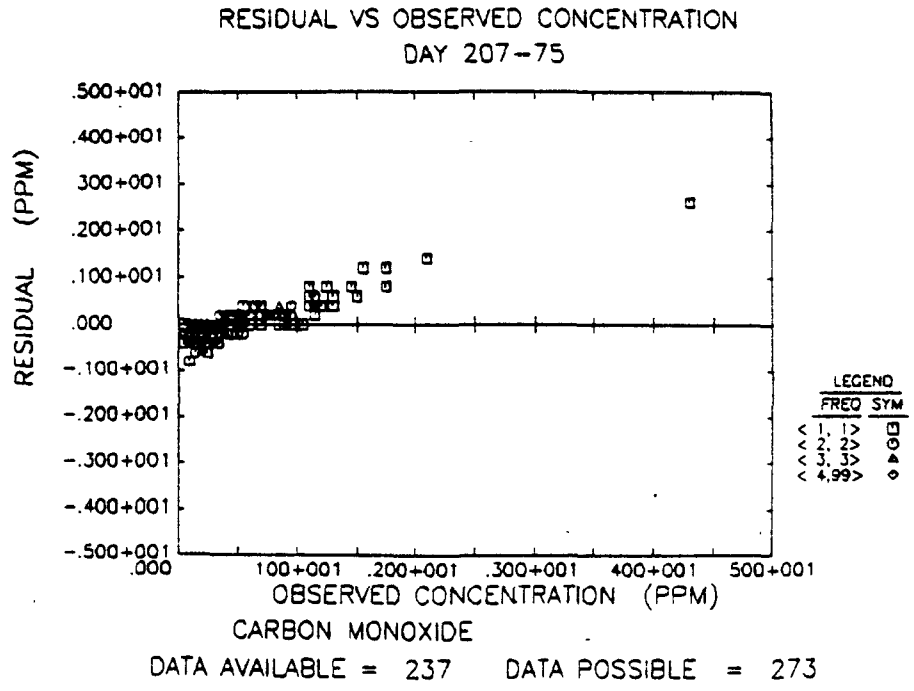

Figure 21b. Residual vs. observed plot for CO from the UAM simulation results for Day 207-75.

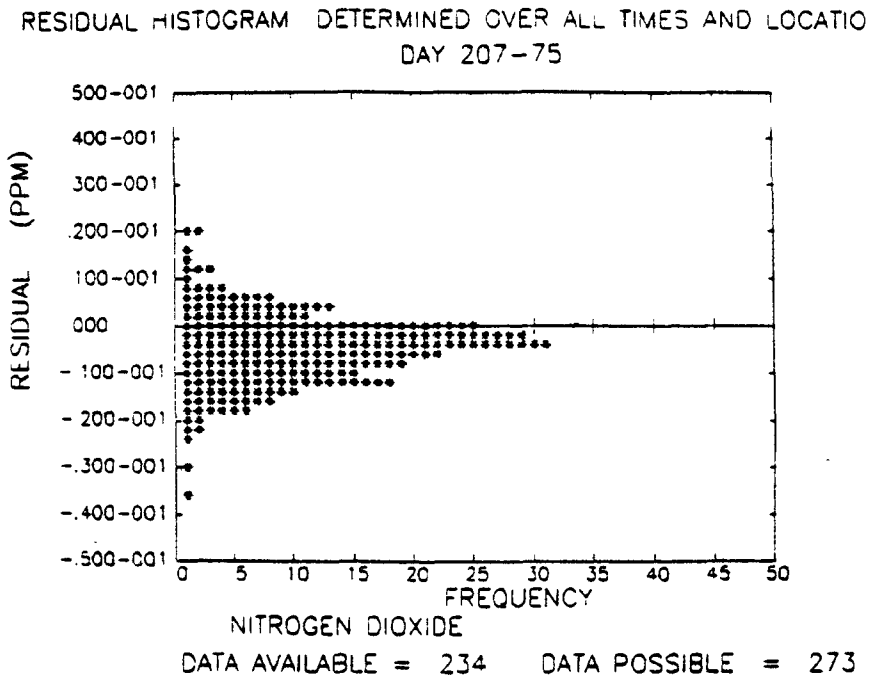

Figure 22a. Residual histogram for NO_2 from the UAM simulation results for Day 207-75.

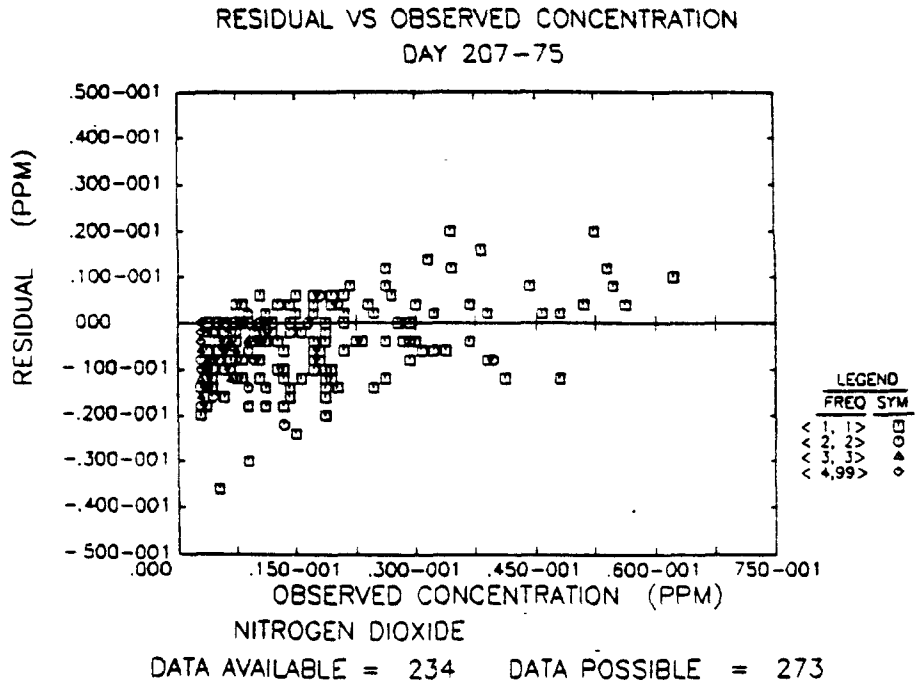

Figure 22b. Residual vs. observed plot for NO_2 from the UAM simulation results for Day 207-75.

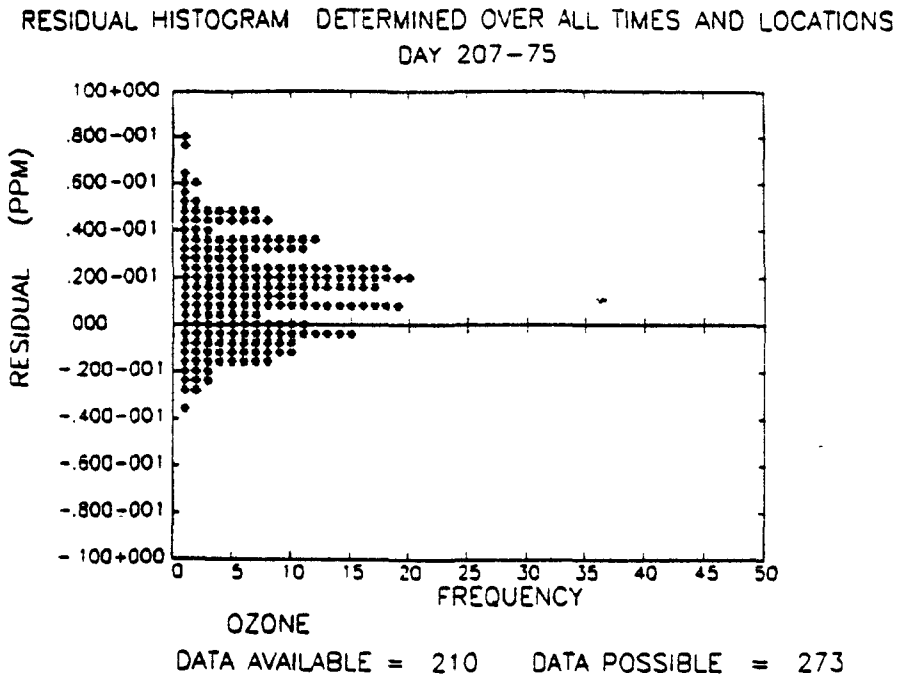

Figure 23a. Residual histogram for O_3 from the UAM simulation results for Day 207-75.

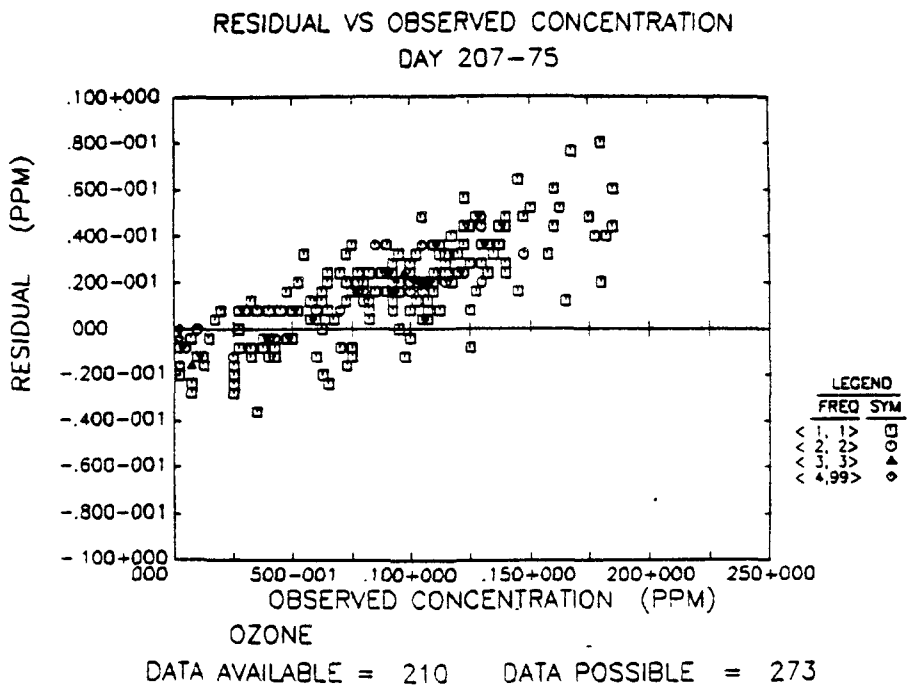

Figure 23b. Residual vs. observed plot for O_3 from the UAM simulation results for Day 207-75.

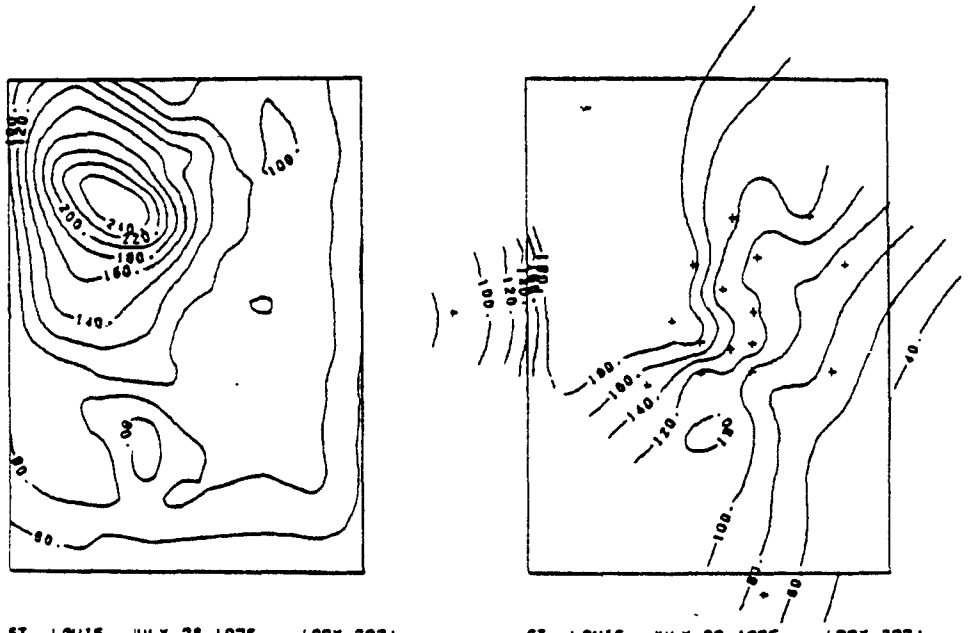

(a) (b)

Figure 24. Contours of (a) predicted and (b) observed fields of O_3 at hour of observed maximum on Day 207-75.

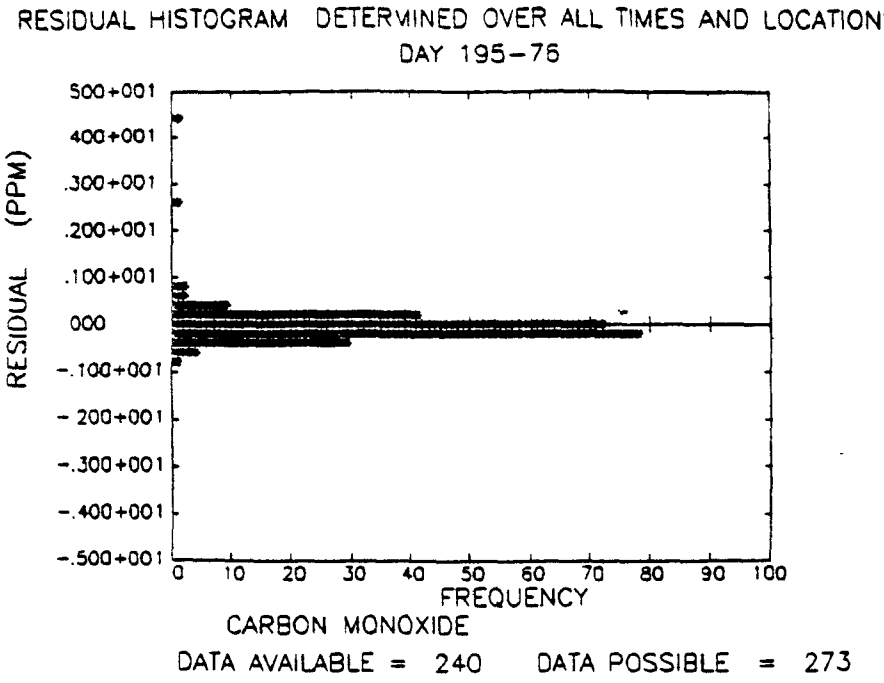

Figure 25a. Residual histogram for CO from the UAM simulation results for Day 195-76.

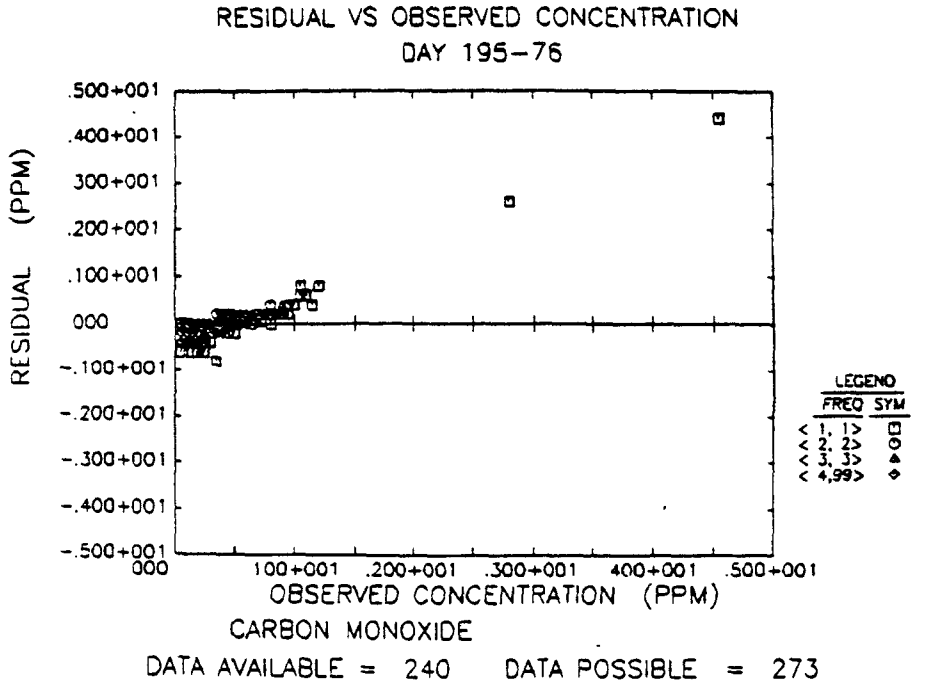

Figure 25b. Residual vs. observed plot for CO from the UAM simulation results for Day 195-76.

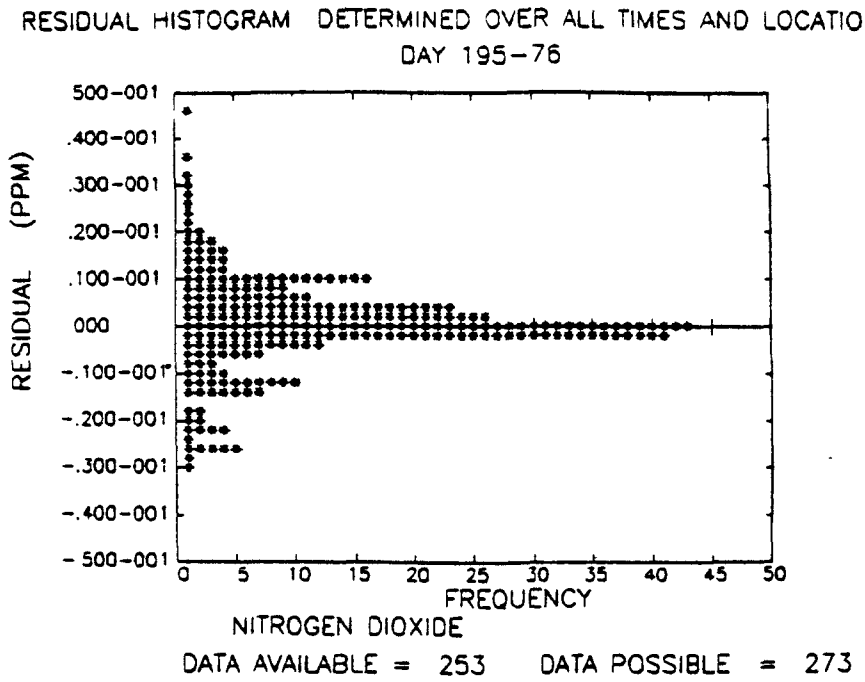

Figure 26a. Residual histogram for NO_2 from the UAM simulation results for Day 195-76.

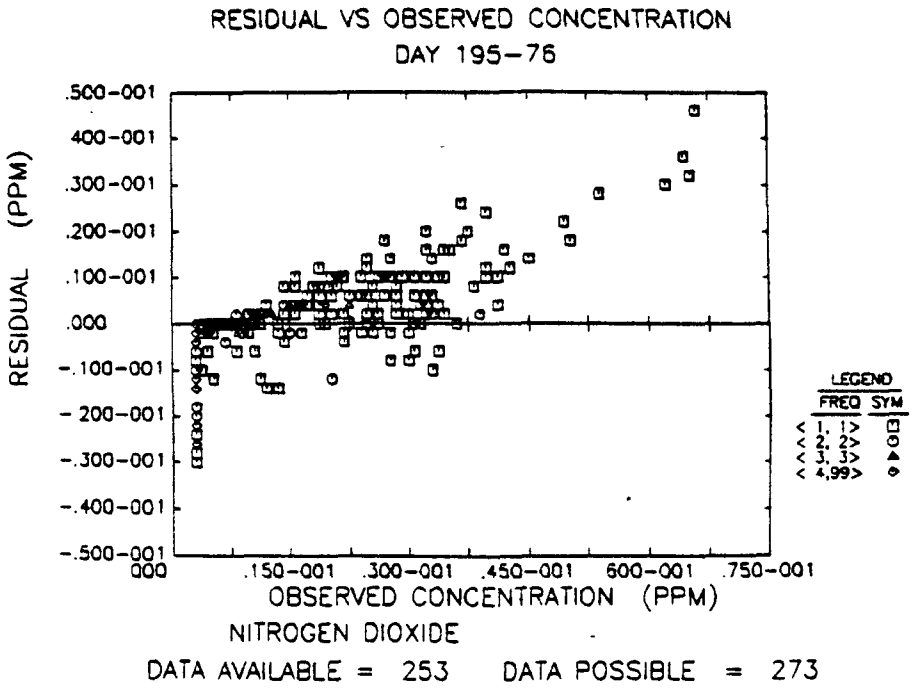

Figure 26b. Residual vs. observed plot for NO_2 from the UAM simulation results for Day 195-76.

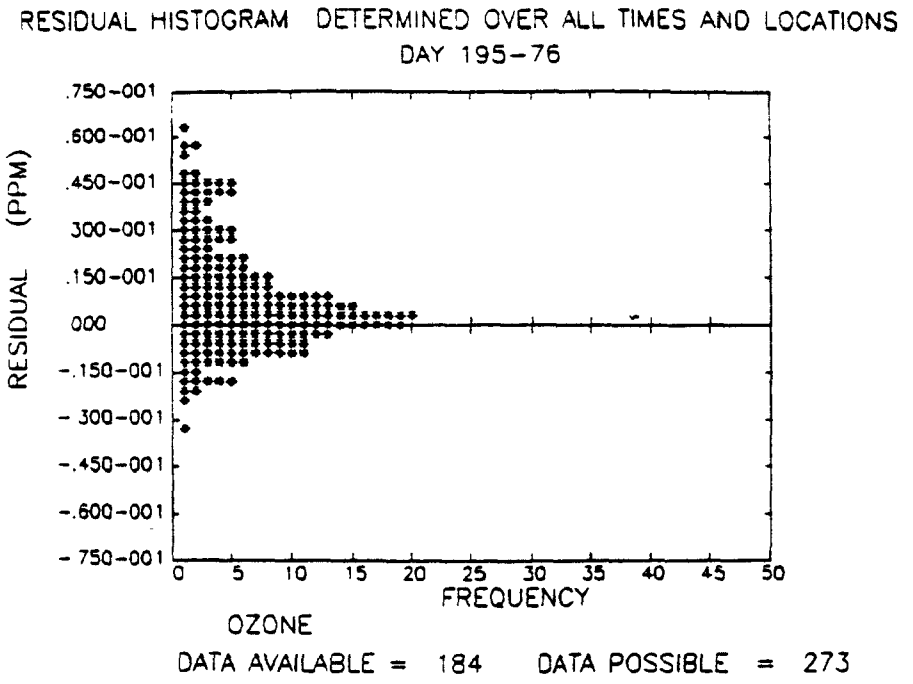

Figure 27a. Residual histogram for O_3 from the UAM simulation results for Day 195-76.

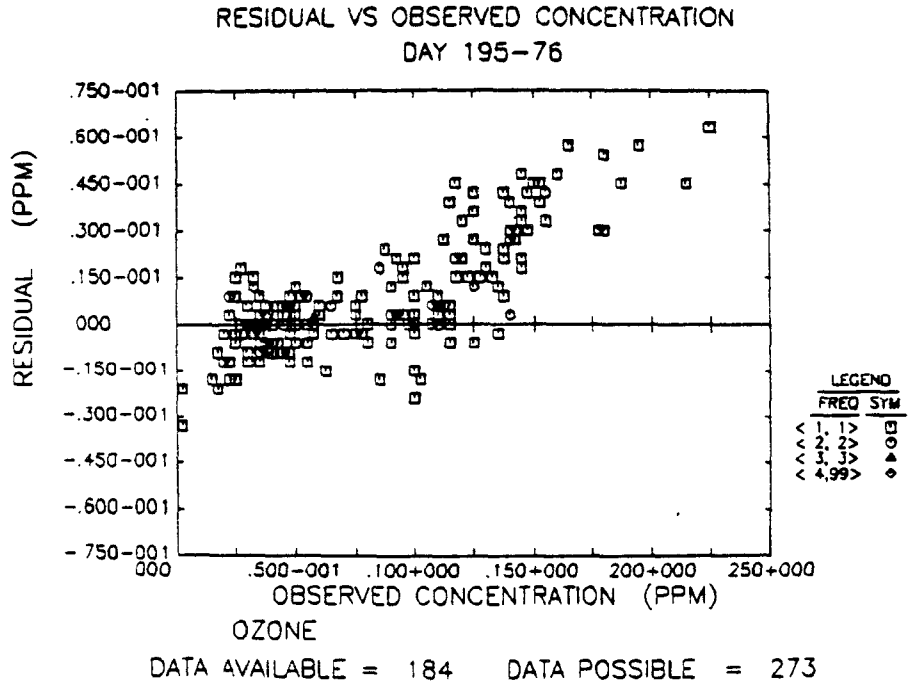

Figure 27b. Residual vs. observed plot for O_3 from the UAM simulation results for Day 195-76.

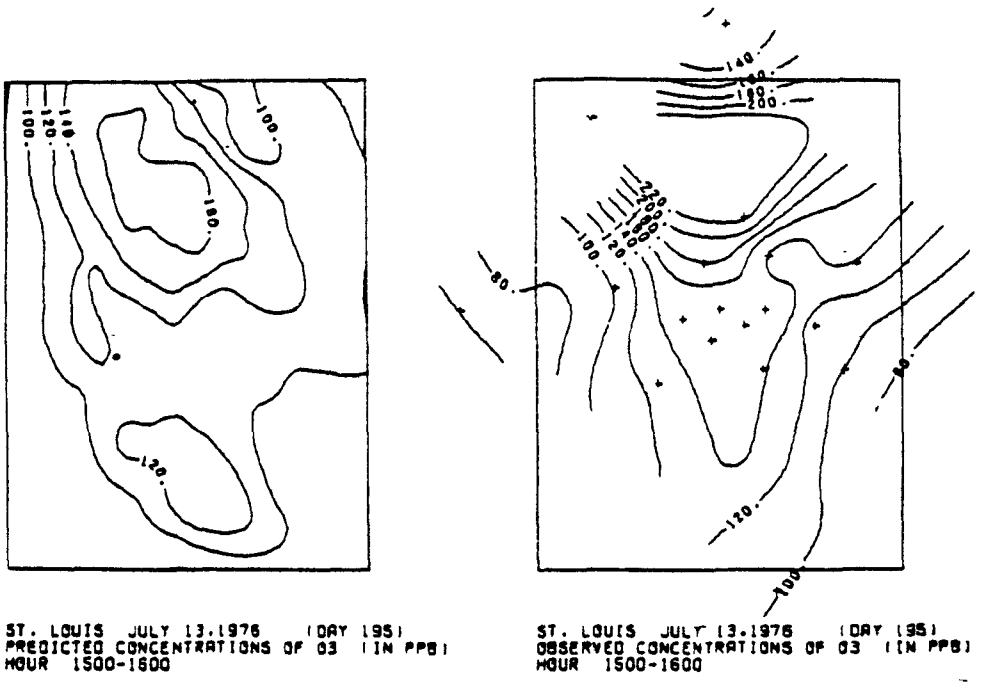

(a) (b)

Figure 28. Contours of (a) predicted and (b) observed fields of O_3 at hour of observed maximum on Day 195-76.

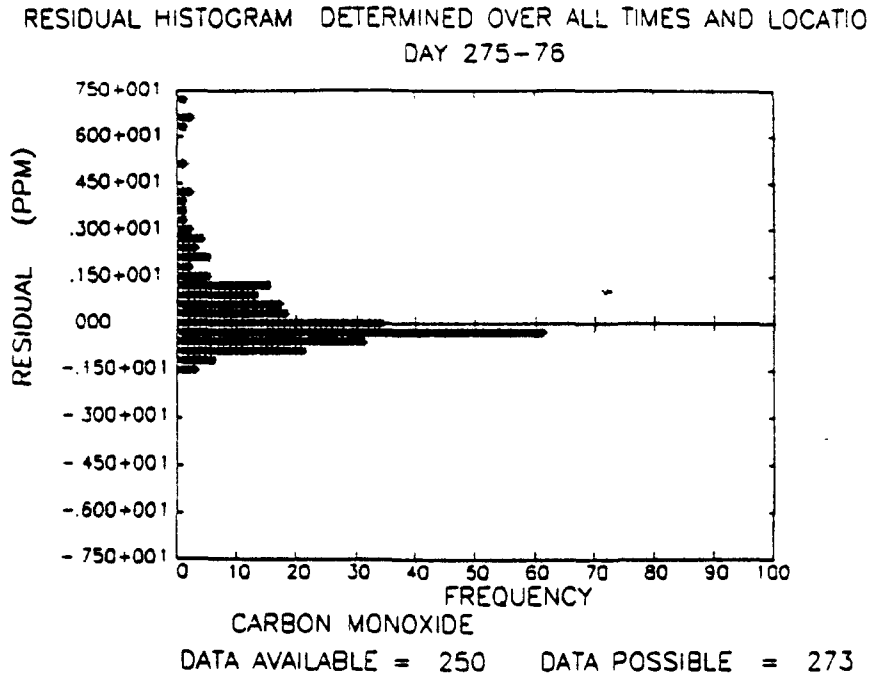

Figure 29a. Residual histogram for CO from the UAM simulation results for Day 275-76.

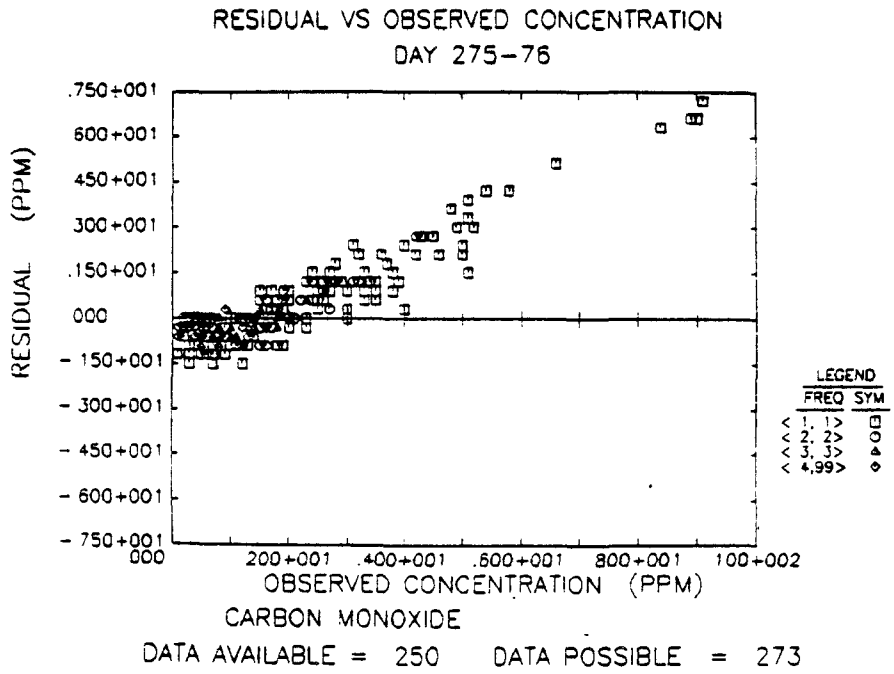

Figure 29b. Residual vs. observed plot for CO from the UAM simulation results for Day 275-76.

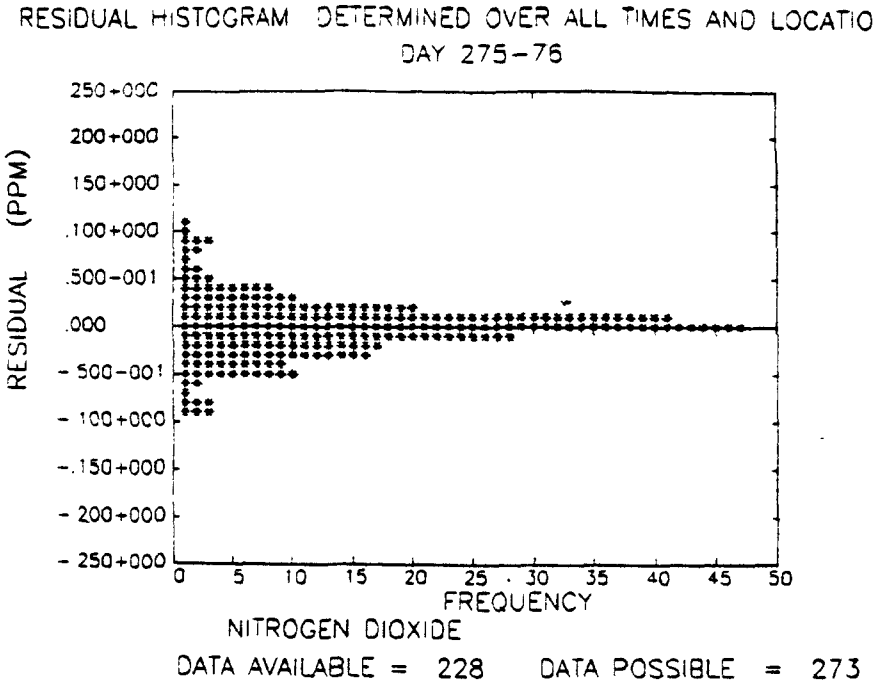

Figure 30a. Residual histogram for NO_2 from the UAM simulation results for Day 275-76.

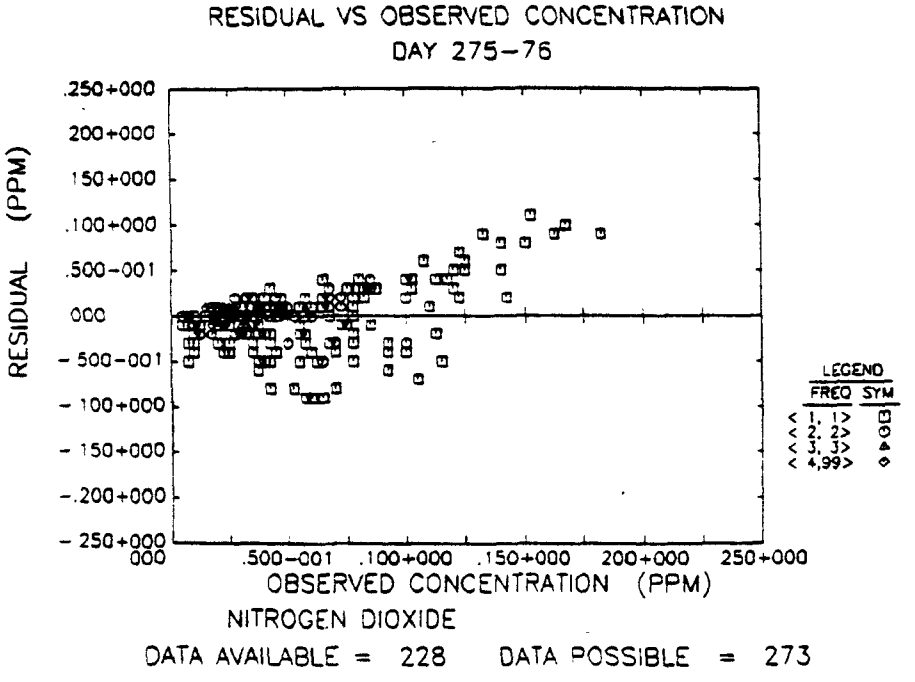

Figure 30b. Residual vs. observed plot for NO_2 from the UAM simulation results for Day 275-76.

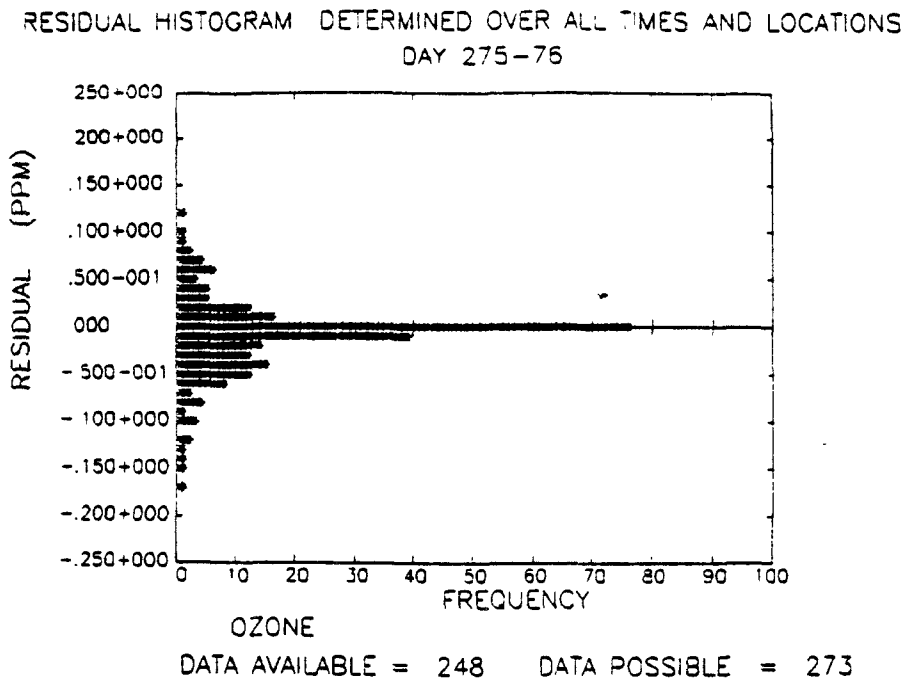

Figure 31a. Residual histogram for O_3 from the UAM simulation results for Day 275-76.

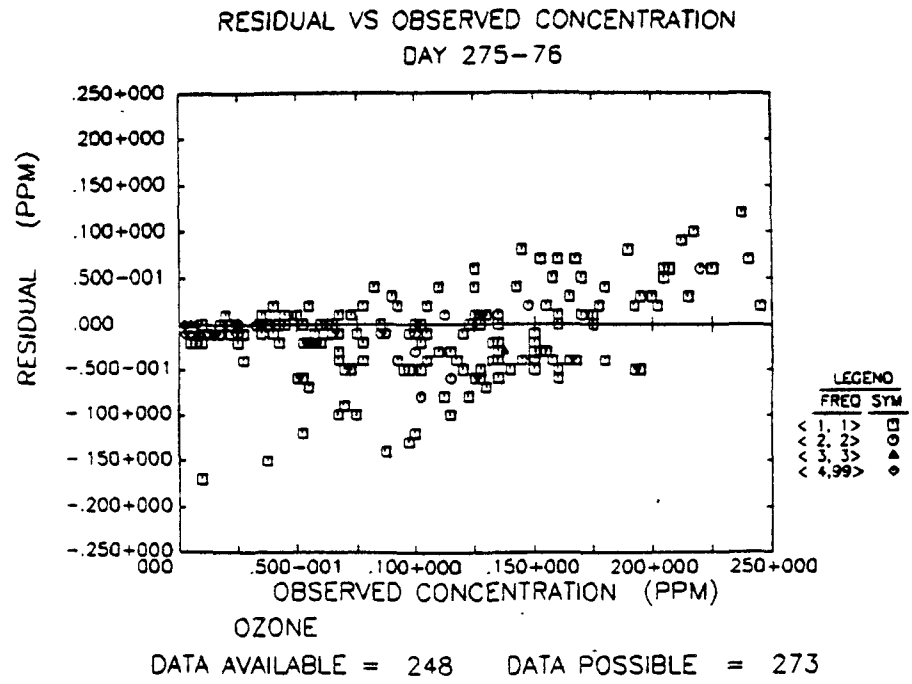

Figure 31b. Residual vs. observed plot for O_3 from the UAM simulation results for Day 275-76.

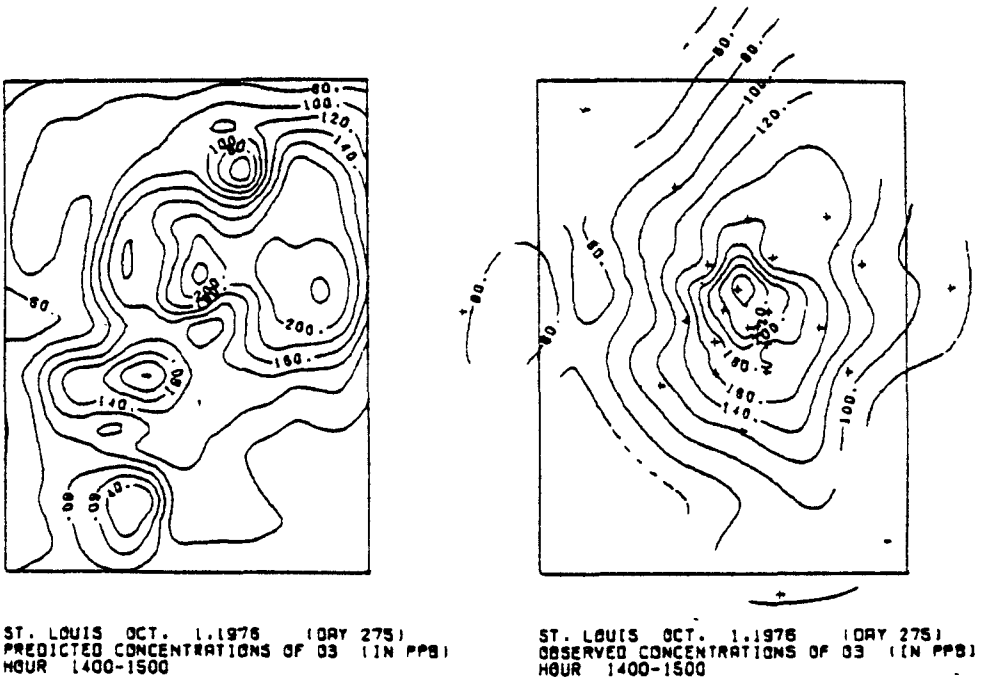

(a) (b)

Figure 32. Contours of (a) predicted and (b) observed fields of O_3 at hour of observed maximum on Day 275-76.

REFERENCES

Bencala, K. E. and J. H. Seinfeld, 1979: An air quality model performance assessment package. Atmos. Environ., 13, 1181-1185.

Littman, F. E., 1979: Regional Air Pollution Study--Emission inventory summarization. Report No. EPA-600/4-79-004, U. S. Environmental Protection Agency, Research Triangle Park, NC 27711.

Lurmann, F., D. Godden, A. C. Lloyd, and R. A. Nordsieck, 1979: A Lagrangian Photochemical Air Quality Simulation Model. Vol. I-Model Formulation, Vol. II-Users Manual. EPA-600/8-79-015a,b (available NTIS).

Lurmann, F., 1980: Modification and Analysis of the Lagrangian Photochemical Air Quality Simulation Model for St. Louis. Environmental Research and Technology, Inc. Document No. P-A095. Westlake Village, CA. 25pp.

Lurmann, F., 1981: Incorporation of Lateral Diffusion in the Lagrangian Photochemical Air Quality Simulation Model. Environmental Research and Technology, Inc. Document No. P-A748. Westlake Village, CA. 32pp.

MacCracken, M. C., D. J. Wuebbles, J. J. Walton, W. H. Duewer, and K. E. Grant, 1978: The Livermore Regional Air Quality Model, I. Concept and development. J. Appl. Met., 17, 254-272.

Schere, K. L. 1981: Air quality model response to objectively analyzed wind fields. In Proceedings of the Fifth Symposium on Turbulence, Diffusion, and Air Pollution, American Meteorological Society, Atlanta, GA, March 9-13, 1981.

Schiermeier, F. A., 1978: Air monitoring milestones: RAPS field measurements are in. Environ. Sci. Technol., 12, 644-651.

Shreffler, J. H. and R. B. Evans, 1982: The surface ozone record from the Regional Air Pollution Study, 1975-1976. Atmos. Environ., 16, 1311-1321.

Shreffler, J. H. and K. L. Schere, 1982: Evaluation of Four Urban-Scale Photochemical Air Quality Simulation Models. EPA Report, U.S. Environmental Protection Agency, Research Triangle Park, NC (in press).

Zalesak, S. T., 1979: Fully multi-dimensional-flux-corrected transport algorithms for fluids. J. Comp. Phys., 31, 335-362.

APPENDIX A

PBM - TIME SERIES FOR REMAINING TEST DAYS

This appendix contains the time series plots for the pollutant species CO, NO_2 and O_3 from the PBM test results for those days that were not specifically discussed within the body of this report. The plots presented here are from test days 182-75, 183-75, 184-75, 209-75, 221-75, 230-75, 231-75, 251-75, 159-76, 160-76, 195-76, 211-76, 225-76, 226-76 and 237-76 of the RAPS data base.

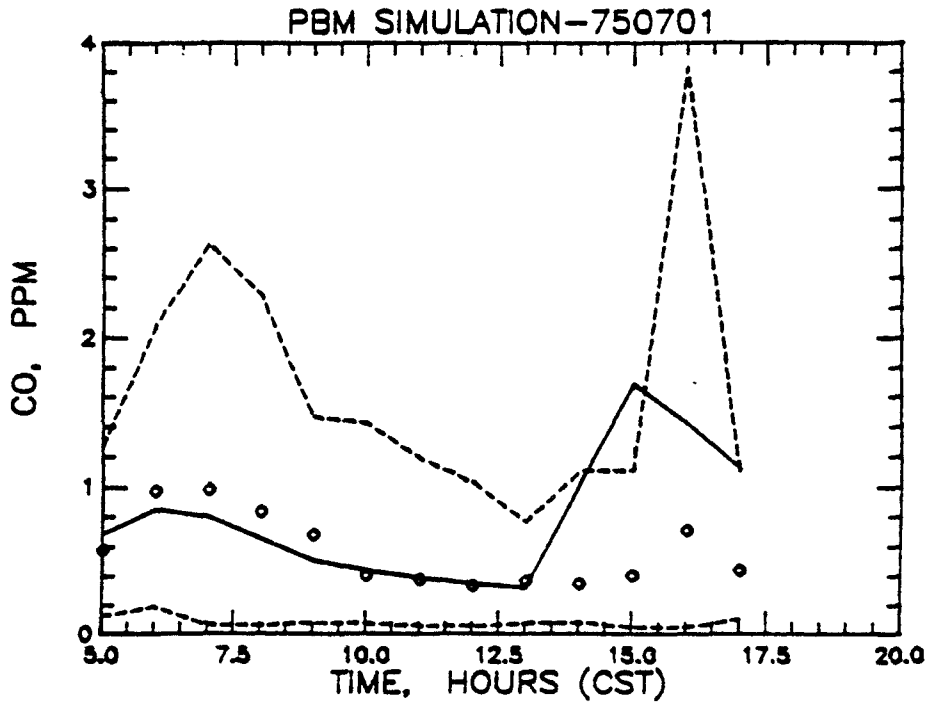

Figure A-1a. PBM simulation results for Day 182 of 1975. Time series of average observed (circles), range of observed (dashed lines), and model-simulated (solid line) hour-average concentrations of CO.

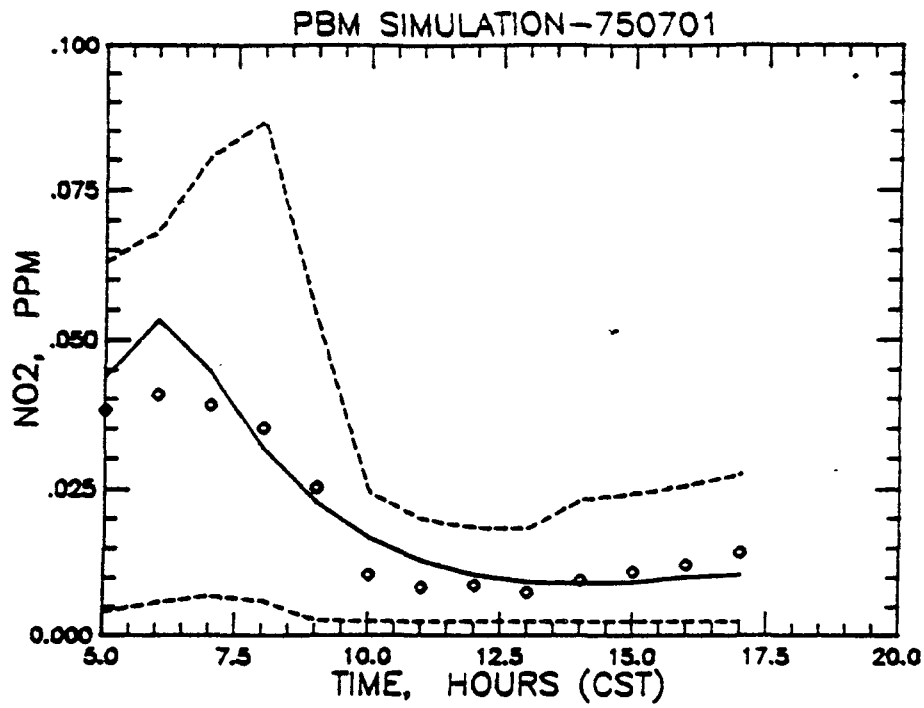

Figure A-1b. PBM simulation results for NO_2 - Day 182 of 1975. Keys to figure described in A-1a.

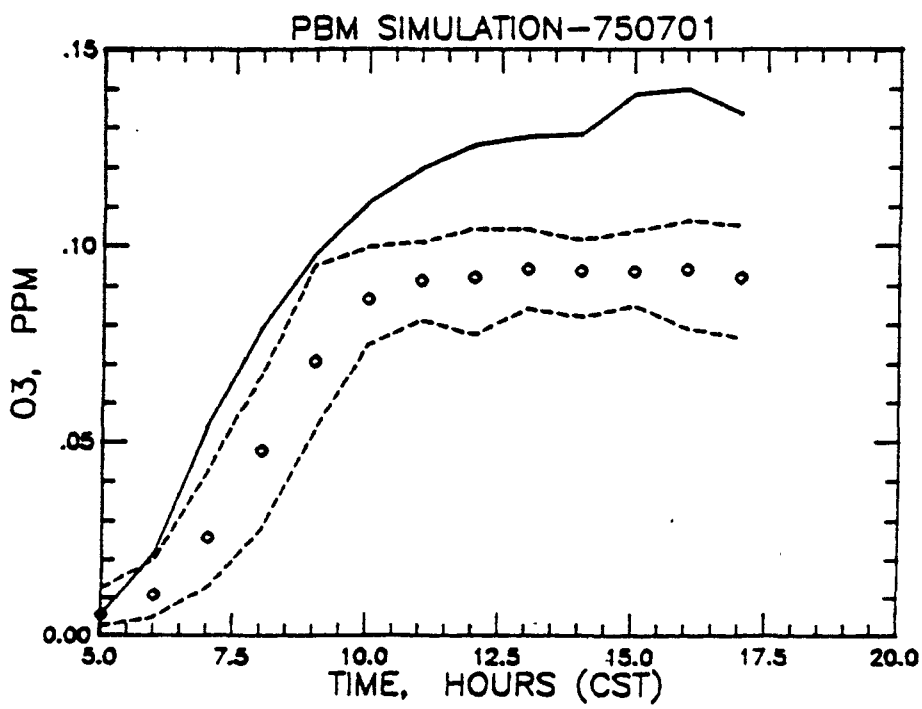

Figure A-1c. PBM simulation results for O_3 - Day 182 of 1975. Keys to figure described in A-1a.

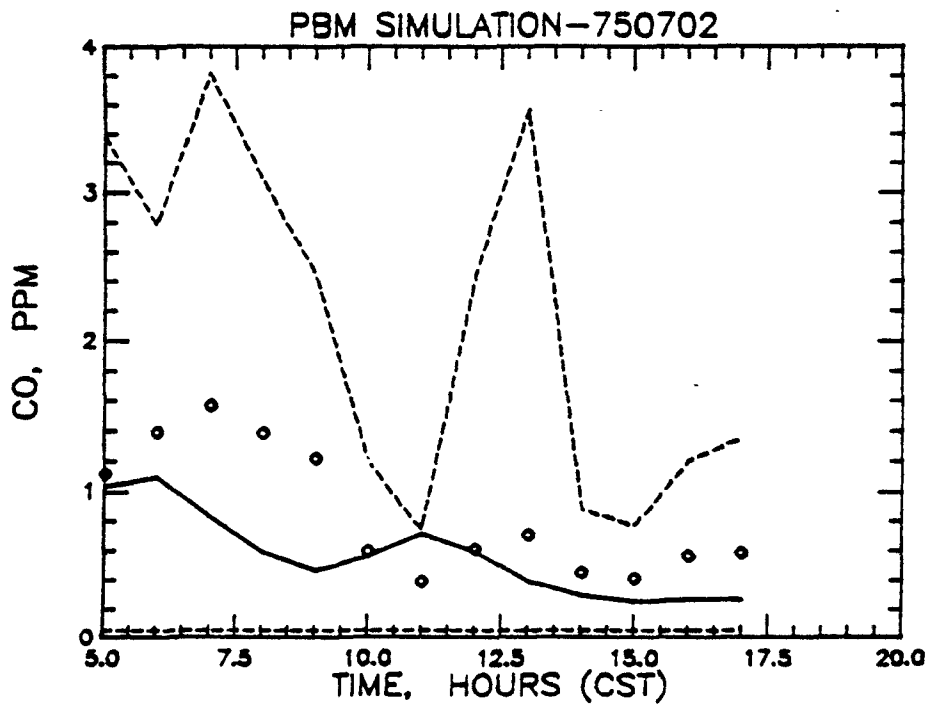

Figure A-2a. PBM simulation results for Day 183 of 1975. Time series of average observed (circles), range of observed (dashed lines), and model-simulated (solid line) hour-average concentrations of CO.

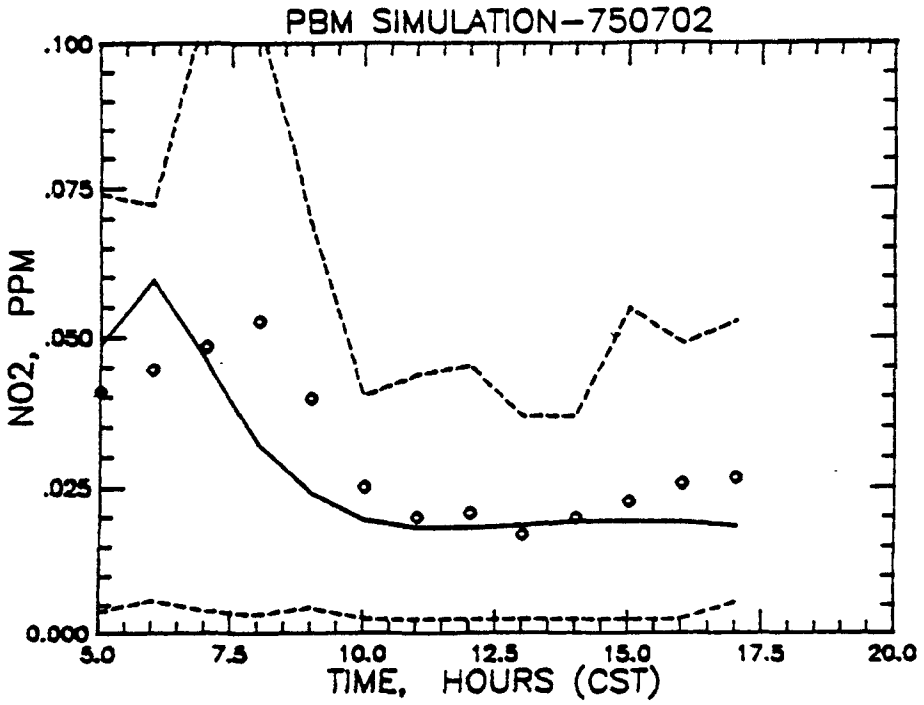

Figure A-2b. PBM simulation results for NO_2 - Day 183 of 1975. Keys to figure described in A-2a.

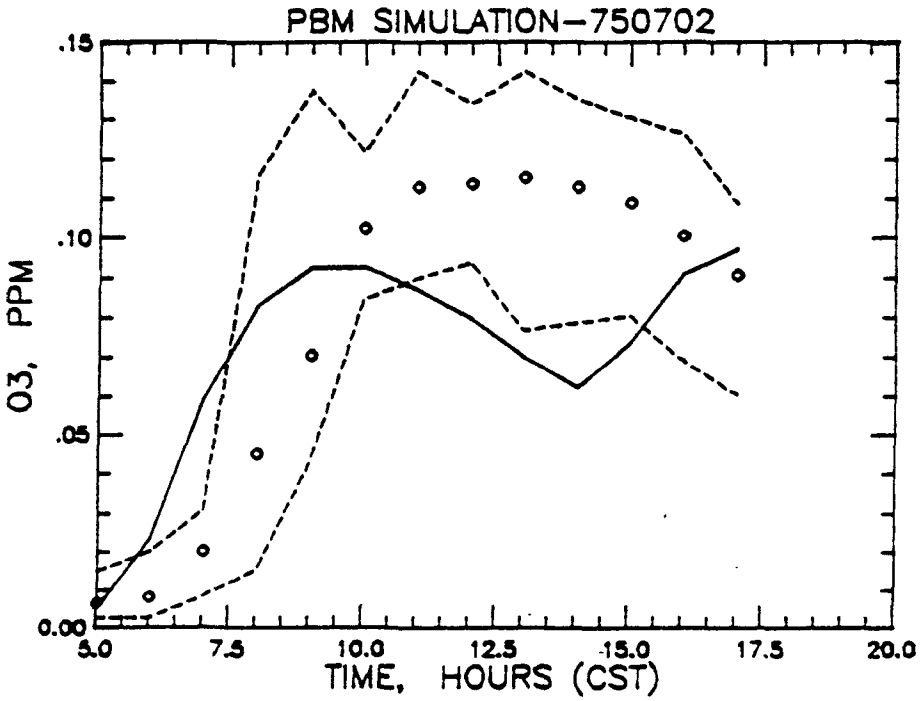

Figure A-2c. PBM simulation results for O_3 - Day 183 of 1975. Keys to figure described in A-2a.

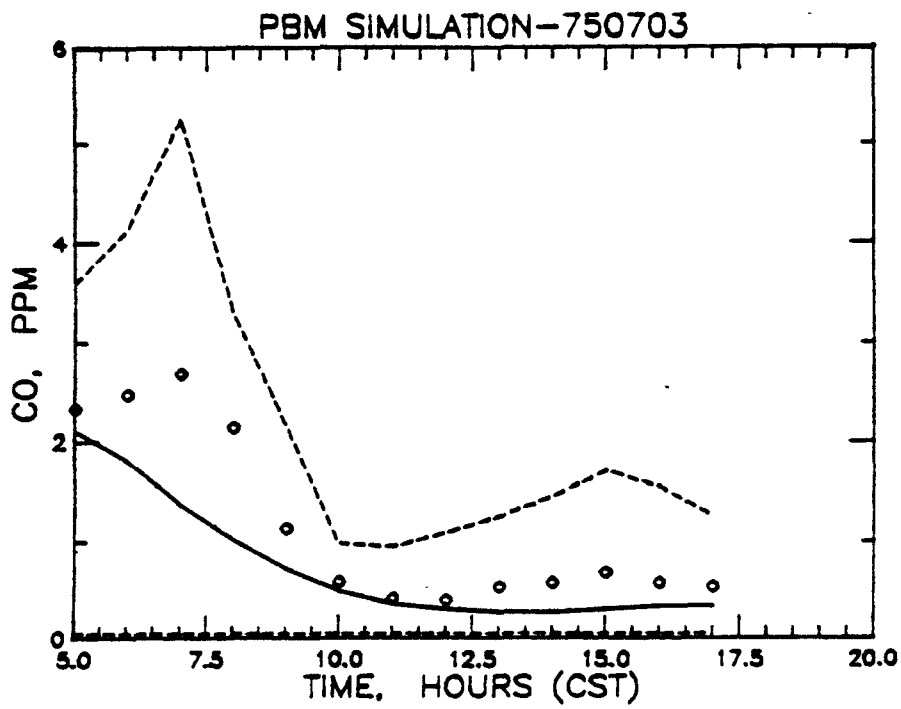

Figure A-3a. PBM simulation results for Day 184 of 1975. Time series of average observed (circles), range of observed (dashed lines), and model-simulated (solid line) hour-average concentrations of CO.

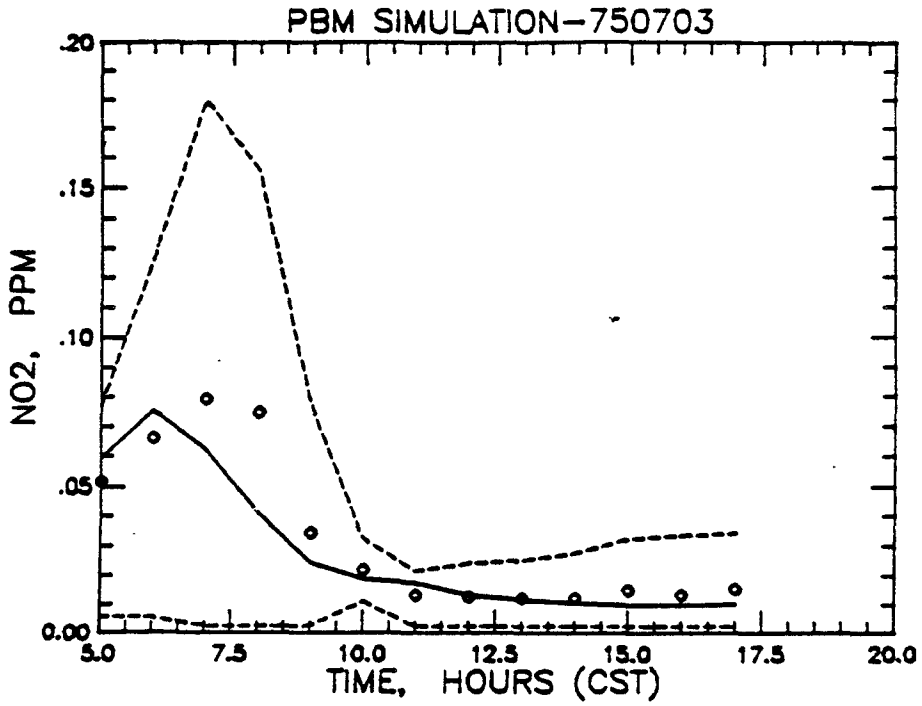

Figure A-3b. PBM simulation results for NO_2 - Day 184 of 1975. Keys to figure described in A-3a.

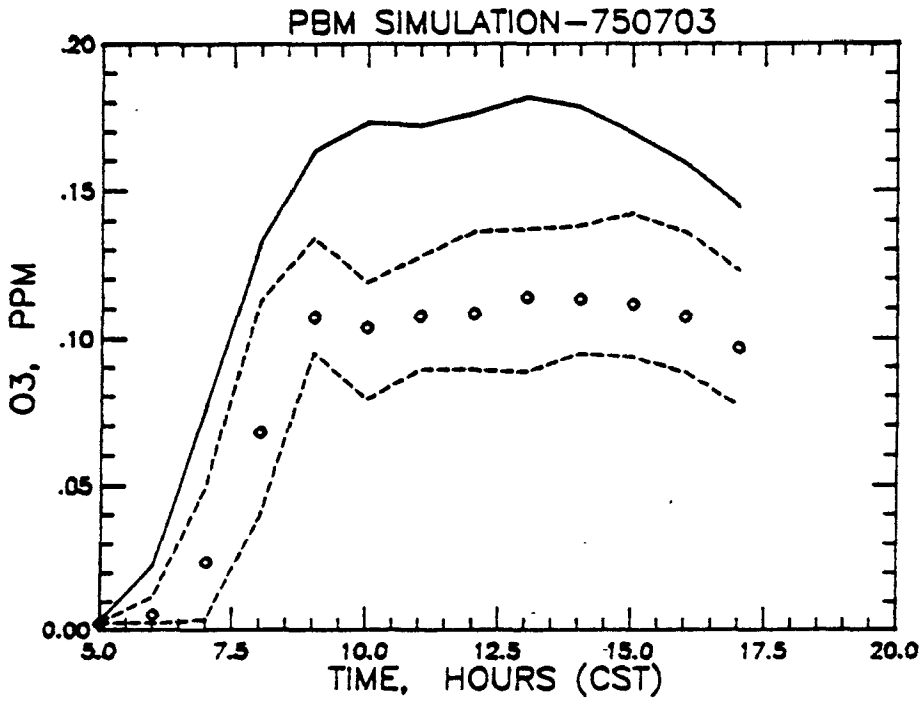

Figure A-3c. PBM simulation results for O_3 - Day 184 of 1975 Keys to figure described in A-3a.

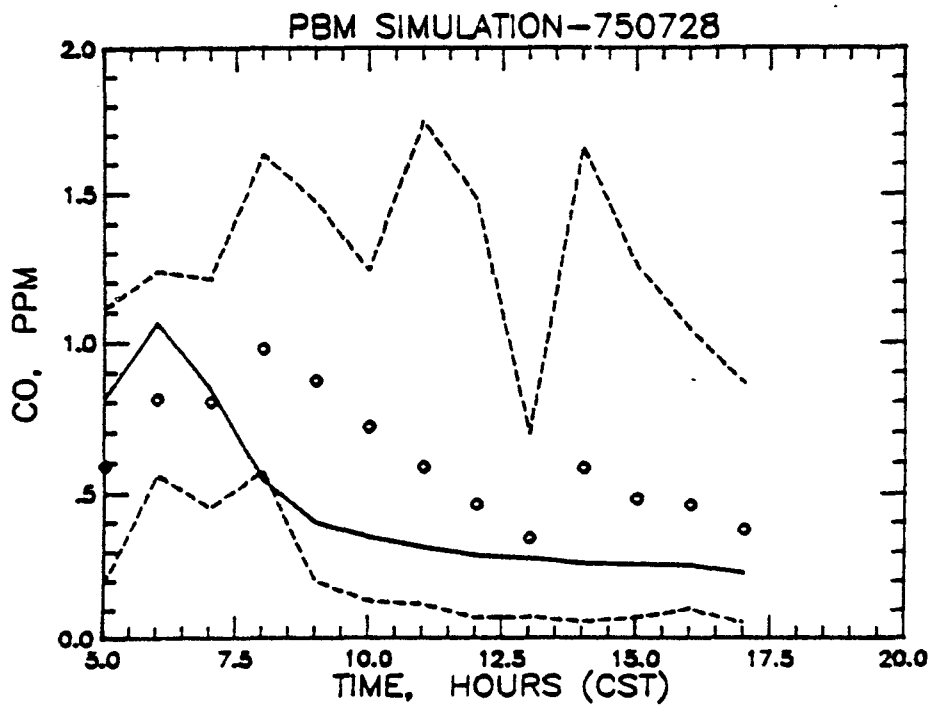

Figure A-4a. PBM simulation results for Day 209 of 1975. Time series of average observed (circles), range of observed (dashed lines), and model-simulated (solid line) hour-average concentrations of CO.

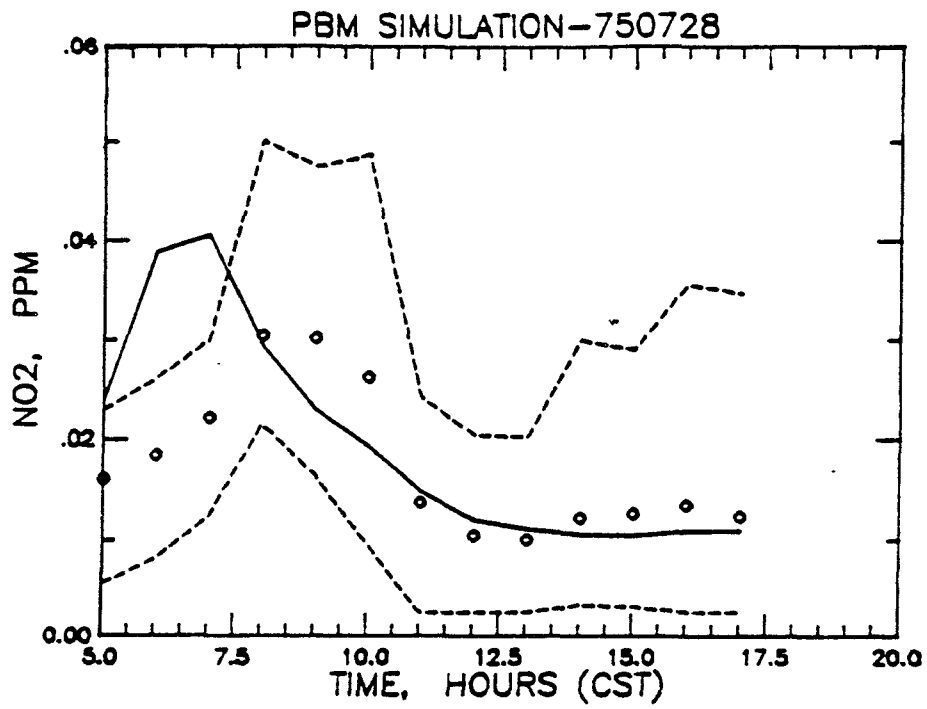

Figure A-4b. PBM simulation results for NO_2 - Day 209 of 1975. Keys to figure described in A-4a.

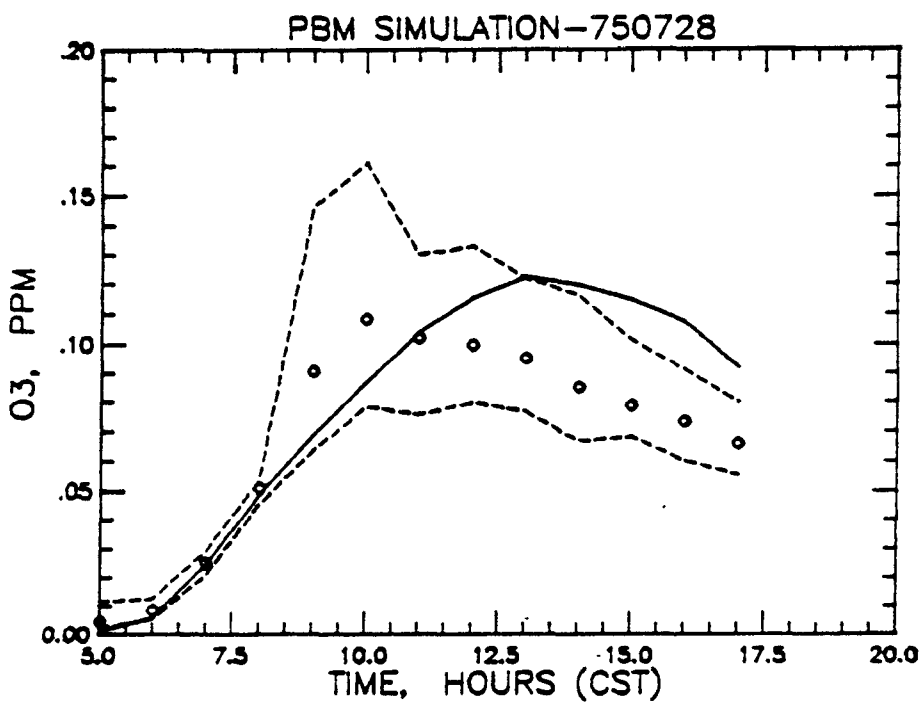

Figure A-4c. PBM simulation results for O_3 - Day 209 of 1975. Keys to figure described in A-4a.

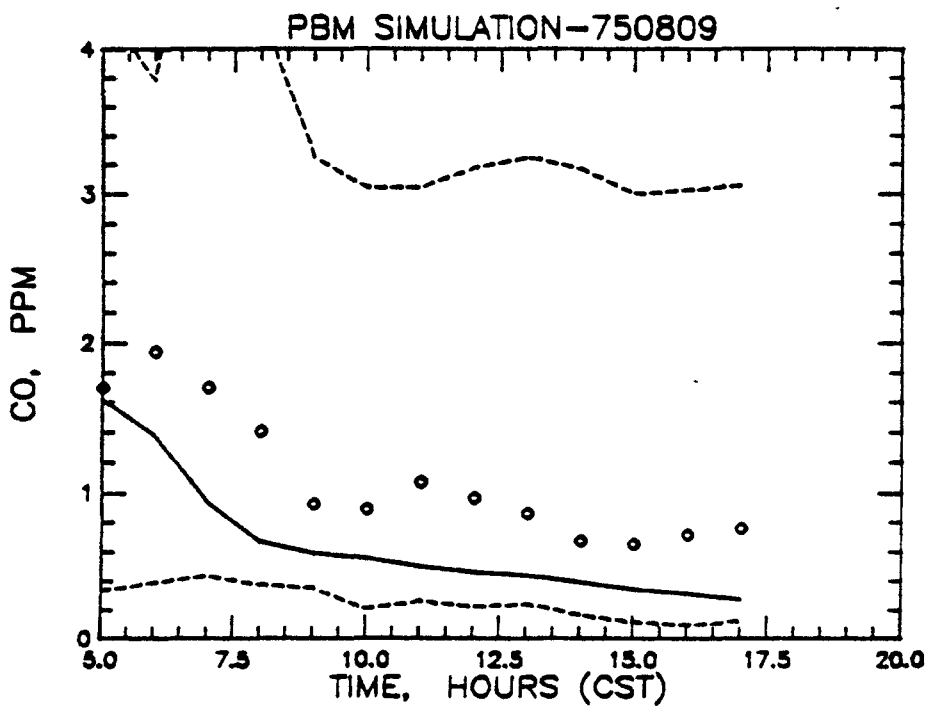

Figure A-5a. PBM simulation results for Day 221 of 1975. Time series of average observed (circles), range of observed (dashed lines), and model-simulated (solid line) hour-average concentrations of CO.

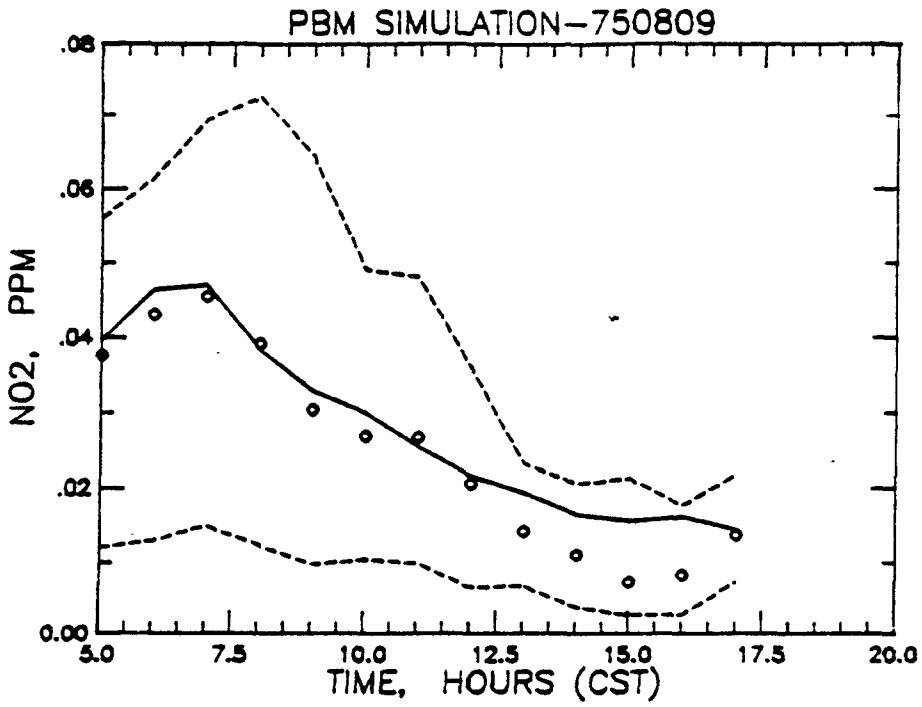

Figure A-5b. PBM simulation results for NO_2 - Day 221 of 1975. Keys to figure described in A-5a.

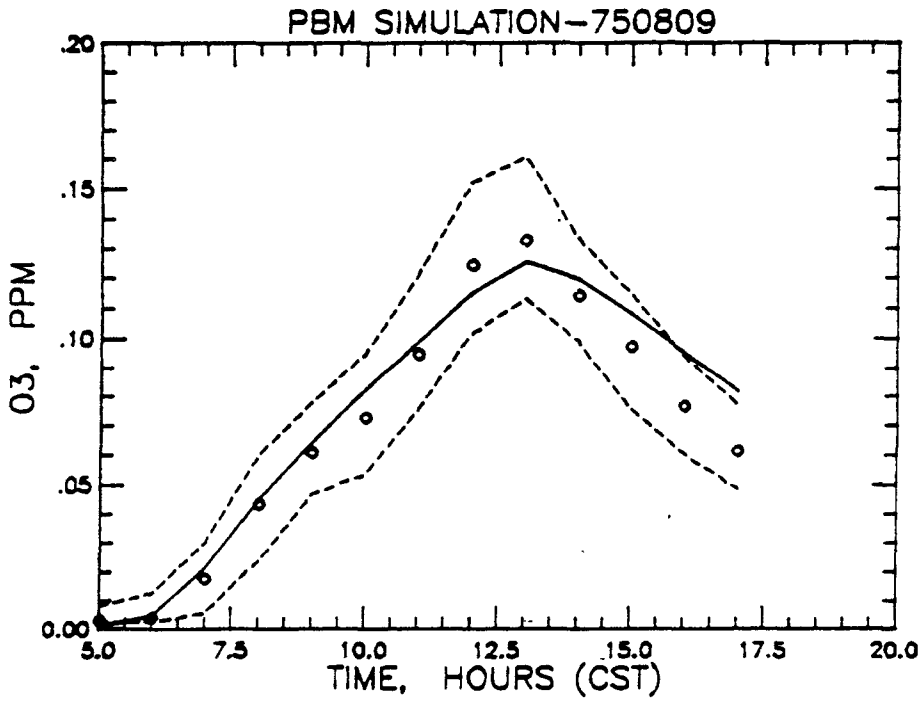

Figure A-5c. PBM simulation results for O_3 - Day 221 of 1975. Keys to figure described in A-5a.

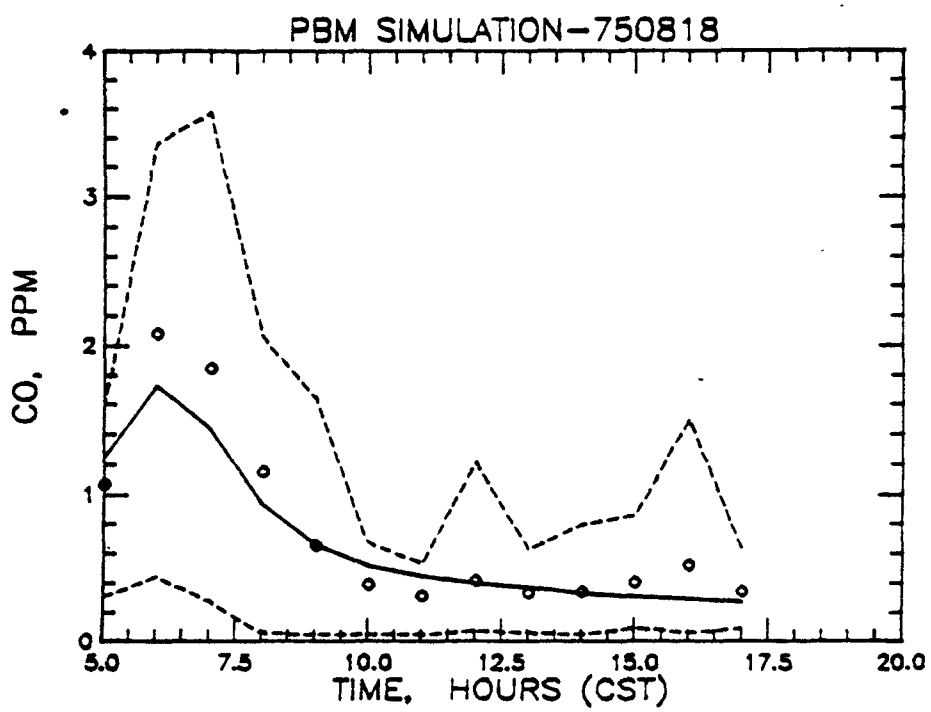

Figure A-6a. PBM simulation results for Day 230 of 1975. Time series of average observed (circles), range of observed (dashed lines), and model-simulated (solid line) hour-average concentrations of CO.

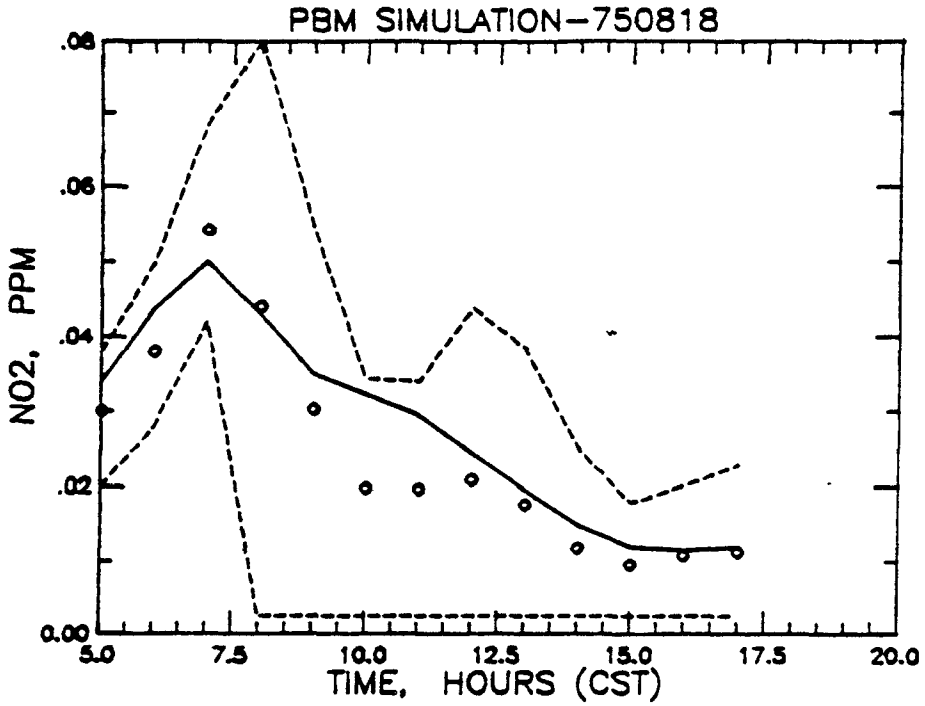

Figure A-6b. PBM simulation results for NO_2 - Day 230 of 1975. Keys to figure described in A-6a.

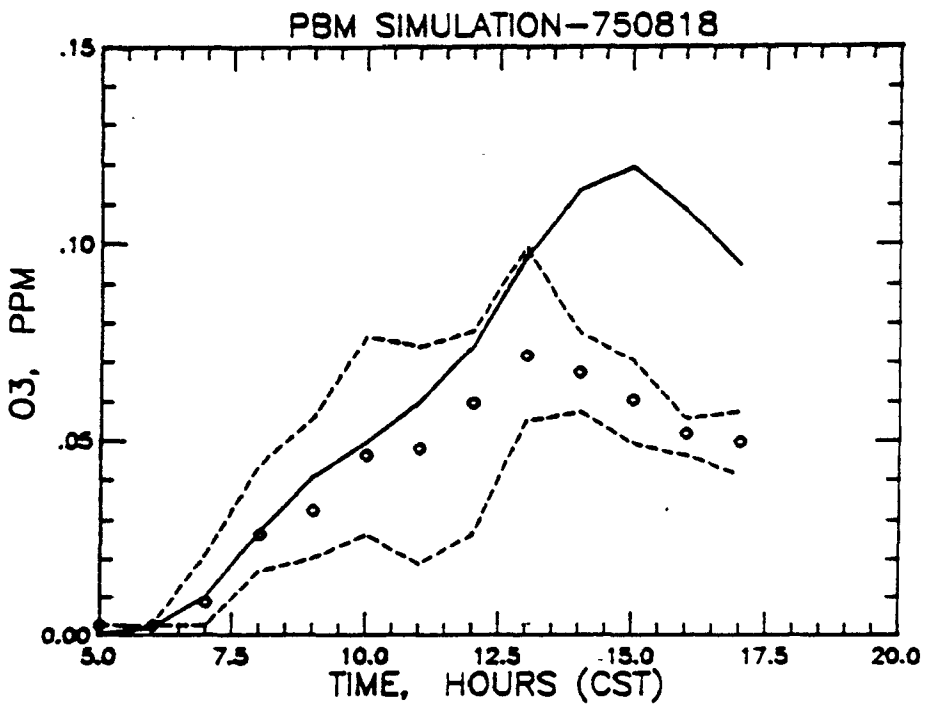

Figure A-6c. PBM simulation results for O_3 - Day 230 of 1975. Keys to figure described in A-6a.

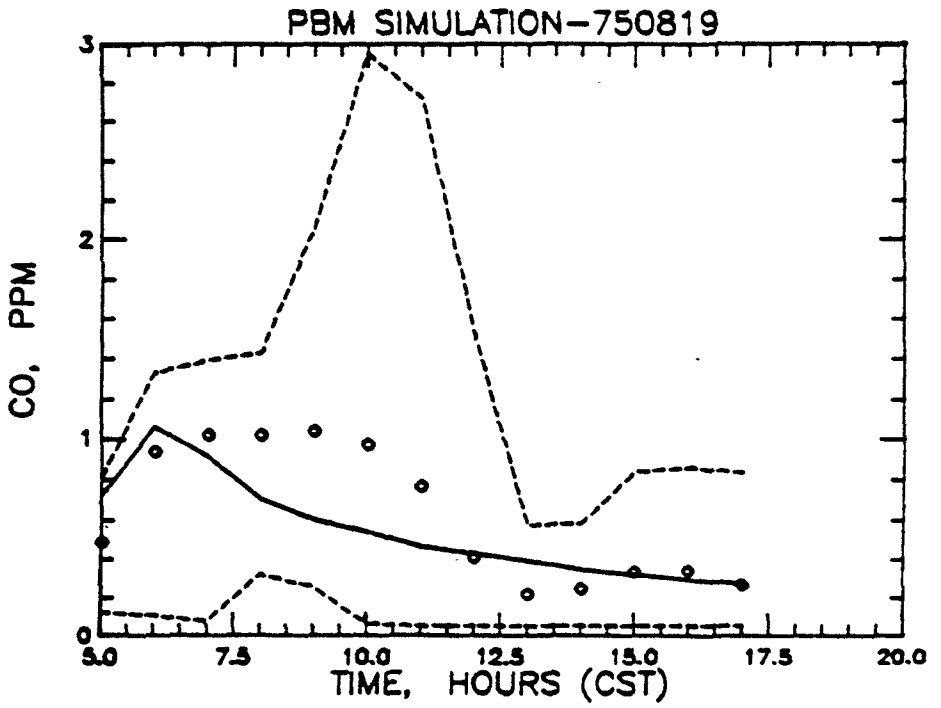

Figure A-7a. PBM simulation results for Day 231 of 1975. Time series of average observed (circles), range of observed (dashed lines), and model-simulated (solid line) hour-average concentrations of CO.

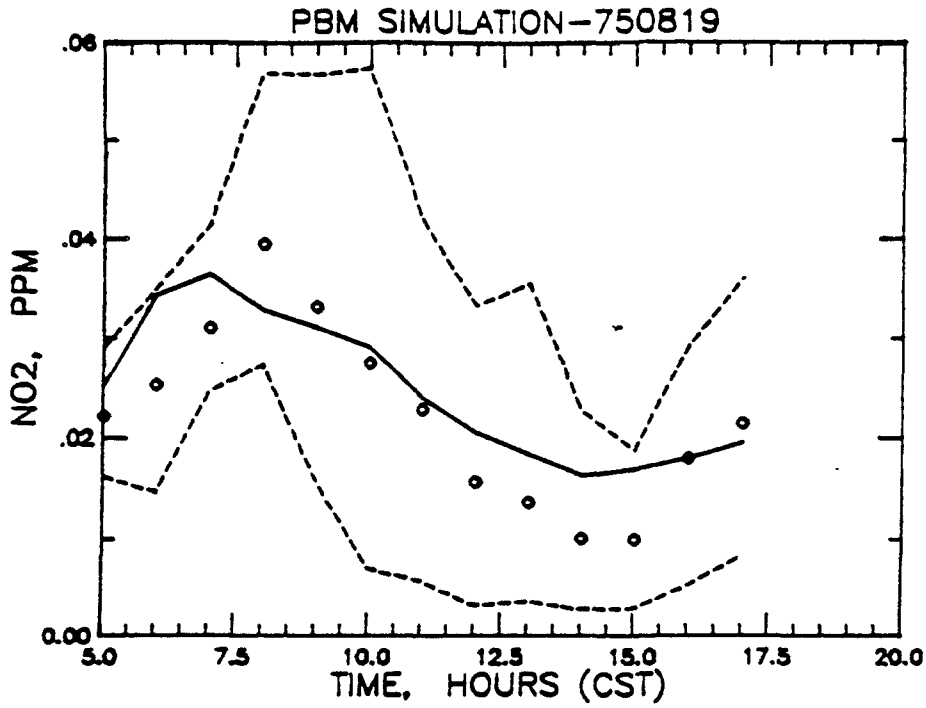

Figure A-7b. PBM simulation results for NO_2 - Day 231 of 1975. Keys to figure described in A-7a.

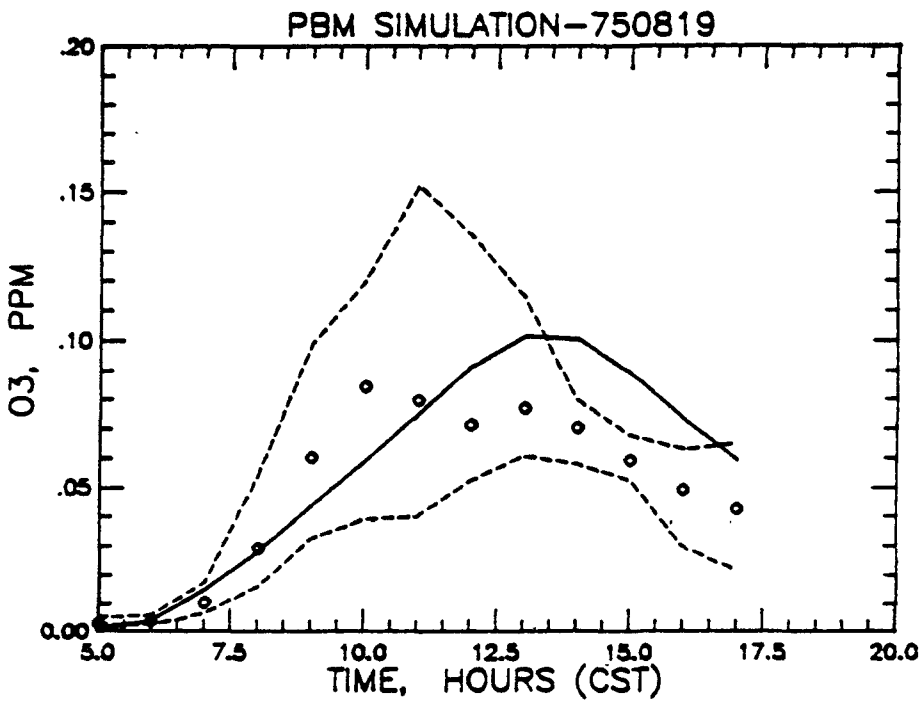

Figure A-7c. PBM simulation results for O_3 - Day 231 of 1975. Keys to figure described in A-7a.

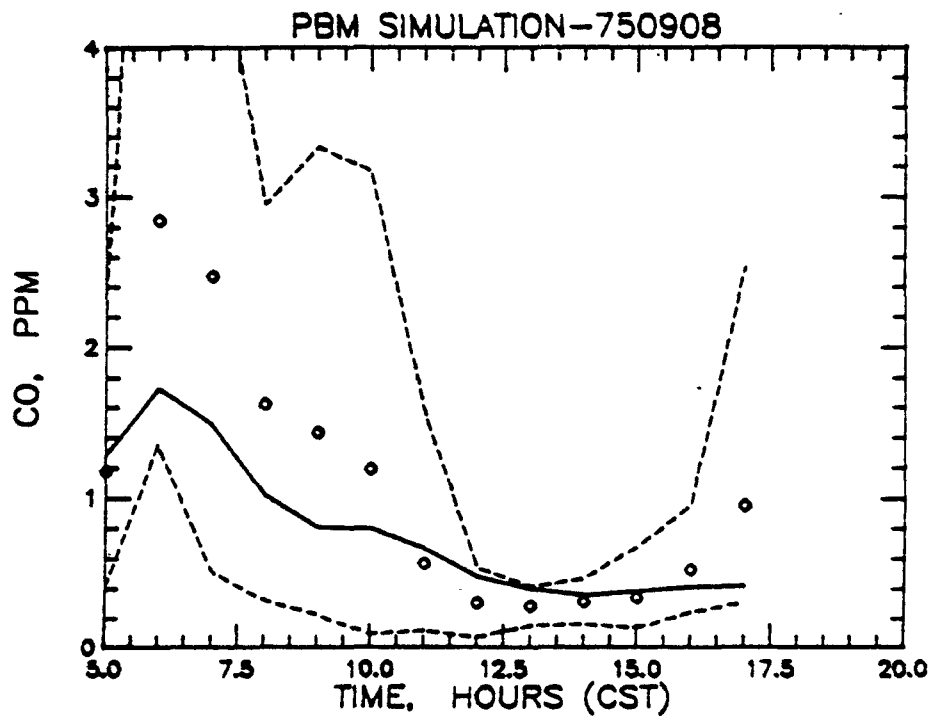

Figure A-8a. PBM simulation results for Day 251 of 1975. Time series of average observed (circles), range of observed (dashed lines), and model-simulated (solid line) hour-average concentrations of CO.

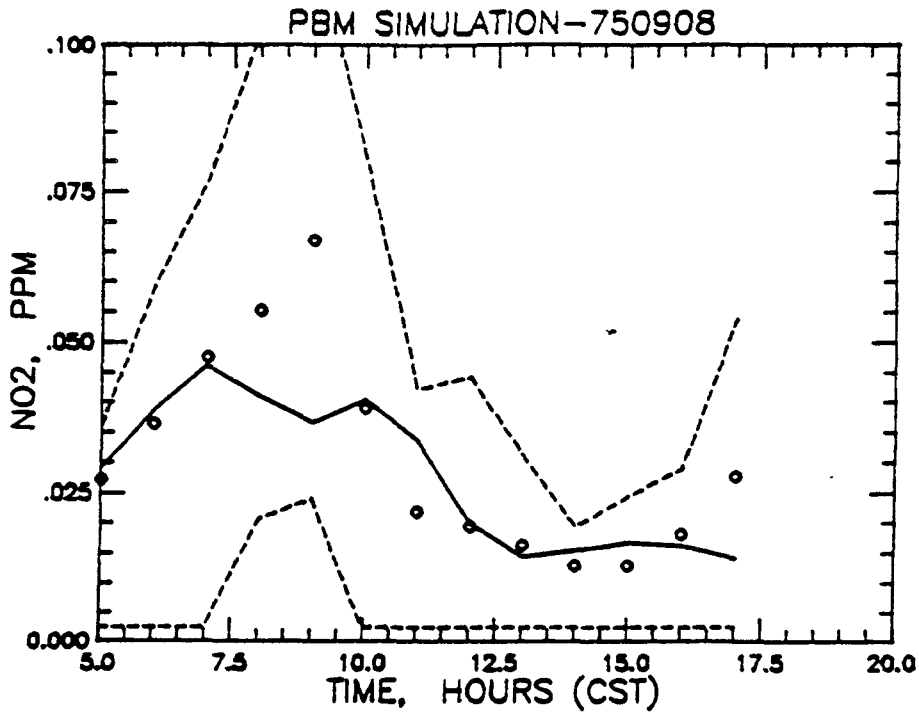

Figure A-8b. PBM simulation results for NO_2 - Day 251 of 1975. Keys to figure described in A-8a.

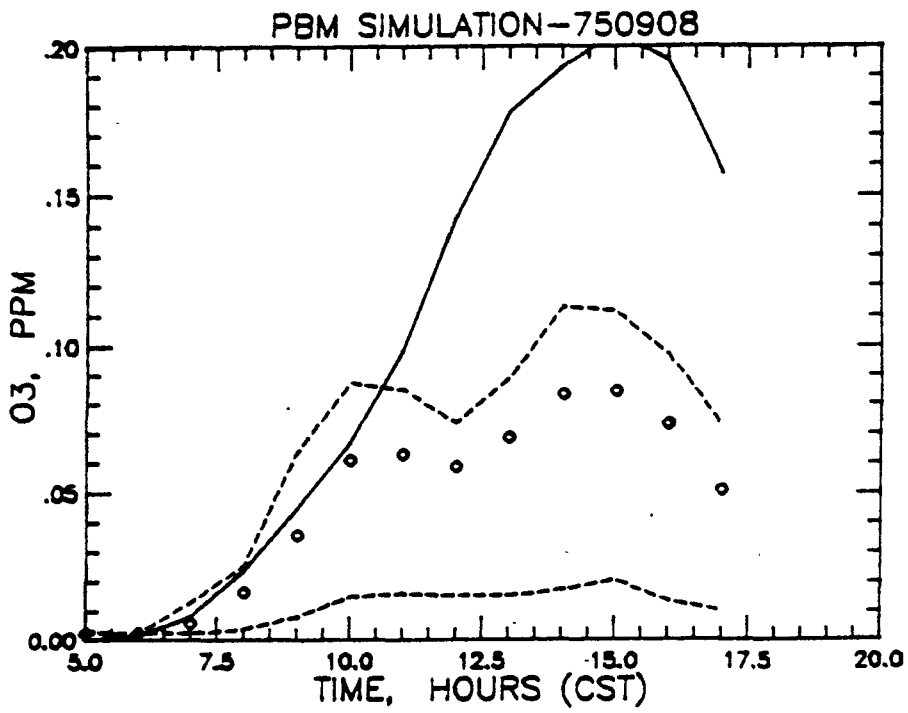

Figure A-8c. PBM simulation results for O_3 - Day 251 of 1975. Keys to figure described in A-8a.

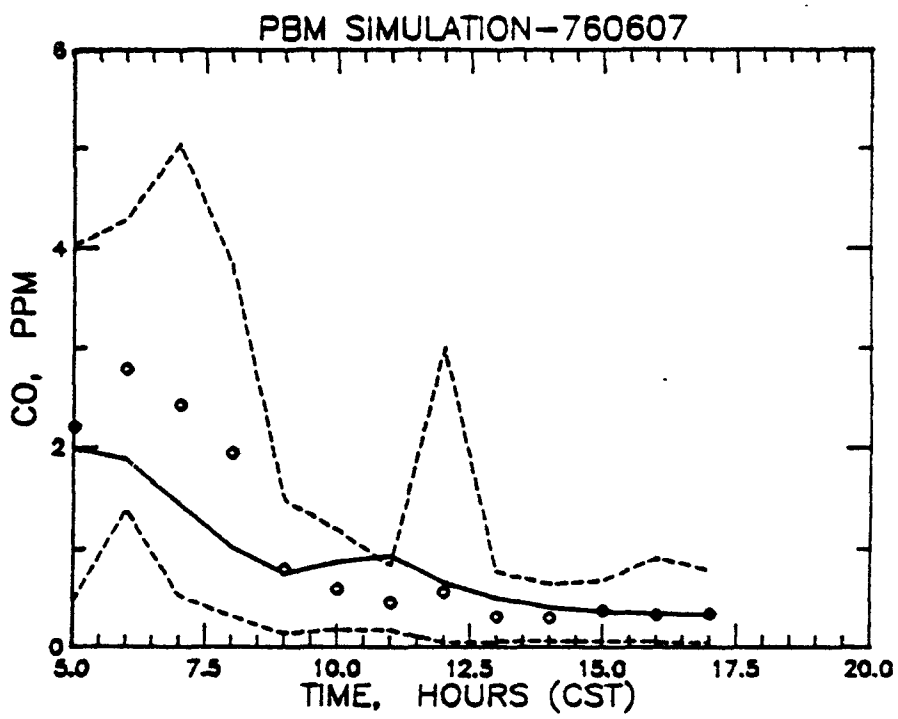

Figure A-9a. PBM simulation results for Day 159 of 1976. Time series of average observed (circles), range of observed (dashed lines), and model-simulated (solid line) hour-average concentrations of CO.

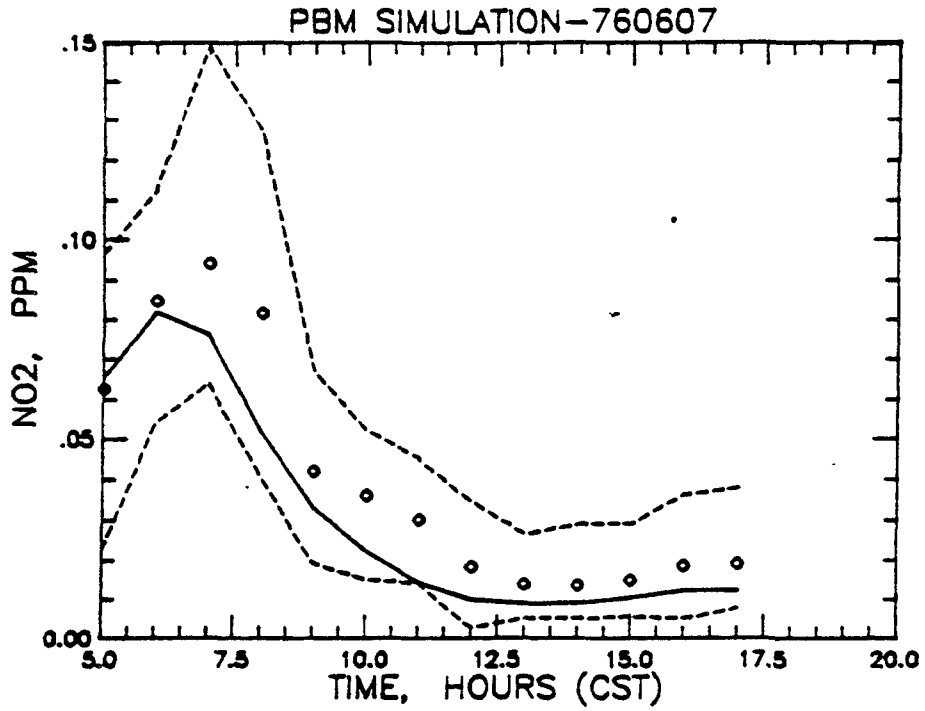

Figure A-9b. PBM simulation results for NO_2 - Day 159 of 1976. Keys to figure described in A-9a.

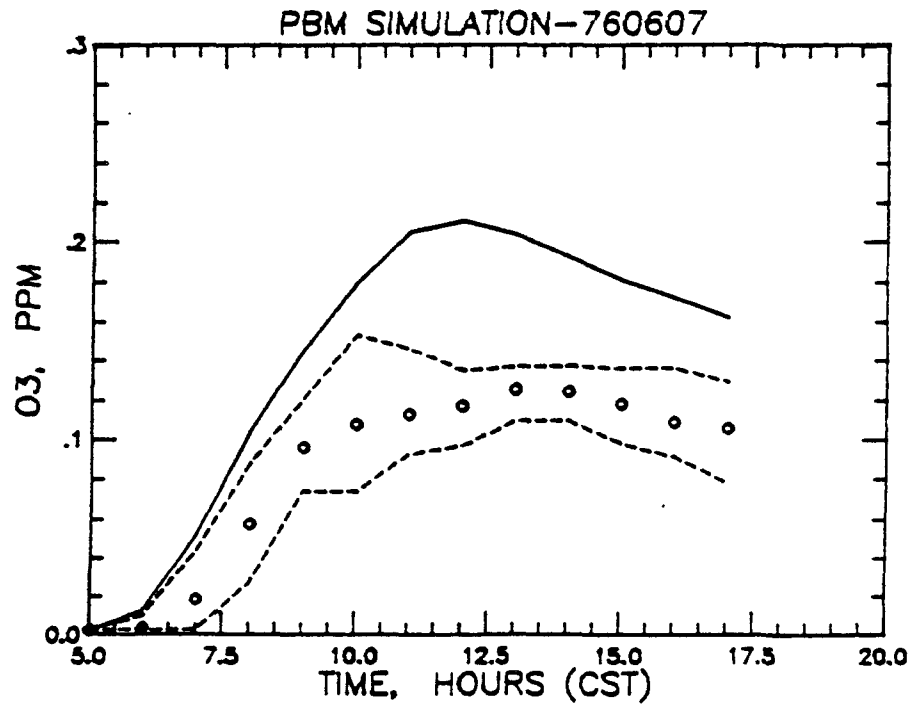

Figure A-9c. PBM simulation results for O_3 - Day 159 of 1976. Keys to figure described in A-9a.

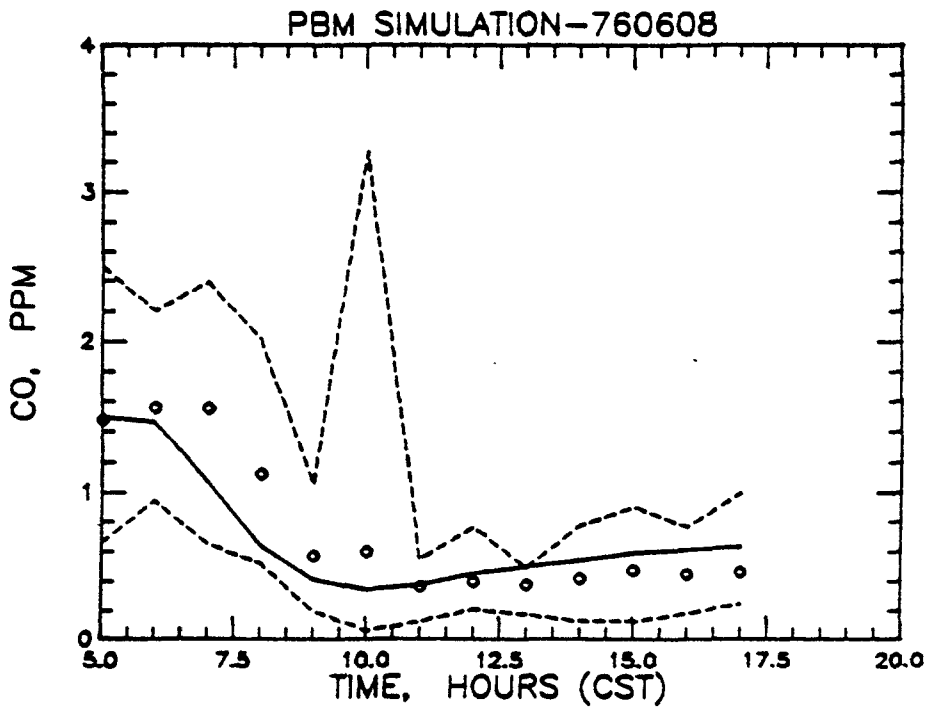

Figure A-10a. PBM simulation results for Day 160 of 1976. Time series of average observed (circles), range of observed (dashed lines), and model-simulated (solid line) hour-average concentrations of CO.

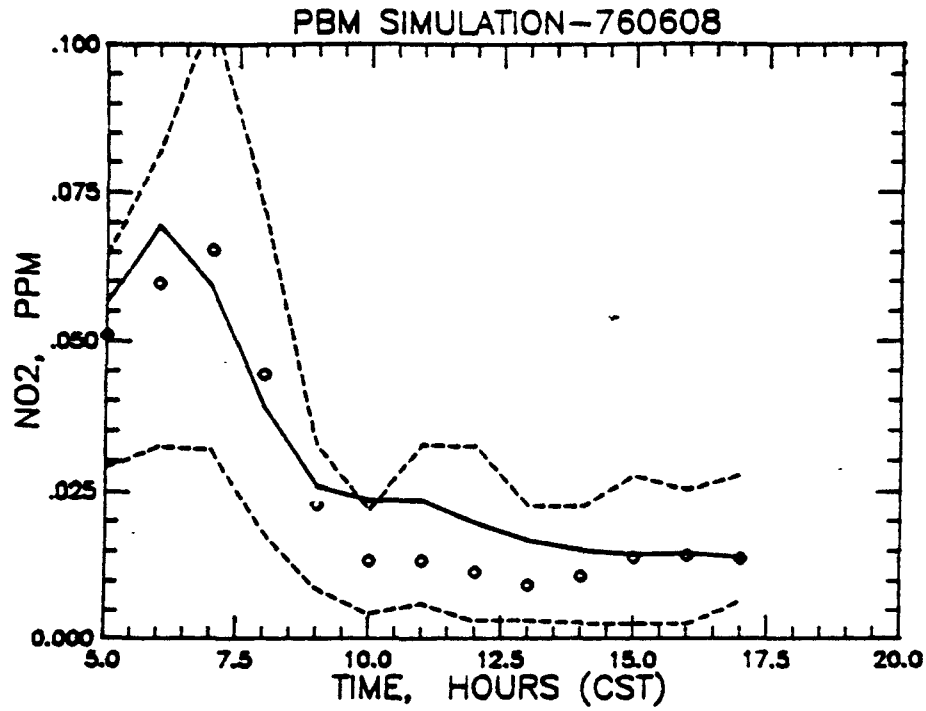

Figure A-10b. PBM simulation results for NO_2 - Day 160 of 1976. Keys to figure described in A-10a.

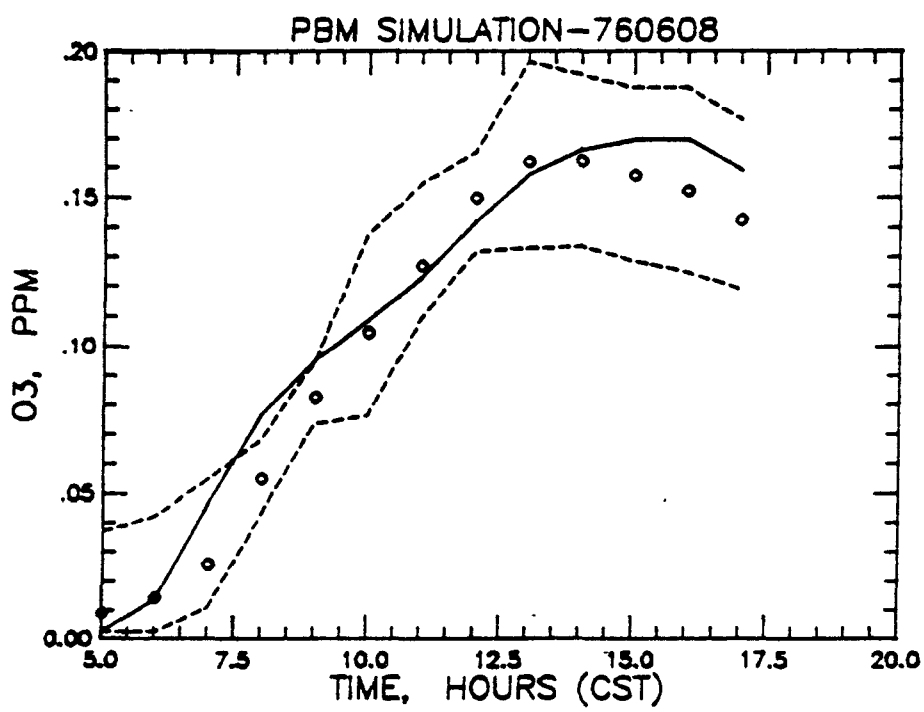

Figure A-10c. PBM simulation results for O_3 - Day 160 of 1976. Keys to figure described in A-10a.

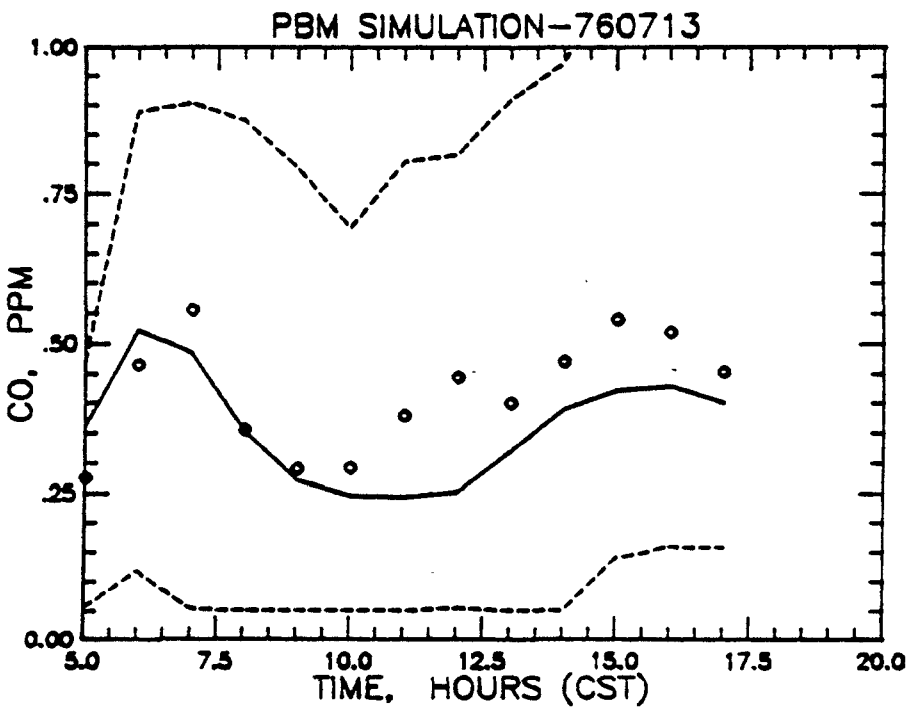

Figure A-11a. PBM simulation results for Day 195 of 1976. Time series of average observed (circles), range of observed (dashed lines), and model-simulated (solid line) hour-average concentrations of CO.

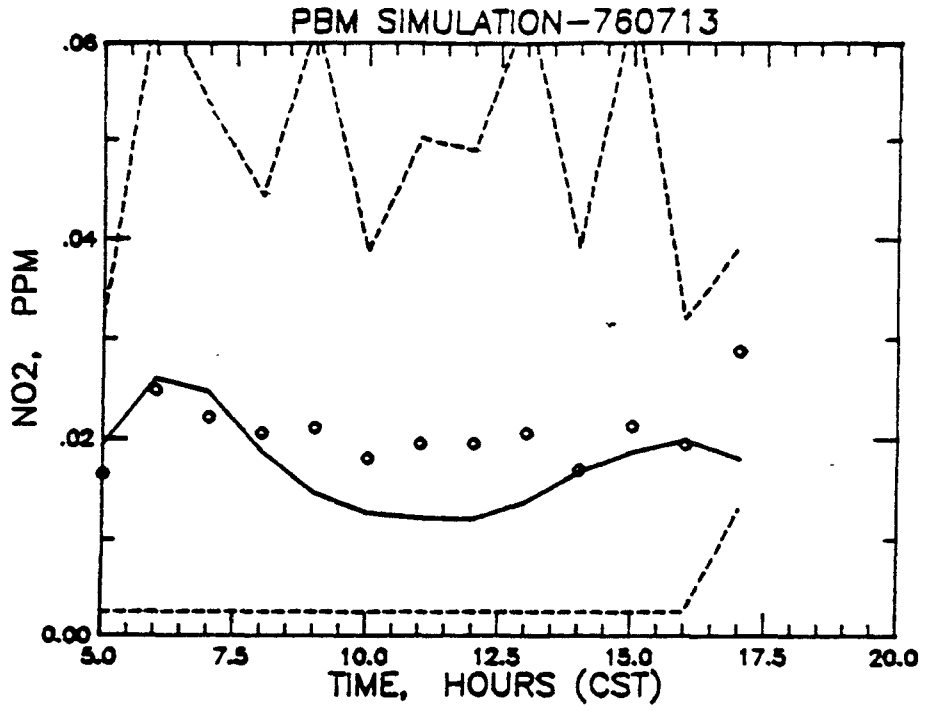

Figure A-11b. PBM simulation results for NO_2 - Day 195 of 1976. Keys to figure described in A-11a.

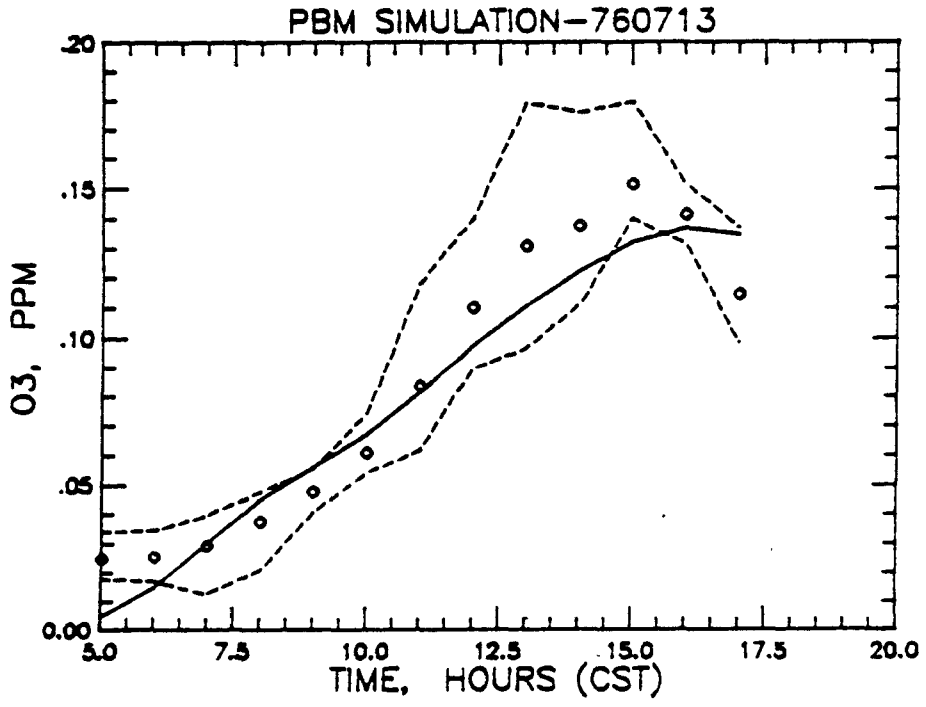

Figure A-11c. PBM simulation results for O_3 - Day 195 of 1976. Keys to figure described in A-11a.

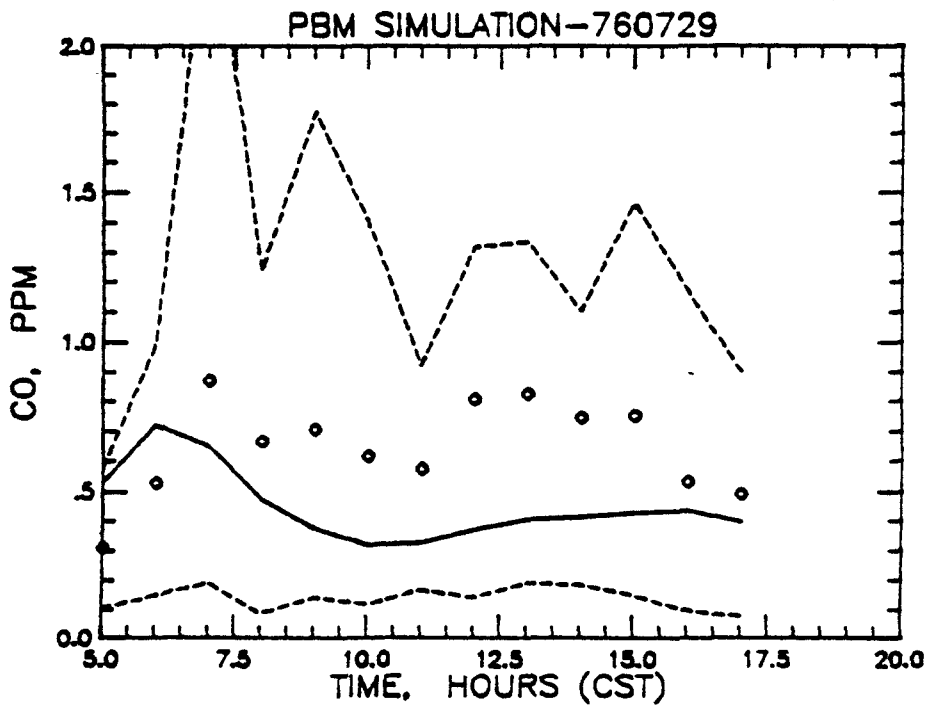

Figure A-12a. PBM simulation results for Day 211 of 1976. Time series of average observed (circles), range of observed (dashed lines), and model-simulated (solid line) hour-average concentrations of CO.

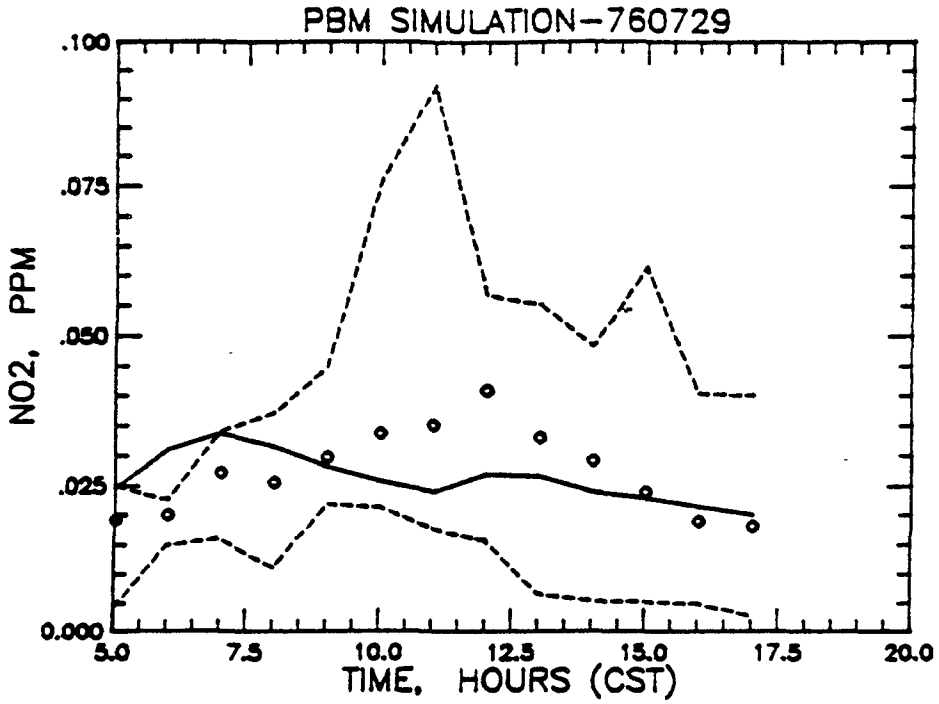

Figure A-12b. PBM simulation results for NO_2 - Day 211 of 1976. Keys to figure described in A-12a.

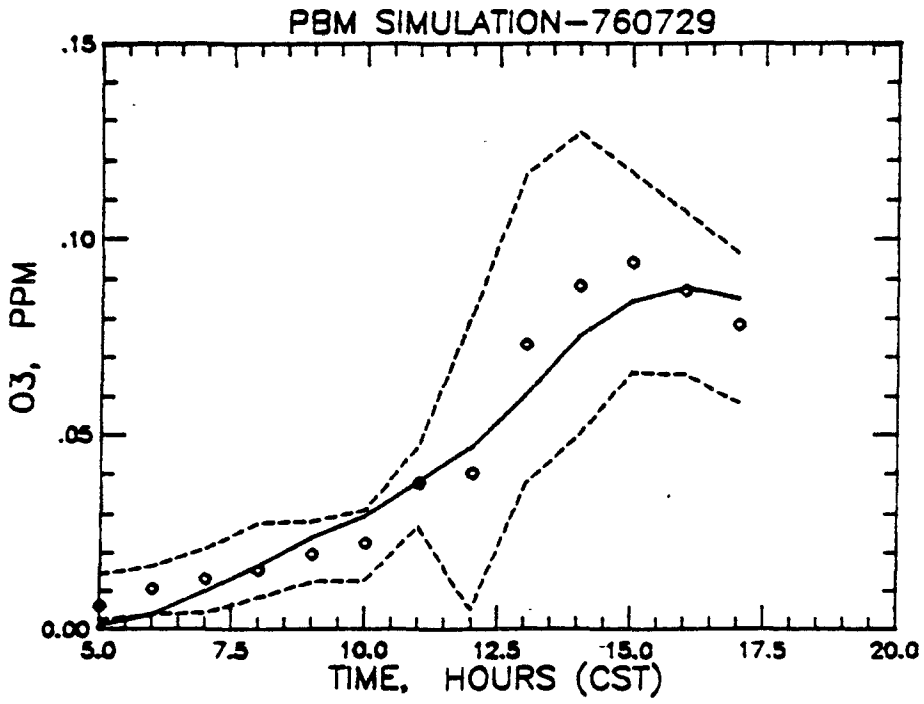

Figure A-12c. PBM simulation results for O_3 - Day 211 of 1976. Keys to figure described in A-12a.

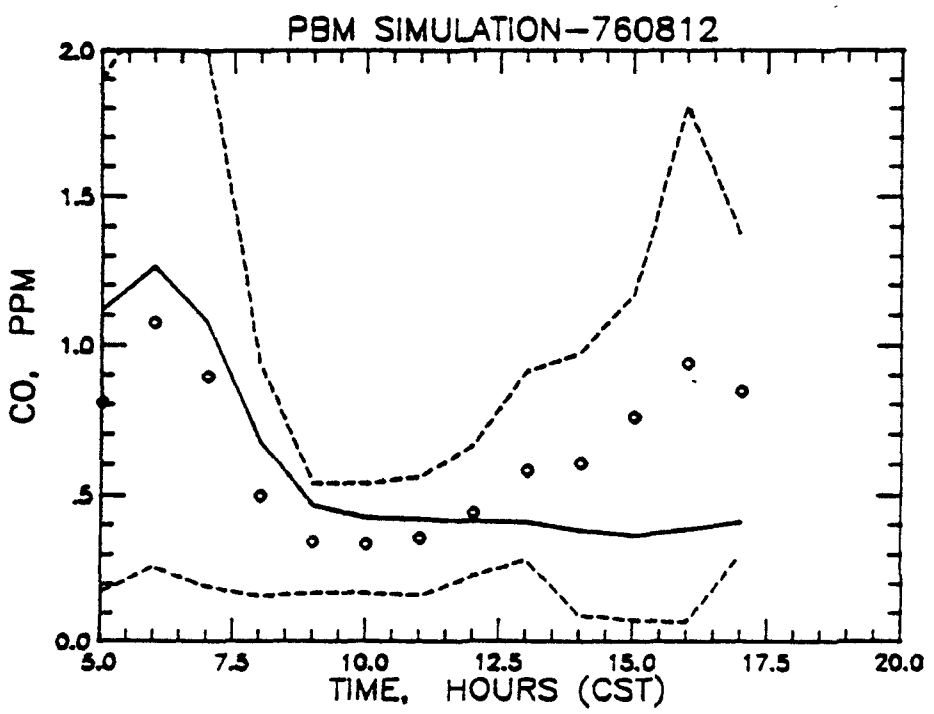

Figure A-13a. PBM simulation results for Day 225 of 1976. Time series of average observed (circles), range of observed (dashed lines), and model-simulated (solid line) hour-average concentrations of CO.

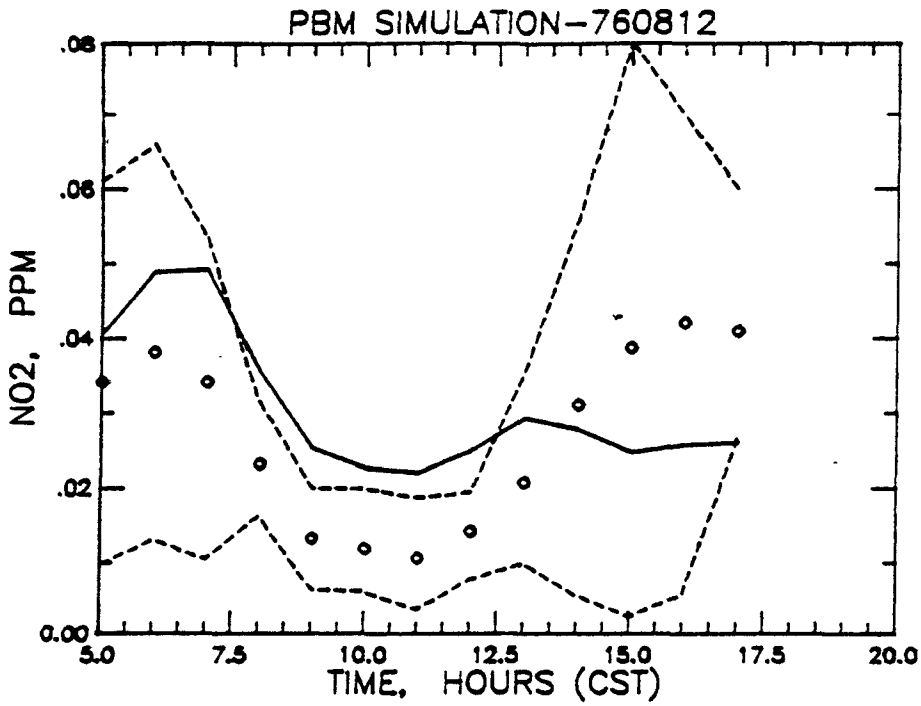

Figure A-13b. PBM simulation results for NO_2 - Day 225 of 1976. Keys to figure described in A-13a.

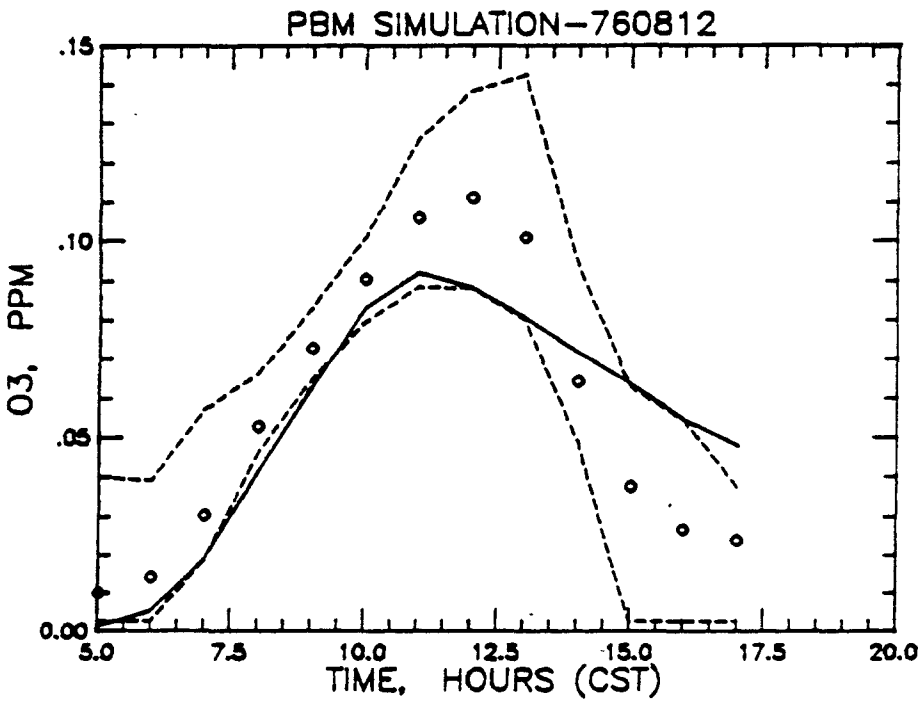

Figure A-13c. PBM simulation results for O_3 - Day 225 of 1976. Keys to figure described in A-13a.

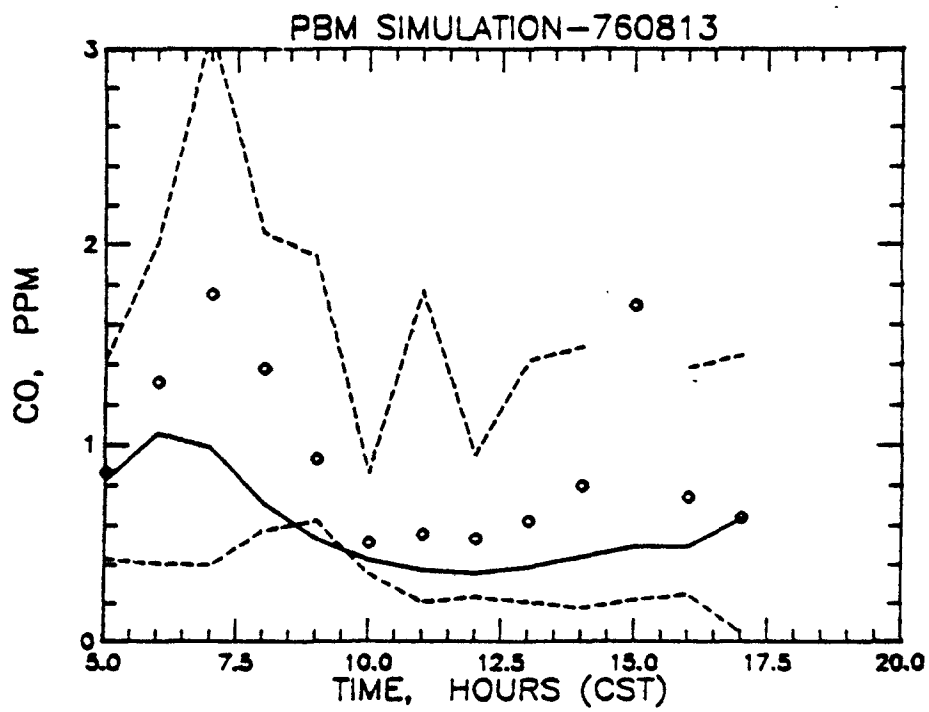

Figure A-14a. PBM simulation results for Day 226 of 1976. Time series of average observed (circles), range of observed (dashed lines), and model-simulated (solid line) hour-average concentrations of CO.

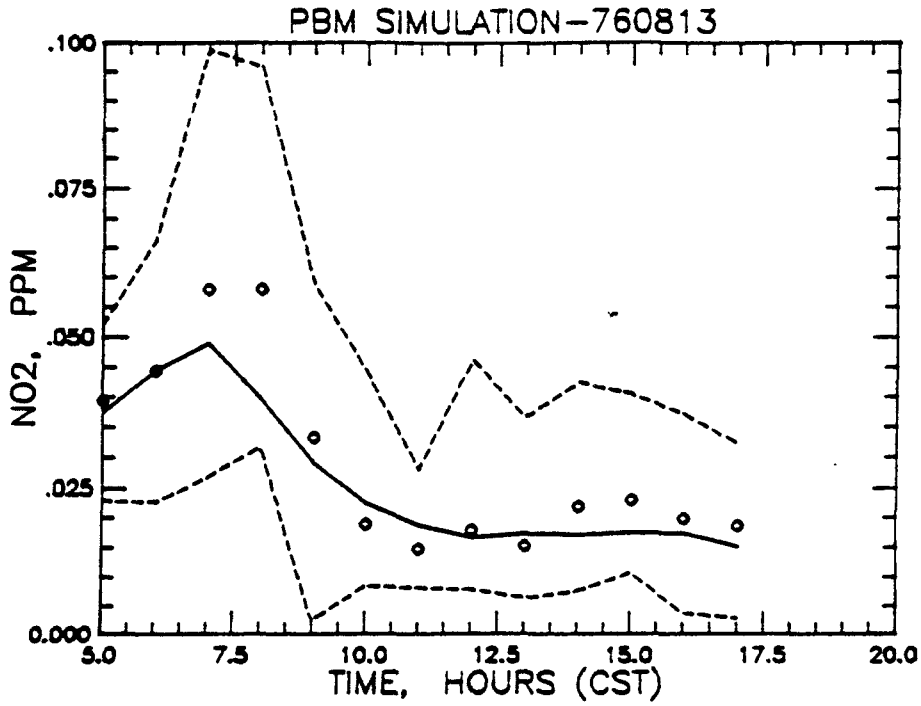

Figure A-14b. PBM simulation results for NO_2 - Day 226 of 1976. Keys to figure described in A-14a.

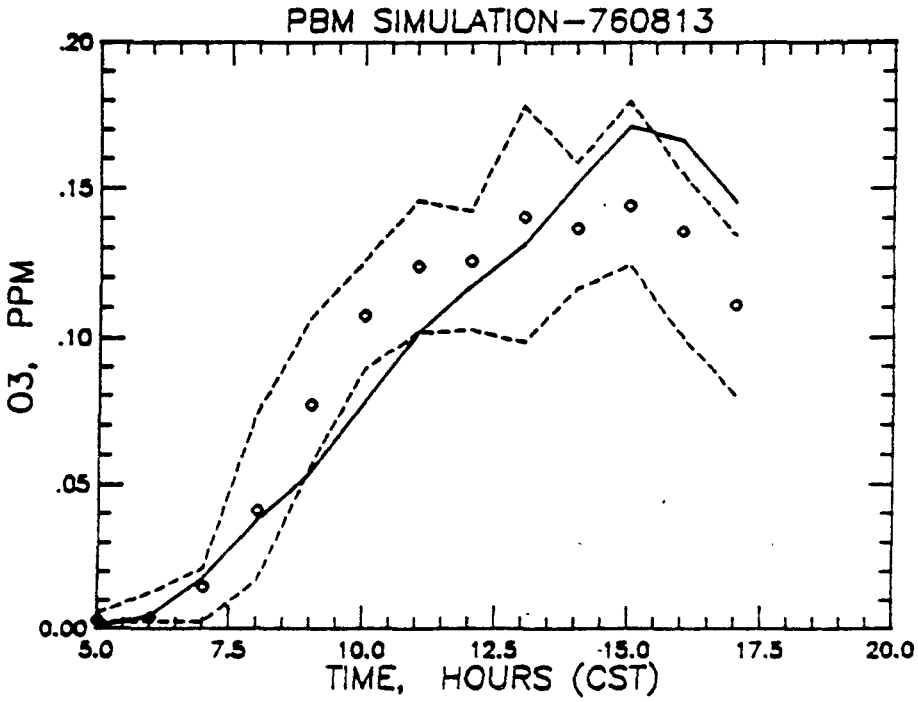

Figure A-14c. PBM simulation results for O_3 - Day 226 of 1976. Keys to figure described in A-14a.

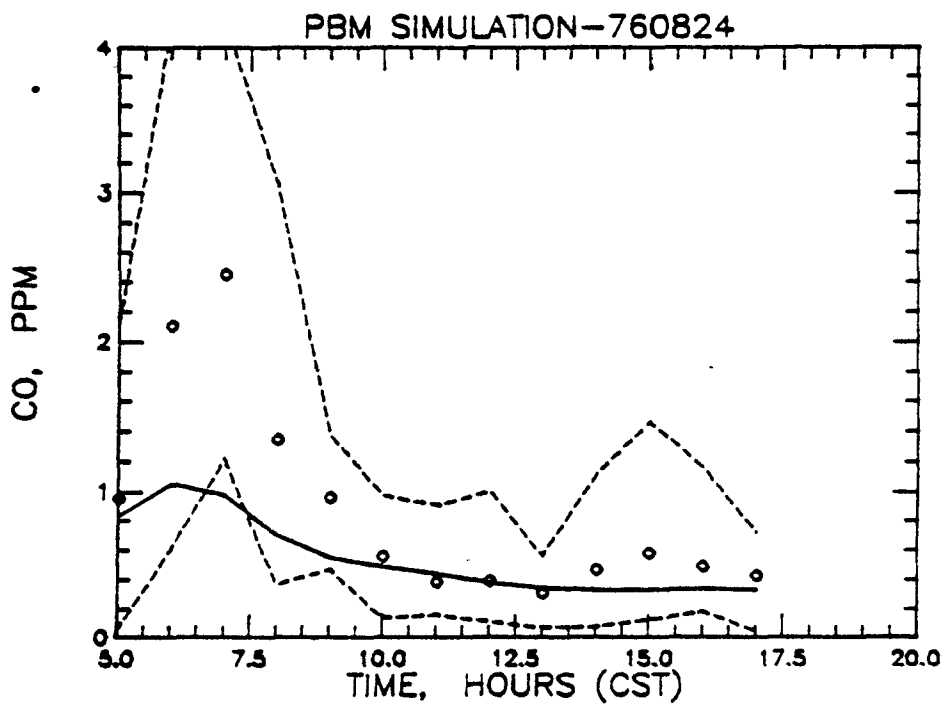

Figure A-15a. PBM simulation results for Day 237 of 1976. Time series of average observed (circles), range of observed (dashed lines), and model-simulated (solid line) hour-average concentrations of CO.

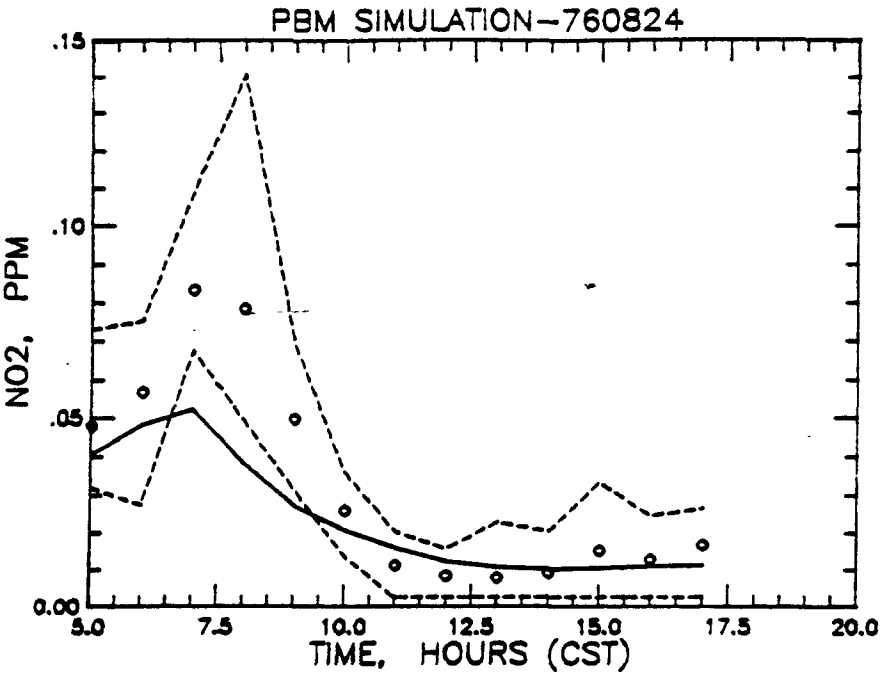

Figure A-15b. PBM simulation results for NO_2 - Day 237 of 1976. Keys to figure described in A-15a.

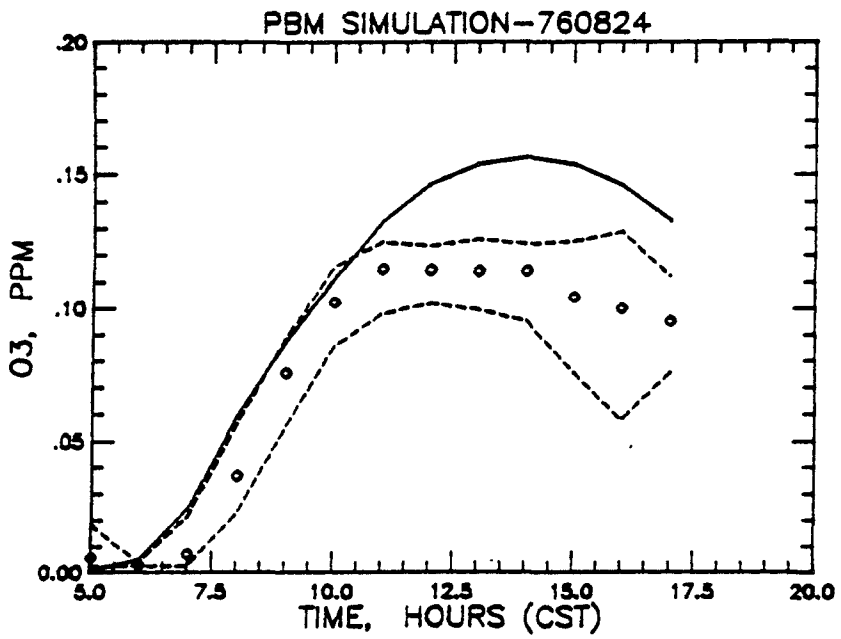

Figure A-15c. PBM simulation results for O_3 - Day 237 of 1976. Keys to figure described in A-15a.

APPENDIX B

PBM - SUMMARY OF STATISTICAL RESULTS

This table summarizes the mean concentration data and the analysis of trends data obtained from PBM simulations on all 20 days for the species NO_2, NO_x, O_3, NMHC and CO. Note that the model internally estimates a measure of NMHC from its explicit structural classes. The table also includes summary statistics on concentration maxima data for all 20 test days for the species NO_2, O_3 and CO. The statistical parameters included in this table are (Bencala and Seinfeld, 1979):

(a) mean observed and mean predicted concentration,

(b) mean residual (measures the average bias in the predictions and indicates whether the model predominantly over- or underpredicts),

(c) root mean square (RMS) error (measures the average spread of the residuals, but is insensitive to bias),

(d) mean residual/mean observed (measures the average percentage of over- or underprediction), and

(e) error band (measures the percentage of predictions that fall within a 25% band around the observations).

The analysis of trends data indicates whether or not the predictions obey the same fundamental relationships as the observations. The parameters contained in this table include:

(a) correlation coefficient (measures the overall degree to which the magnitude of the predictions increases linearly with the magnitude of the observations, but is insensitive to the extent of the increase),

(b) slope (the linear least-squares curve fit measure of the average increase in the observations as the predictions increase),

(c) intercept (the linear least-squares curve fit measure of the bias if the slope parameter is very nearly one; otherwise no independent meaning), and

(d) sum of the squared error (a relative measure of the scatter about the linear least-squares fit to the data).

Concentration maxima data are presented for the species NO_2, O_3 and CO for each test day. The parameters listed here are:

(a) peak observed concentration (and the time of occurrence),

(b) peak predicted concentration (and the time of occurrence),

(c) residual concentration of the peak, and

(d) residual/observed concentration (percentage over- or underprediction of the peak).

In all tables a positive residual indicates an underprediction by the model and a negative residual indicates an overprediction.

TABLE B-1. SUMMARY OF MODEL PERFORMANCE STATISTICS FROM THE PBM[a]

Mean Concentration Data

Species	Mean observed concentration (ppm)	Mean predicted concentration (ppm)	Mean residual (ppm)	RMS error (ppm)	Mean residual / Mean obs. conc. (%)	Error band[b] (%)
NO_2	0.0285	0.0281	0.00039	0.00931	1.4	60.0
NO_x	0.0440	0.0412	0.00284	0.0148	6.5	56.5
O_3	0.0725	0.0879	-0.0154	0.0289	-21.2	45.4
NMHC	0.402	0.350	0.0520	0.188	12.9	43.1
CO	0.869	0.676	0.193	0.356	22.2	43.5

Analysis of Trends Data

Species	Correlation coefficient	Slope	Intercept (ppm)	Sum of squared error (ppm^2)
NO_2	0.876	0.753	0.00734	0.0276
NO_x	0.923	0.832	0.00976	0.0685
O_3	0.871	1.09	-0.0230	0.269
NMHC	0.837	0.666	0.169	12.1
CO	0.848	0.599	0.464	50.6

TABLE B-1. (Continued)

SUMMARY OF MODEL PERFORMANCE STATISTICS FROM THE PBM[a]

Concentration Maxima Data

Julian date	Species	Observed Peak Concentration Value (ppm)	Observed Peak Concentration Time (CST)	Predicted Peak Concentration Value (ppm)	Predicted Peak Concentration Time (CST)	Residual (ppm)	Residual / Obs. conc. (%)
142-75	NO_2	0.0367	0600	0.0421	0700	-0.0054	-14.7
	O_3	0.137	1200	0.148	1300	-0.0110	-8.0
	CO	1.31	0700	1.18	0600	0.130	9.9
178-75	NO_2	0.0535	0700	0.0456	0600	0.0079	14.8
	O_3	0.159	1400	0.173	1600	-0.0140	-8.8
	CO	1.85	0600	1.07	0600	0.780	42.2
182-75	NO_2	0.0408	0600	0.0532	0600	-0.0124	-30.4
	O_3	0.0939	1300	0.140	1600	-0.0461	-49.1
	CO	0.979	0700	1.68	1500	-0.7001	-71.6
183-75	NO_2	0.0526	0800	0.0594	0600	-0.0068	-12.9
	O_3	0.115	1300	0.0971	1700	0.0179	-15.6
	CO	1.57	0700	1.09	0600	0.480	30.6
184-75	NO_2	0.0792	0700	0.0753	0600	0.0039	4.9
	O_3	0.114	1300	0.182	1300	-0.0680	-59.6
	CO	2.68	0700	2.11	0500	0.570	21.3
207-75	NO_2	0.0416	0600	0.0509	0600	-0.00093	-22.4
	O_3	0.140	1400	0.145	1500	-0.0050	-3.6
	CO	1.24	0500	1.02	0500	0.220	17.7
209-75	NO_2	0.0304	0800	0.0406	0700	-0.0102	-33.6
	O_3	0.108	1000	0.122	1300	-0.0140	-13.0
	CO	0.976	0800	1.06	0600	-0.0840	-8.6

TABLE B-1. (Continued)

SUMMARY OF MODEL PERFORMANCE STATISTICS FROM THE PBM[a]

Concentration Maxima Data

Julian date	Species	Observed Peak Concentration Value (ppm)	Observed Peak Concentration Time (CST)	Predicted Peak Concentration Value (ppm)	Predicted Peak Concentration Time (CST)	Residual (ppm)	Residual / Obs. conc. (%)
221-75	NO_2	0.0453	0700	0.0469	0700	-0.0016	-3.5
	O_3	0.132	1300	0.125	1300	0.0070	5.3
	CO	1.94	0600	1.62	0500	0.320	16.5
230-75	NO_2	0.0541	0700	0.0499	0700	0.0042	7.8
	O_3	0.0717	1300	0.119	1500	-0.0473	-66.0
	CO	2.08	0600	1.72	0600	0.360	17.3
231-75	NO_2	0.0394	0800	0.0364	0700	0.0030	7.6
	O_3	0.0842	1000	0.101	1300	-0.0168	-20.0
	CO	1.04	0900	1.06	0600	-0.0200	-1.9
251-75	NO_2	0.0667	0900	0.0461	0700	0.0206	30.9
	O_3	0.0841	1500	0.205	1500	-0.121	-143.9
	CO	2.85	0600	1.72	0600	1.13	39.6
159-76	NO_2	0.0938	0700	0.0816	0600	0.0122	13.0
	O_3	0.125	1300	0.210	1200	-0.0850	-68.0
	CO	2.78	0600	1.98	0500	0.800	28.8
160-76	NO_2	0.0652	0700	0.0693	0600	-0.0041	-6.3
	O_3	0.162	1400	0.170	1500	-0.0080	-4.9
	CO	1.56	0600	1.50	0500	0.0600	3.8
195-76	NO_2	0.0287	1700	0.0260	0600	0.0027	9.4
	O_3	0.151	1500	0.137	1600	0.0140	9.3
	CO	0.555	0700	0.522	0600	0.0330	5.9

TABLE 8-1. (Continued)

SUMMARY OF MODEL PERFORMANCE STATISTICS FROM THE PBM[a]

Concentration Maxima Data

Julian date	Species	Observed Peak Concentration Value (ppm)	Observed Peak Concentration Time (CST)	Predicted Peak Concentration Value (ppm)	Predicted Peak Concentration Time (CST)	Residual (ppm)	Residual / Obs. conc. (%)
211-76	NO_2	0.0409	1200	0.0338	0700	0.0071	17.6
	O_3	0.0939	1500	0.0878	1600	0.0061	6.5
	CO	0.869	0700	0.719	0600	0.150	17.3
212-76	NO_2	0.0609	0700	0.0528	0600	0.0081	13.3
	O_3	0.127	1200	0.121	1400	0.0060	4.7
	CO	1.73	0600	1.42	0500	0.310	17.9
225-76	NO_2	0.0421	1600	0.0491	0700	-0.0070	-16.6
	O_3	0.111	1200	0.0919	1100	0.0191	17.2
	CO	1.08	0600	1.26	0600	-0.180	-16.7
226-76	NO_2	0.0580	0700	0.0489	0700	0.0091	15.7
	O_3	0.144	1500	0.171	1500	-0.0270	-18.8
	CO	1.75	0700	1.05	0600	0.700	40.0
237-76	NO_2	0.0832	0700	0.0521	0700	0.0311	37.4
	O_3	0.115	1100	0.156	1400	-0.0410	-35.7
	CO	2.45	0700	1.05	0600	1.40	57.1
275-76	NO_2	0.108	1700	0.0869	1000	0.0211	19.5
	O_3	0.183	1400	0.223	1500	-0.0400	-21.9
	CO	4.17	0700	3.00	0700	1.17	28.1

[a]Statistics for Mean Concentration and Analysis of Trends data are developed for all 20 test days;
Statistics for Concentration Maxima are listed for each test day.
All concentration values represent an average over the model domain.

[b]Percent of predictions within 25% of observations.

APPENDIX C

LPM TEMPORAL CORRELATION COEFFICIENTS AND TIME SERIES FOR REMAINING TEST DAYS

This appendix presents temporal correlation coefficients for O_3, NO, and NO_2 for all 20 days and time series from LPM simulations for the 15 days not presented in the body of the report.

The temporal correlation coefficients were computed between observed and predicted series from the start time to the lesser of 1700 CST or the end of the run. These coefficients for Levels 1 and 3 appear in Table C-1. The choice of a termination time can have significant influence on the correlation. For instance, the correlation for O_3 on Day 231 is below the average for the 20 days, but the simulation was fairly successful. A part of the problem with the correlation is the discrepancy between prediction and observation after the time of the observed maximum. As explained previously for Day 231, this discrepancy is expected because the modeled parcel has moved away from the stations contributing to the "observed" value. The correlations for NO and NO_2 tend to be low, perhaps reflecting the low concentrations and the consequent difficulty in obtaining accurate measurements.

TABLE C-1. TEMPORAL CORRELATION COEFFICIENT BETWEEN OBSERVED AND LPM PREDICTED POLLUTANT CONCENTRATIONS FOR THE PERIOD FROM THE START OF THE SIMULATION TO 1700 CST OR EARLIER TERMINATION.

Day	O_3		NO		NO_2	
	L-1	L-3	L-1	L-3	L-1	L-3
142 (1975)	0.53	0.66	-0.03	0.34	-0.26	-0.03
178	0.52	0.88	0.54	0.51	-0.39	-0.71
182	0.99	0.98	0.95	0.70	0.94	0.94
183	0.95	0.97	0.90	0.39	0.65	0.65
184	0.89	0.83	0.90	0.48	0.77	0.81
207	0.73	0.78	0.18	0.41	0.32	0.53
209	0.64	0.58	0.53	0.17	0.93	0.93
221	0.82	0.76	0.82	0.56	0.77	0.85
230	0.85	0.83	0.30	0.20	0.43	0.42
231	0.64	0.58	0.79	0.15	0.62	0.57
251	0.67	0.64	0.91	0.87	0.84	0.92
159 (1976)	0.97	0.97	0.94	0.88	0.89	0.92
160	0.94	0.92	-0.12	-0.02	-0.09	0.23
195	0.94	0.95	0.77	0.50	0.61	0.44
211	0.90	0.89	0.50	-0.28	0.70	0.78
212	0.80	0.73	-0.01	0.07	0.30	0.30
225	0.11	0.06	0.13	0.34	-0.36	0.07
226	0.92	0.83	0.78	0.48	0.28	0.88
237	0.89	0.84	0.73	0.70	0.83	0.87
275	0.90	0.80	0.45	0.88	0.66	0.87
$\bar{r}$ =	0.78	0.77	0.49	0.42	0.47	0.56
σ_r	0.21	0.20	0.42	0.30	0.42	0.42

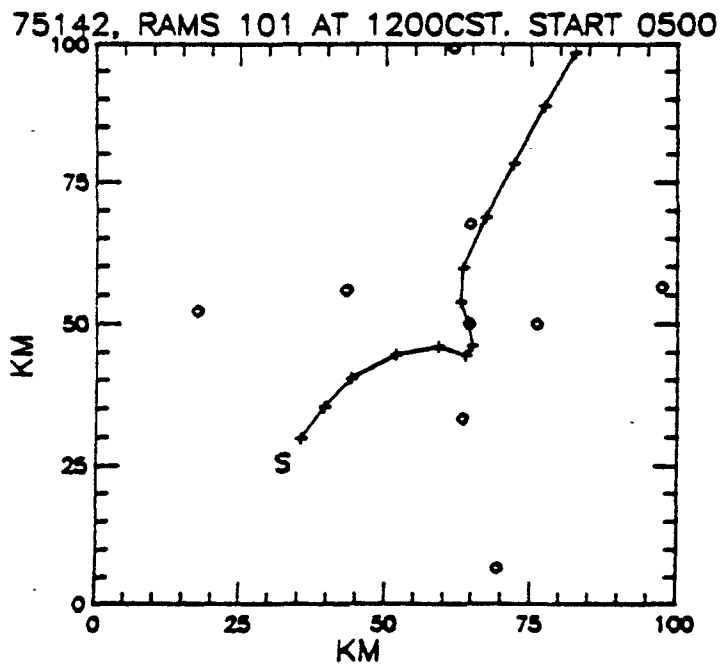

Figure C-1a. LPM parcel trajectory for Day 142 of 1975.

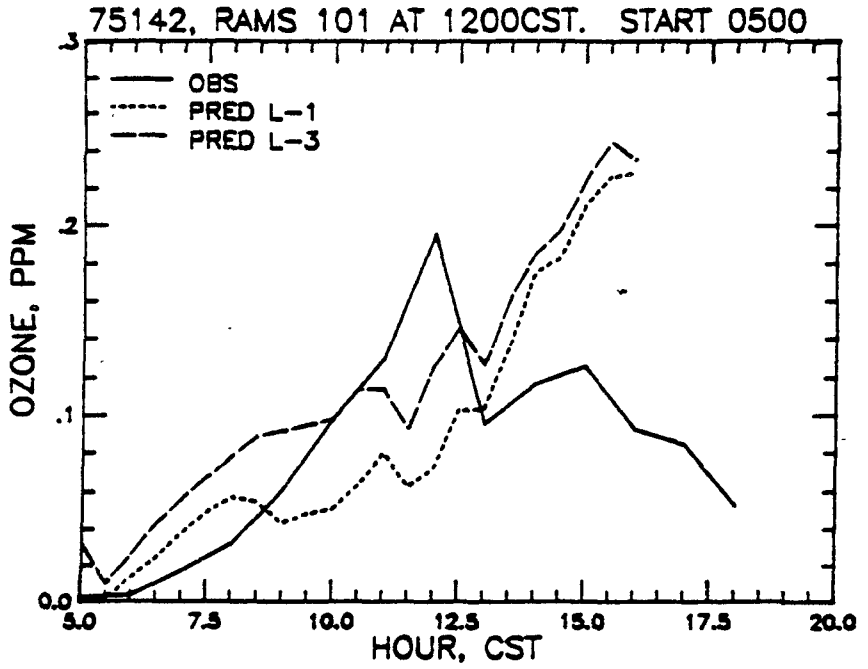

Figure C-1b. LPM time series of observed and predicted O_3 hourly concentrations on Day 142 of 1975.

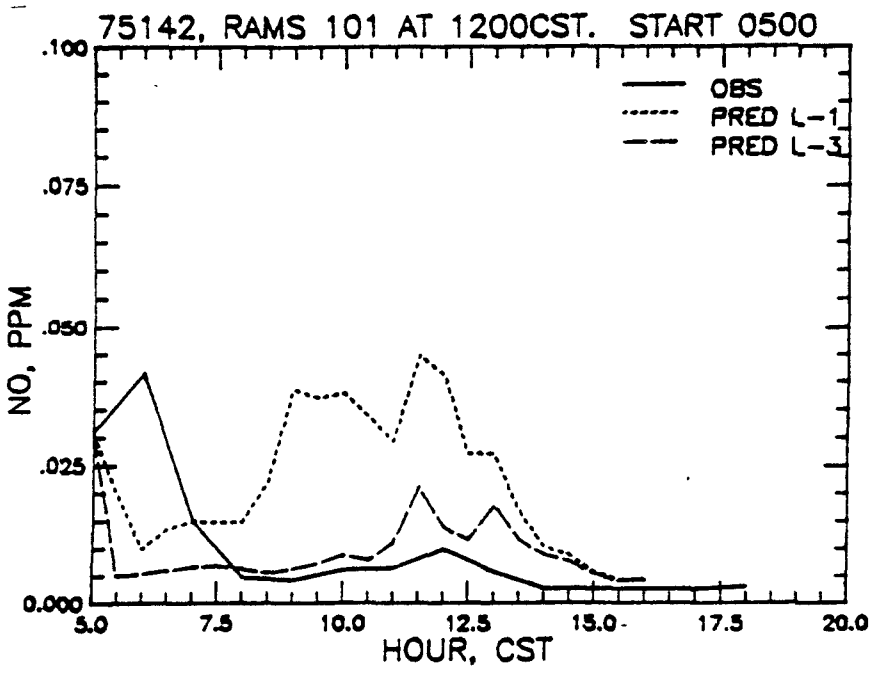

Figure C-1c. LPM time series of observed and predicted NO hourly concentrations on Day 142 of 1975.

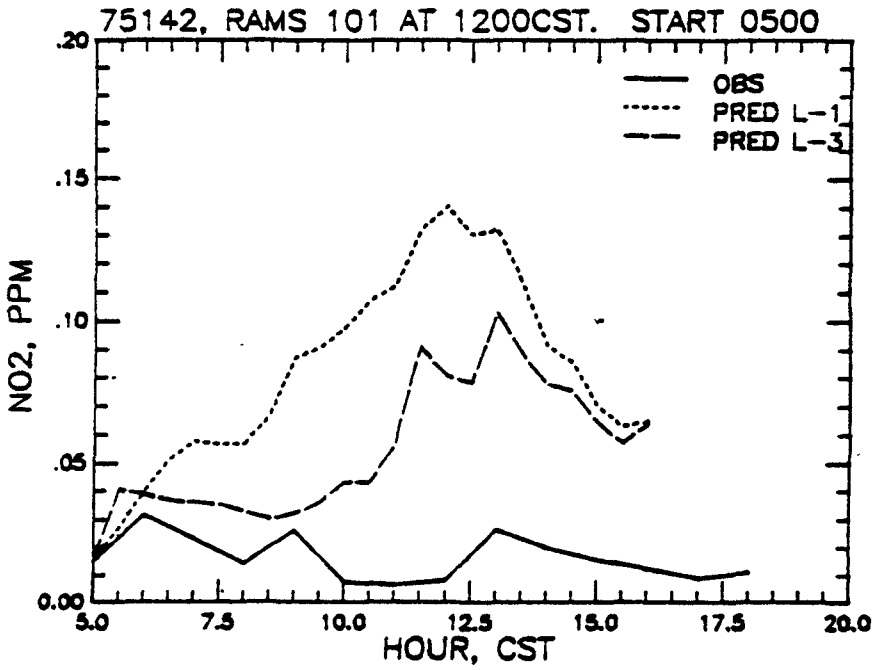

Figure C-1d. LPM time series of observed and predicted NO_2 hourly concentrations on Day 142 of 1975.

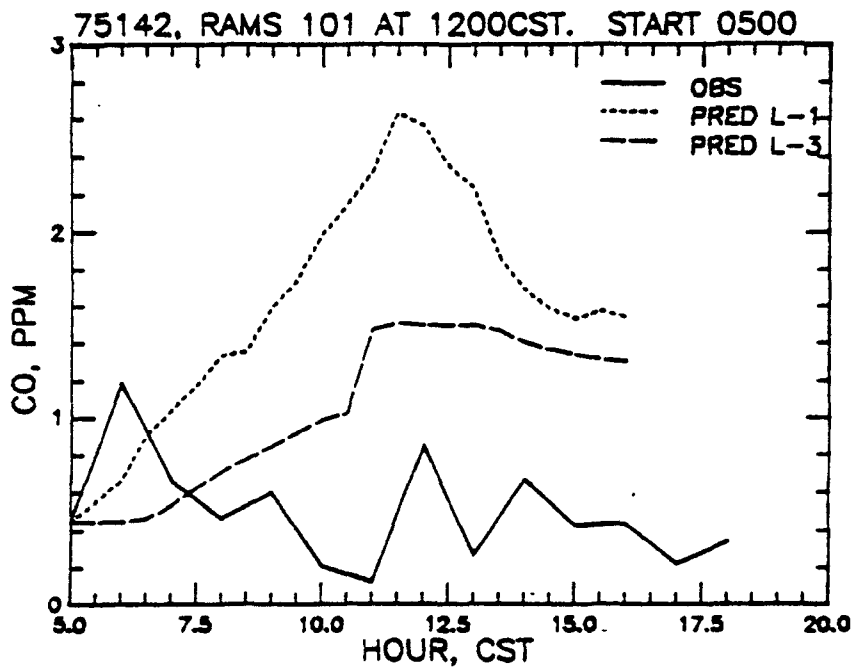

Figure C-1e. LPM time series of observed and predicted CO hourly concentrations on Day 142 of 1975.

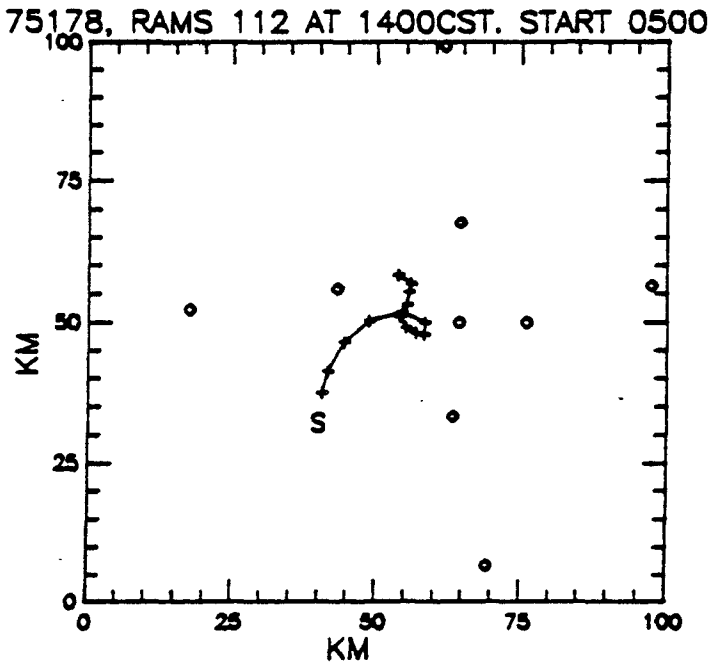

Figure C-2a. LPM parcel trajectory for Day 178 of 1975.

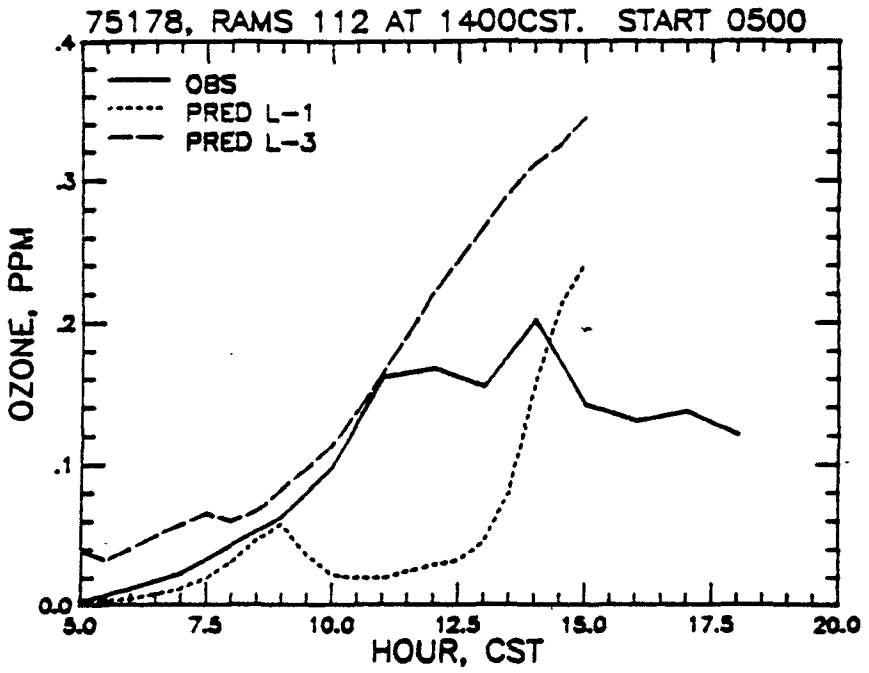

Figure C-2b. LPM time series of observed and predicted O_3 hourly concentrations on Day 178 of 1975.

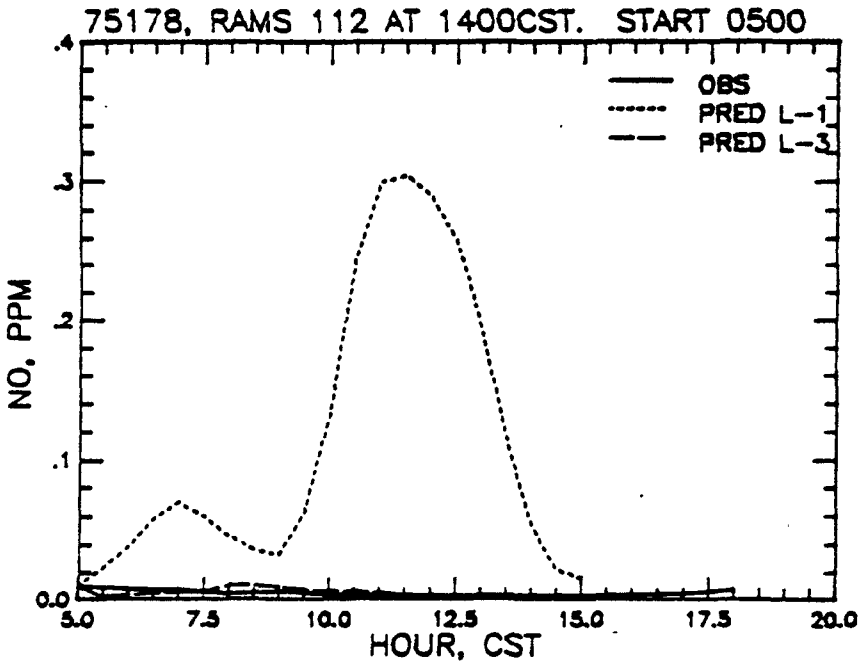

Figure C-2c. LPM time series of observed and predicted NO hourly concentrations on Day 178 of 1975.

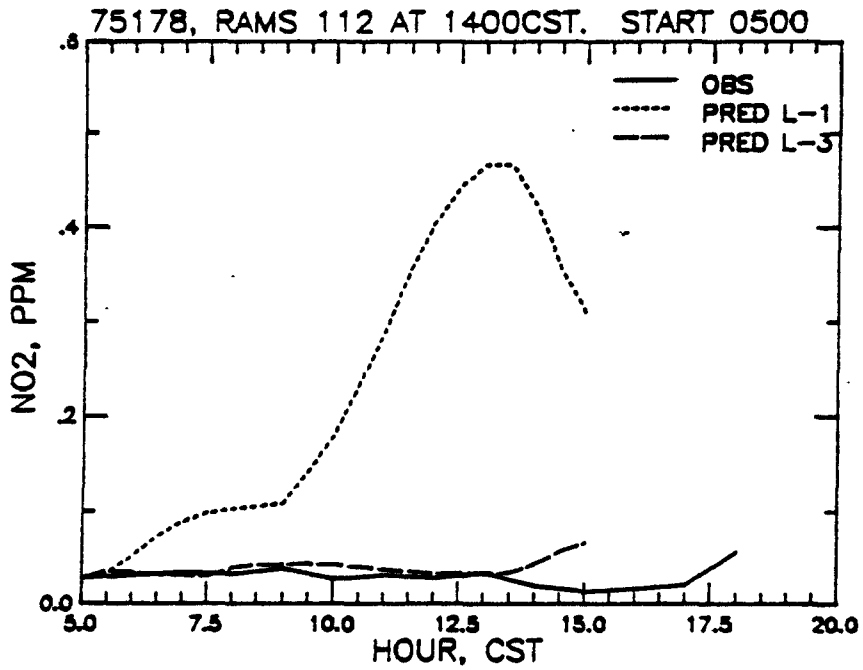

Figure C-2d. LPM time series of observed and predicted NO_2 hourly concentrations on Day 178 of 1975.

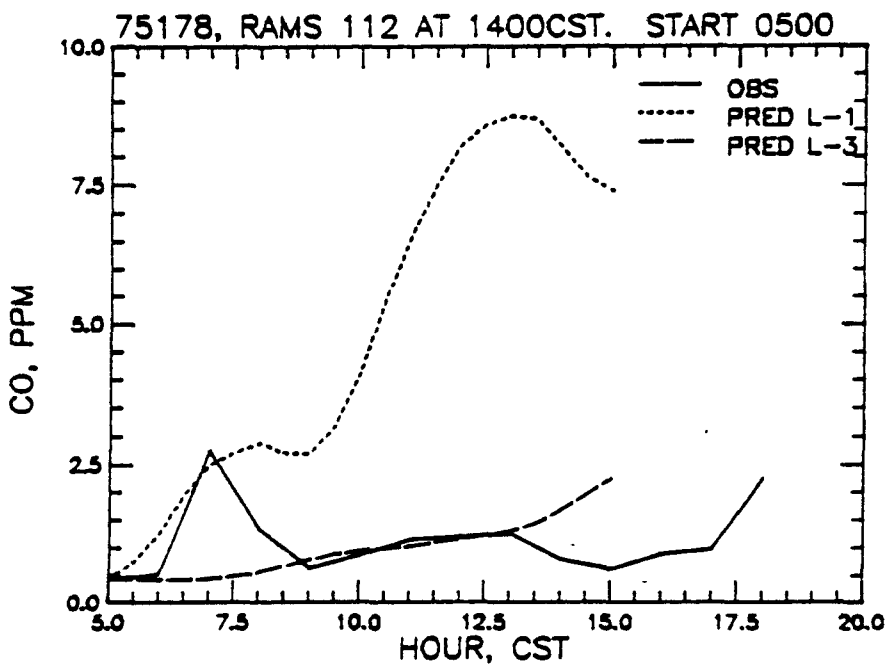

Figure C-2e. LPM time series of observed and predicted CO hourly concentrations on Day 178 of 1975.

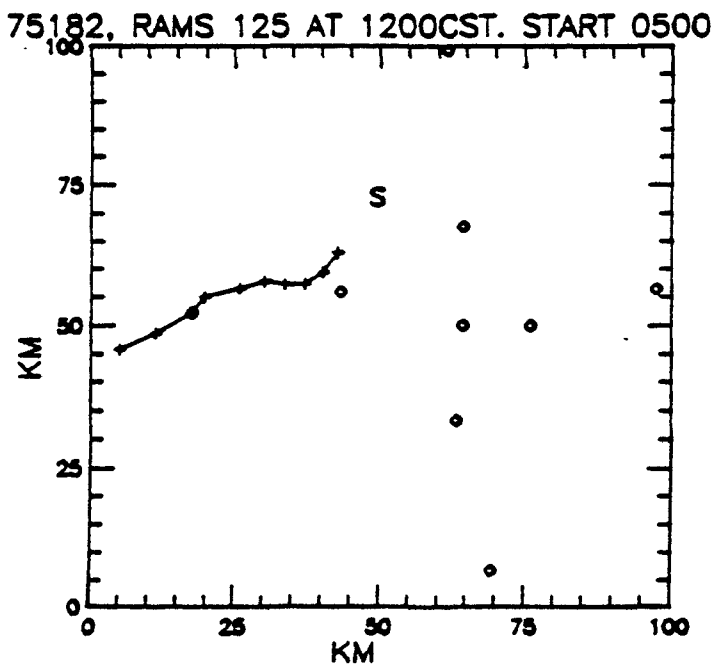

Figure C-3a. LPM parcel trajectory for Day 182 of 1975.

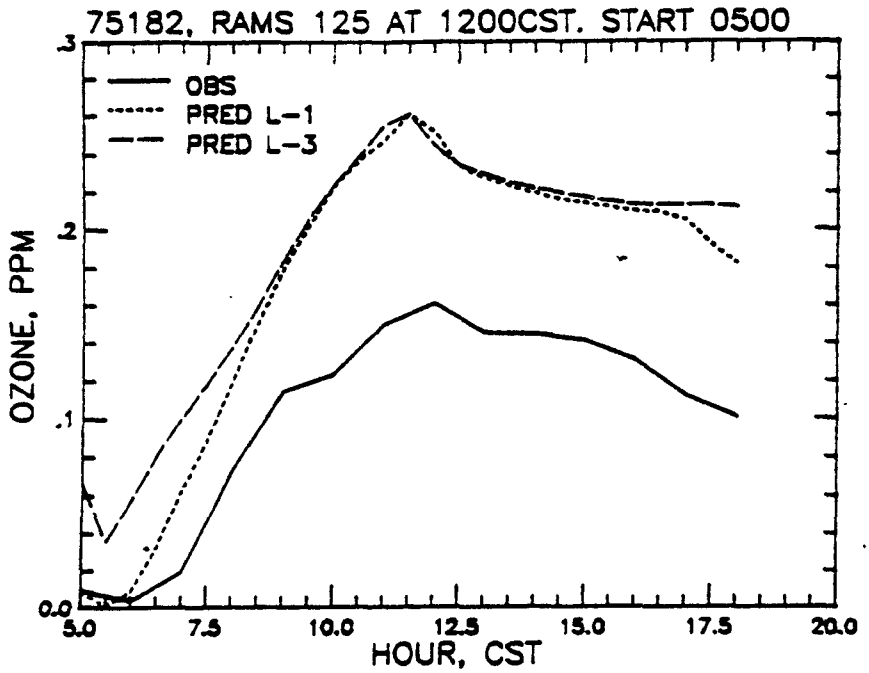

Figure C-3b. LPM time series of observed and predicted O_3 hourly concentrations on Day 182 of 1975.

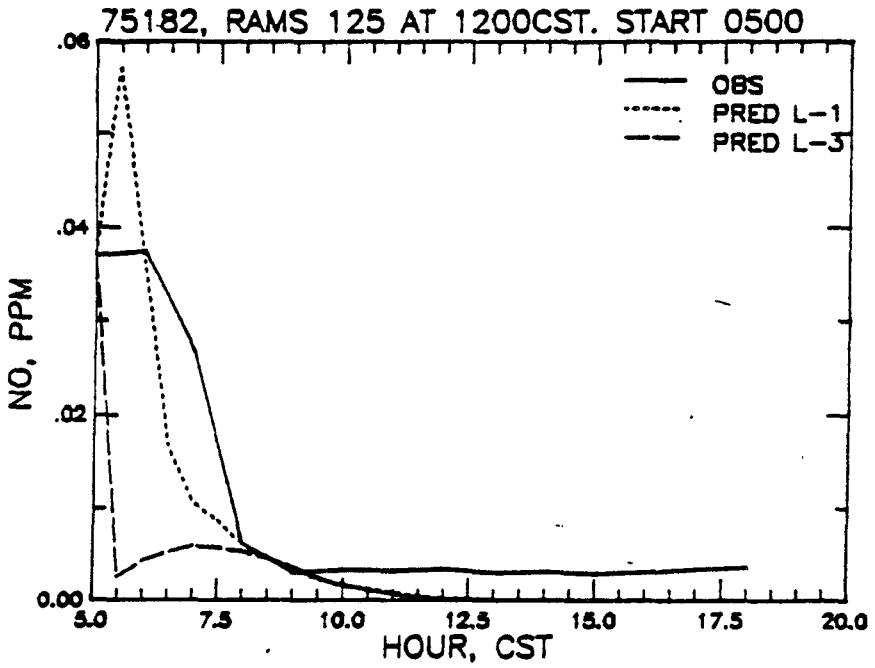

Figure C-3c. LPM time series of observed and predicted NO hourly concentrations on Day 182 of 1975.

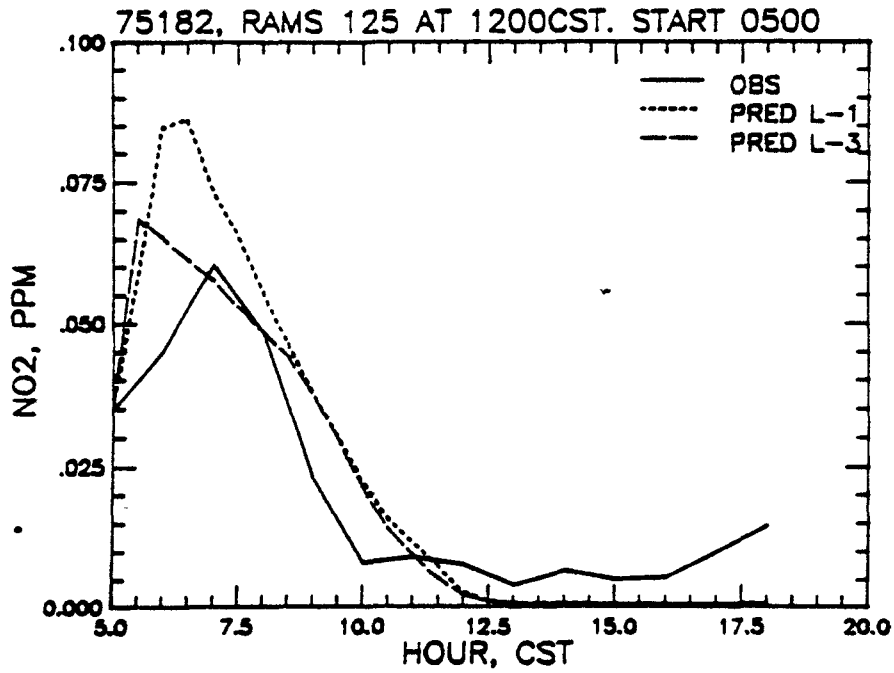

Figure C-3d. LPM time series of observed and predicted NO_2 hourly concentrations on Day 182 of 1975.

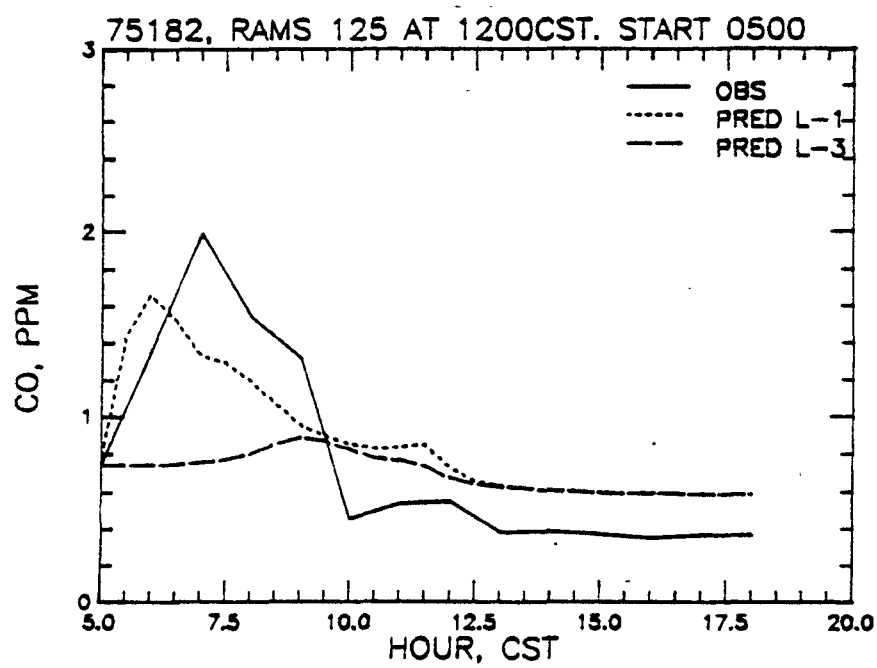

Figure C-3e. LPM time series of observed and predicted O_3 hourly concentrations on Day 182 of 1975.

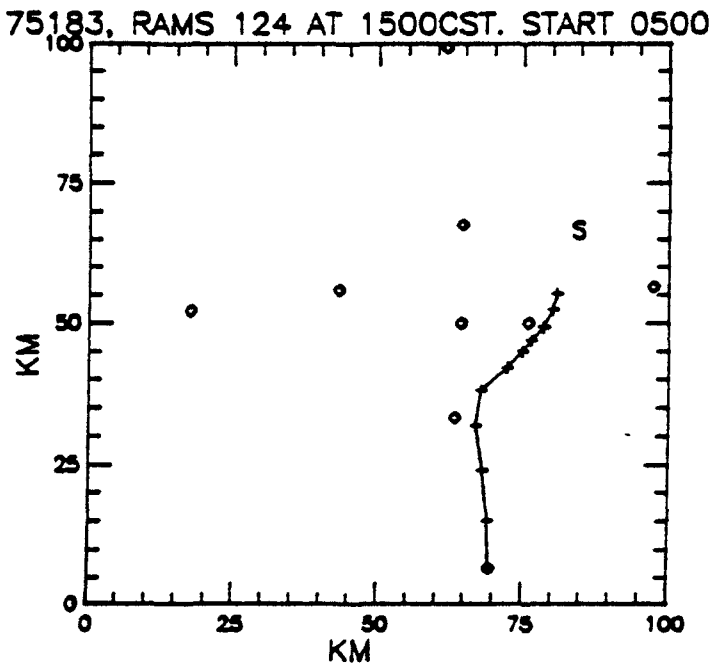

Figure C-4a. LPM parcel trajectory for Day 183 of 1975.

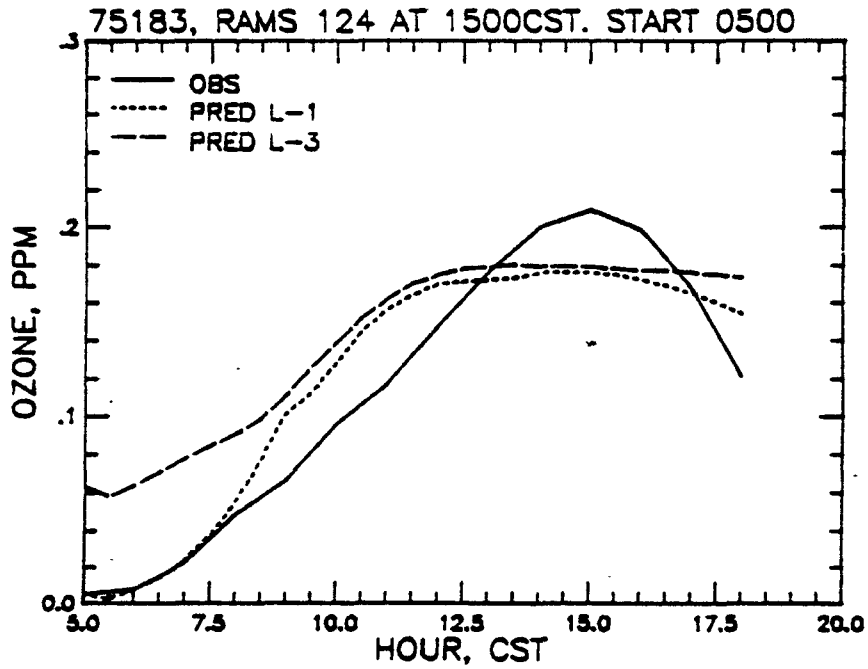

Figure C-4b. LPM time series of observed and predicted O_3 hourly concentrations on Day 183 of 1975.

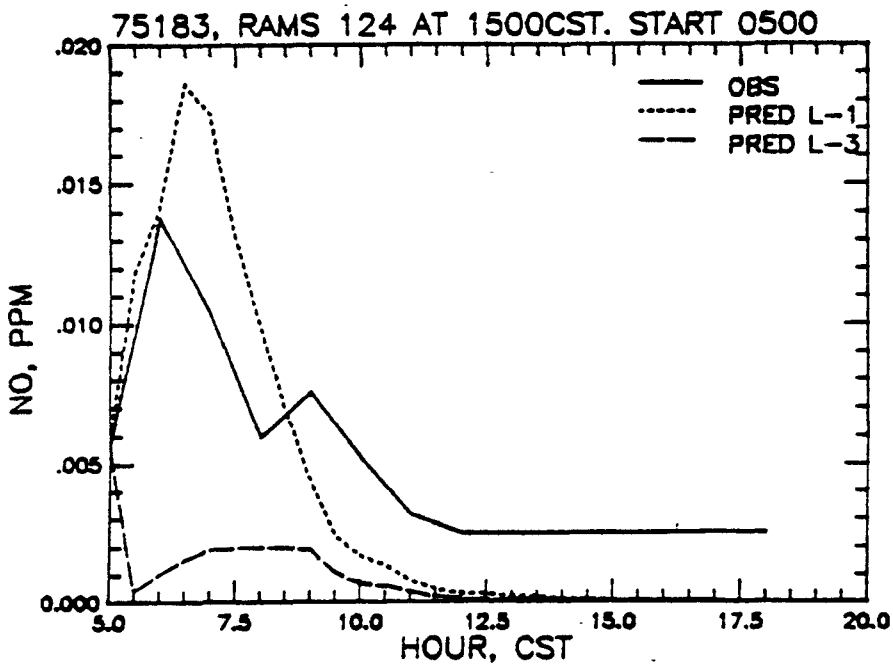

Figure C-4c. LPM time series of observed and predicted NO hourly concentrations on Day 183 of 1975.

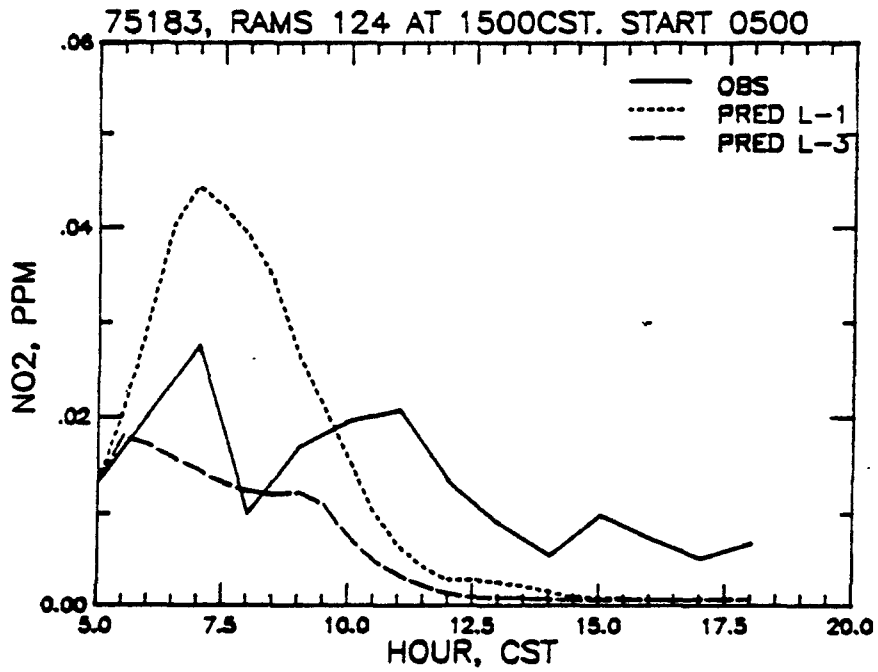

Figure C-4d. LPM time series of observed and predicted NO_2 hourly concentrations on Day 183 of 1975.

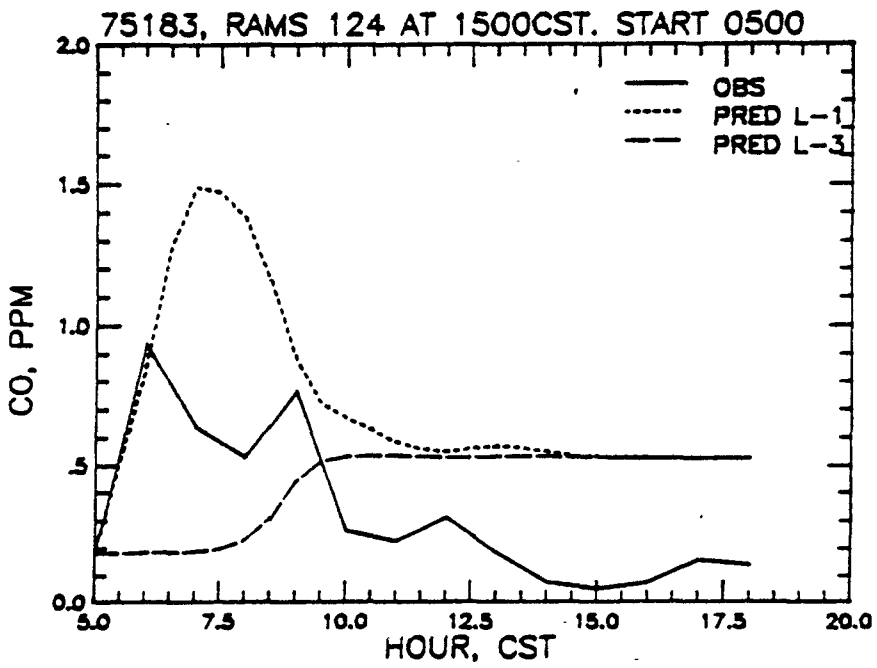

Figure C-4e. LPM time series of observed and predicted CO hourly concentrations on Day 183 of 1975.

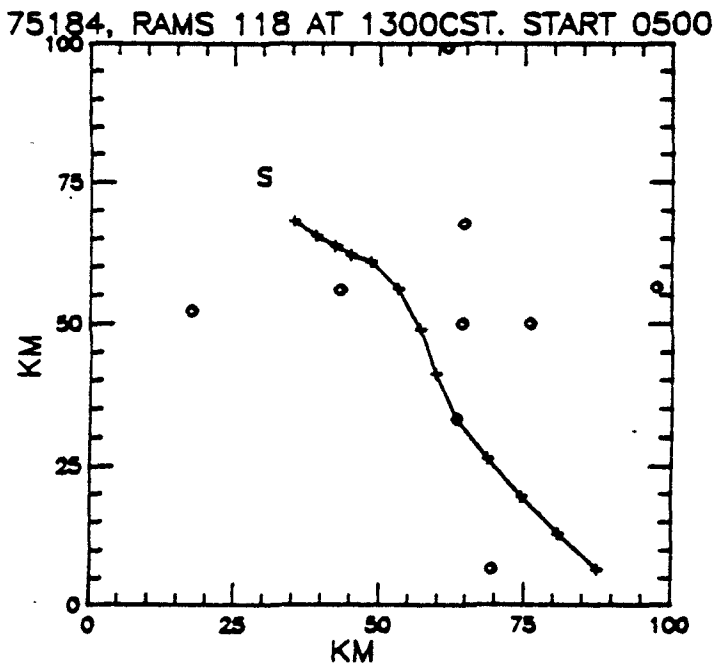

Figure C-5a. LPM parcel trajectory for Day 184 of 1975.

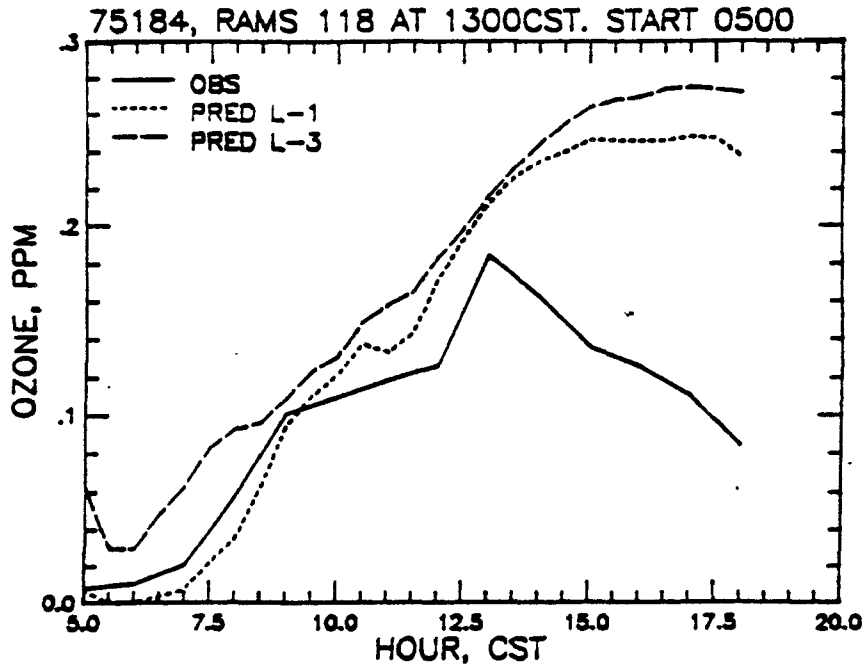

Figure C-5b. LPM time series of observed and predicted O_3 hourly concentrations on Day 184 of 1975.

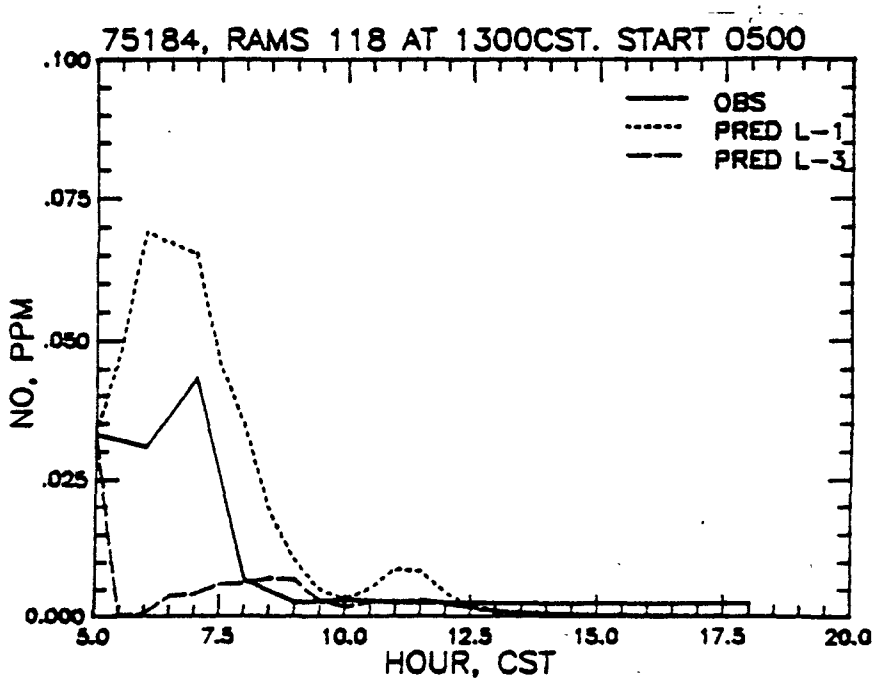

Figure C-5c. LPM time series of observed and predicted NO hourly concentrations on Day 184 of 1975.

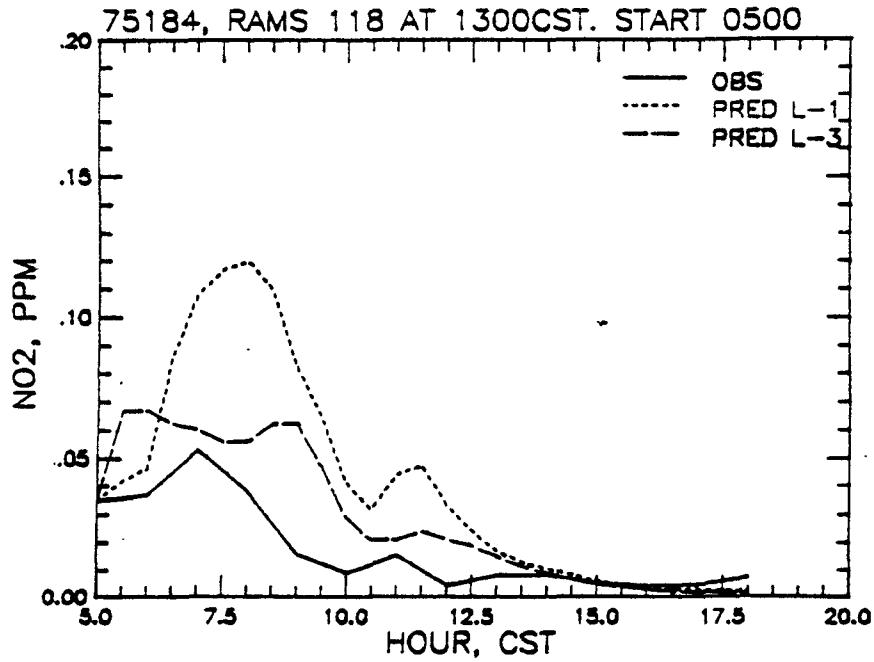

Figure C-5d. LPM time series of observed and predicted NO_2 hourly concentrations on Day 184 of 1975.

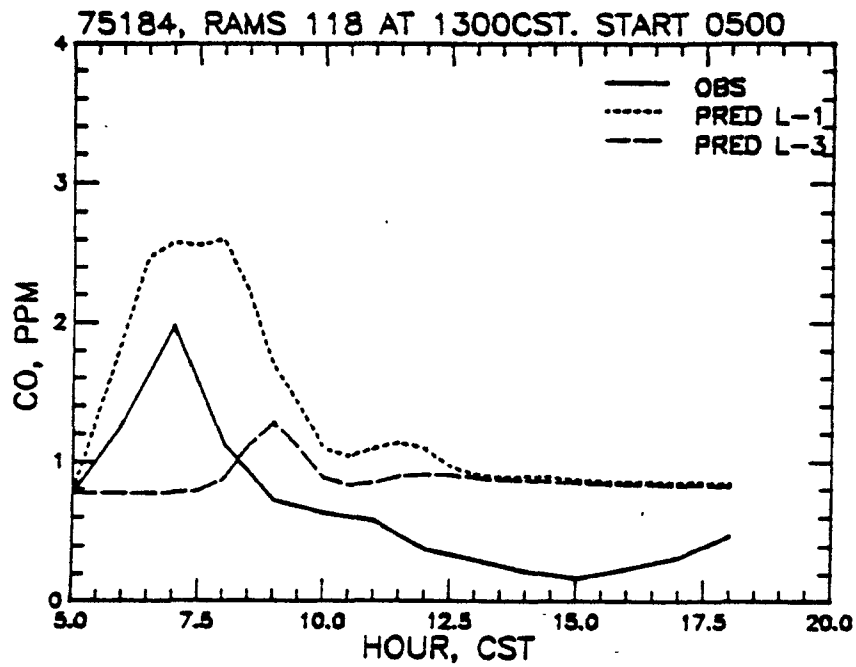

Figure C-5e. LPM time series of observed and predicted CO hourly concentrations on Day 184 of 1975.

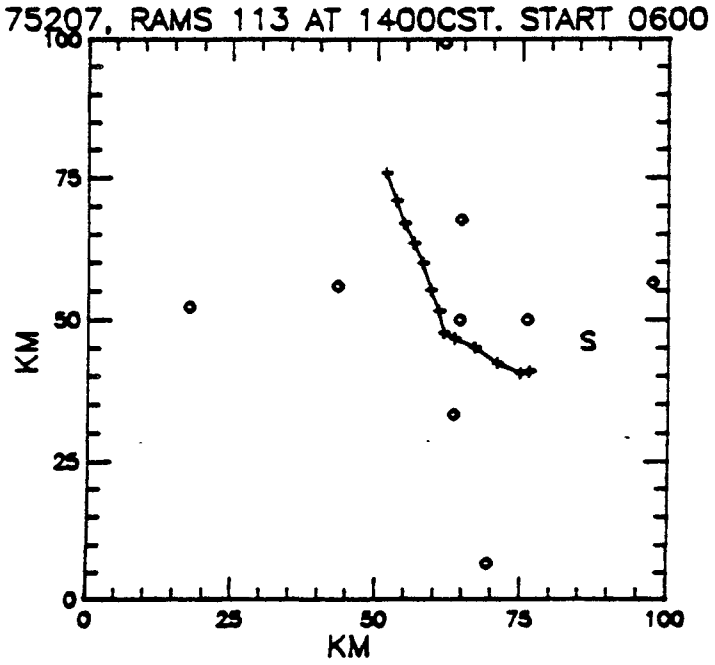

Figure C-6a. LPM parcel trajectory for Day 207 of 1975.

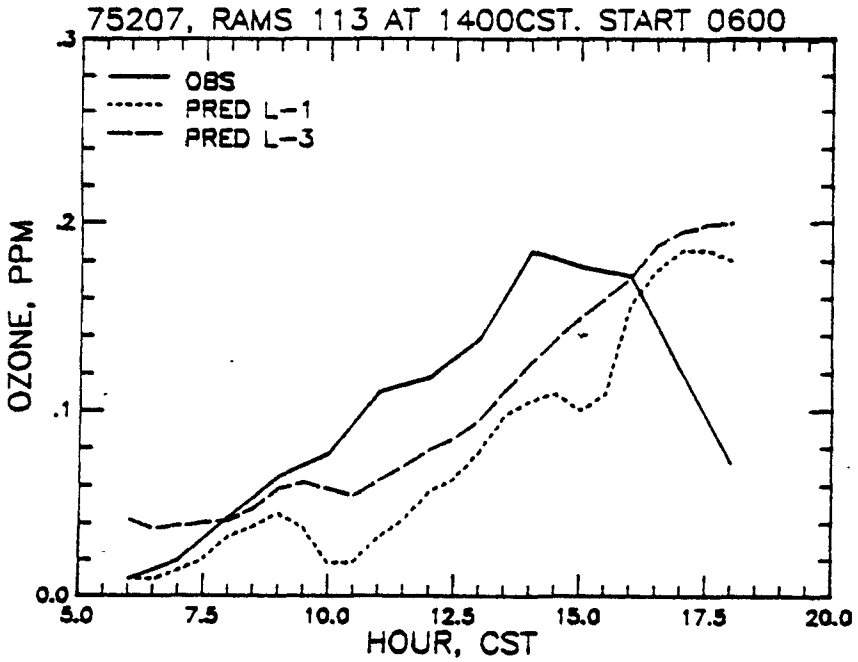

Figure C-6b. LPM time series of observed and predicted O_3 hourly concentrations on Day 207 of 1975.

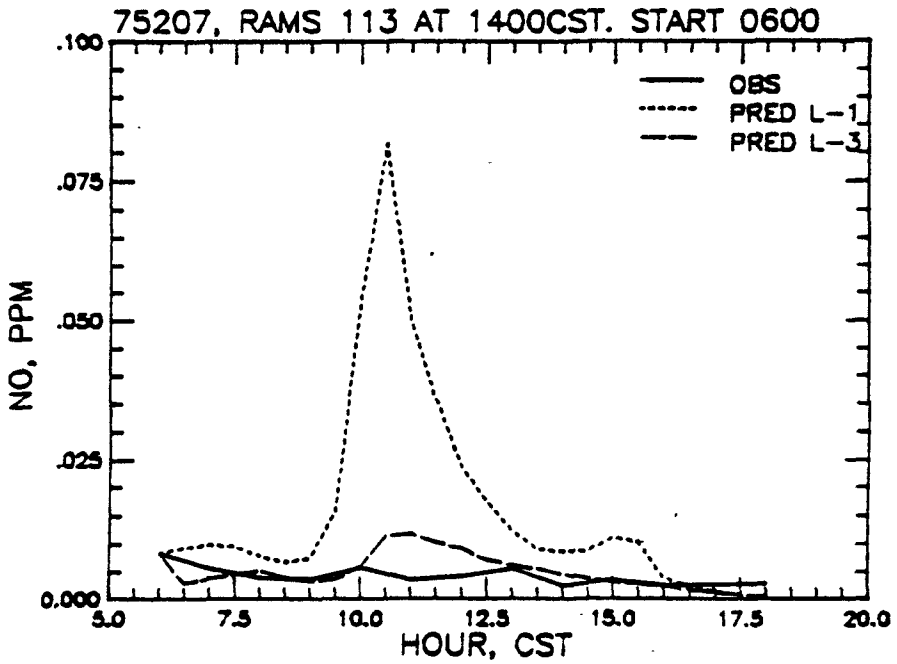

Figure C-6c. LPM time series of observed and predicted NO hourly concentrations on Day 207 of 1975.

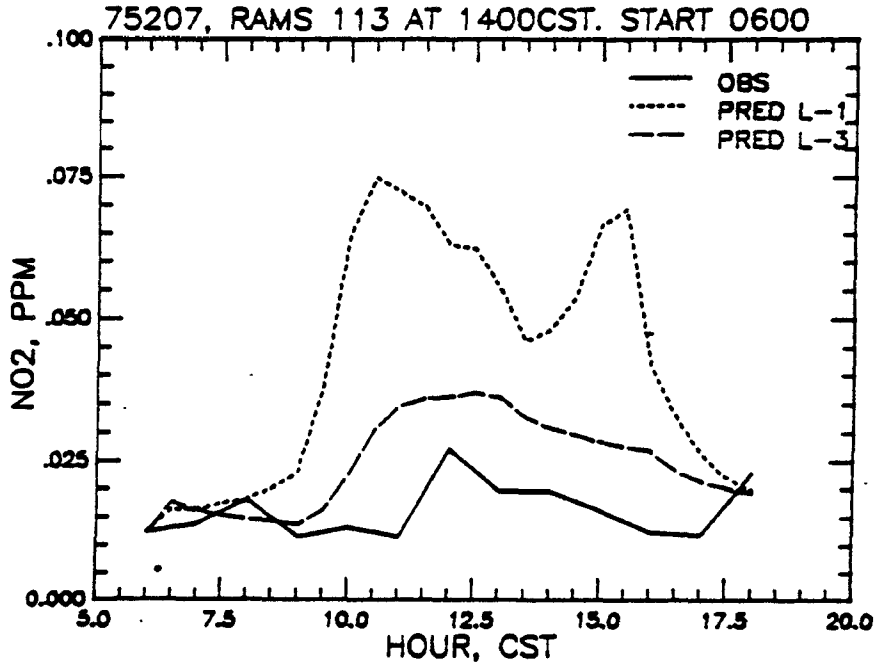

Figure C-6d. LPM time series of observed and predicted NO_2 hourly concentrations on Day 207 of 1975.

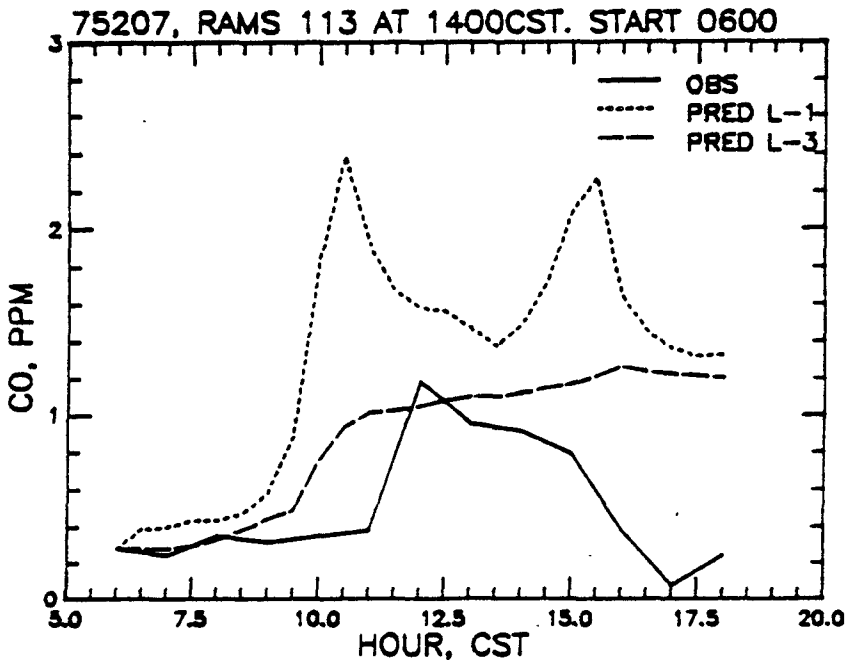

Figure C-6e. LPM time series of observed and predicted CO hourly concentrations on Day 207 of 1975.

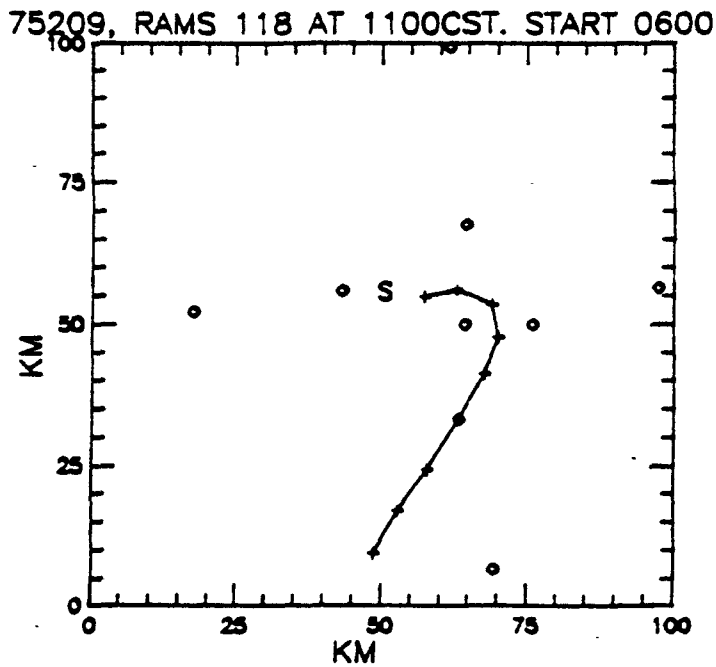

Figure C-7a. LPM parcel trajectory for Day 209 of 1975.

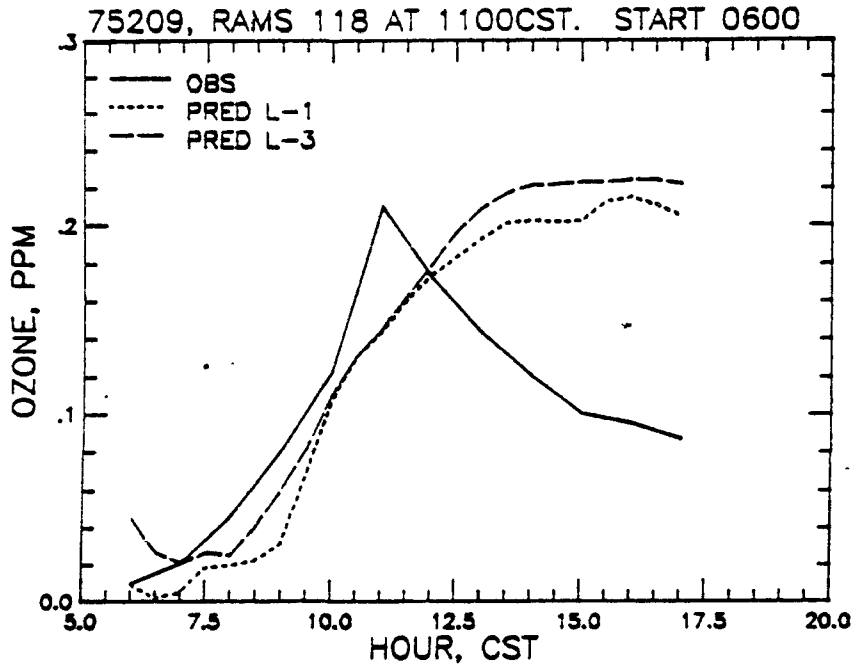

Figure C-7b. LPM time series of observed and predicted O_3 hourly concentrations on Day 209 of 1975.

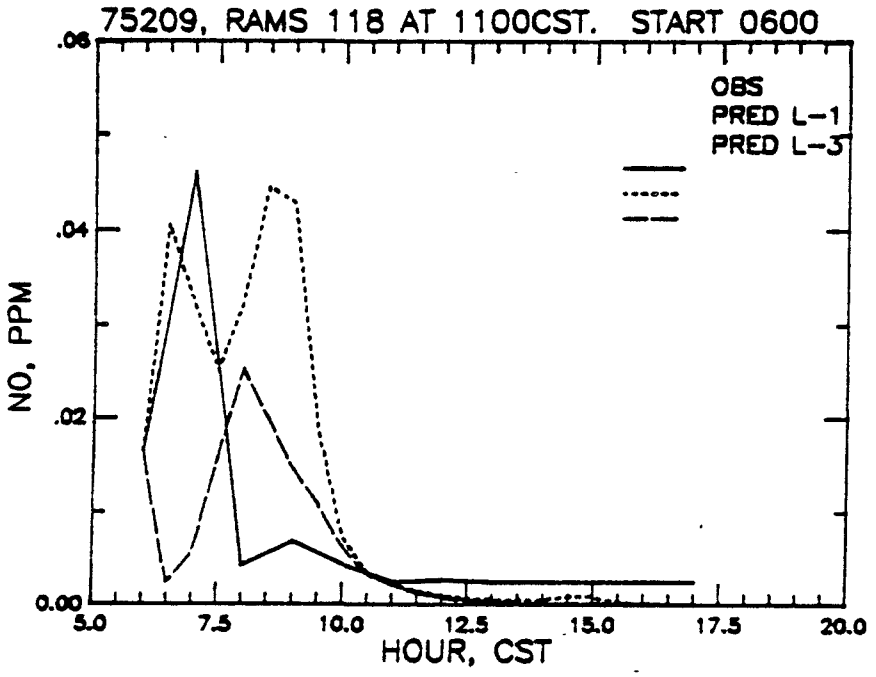

Figure C-7c. LPM time series of observed and predicted NO hourly concentrations on Day 209 of 1975.

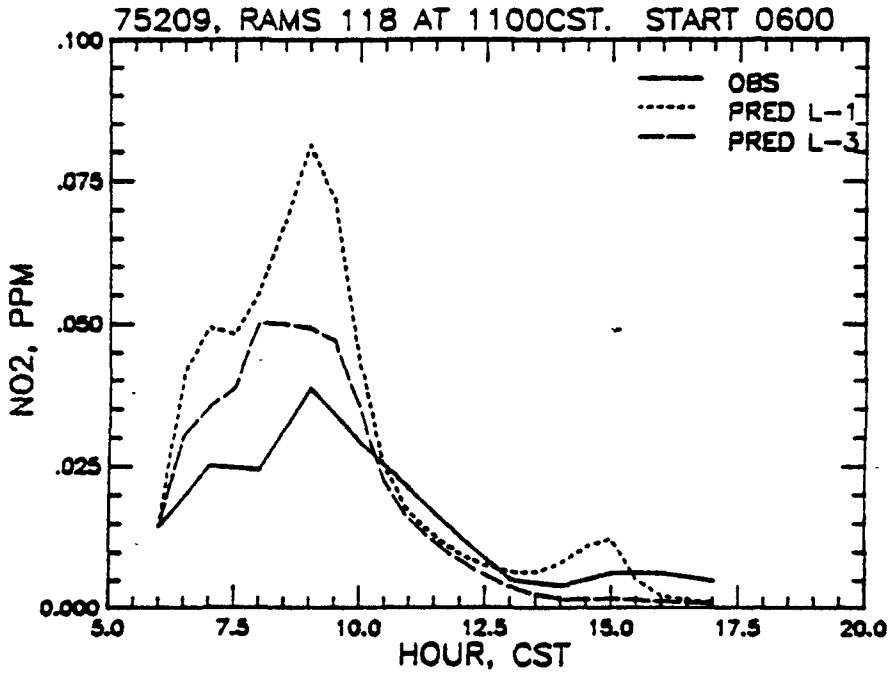

Figure C-7d. LPM time series of observed and predicted NO_2 hourly concentrations on Day 209 of 1975.

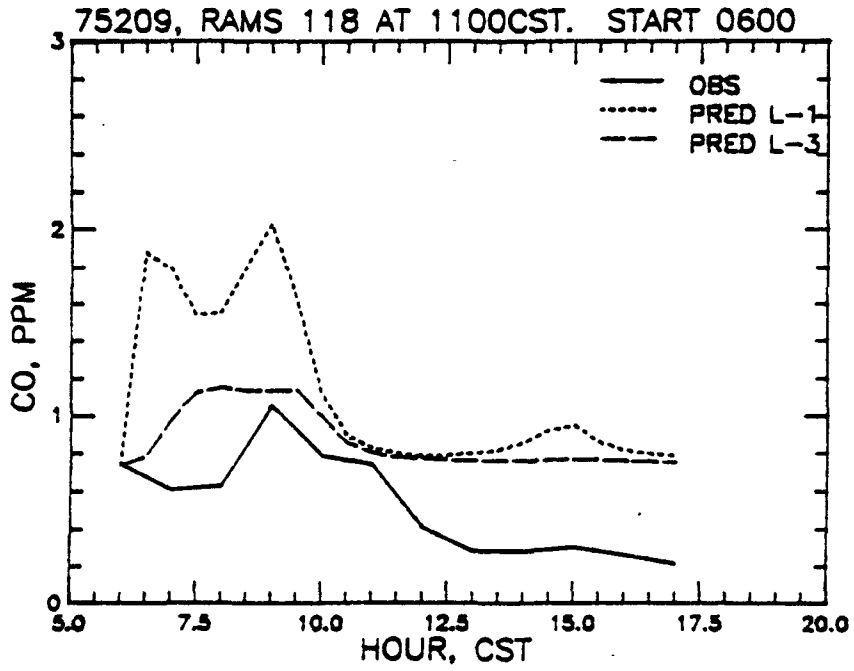

Figure C-7e. LPM time series of observed and predicted CO hourly concentrations on Day 209 of 1975.

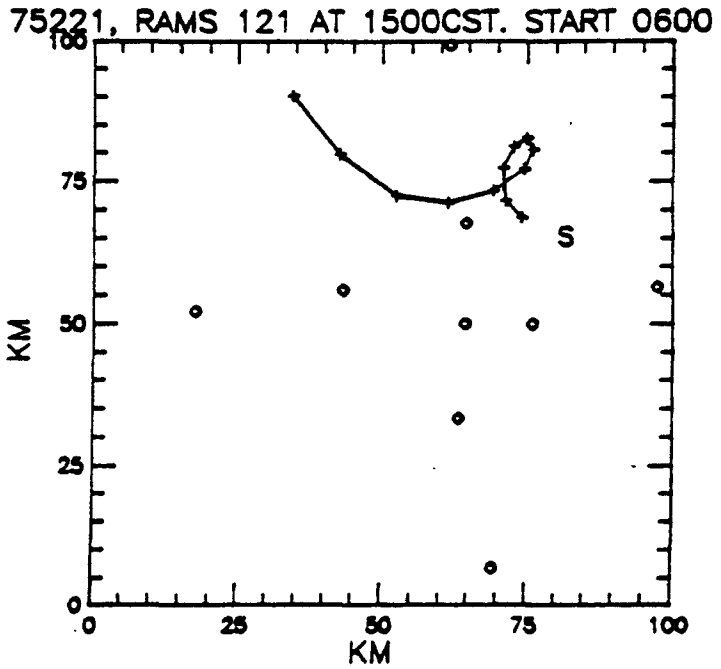

Figure C-8a. LPM parcel trajectory for Day 221 of 1975.

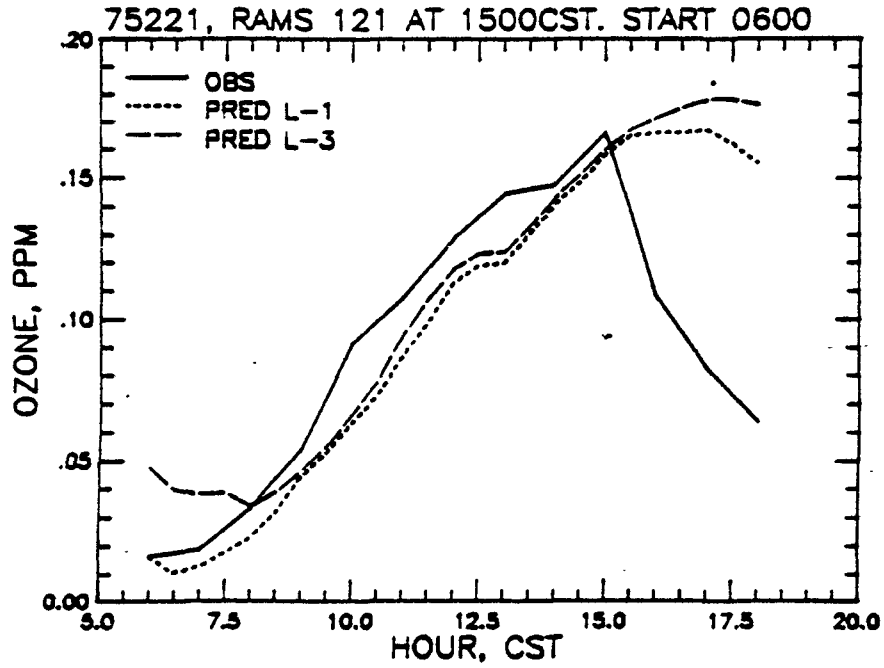

Figure C-8b. LPM time series of observed and predicted O_3 hourly concentrations on Day 221 of 1975.

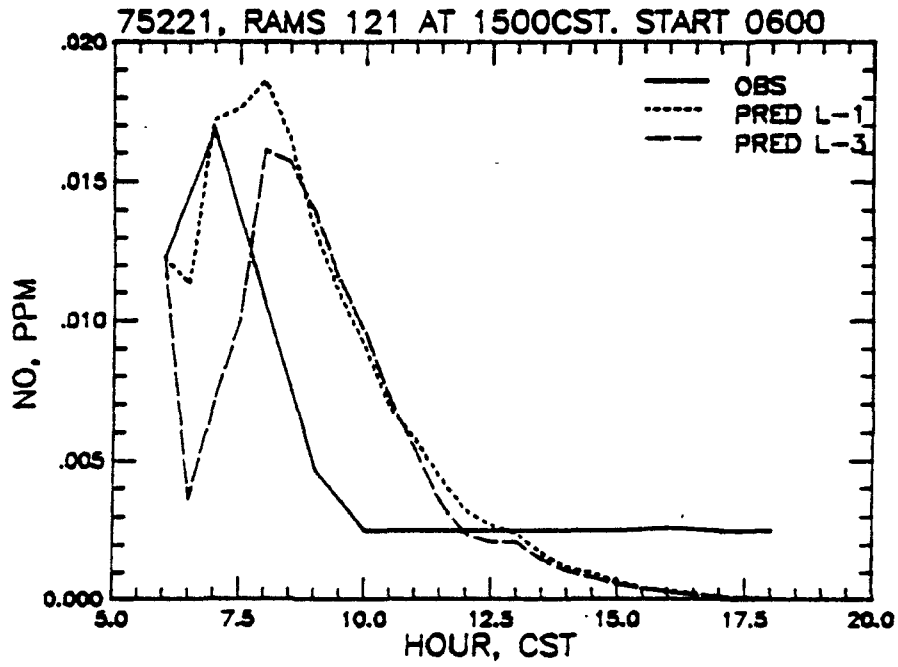

Figure C-8c. LPM time series of observed and predicted NO hourly concentrations on Day 221 of 1975.

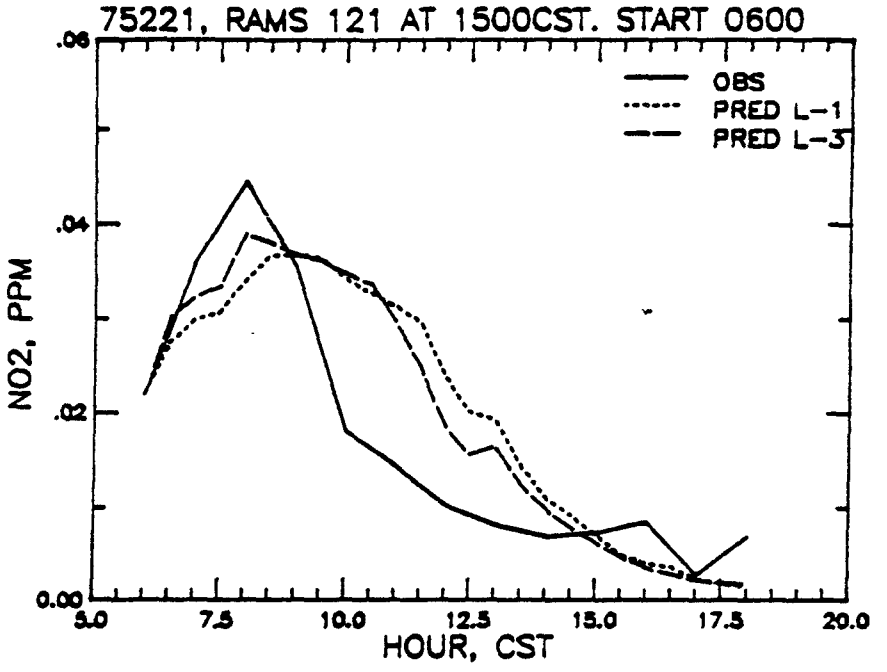

Figure C-8d. LPM time series of observed and predicted NO_2 hourly concentrations on Day 221 of 1975.

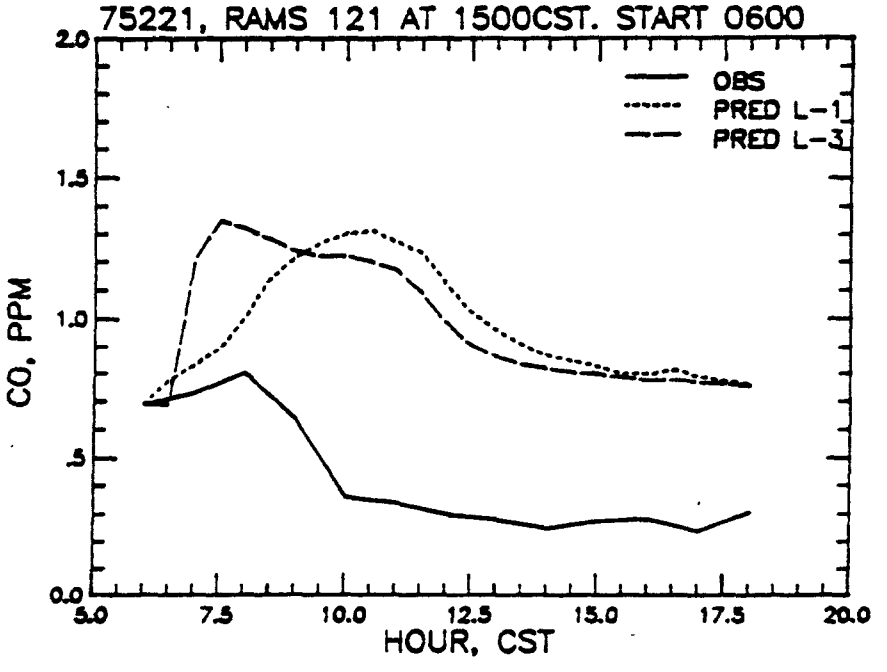

Figure C-8e. LPM time series of observed and predicted CO hourly concentrations on Day 221 of 1975.

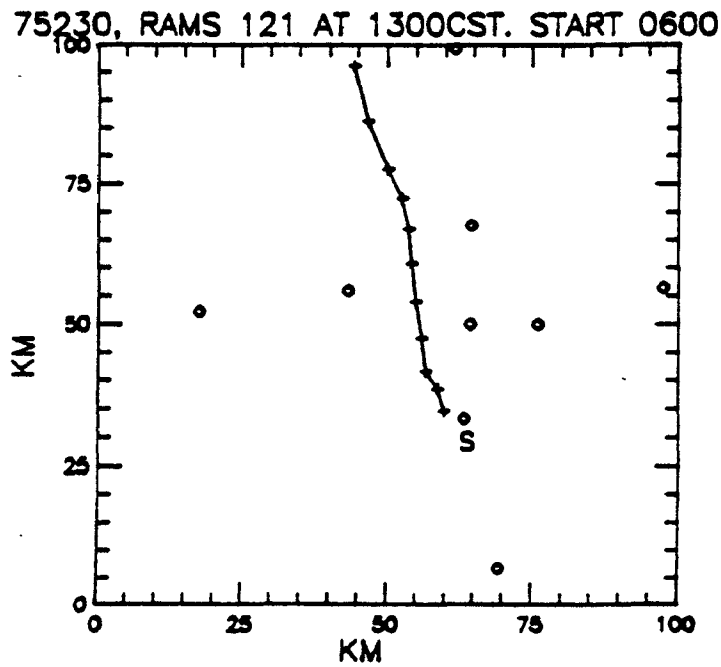

Figure C-9a. LPM parcel trajectory for Day 230 of 1975.

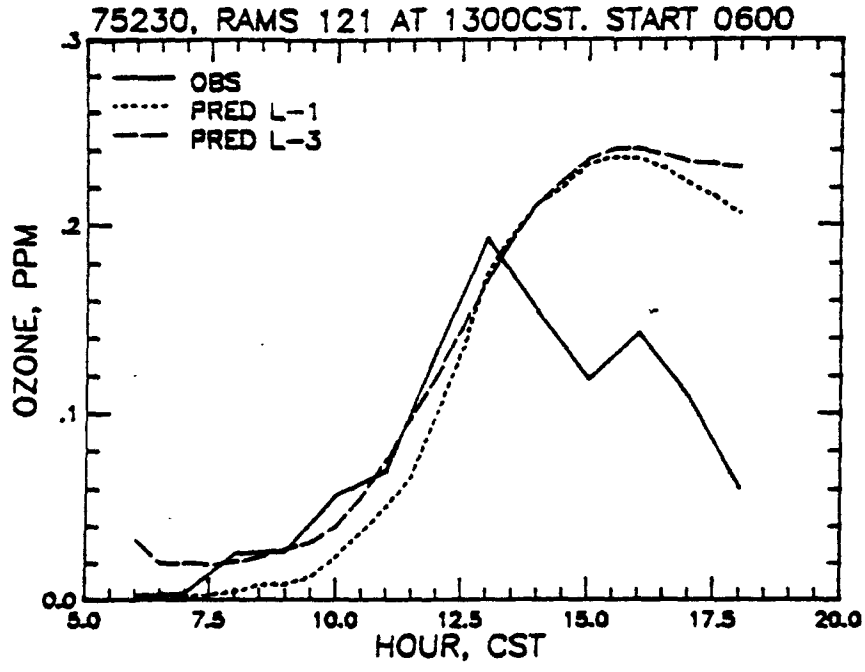

Figure C-9b. LPM time series of observed and predicted O_3 hourly concentrations on Day 230 of 1975.

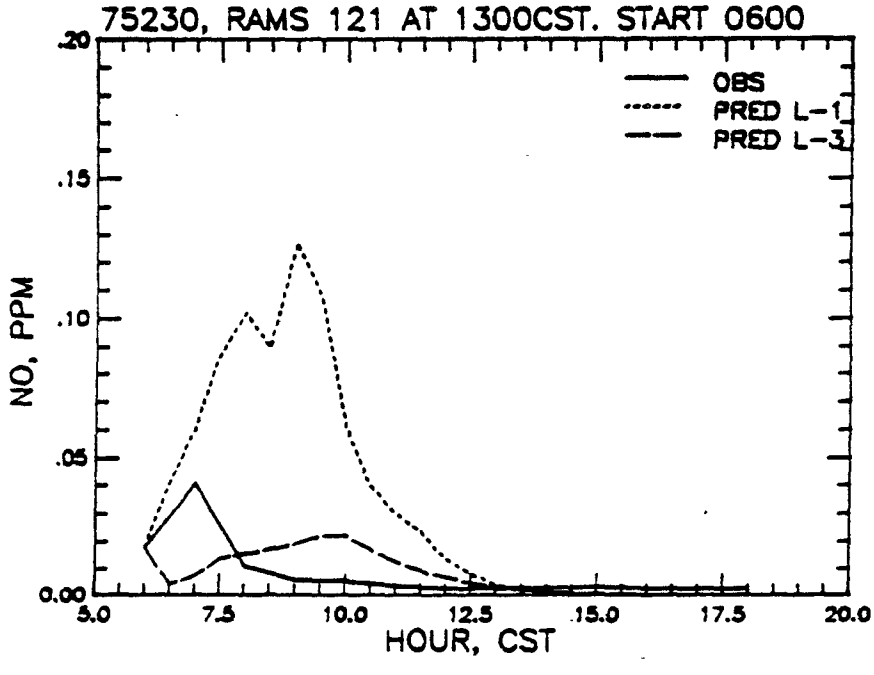

Figure C-9c. LPM time series of observed and predicted NO hourly concentrations on Day 230 of 1975.

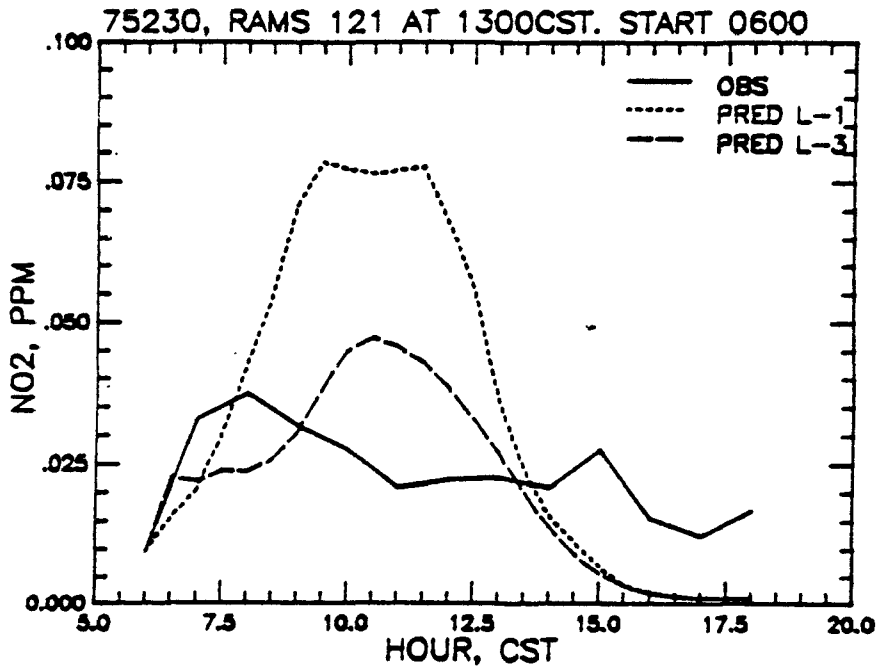

Figure C-9d. LPM time series of observed and predicted NO_2 hourly concentrations on Day 230 of 1975.

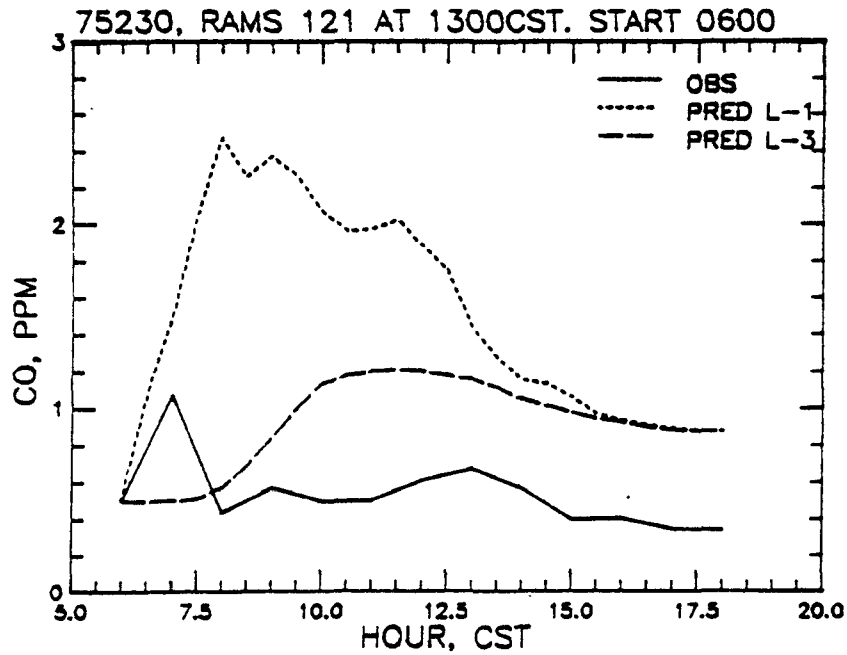

Figure C-9e. LPM time series of observed and predicted CO hourly concentrations on Day 230 of 1975.

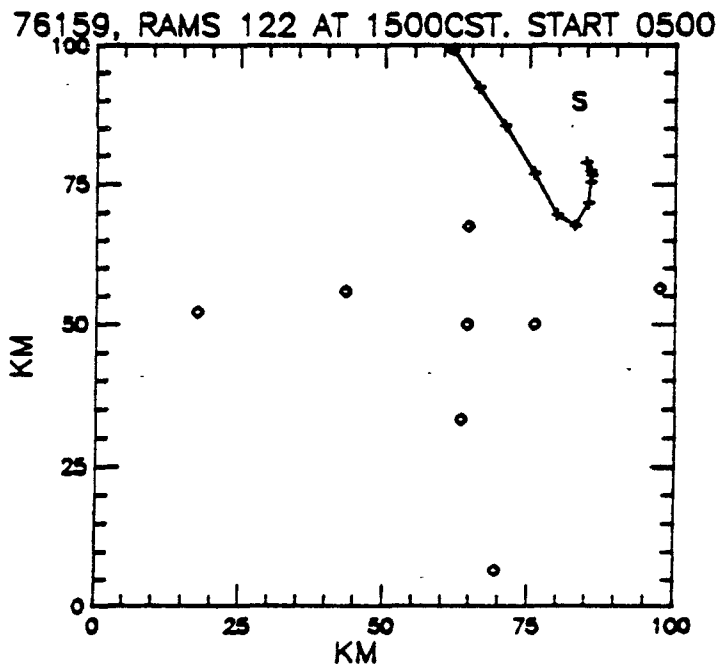

Figure C-10a. LPM parcel trajectory for Day 159 of 1976.

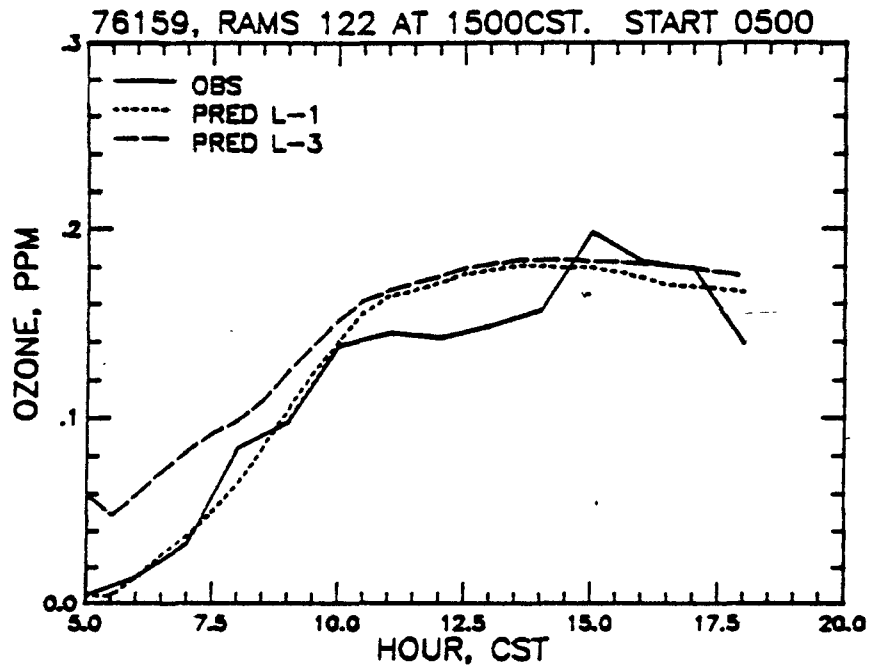

Figure C-10b. LPM time series of observed and predicted O_3 hourly concentrations on Day 159 of 1976.

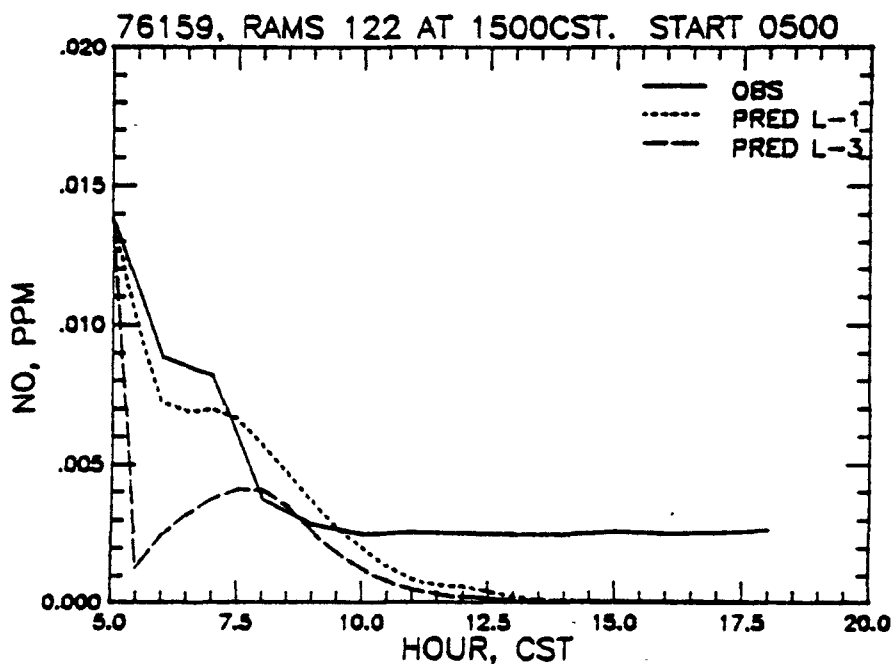

Figure C-10c. LPM time series of observed and predicted NO hourly concentrations on Day 159 of 1976.

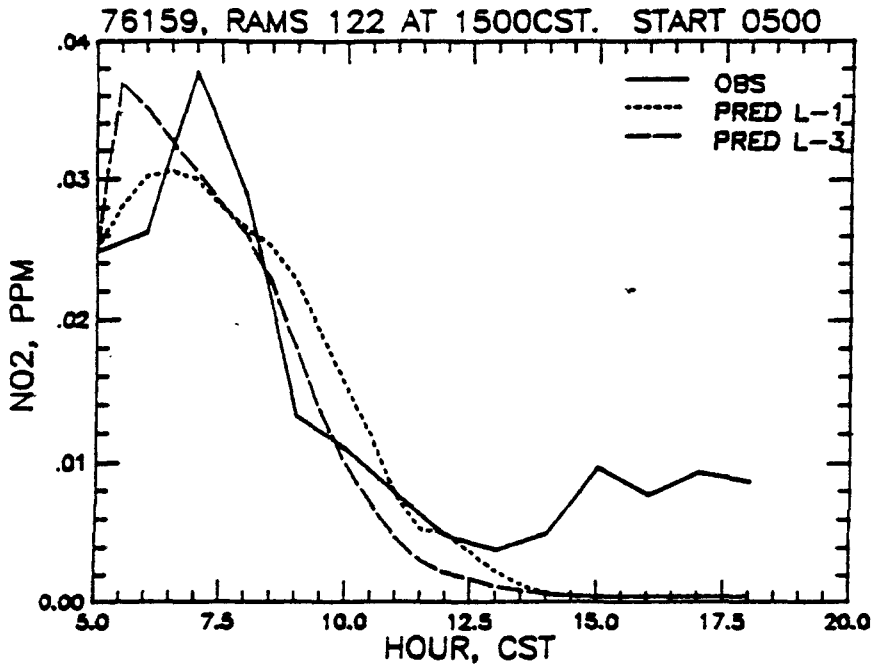

Figure C-10d. LPM time series of observed and predicted NO_2 hourly concentrations on Day 159 of 1976.

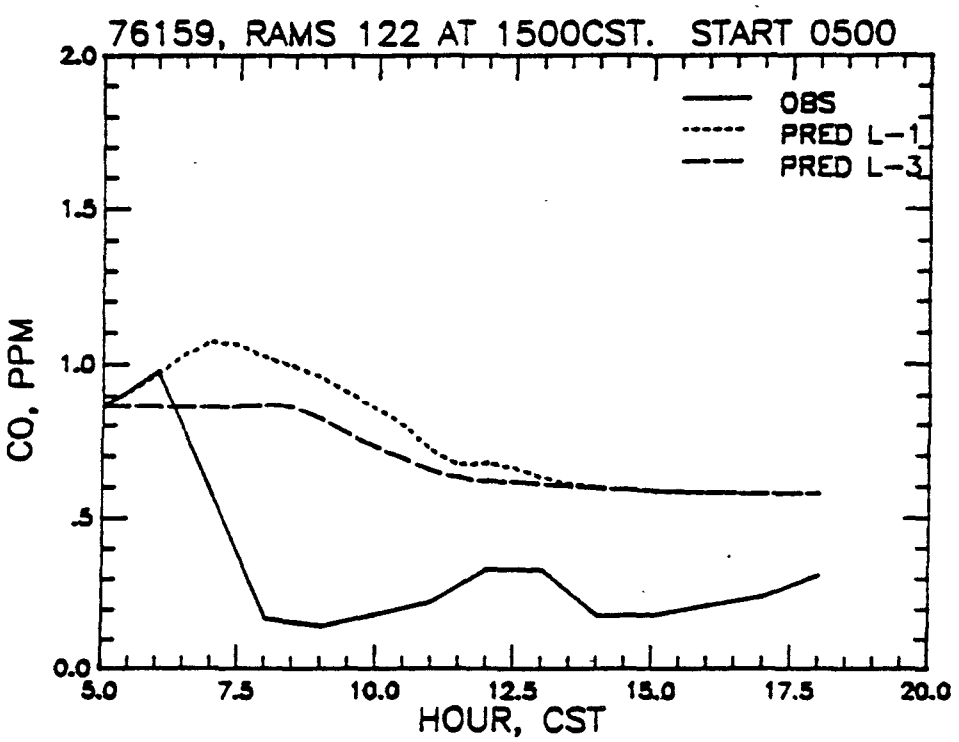

Figure C-10e. LPM time series of observed and predicted CO hourly concentrations on Day 159 of 1976.

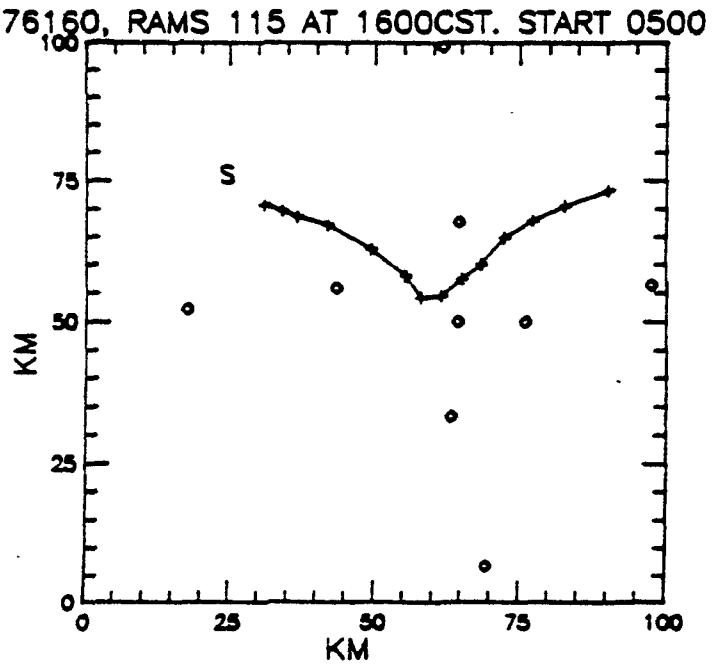

Figure C-11a. LPM parcel trajectory for Day 160 of 1976.

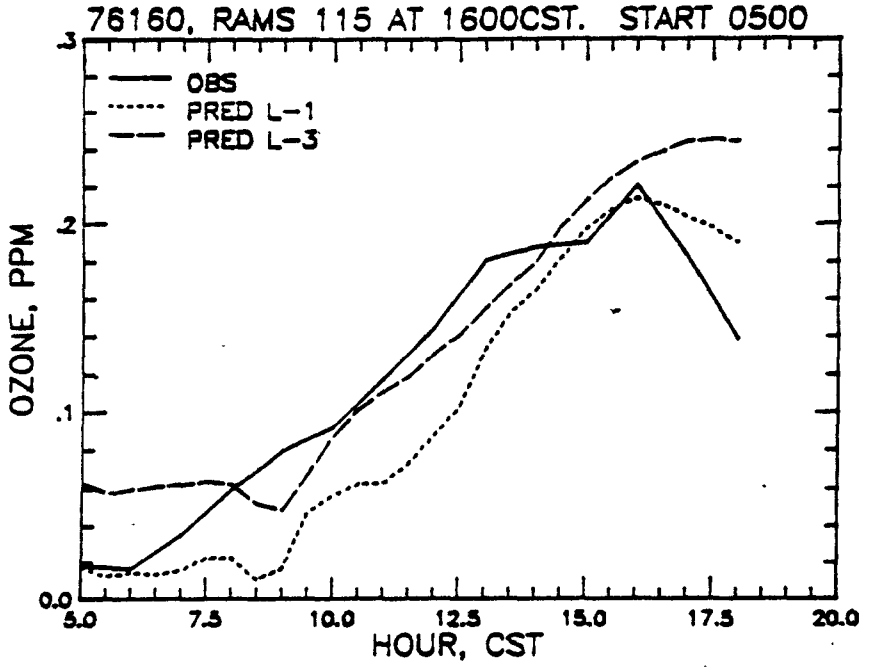

Figure C-11b. LPM time series of observed and predicted O_3 hourly concentrations on Day 160 of 1976.

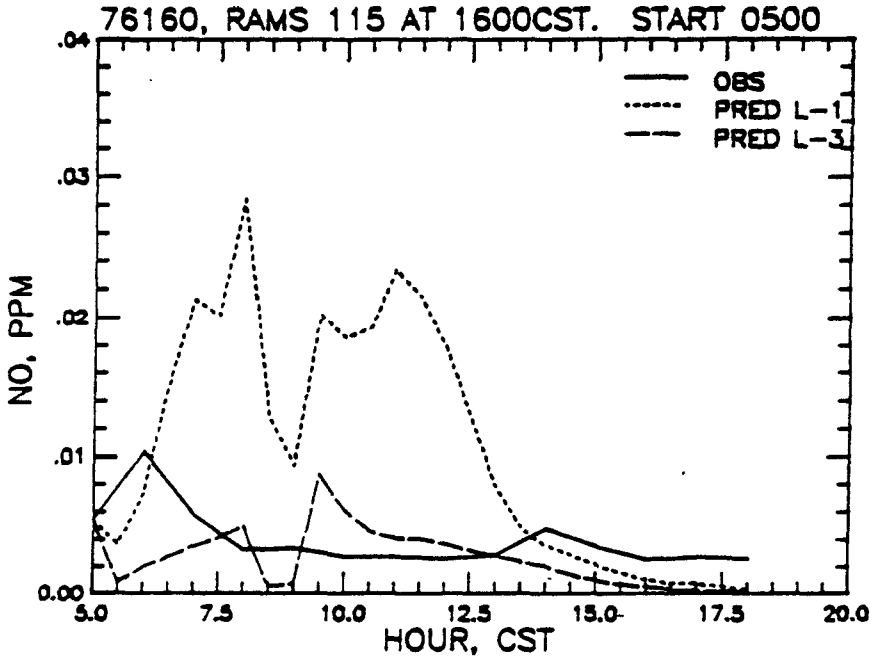

Figure C-11c. LPM time series of observed and predicted NO hourly concentrations on Day 160 of 1976.

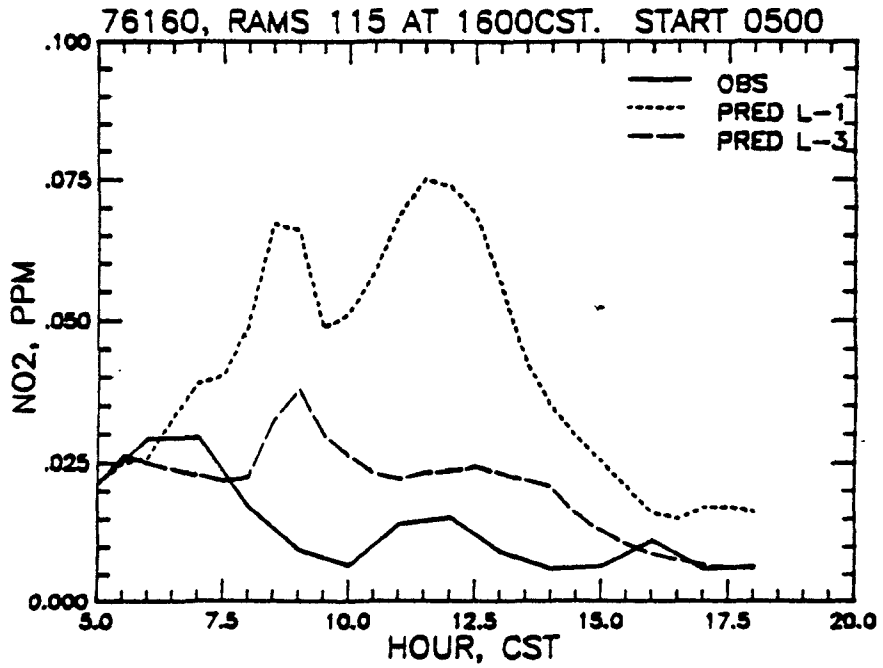

Figure C-11d. LPM time series of observed and predicted NO_2 hourly concentrations on Day 160 of 1976.

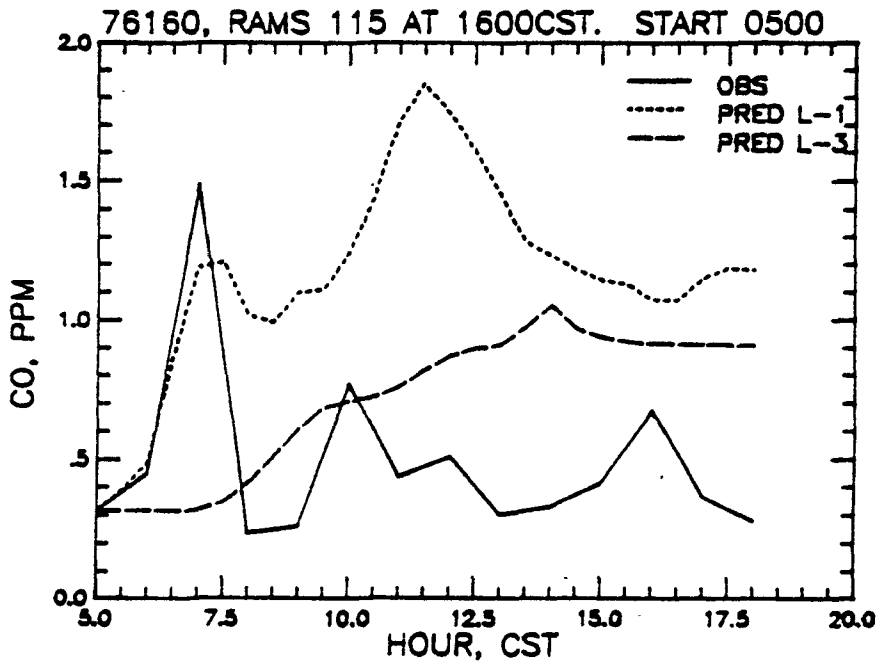

Figure C-11e. LPM time series of observed and predicted CO hourly concentrations on Day 160 of 1976.

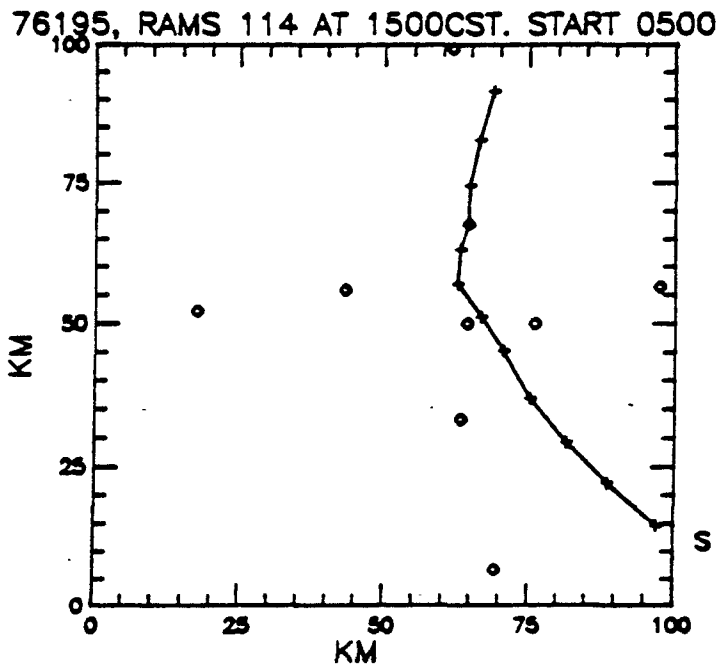

Figure C-12a. LPM parcel trajectory for Day 195 of 1976.

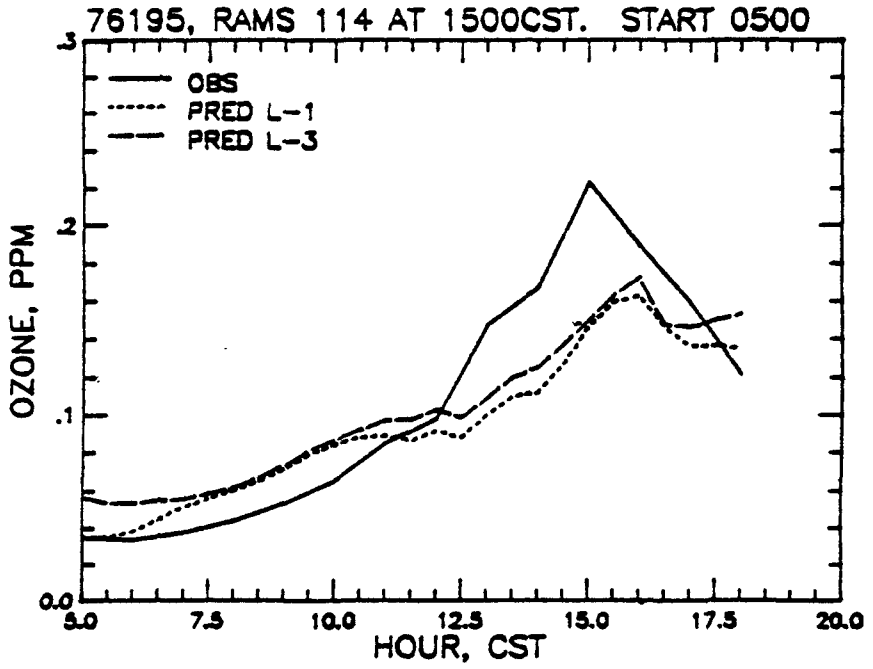

Figure C-12b. LPM time series of observed and predicted O_3 hourly concentrations on Day 195 of 1976.

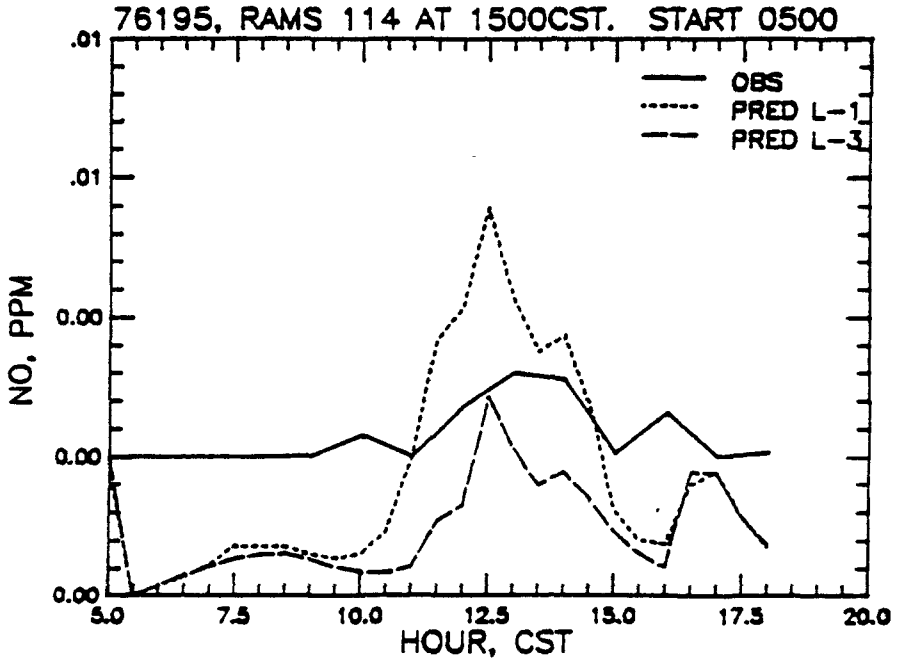

Figure C-12c. LPM time series of observed and predicted NO hourly concentrations on Day 195 of 1976.

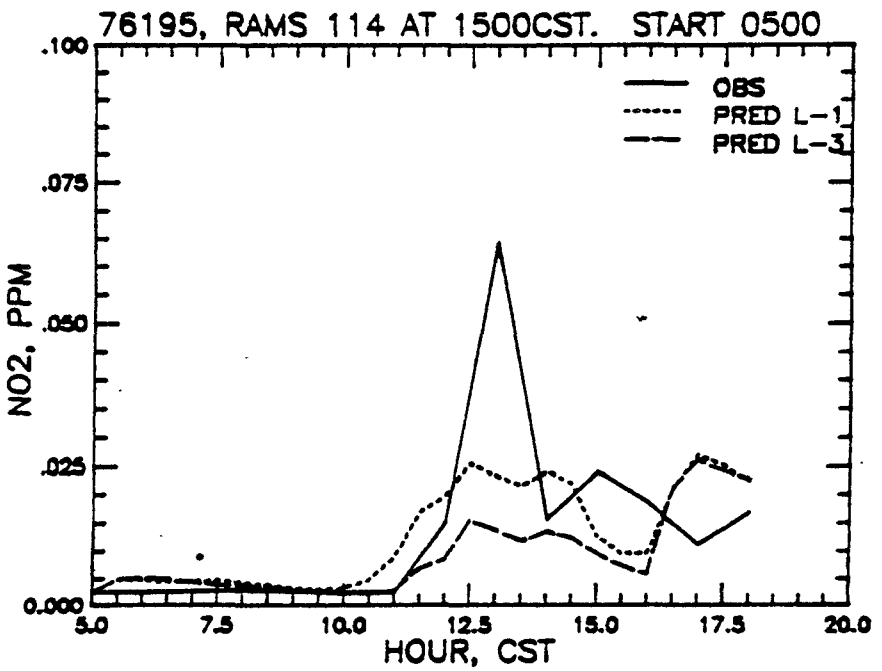

Figure C-12d. LPM time series of observed and predicted NO_2 hourly concentrations on Day 195 of 1976.

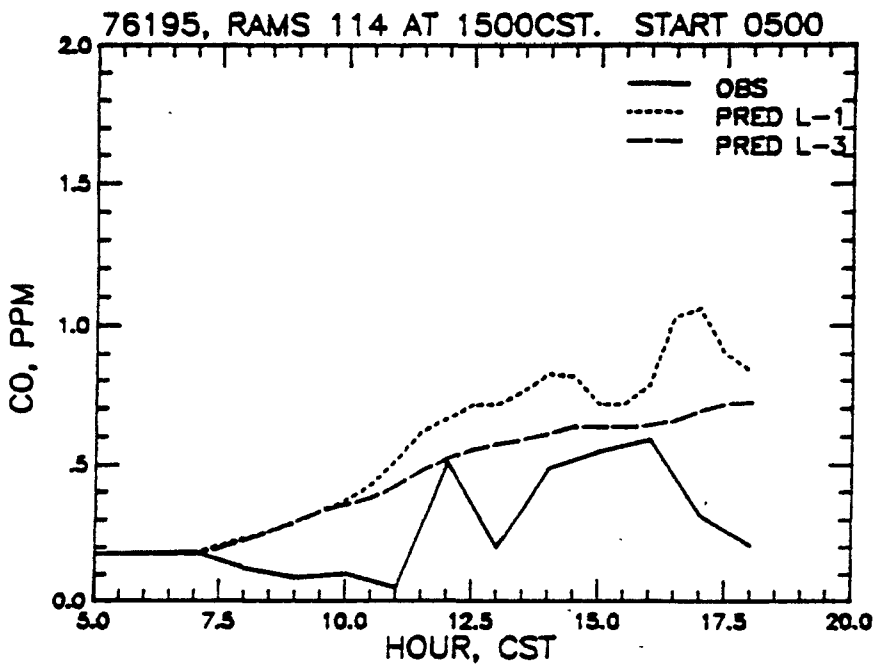

Figure C-12e. LPM time series of observed and predicted CO hourly concentrations on Day 195 of 1976.

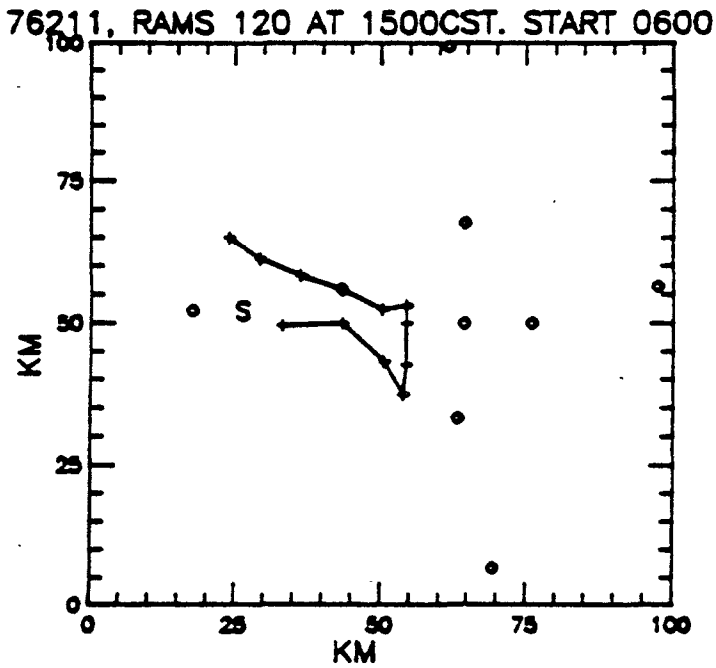

Figure C-13a. LPM parcel trajectory for Day 211 of 1976.

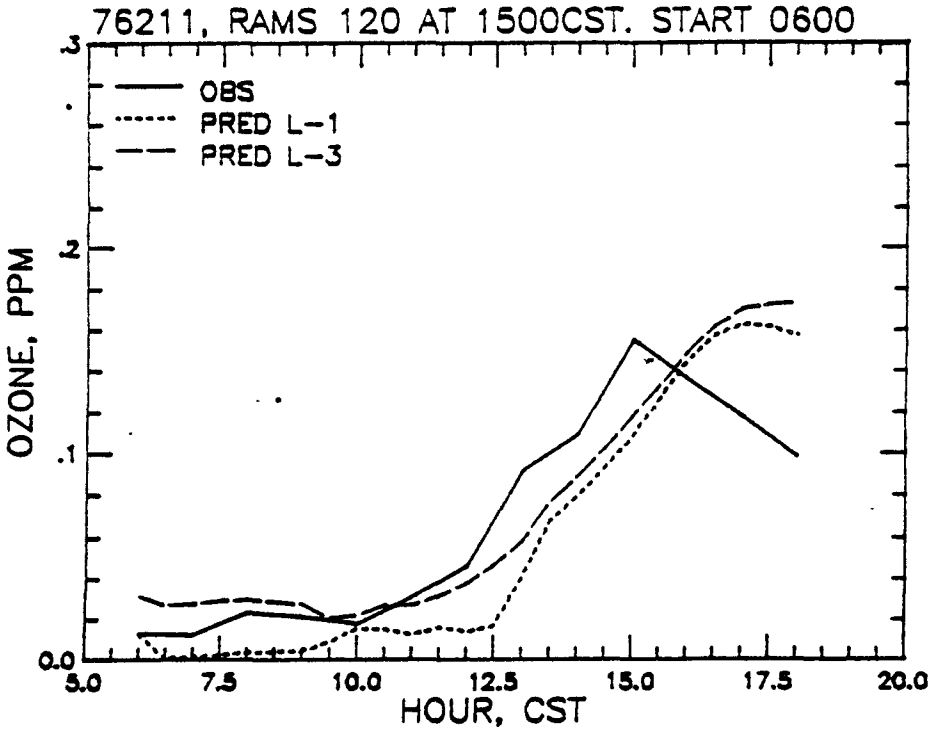

Figure C-13b. LPM time series of observed and predicted O_3 hourly concentrations on Day 211 of 1976.

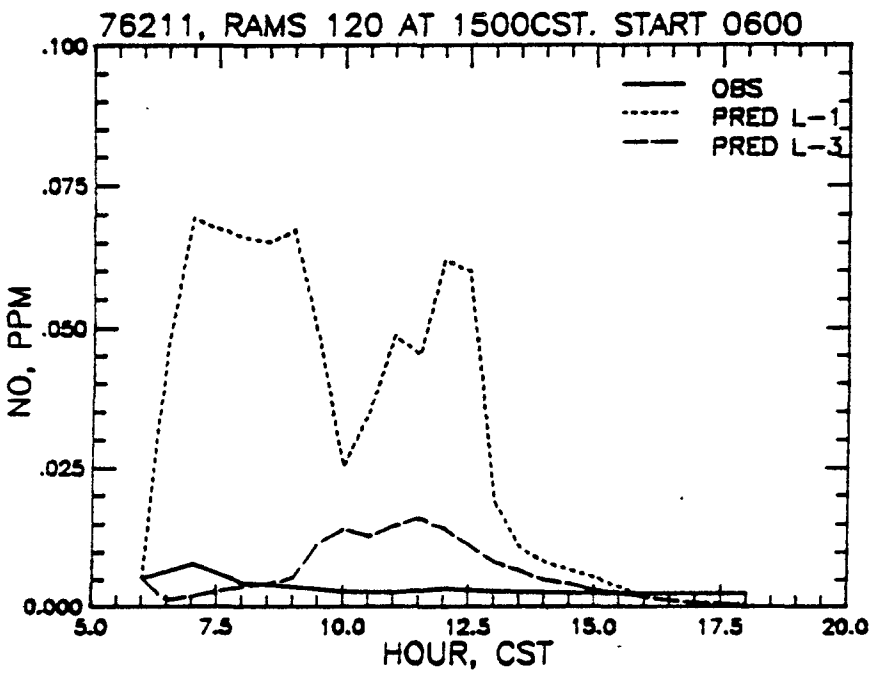

Figure C-13c. LPM time series of observed and predicted NO hourly concentrations on Day 211 of 1976.

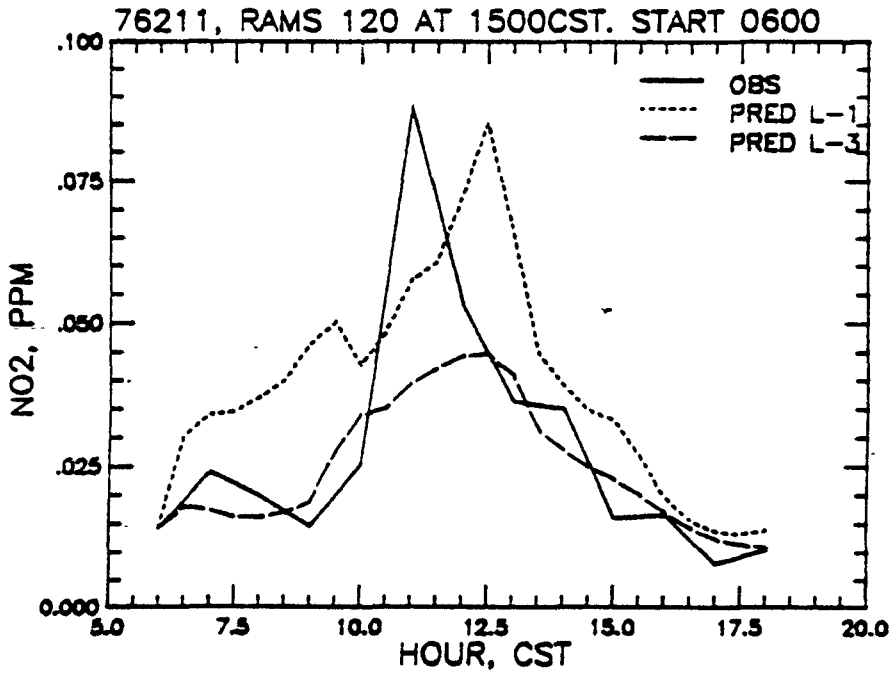

Figure C-13d. LPM time series of observed and predicted NO_2 hourly concentrations on Day 211 of 1976.

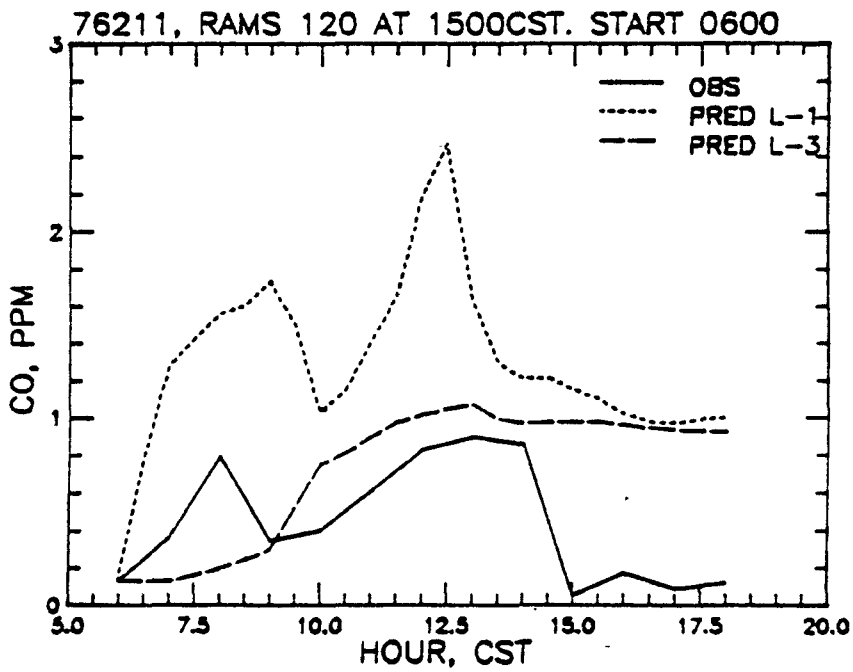

Figure C-13e. LPM time series of observed and predicted CO hourly concentrations on Day 211 of 1976.

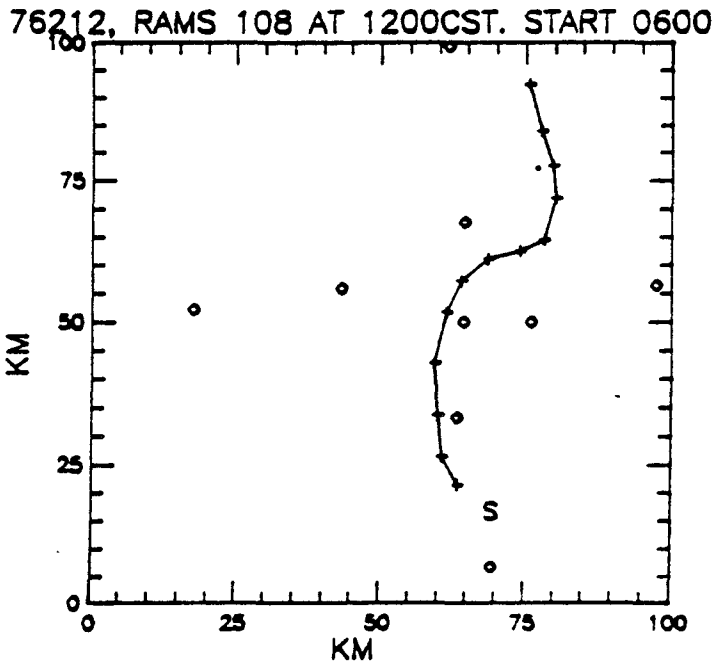

Figure C-14a. LPM parcel trajectory for Day 212 of 1976.

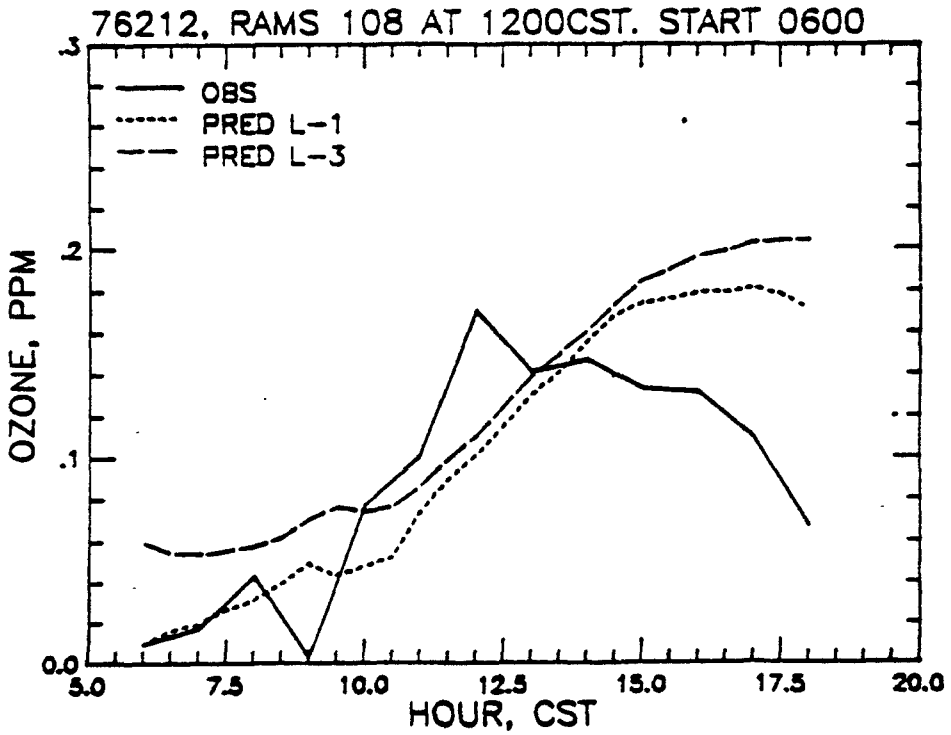

Figure C-14b. LPM time series of observed and predicted O_3 hourly concentrations on Day 212 of 1976.

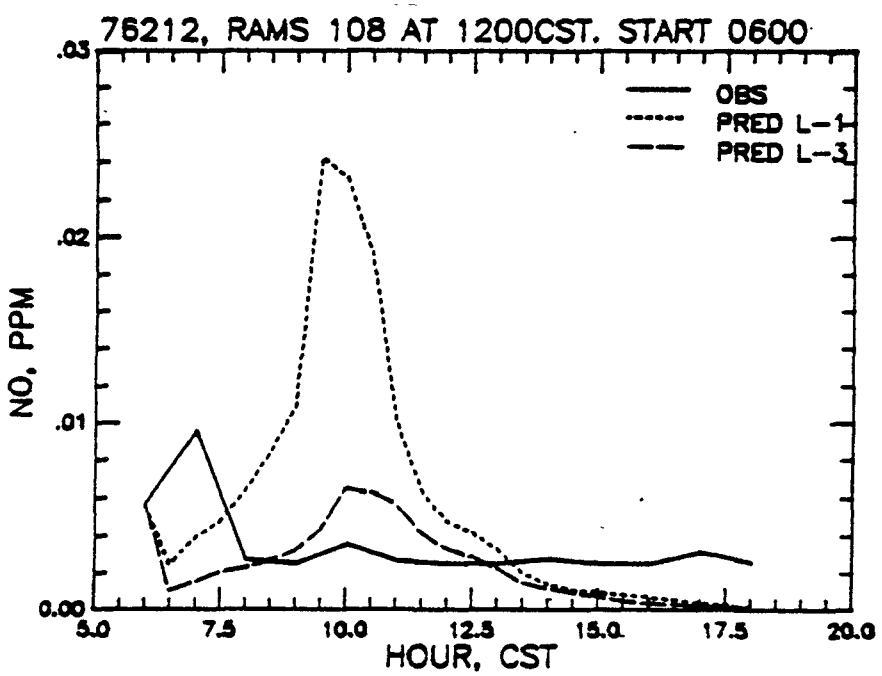

Figure C-14c. LPM time series of observed and predicted NO hourly concentrations on Day 212 of 1976.

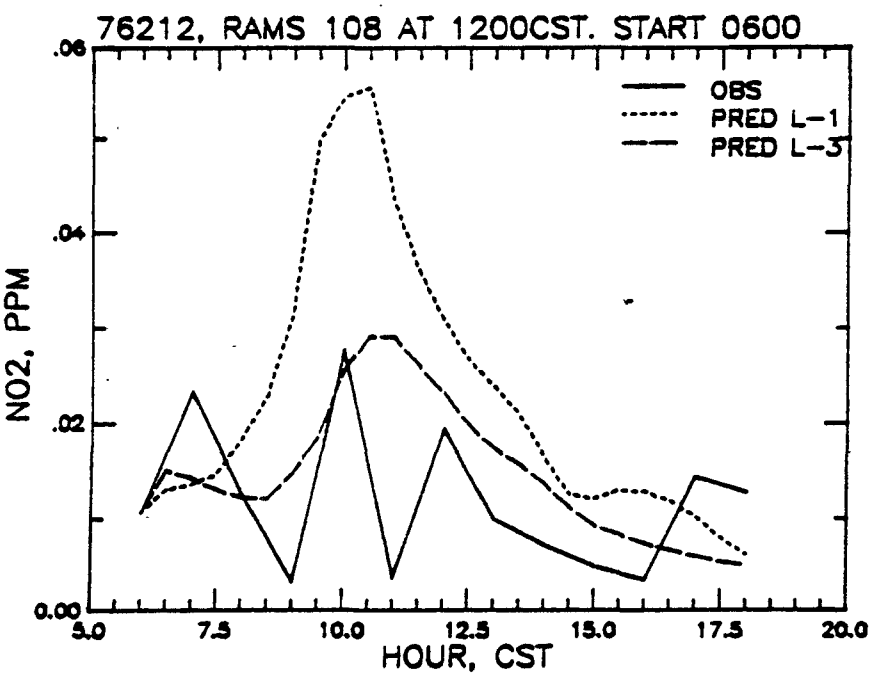

Figure C-14d. LPM time series of observed and predicted NO_2 hourly concentrations on Day 212 of 1976.

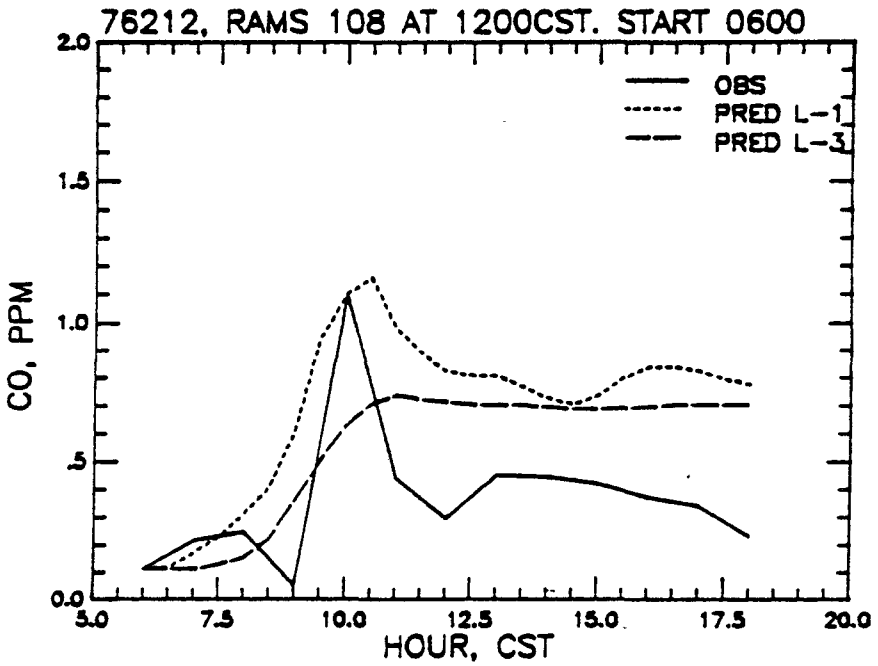

Figure C-14e. LPM time series of observed and predicted CO hourly concentrations on Day 212 of 1976.

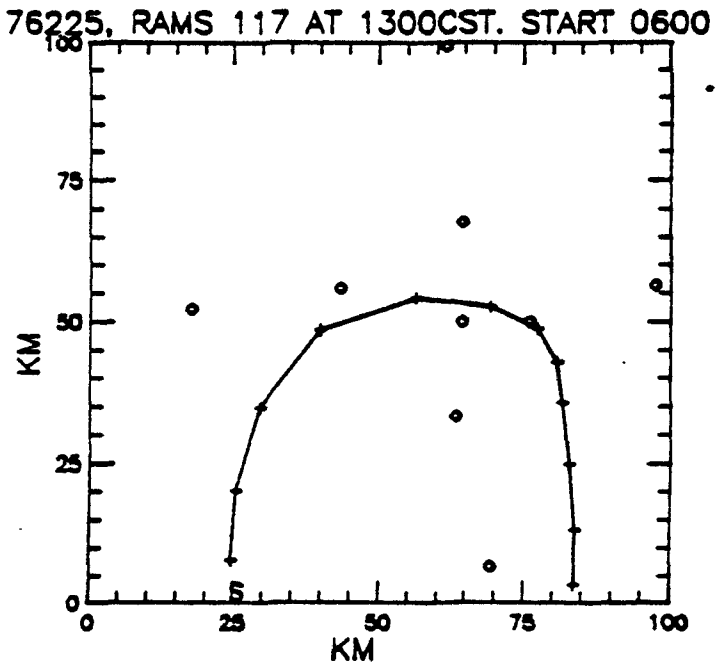

Figure C-15a. LPM parcel trajectory for Day 225 of 1976.

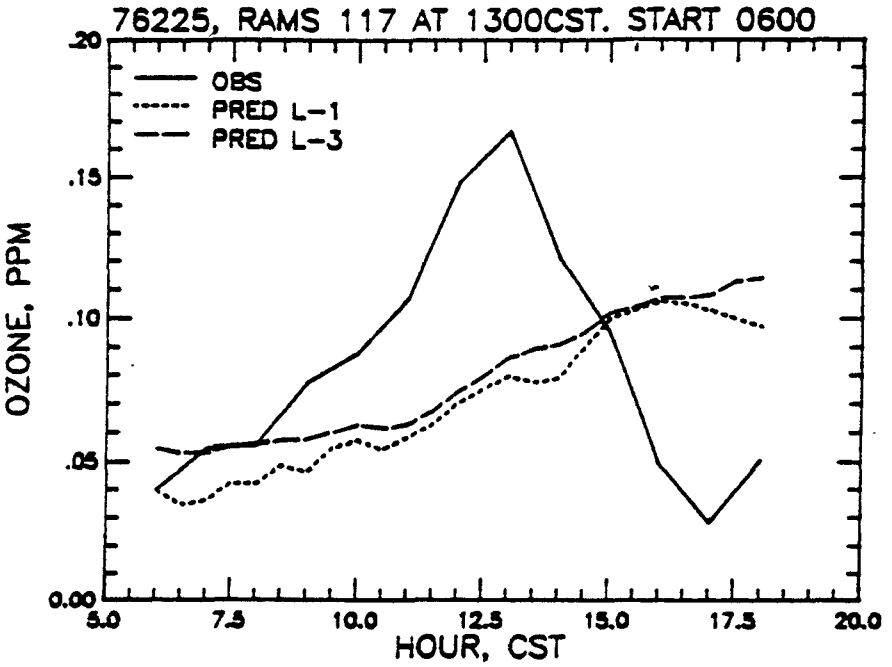

Figure C-15b. LPM time series of observed and predicted O_3 hourly concentrations on Day 225 of 1976.

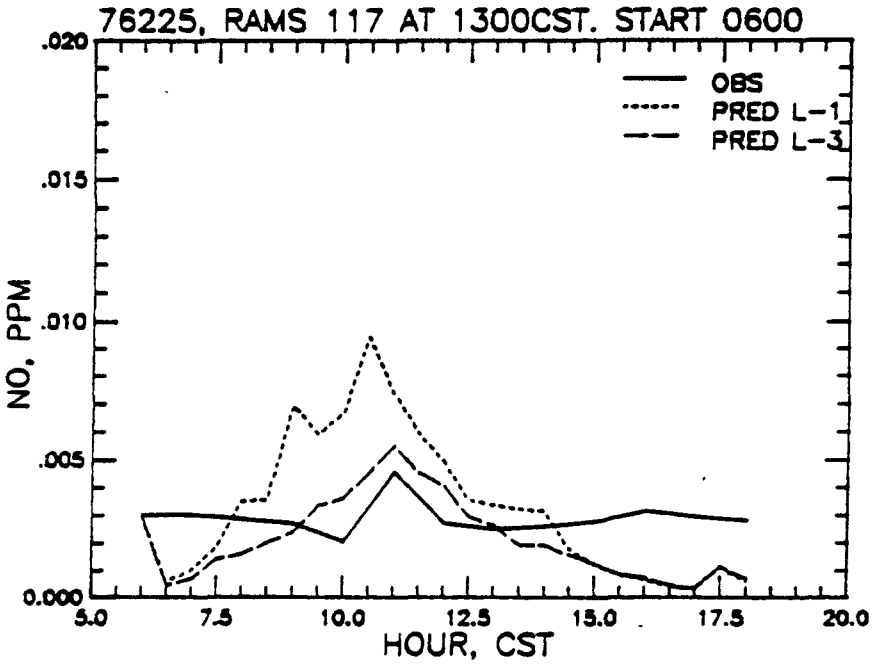

Figure C-15c. LPM time series of observed and predicted NO hourly concentrations on Day 225 of 1976.

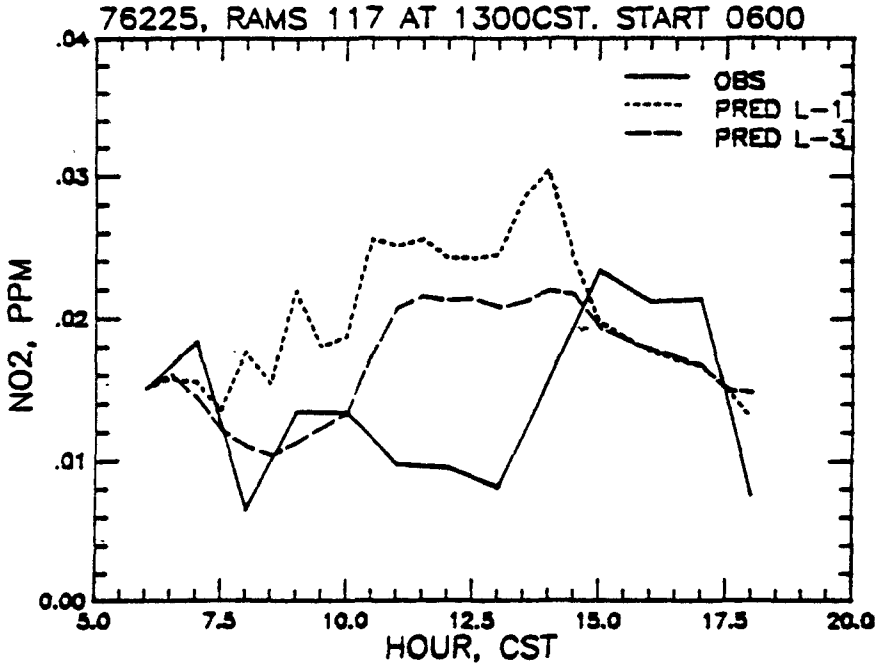

Figure C-15d. LPM time series of observed and predicted NO_2 hourly concentrations on Day 225 of 1976.

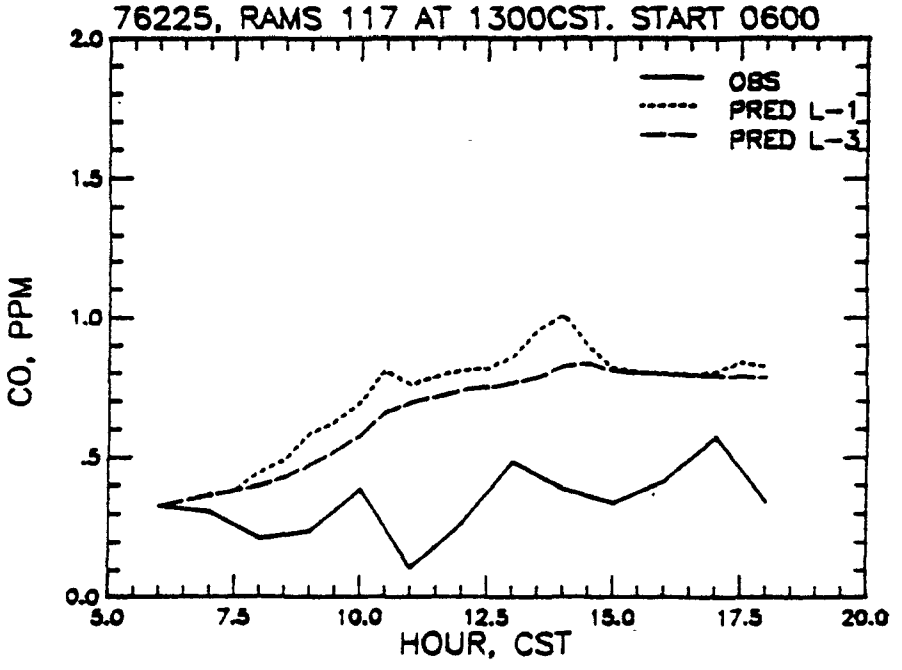

Figure C-15e. LPM time series of observed and predicted CO hourly concentrations on Day 225 of 1976.

APPENDIX D

UAM - RS AND RO PLOTS FOR REMAINING TEST DAYS

This appendix contains the residual histogram (RS) and residual vs. observed plots (RO) for the species NO_2, O_3 and CO from the UAM statistical analysis that were not specifically discussed within the body of this report. The plots presented here are from test days 178-75, 182-75, 183-75, 184-75, 209-75, 221-75, 230-75, 231-75, 251-75, 159-76, 160-76, 211-76, 212-76, 225-76, 226-76 and 237-76 of the RAPS data base.

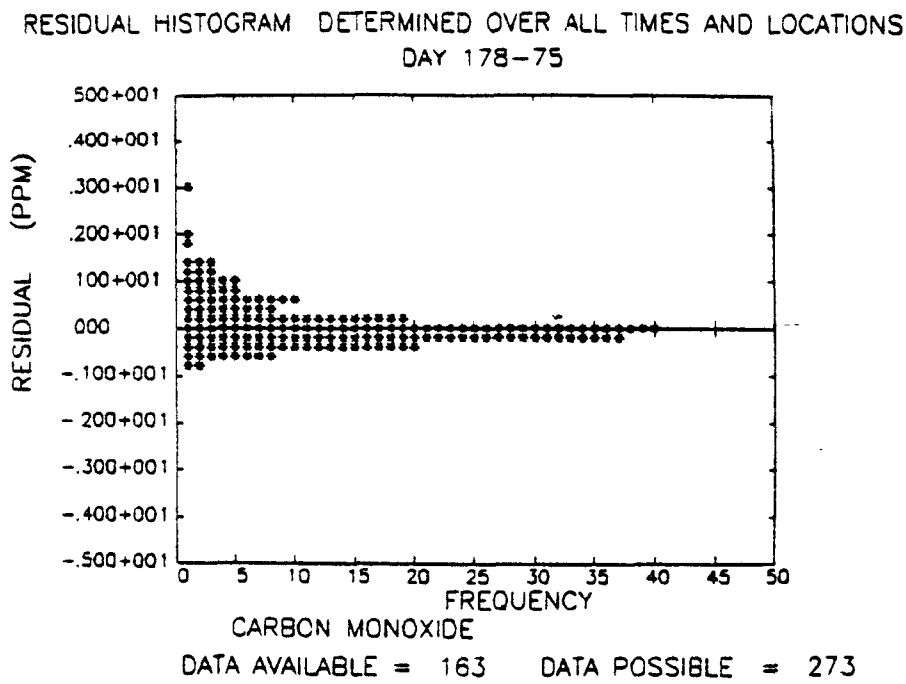

Figure D-1a. Residual histogram for CO from the UAM simulation results for Day 178-75.

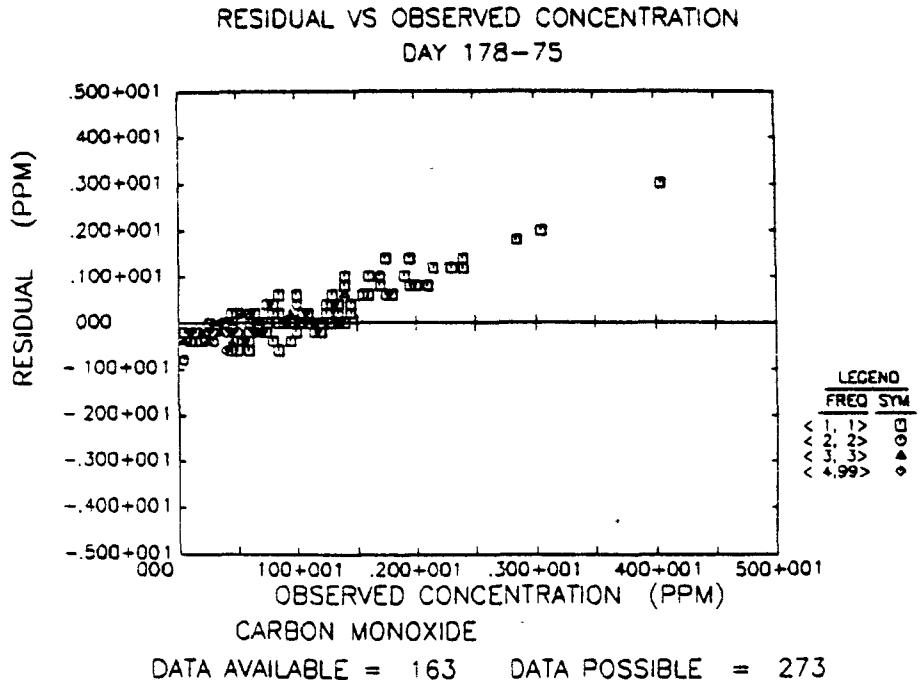

Figure D-1b. Residual vs. observed plot for CO from the UAM simulation results for Day 178-75.

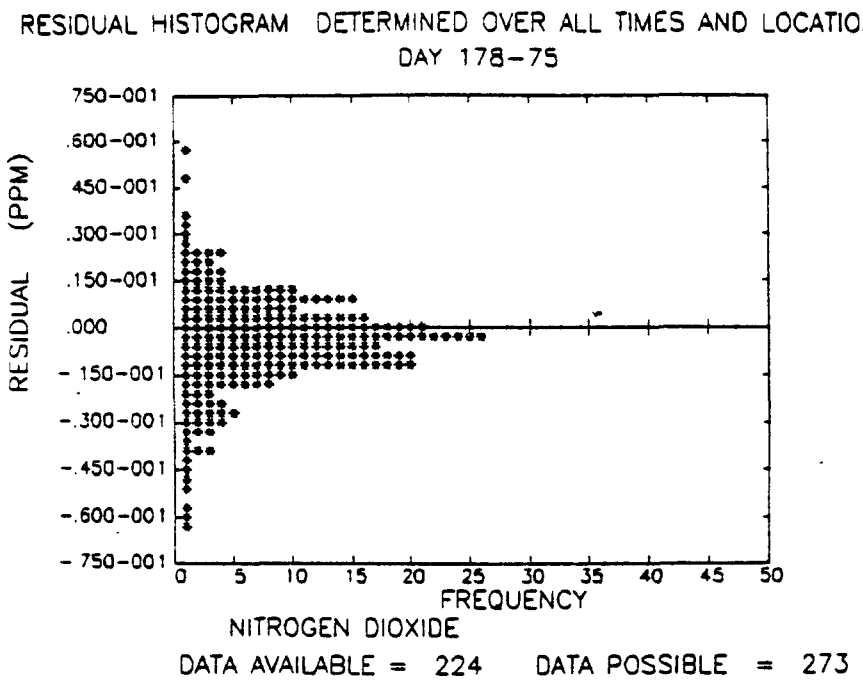

Figure D-2a. Residual histogram for NO_2 from the UAM simulation results for Day 178-75.

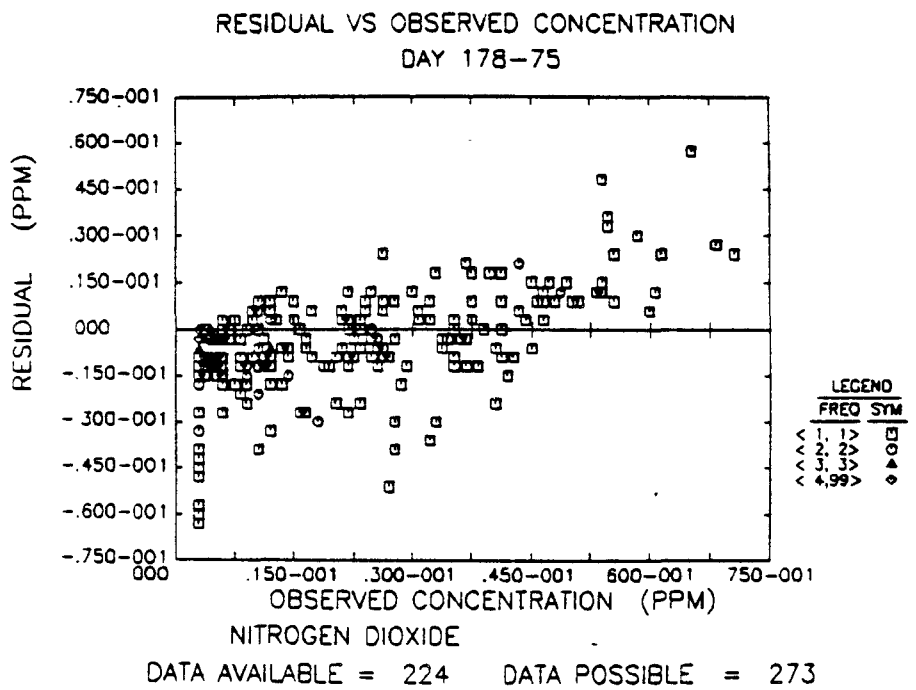

Figure D-2b. Residual vs. observed plot for NO_2 from the UAM simulation results for Day 178-75.

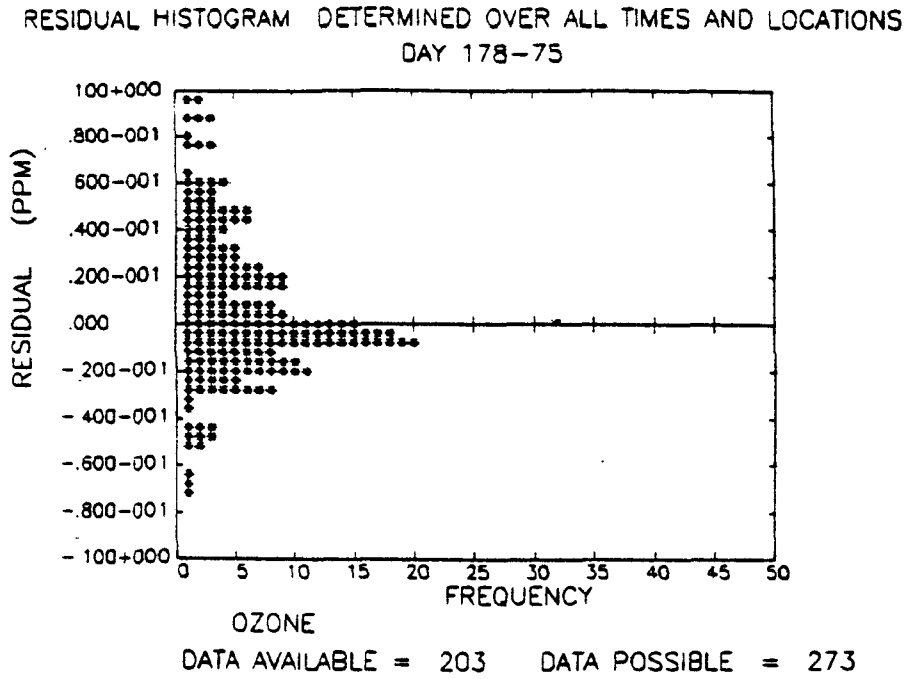

Figure D-3a. Residual histogram for O_3 from the UAM simulation results for Day 178-75.

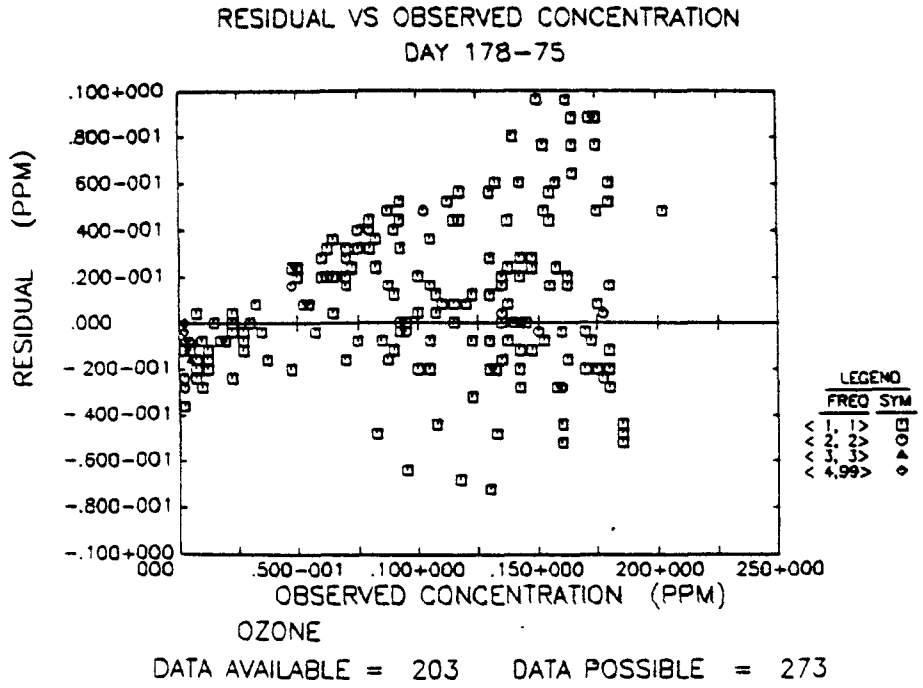

Figure D-3b. Residual vs. observed plot for O_3 from the UAM simulation results for Day 178-75.

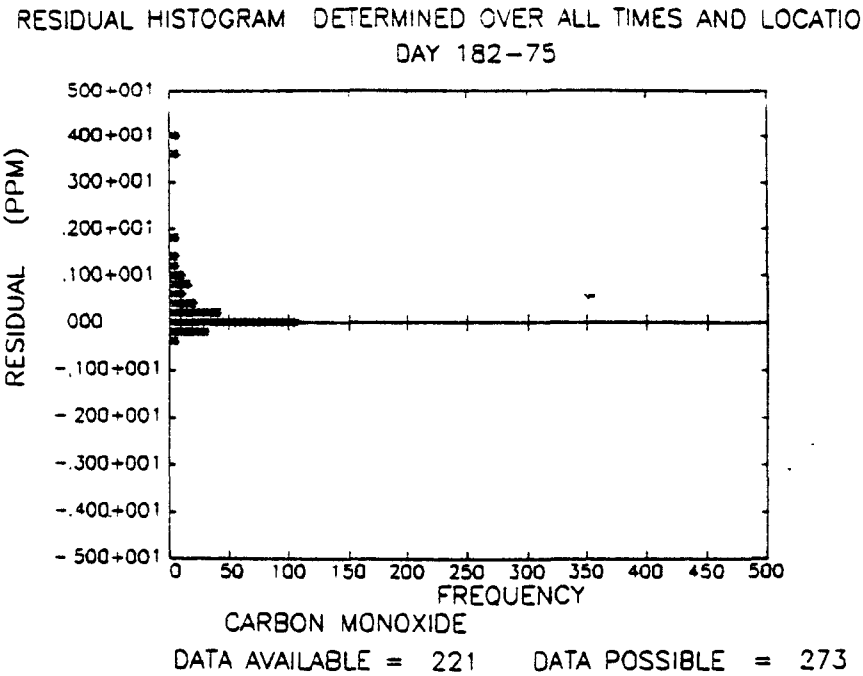

Figure D-4a. Residual histogram for CO from the UAM simulation results for Day 182-75.

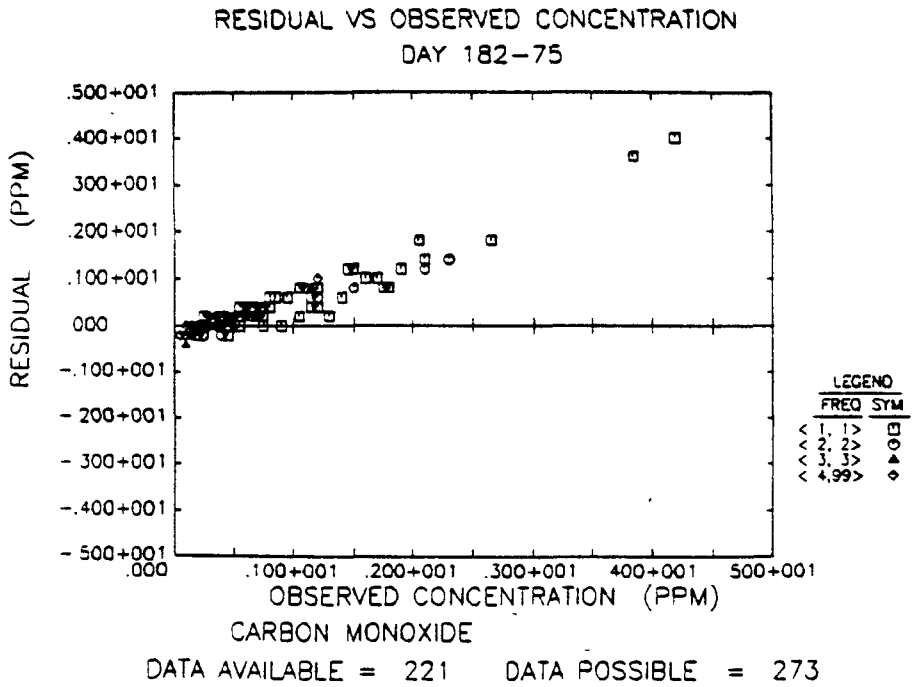

Figure D-4b. Residual vs. observed plot for CO from the UAM simulation results for Day 182-75.

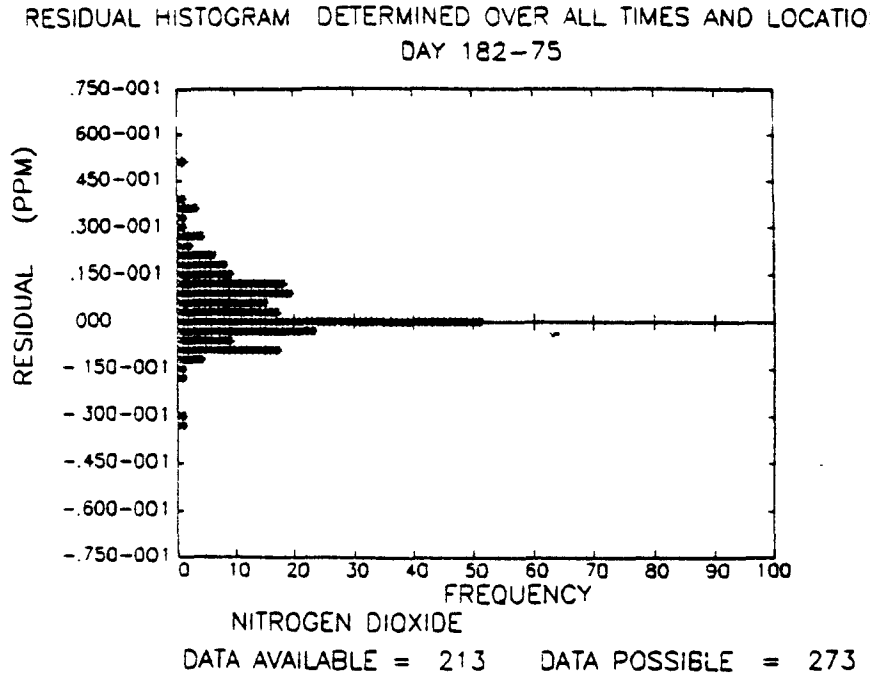

Figure D-5a. Residual histogram for NO_2 from the UAM simulation results for Day 182-75.

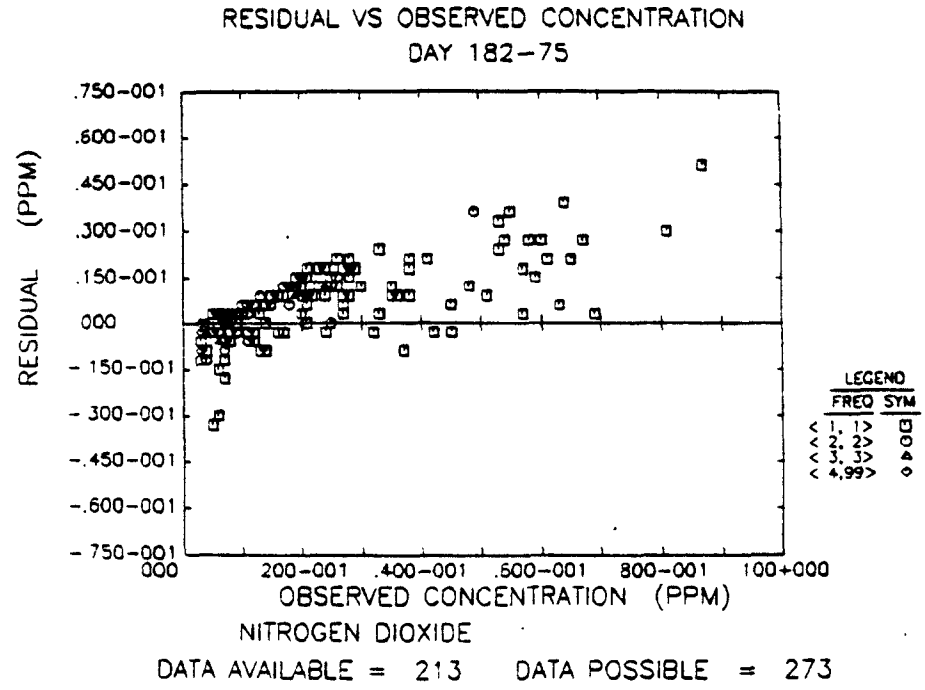

Figure D-5b. Residual vs. observed plot for NO_2 from the UAM simulation results for Day 182-75.

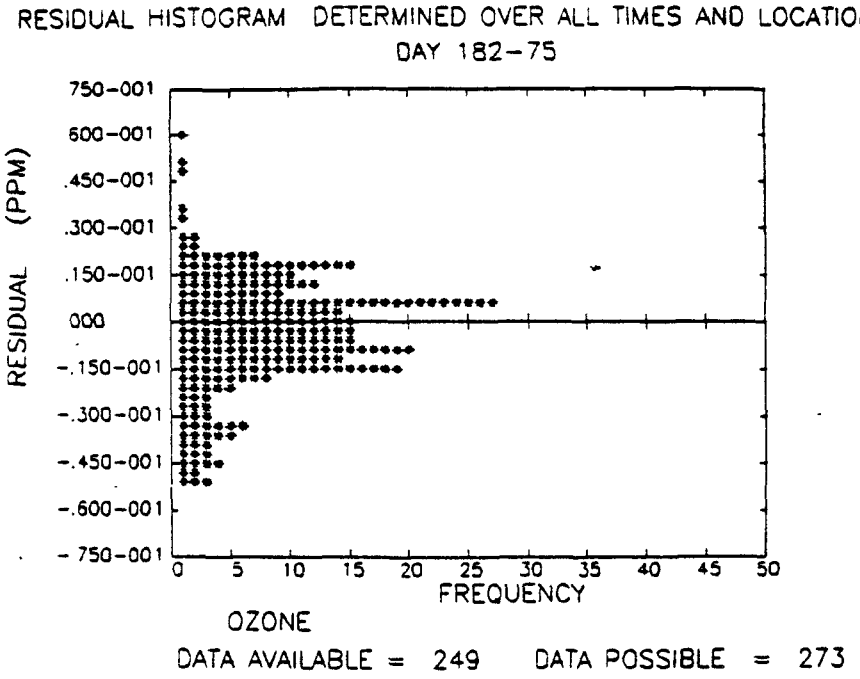

Figure D-6a. Residual histogram for O_3 from the UAM simulation results for Day 182-75.

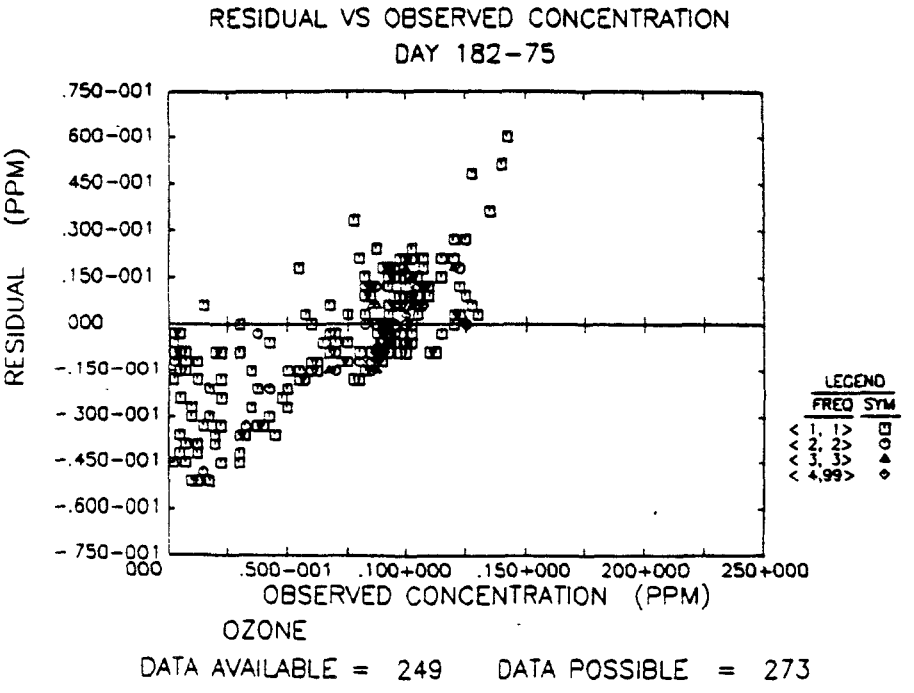

Figure D-6b. Residual vs. observed plot for O_3 from the UAM simulation results for Day 182-75.

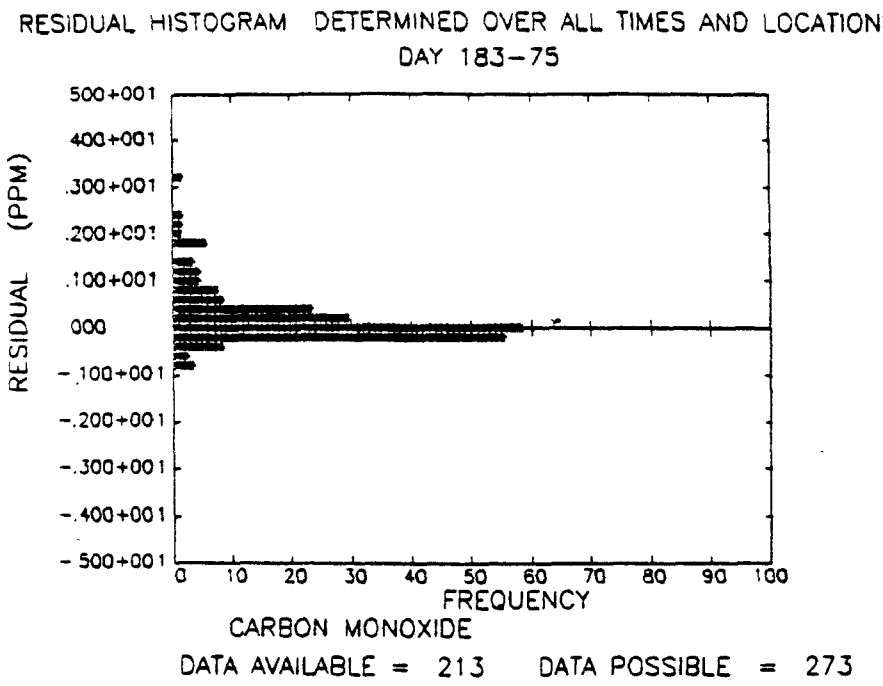

Figure D-7a. Residual histogram for CO from the UAM simulation results for Day 183-75.

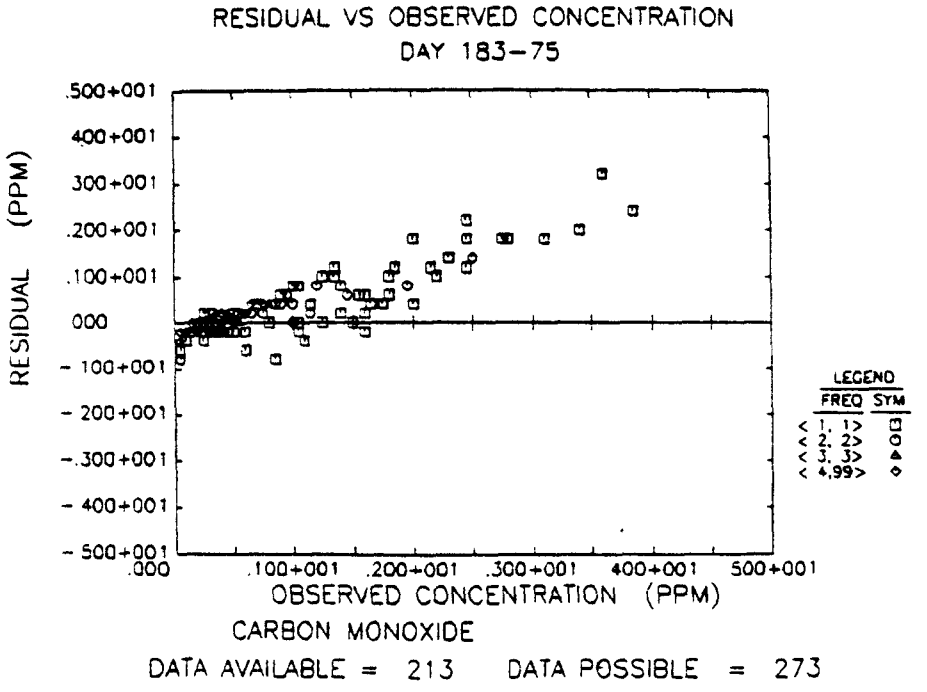

Figure D-7b. Residual vs. observed plot for CO from the UAM simulation results for Day 183-75.

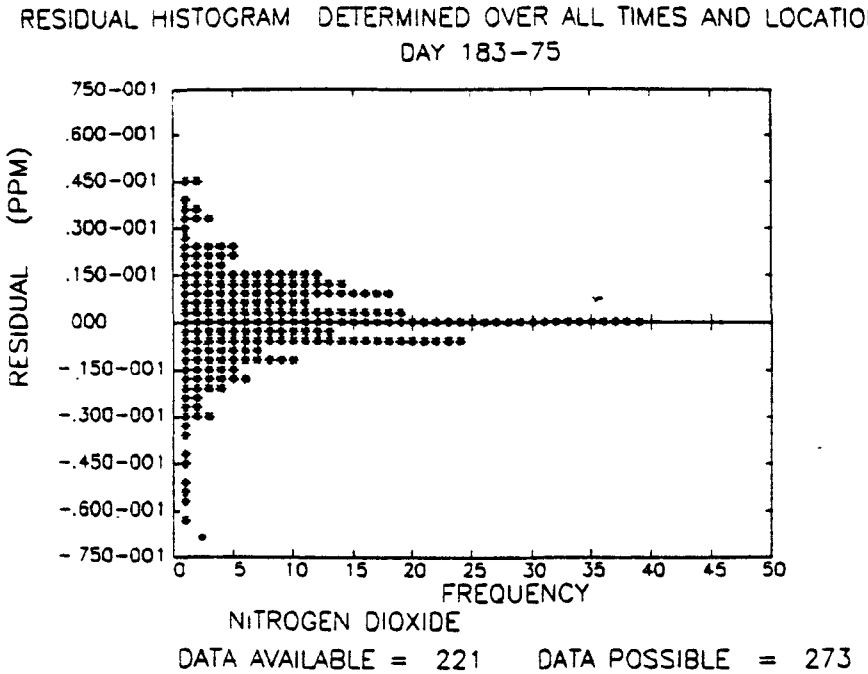

Figure D-8a. Residual histogram for NO_2 from the UAM simulation results for Day 183-75.

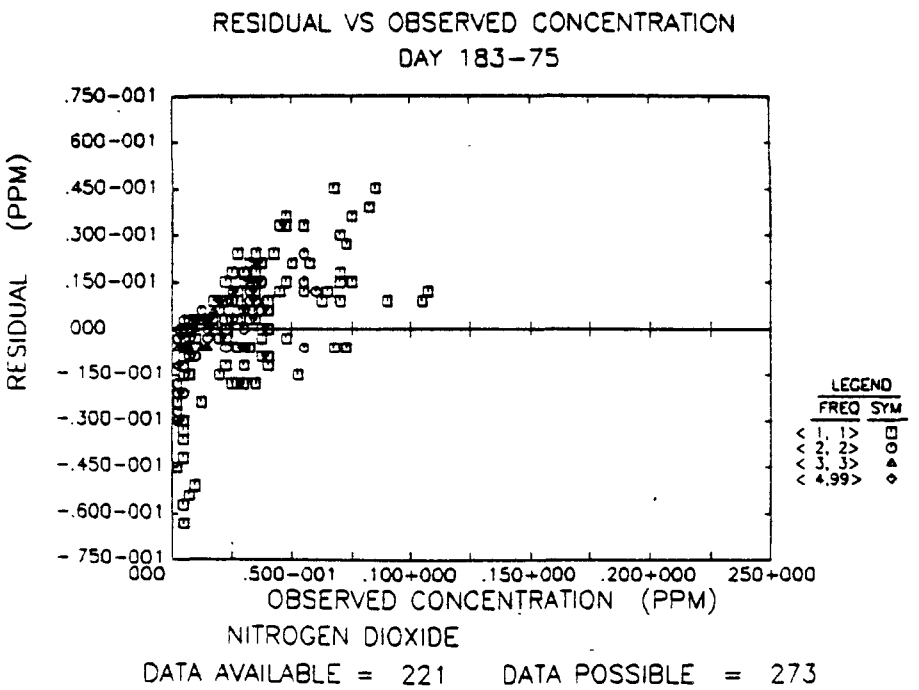

Figure D-8b. Residual vs. observed plot for NO_2 from the UAM simulation results for Day 183-75.

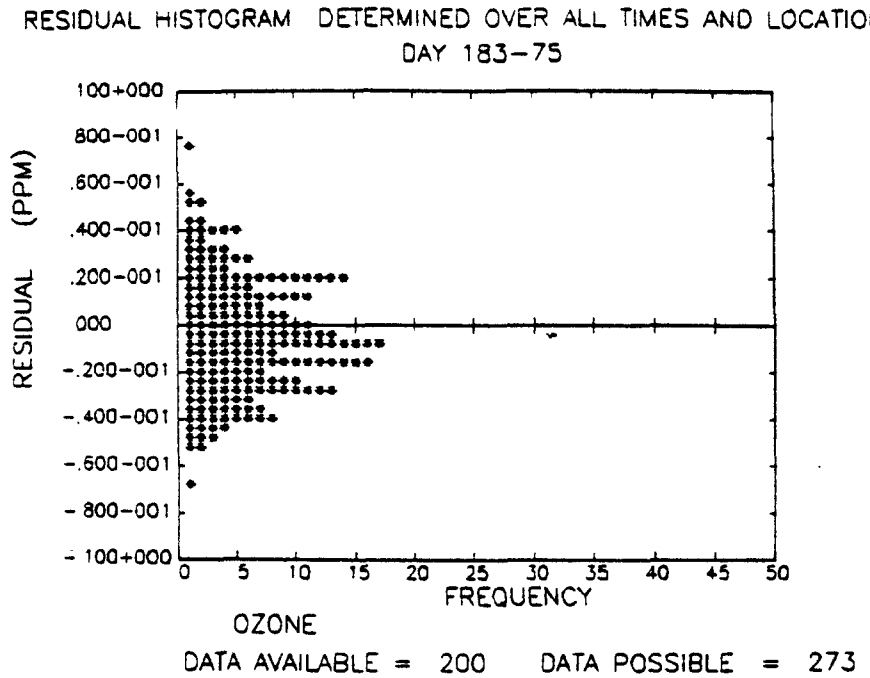

Figure D-9a. Residual histogram for O_3 from the UAM simulation results for Day 183-75.

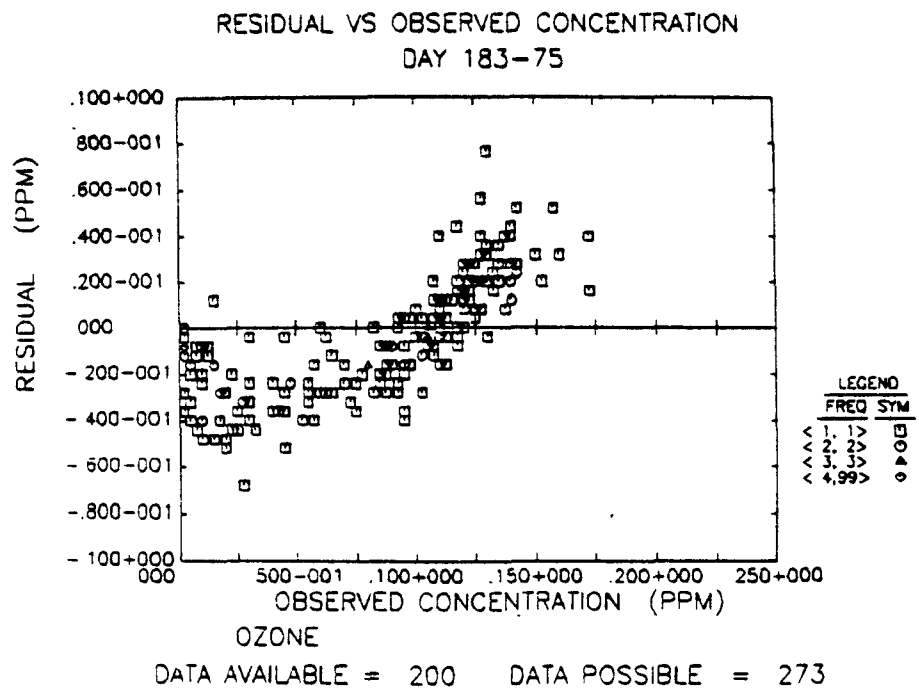

Figure D-9b. Residual vs. observed plot for O_3 from the UAM simulation results for Day 183-75.

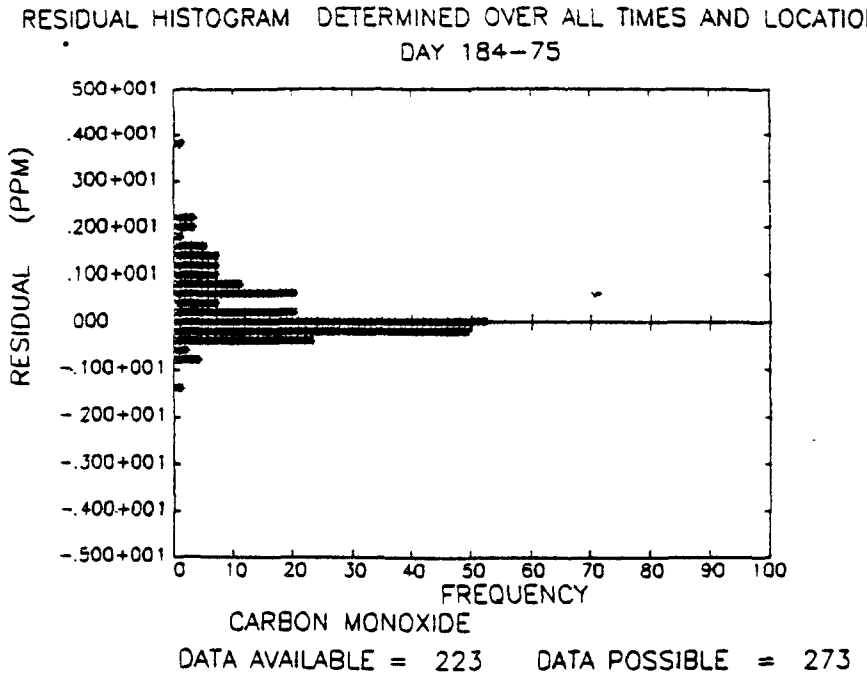

Figure D-10a. Residual histogram for CO from the UAM simulation results for Day 184-75.

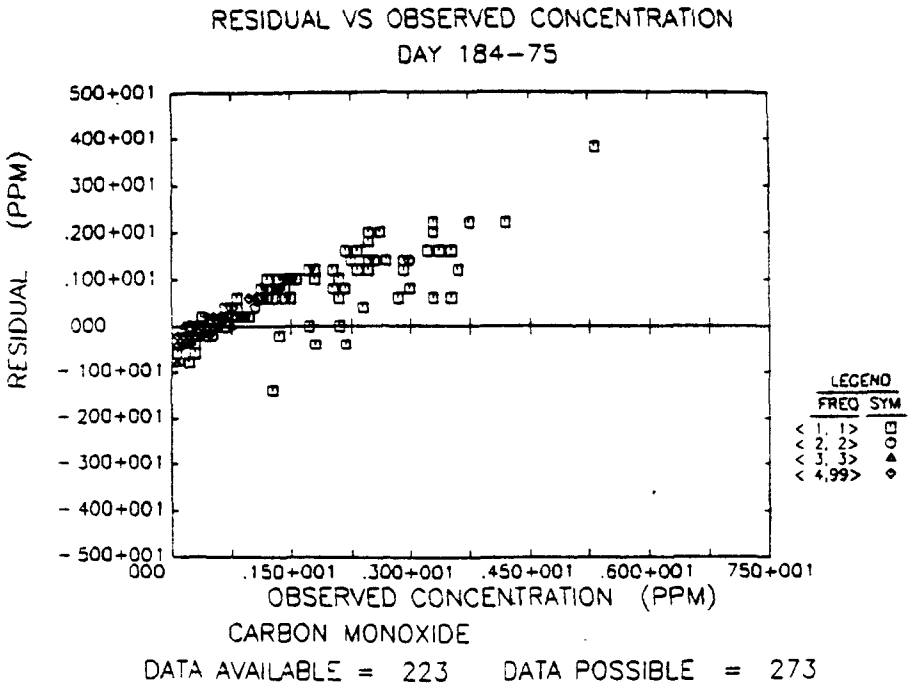

Figure D-10b. Residual vs. observed plot for CO from the UAM simulation results for Day 184-75.

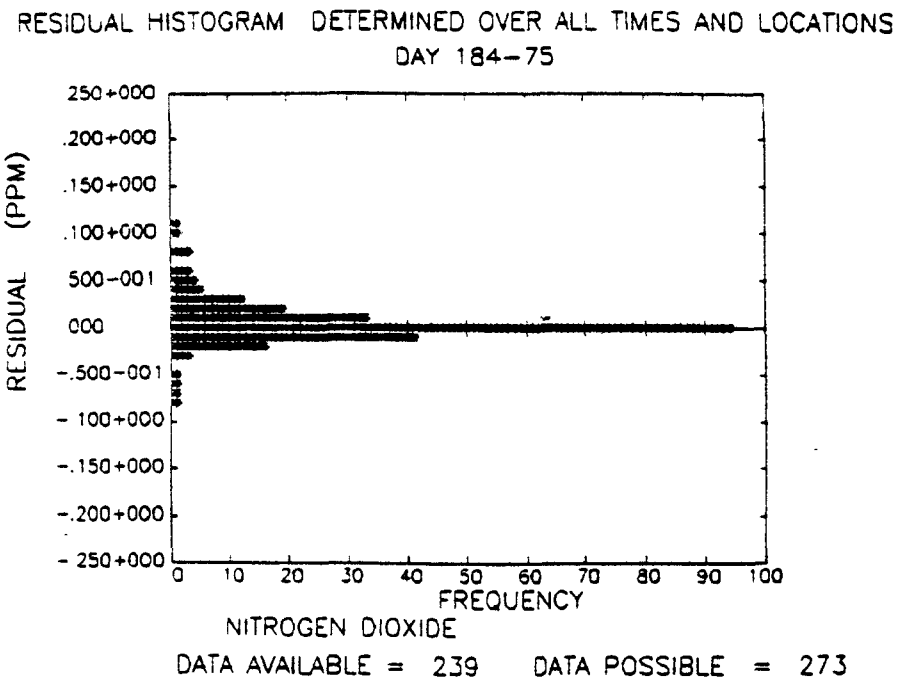

Figure D-11a. Residual histogram for NO_2 from the UAM simulation results for Day 184-75.

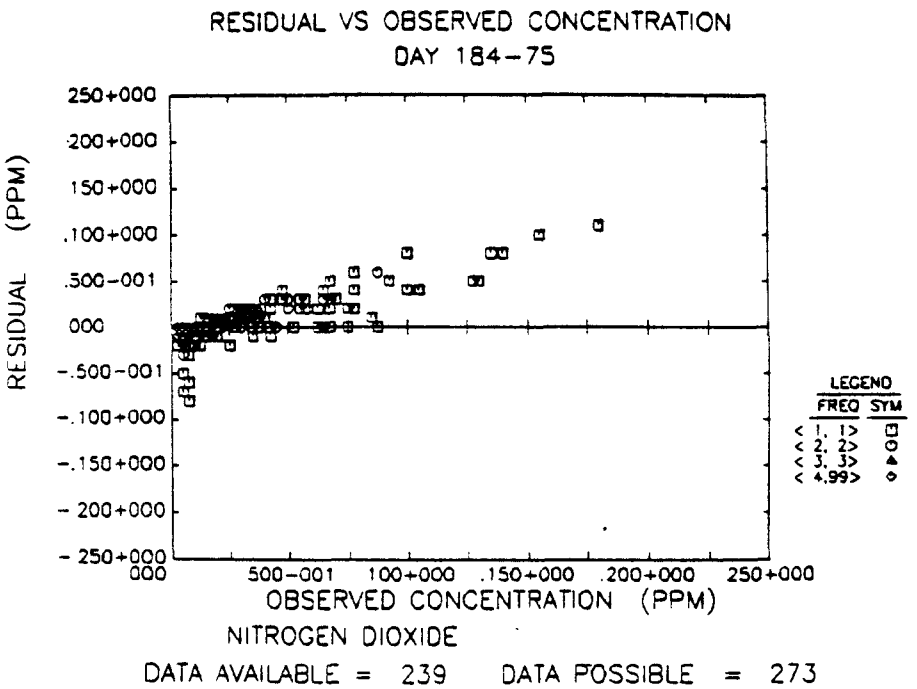

Figure D-11b. Residual vs. observed plot for NO_2 from the UAM simulation results for Day 184-75.

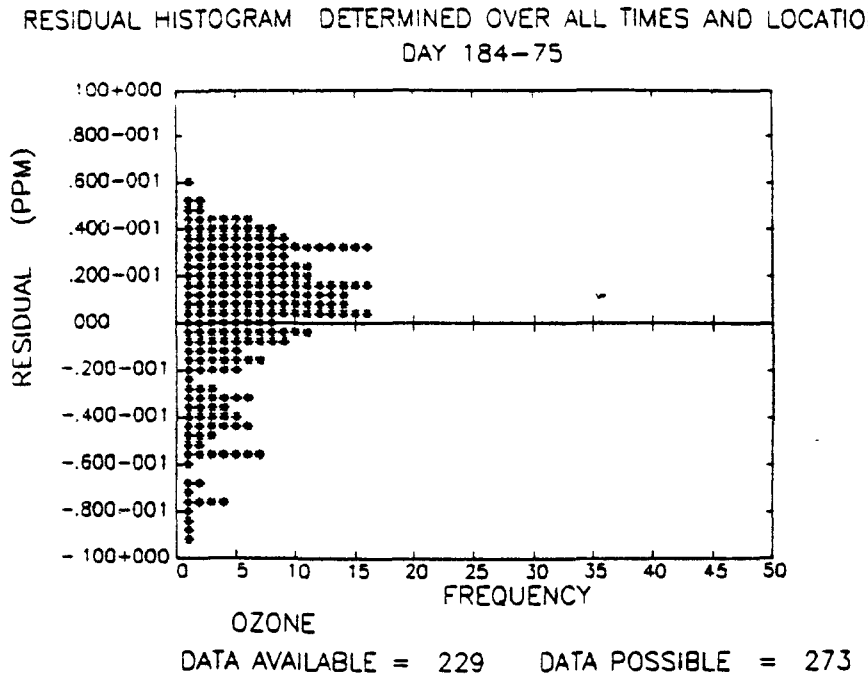

Figure D-12a. Residual histogram for O_3 from the UAM simulation results for Day 184-75.

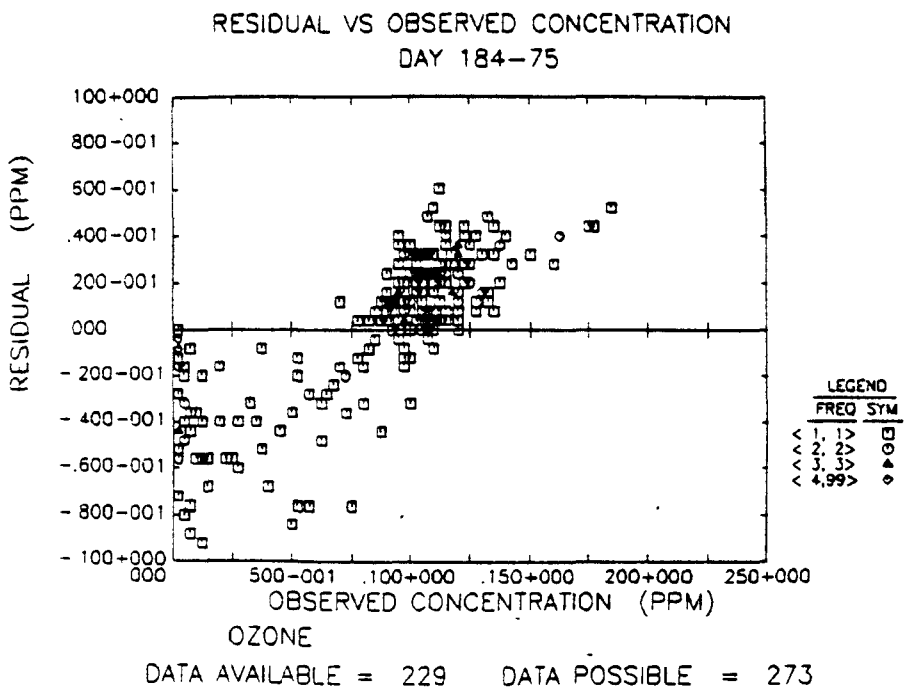

Figure D-12b. Residual vs. observed plot for O_3 from the UAM simulation results for Day 184-75.

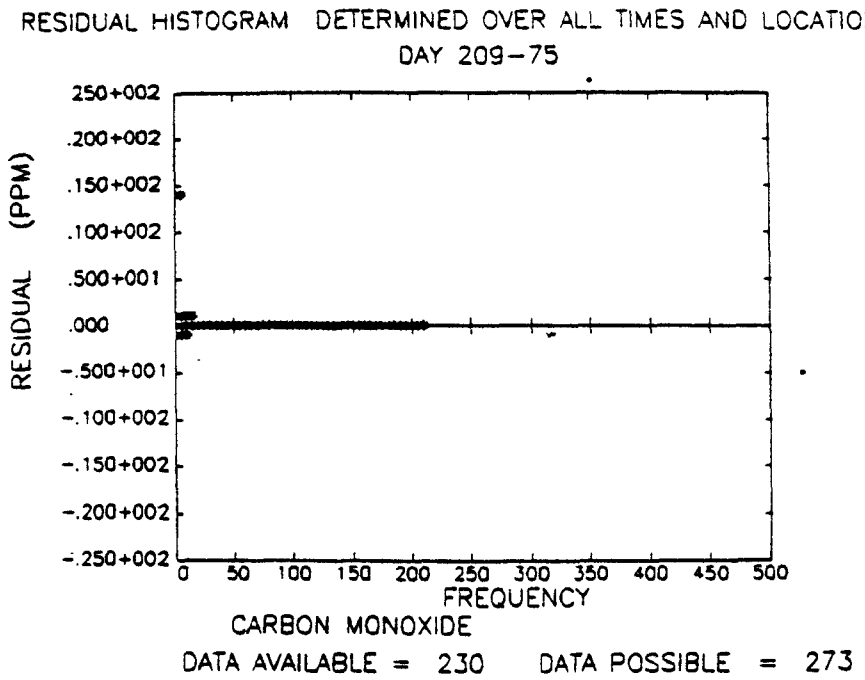

Figure D-13a. Residual histogram for CO from the UAM simulation results for Day 209-75.

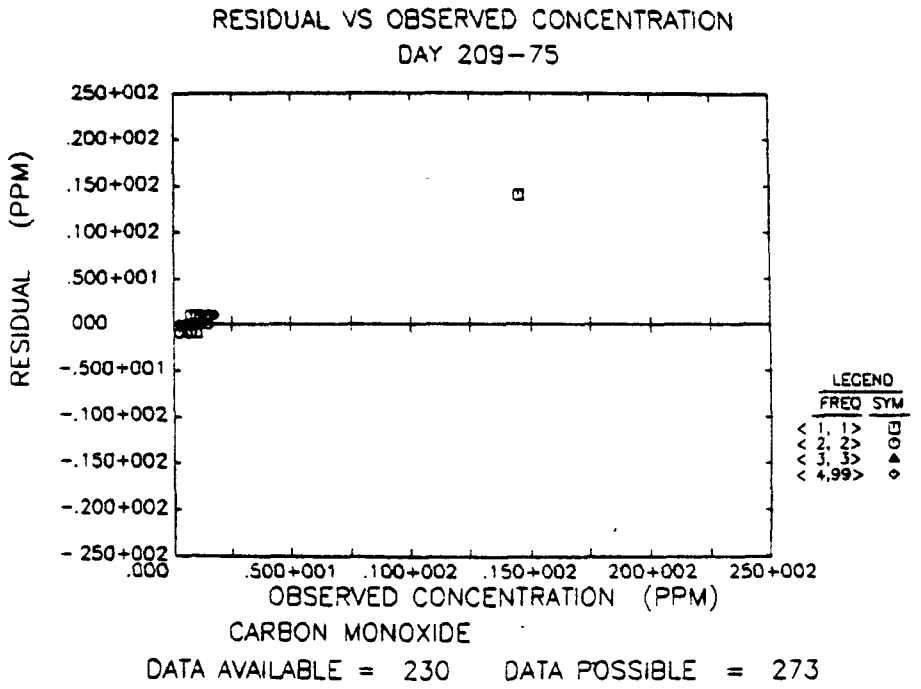

Figure D-13b. Residual vs. observed plot for CO from the UAM simulation results for Day 209-75.

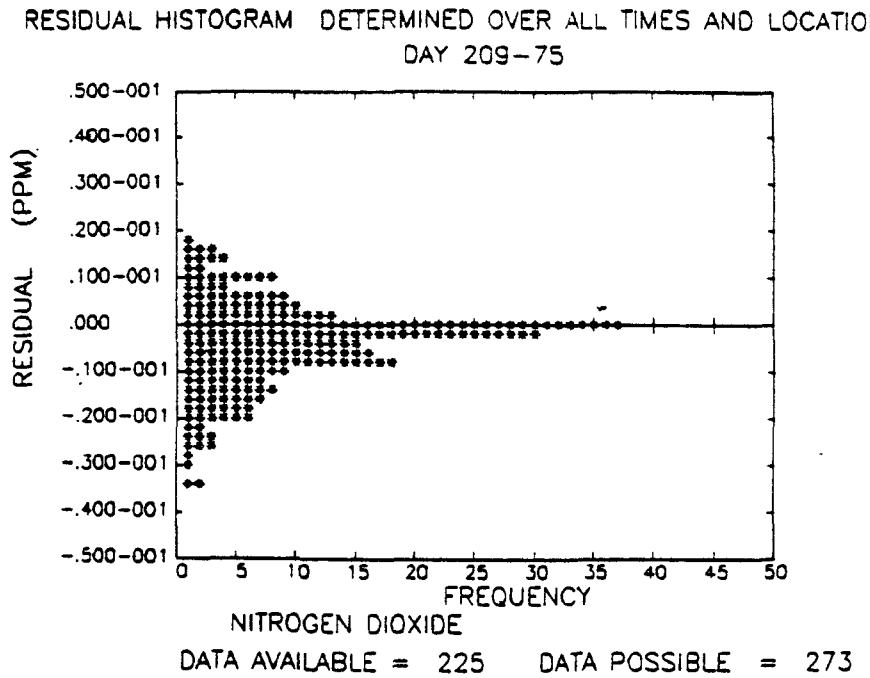

Figure D-14a. Residual histogram for NO_2 from the UAM simulation results for Day 209-75.

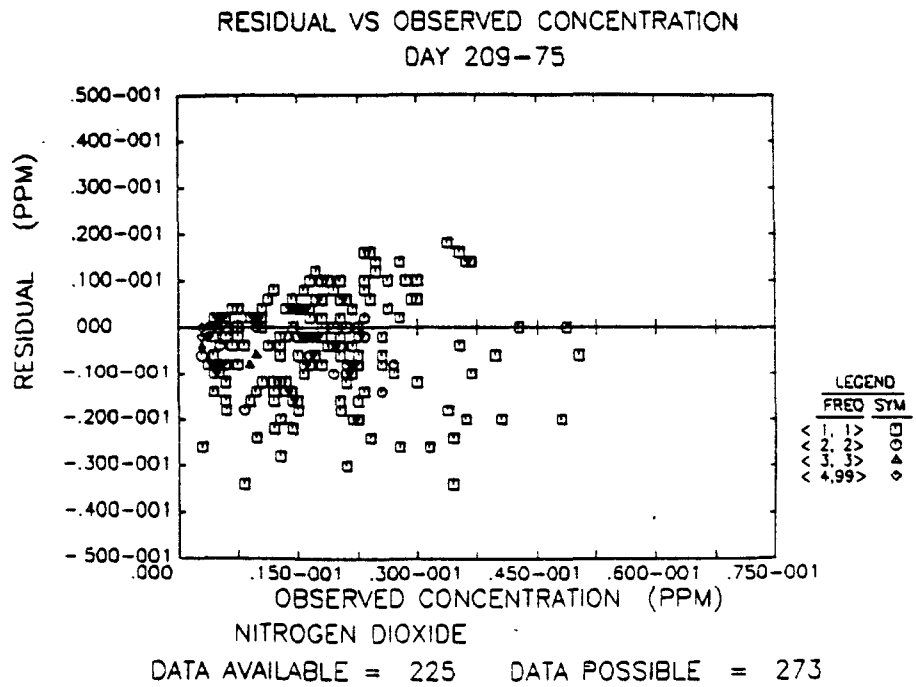

Figure D-14b. Residual vs. observed plot for NO_2 from the UAM simulation results for Day 209-75.

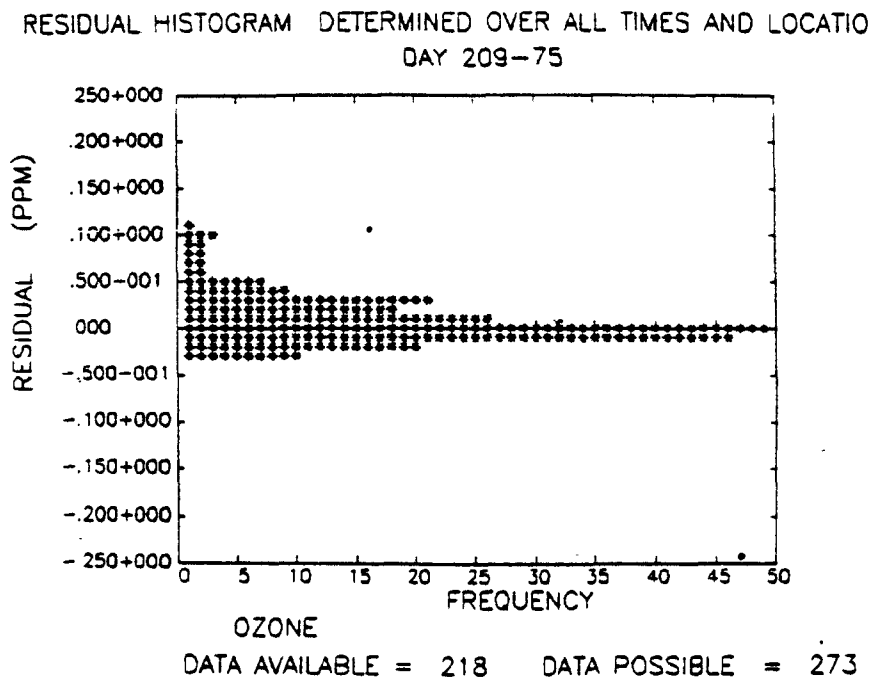

Figure D-15a. Residual histogram for O_3 from the UAM simulation results for Day 209-75.

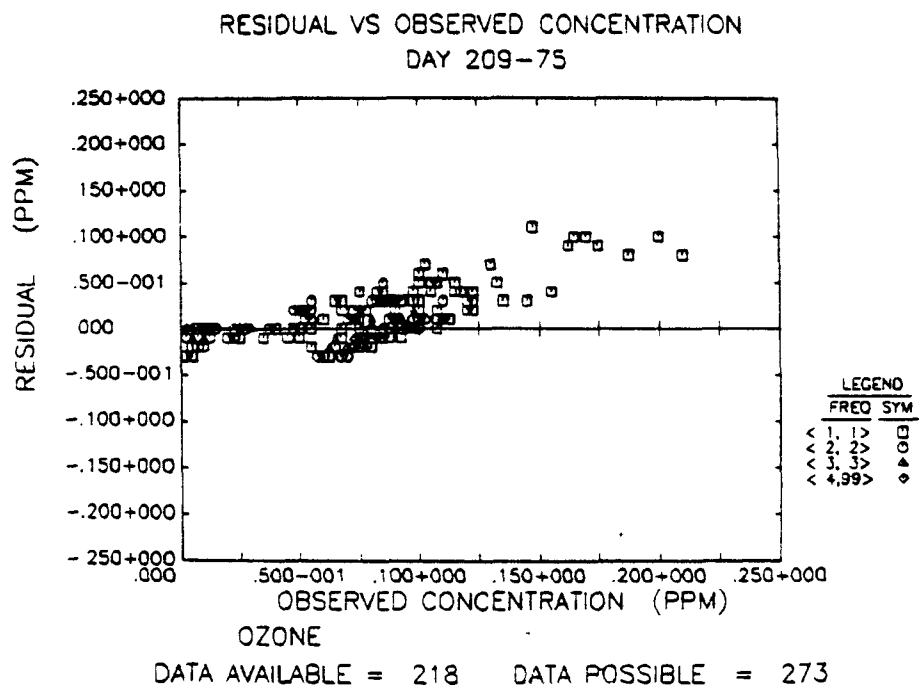

Figure D-15b. Residual vs. observed plot for O_3 from the UAM simulation results for Day 209-75.

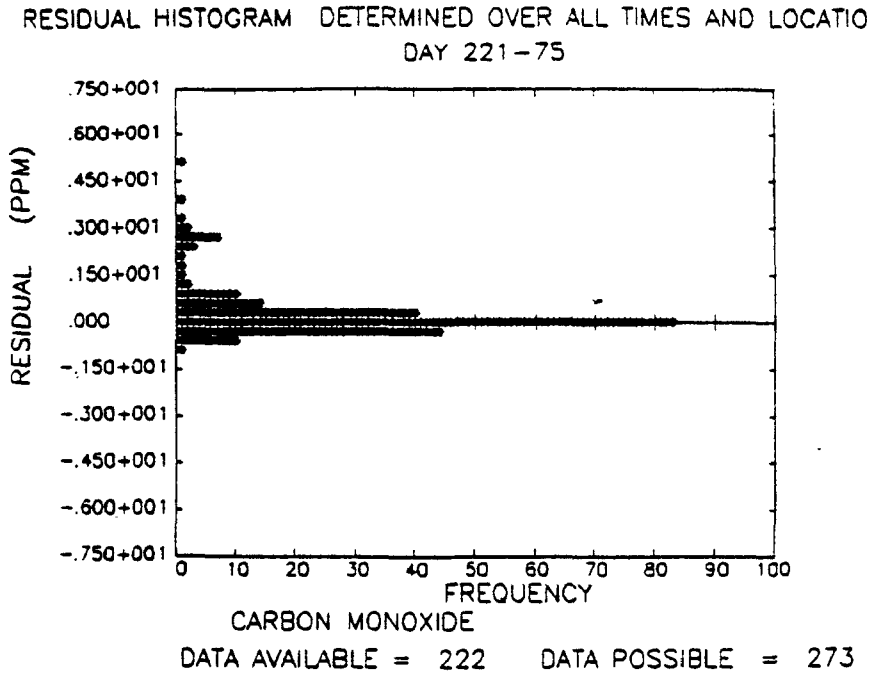

Figure D-16a. Residual histogram for CO from the UAM simulation results for Day 221-75.

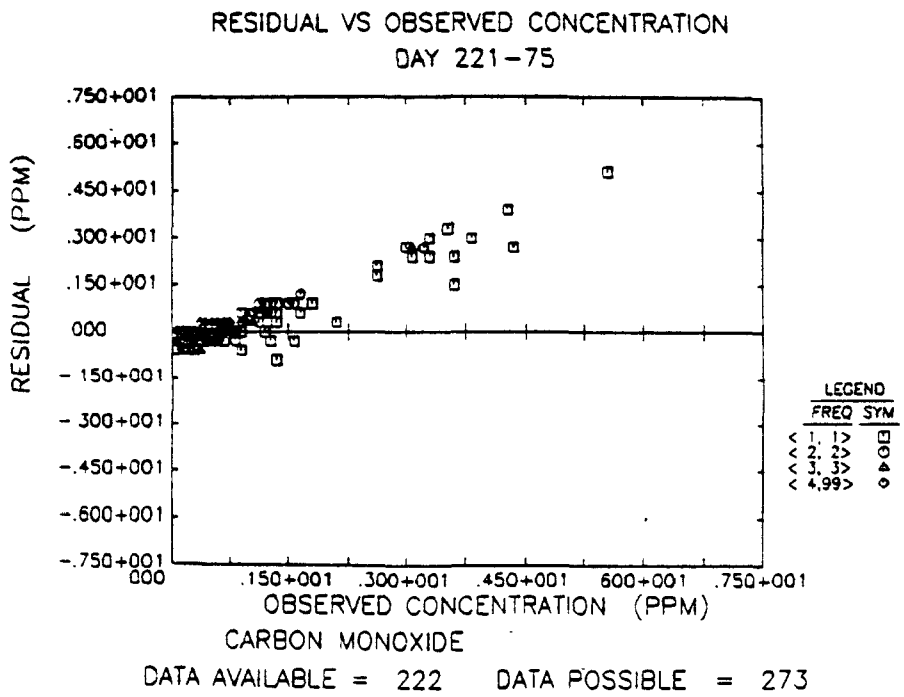

Figure D-16b. Residual vs. observed plot for CO from the UAM simulation results for Day 221-75.

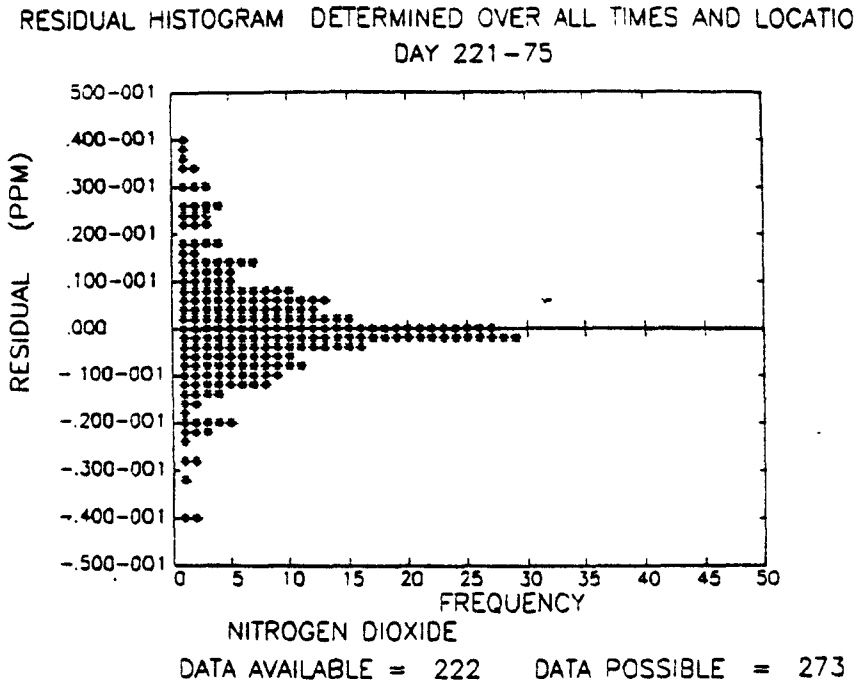

Figure D-17a. Residual histogram for NO_2 from the UAM simulation results for Day 221-75.

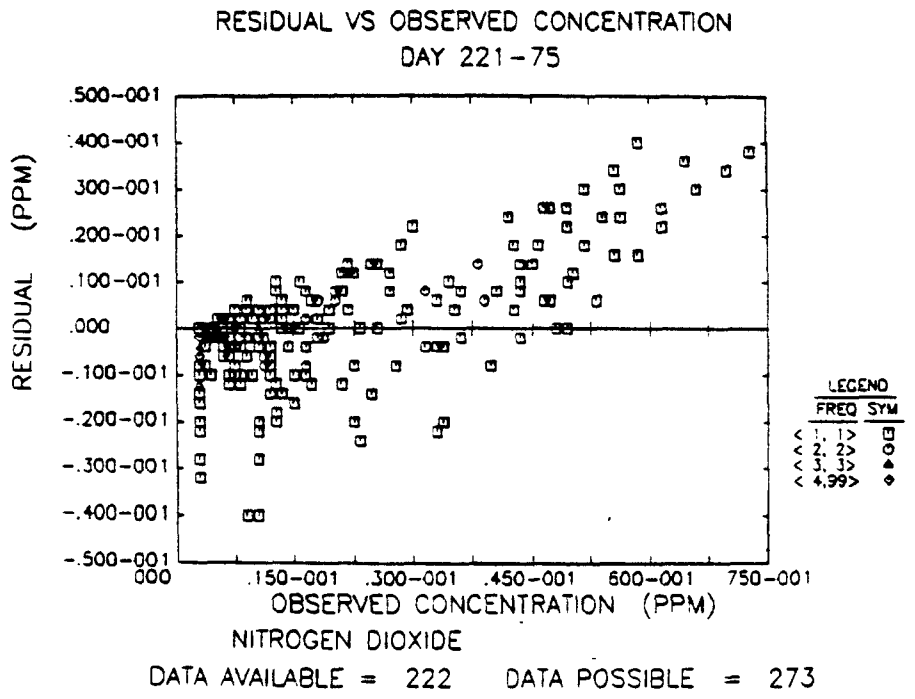

Figure D-17b. Residual vs. observed plot for NO_2 from the UAM simulation results for Day 221-75.

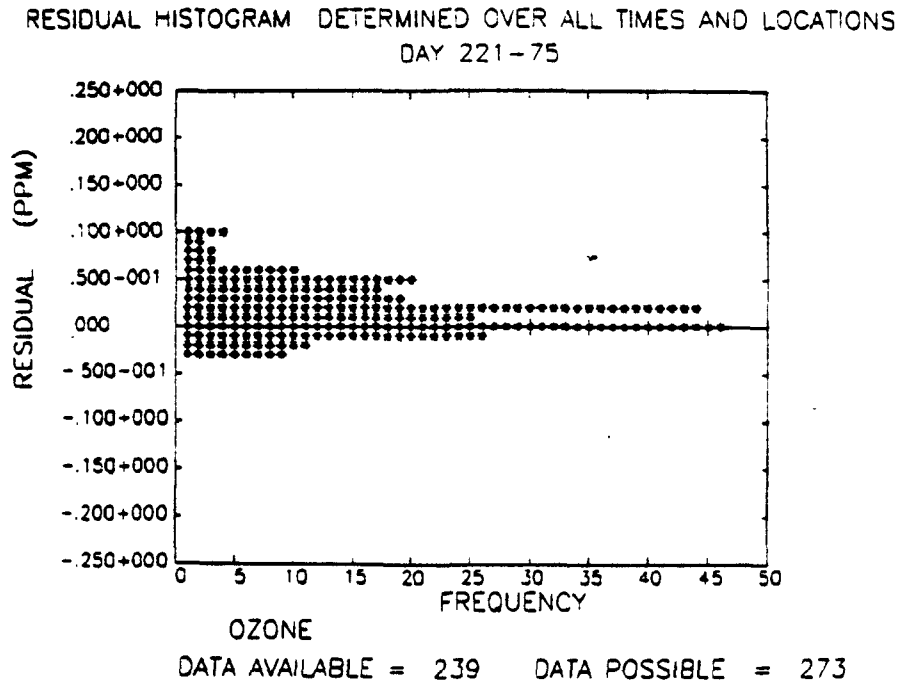

Figure D-18a. Residual histogram for O_3 from the UAM simulation results for Day 221-75.

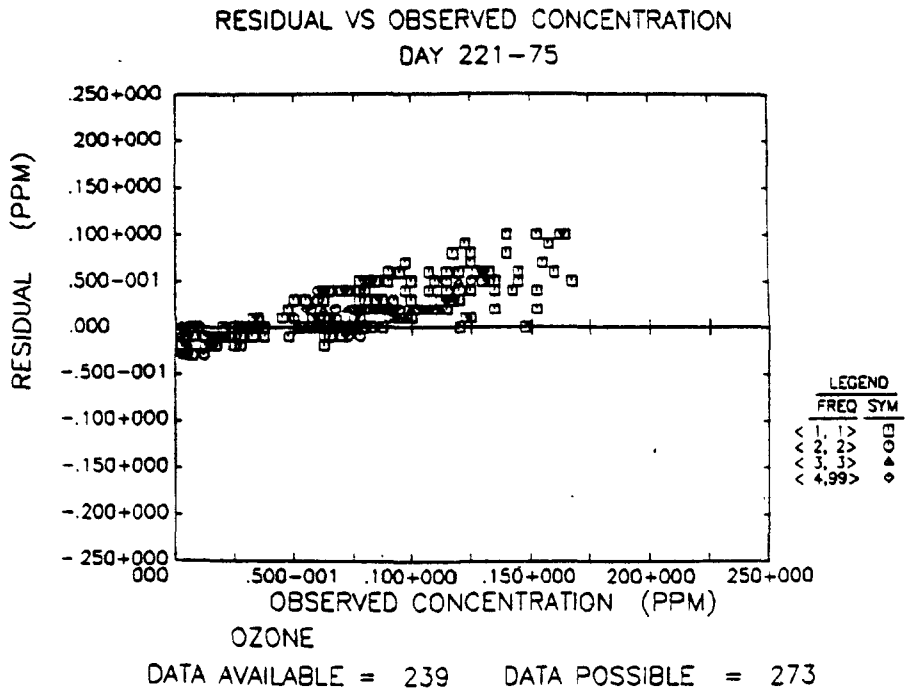

Figure D-18b. Residual vs. observed plot for O_3 from the UAM simulation results for Day 221-75.

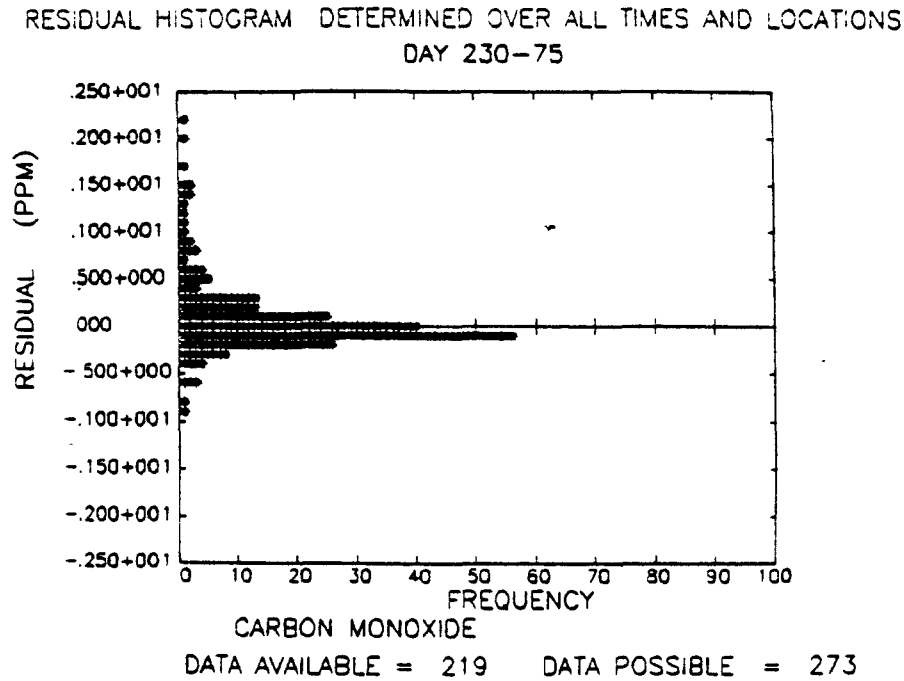

Figure D-19a. Residual histogram for CO from the UAM simulation results for Day 230-75.

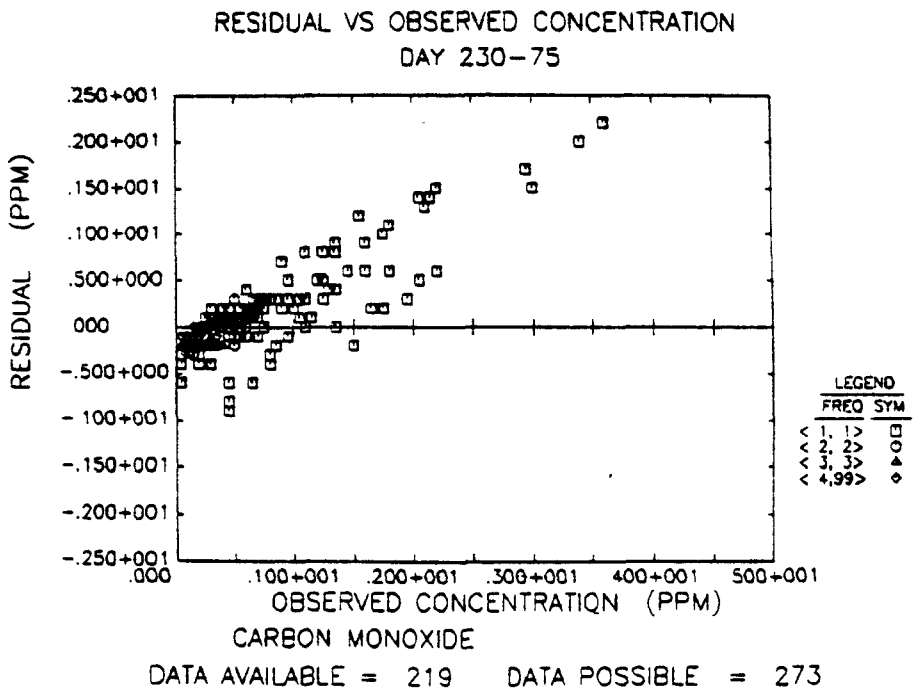

Figure D-19b. Residual vs. observed plot for CO from the UAM simulation results for Day 230-75.

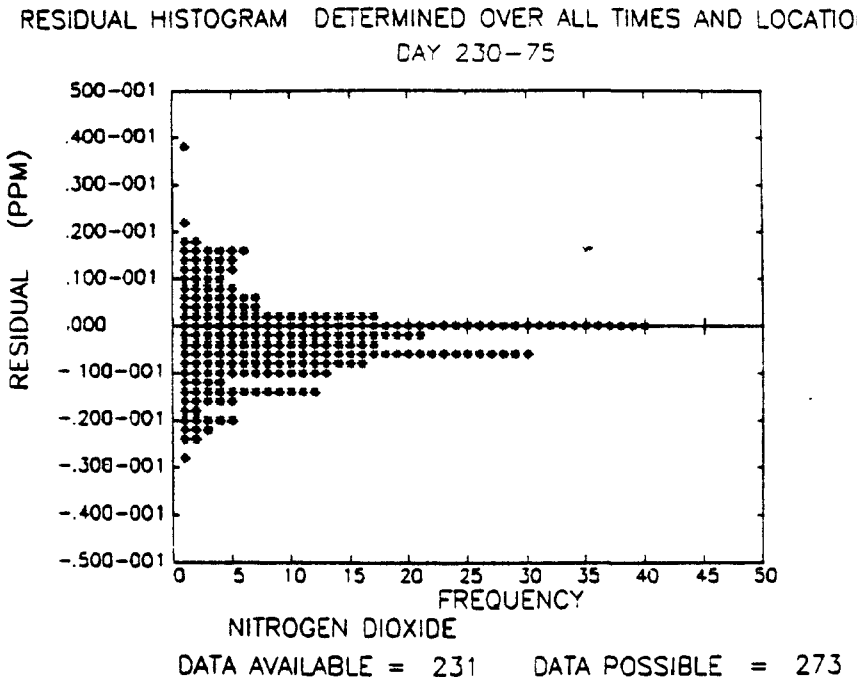

Figure D-20a. Residual histogram for NO_2 from the UAM simulation results for Day 230-75.

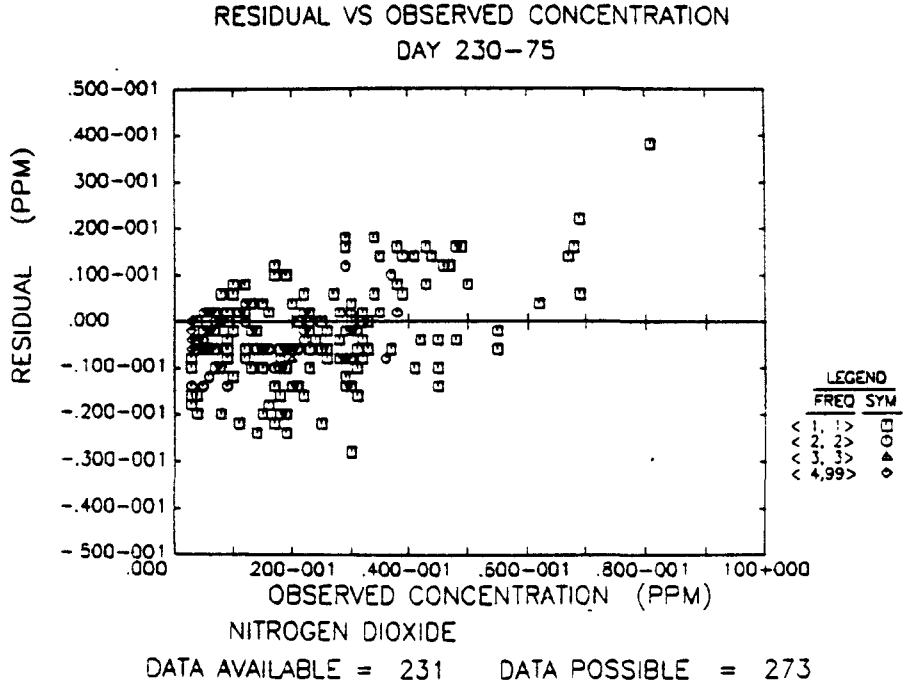

Figure D-20b. Residual vs. observed plot for NO_2 from the UAM simulation results for Day 230-75.

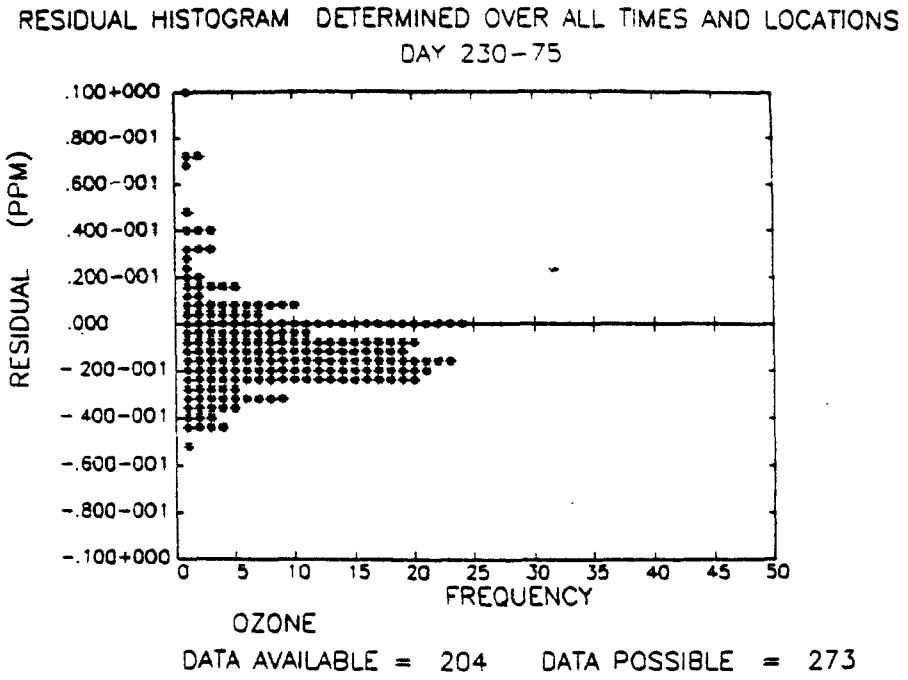

Figure D-21a. Residual histogram for O_3 from the UAM simulation results for Day 230-75.

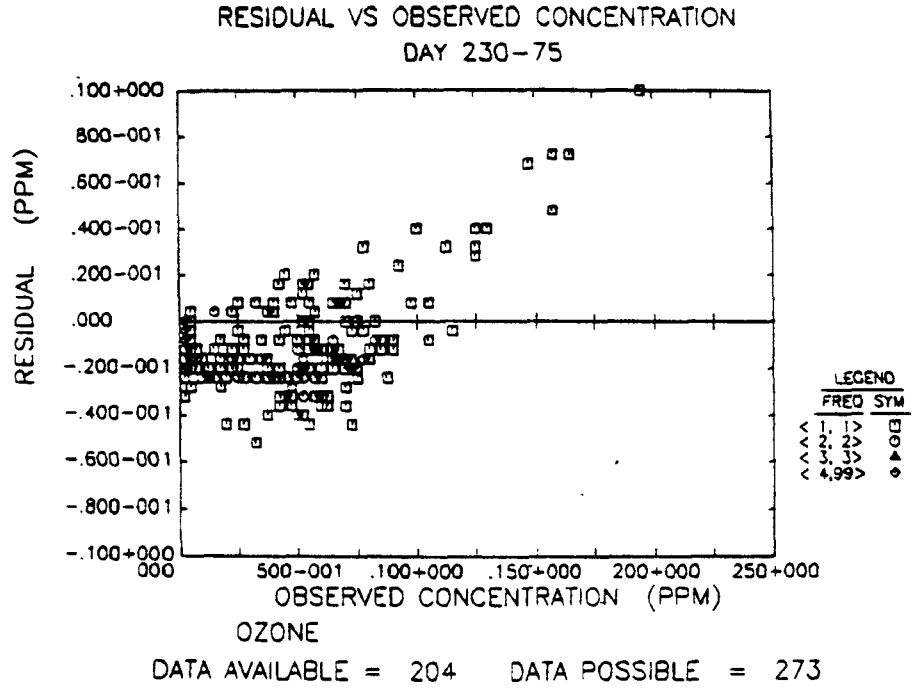

Figure D-21b. Residual vs. observed plot for O_3 from the UAM simulation results for Day 230-75.

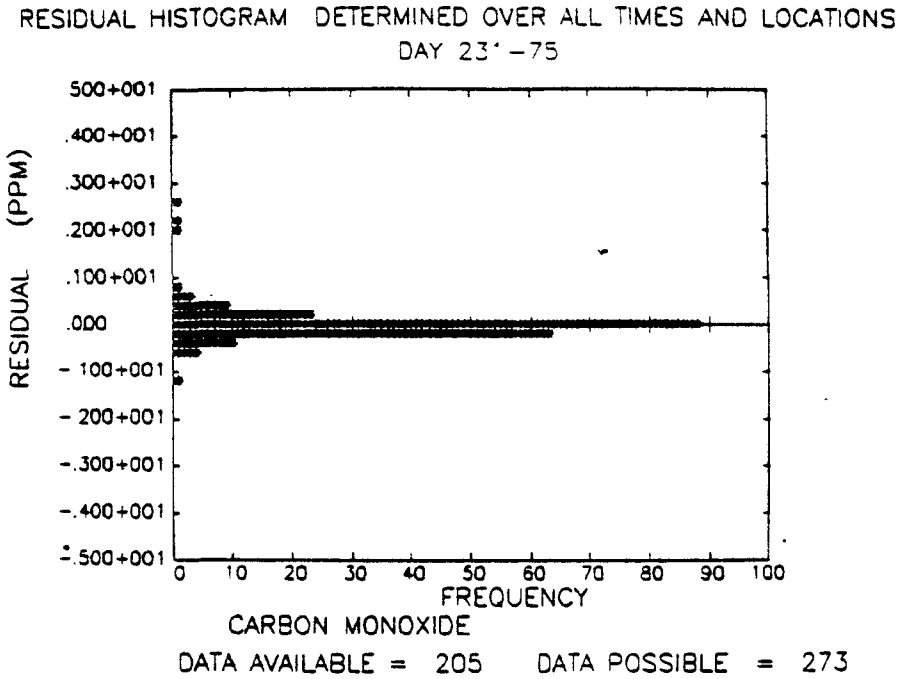

Figure D-22a. Residual histogram for CO from the UAM simulation results for Day 231-75.

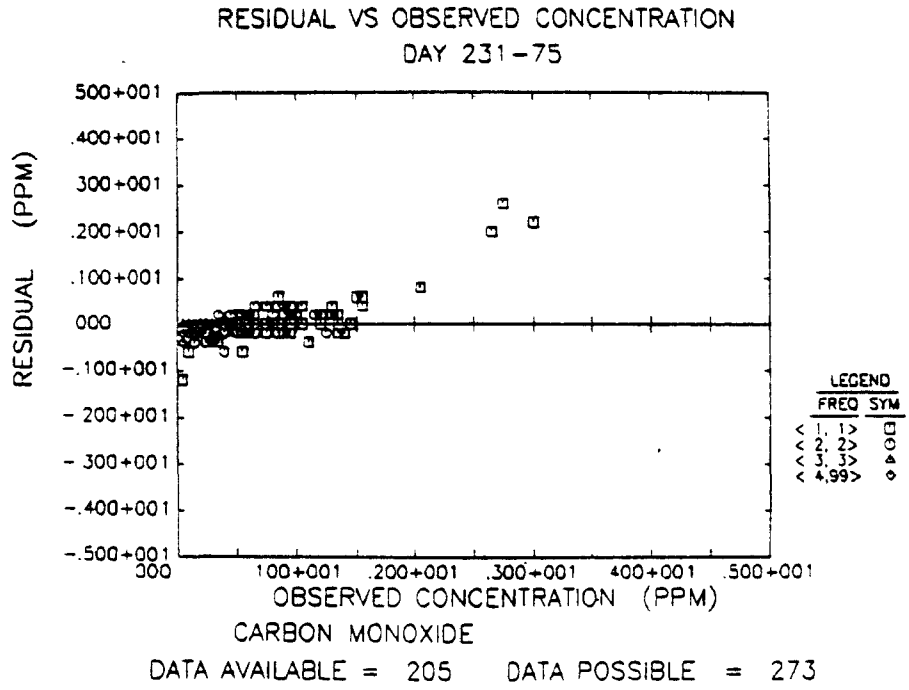

Figure D-22b. Residual vs. observed plot for CO from the UAM simulation results for Day 231-75.

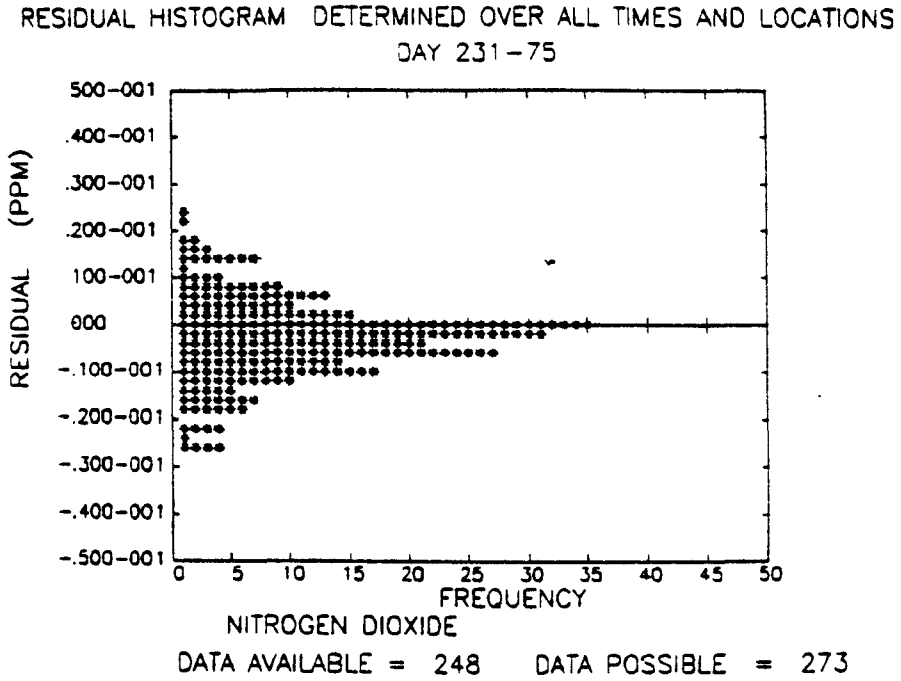

Figure D-23a. Residual histogram for NO_2 from the UAM simulation results for Day 231-75.

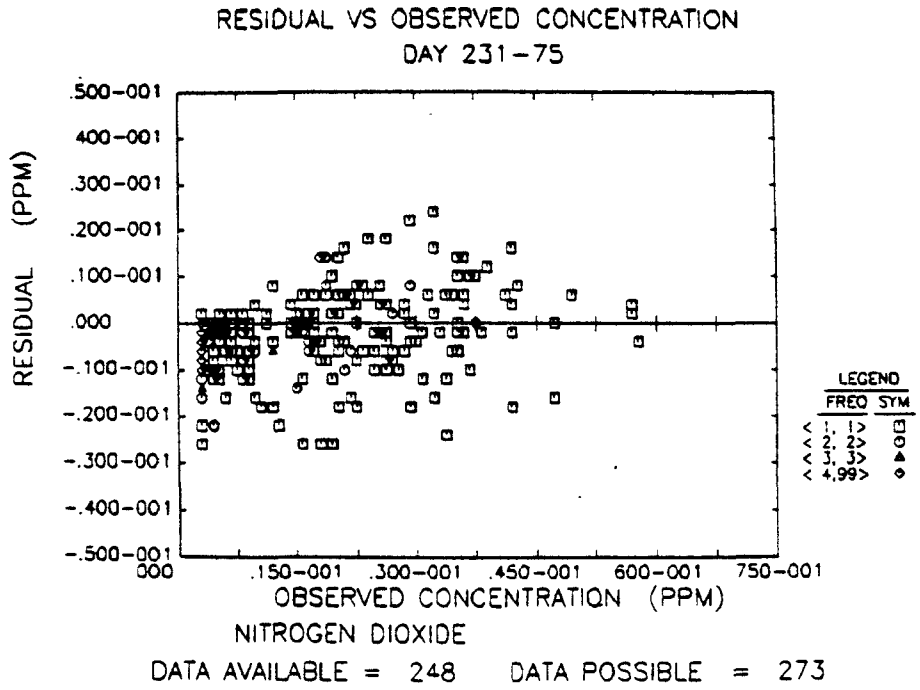

Figure D-23b. Residual vs. observed plot for NO_2 from the UAM simulation results for Day 231-75.

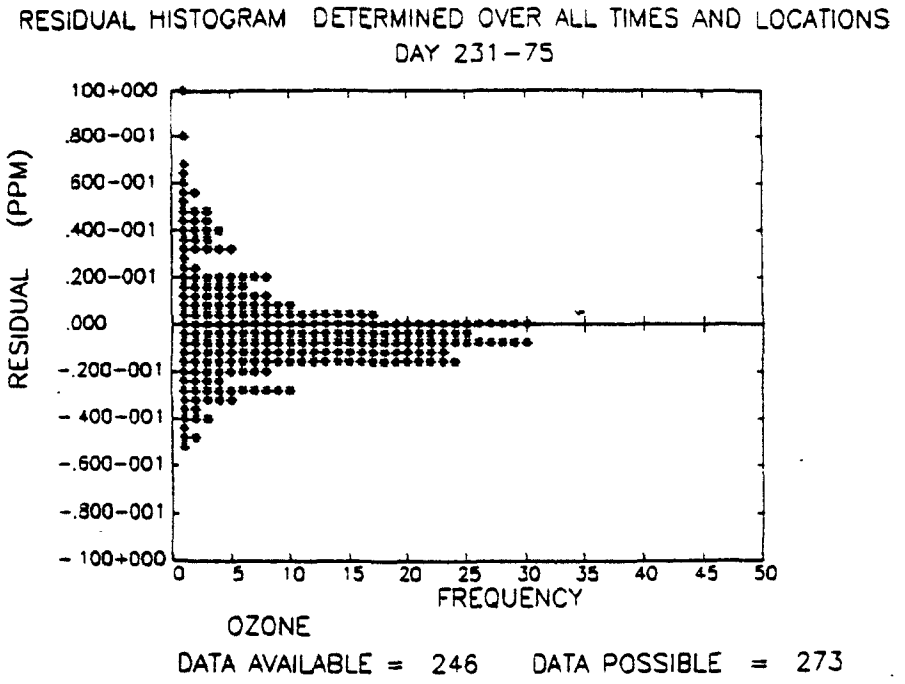

Figure D-24a. Residual histogram for O_3 from the UAM simulation results for Day 231-75.

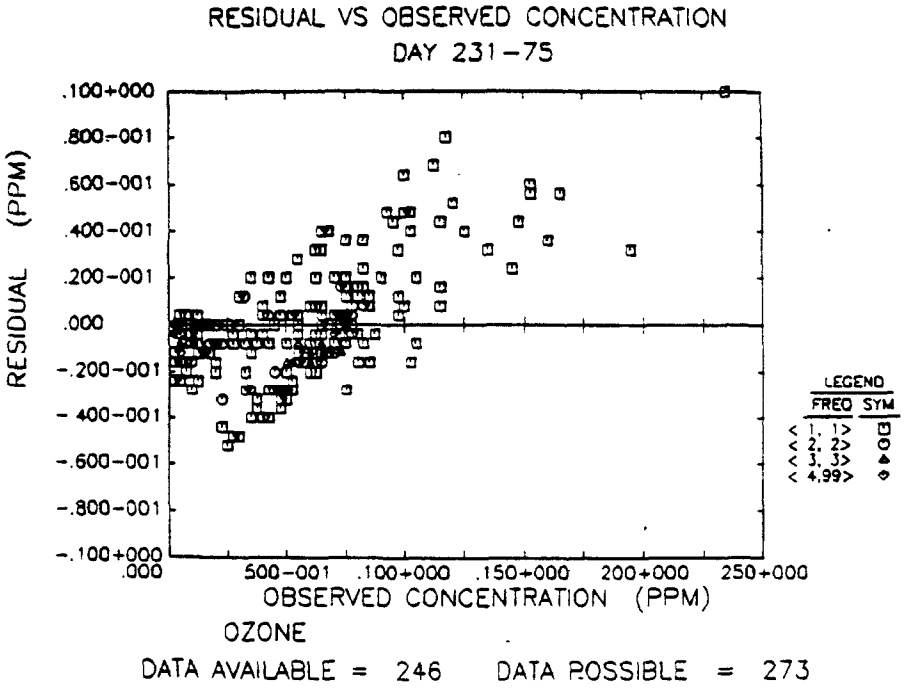

Figure D-24b. Residual vs. observed plot for O_3 from the UAM simulation results for Day 231-75.

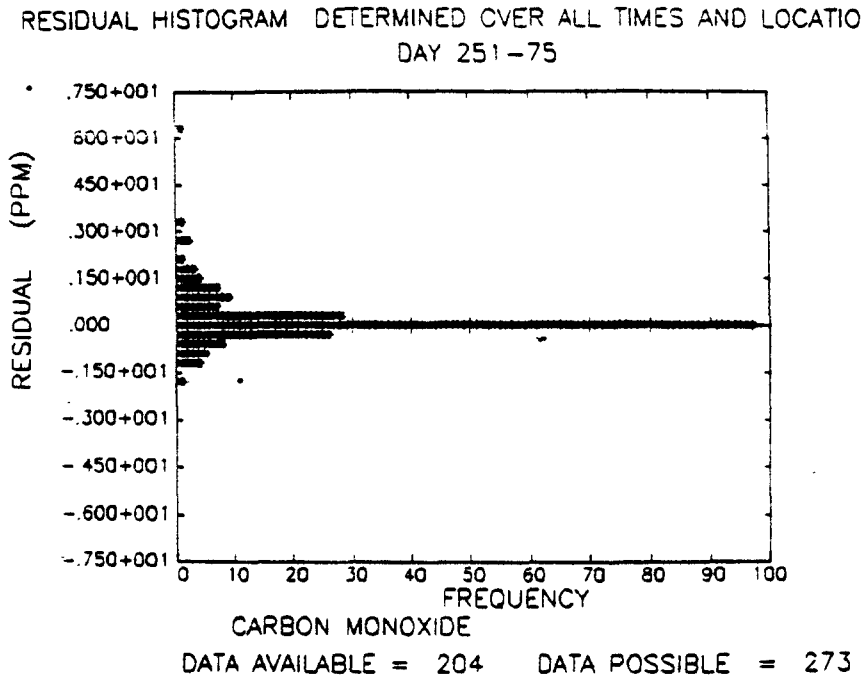

Figure D-25a. Residual histogram for CO from the UAM simulation results for Day 251-75.

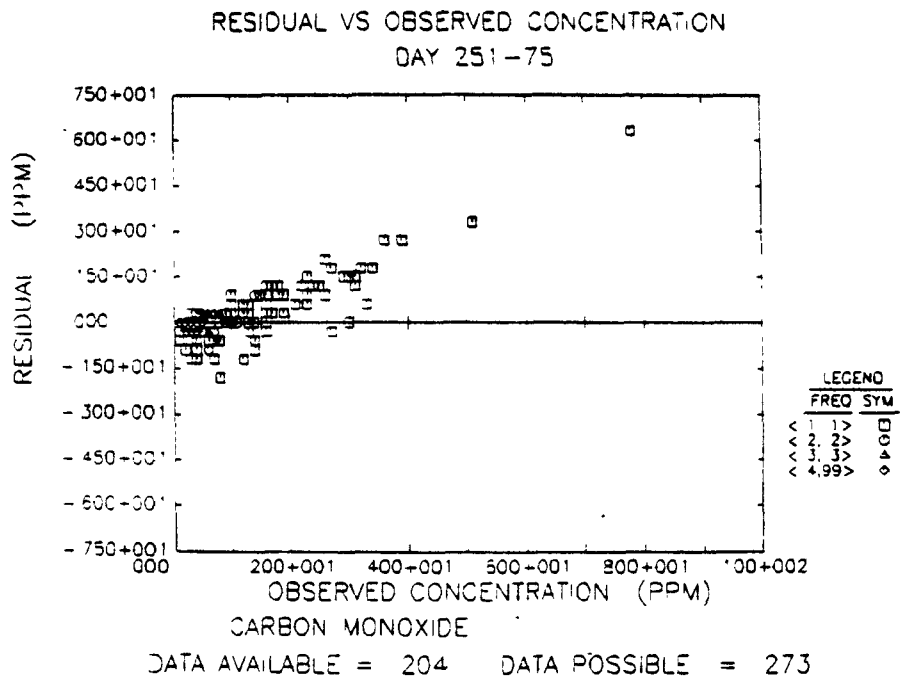

Figure D-25b. Residual vs. observed plot for CO from the UAM simulation results for Day 251-75.

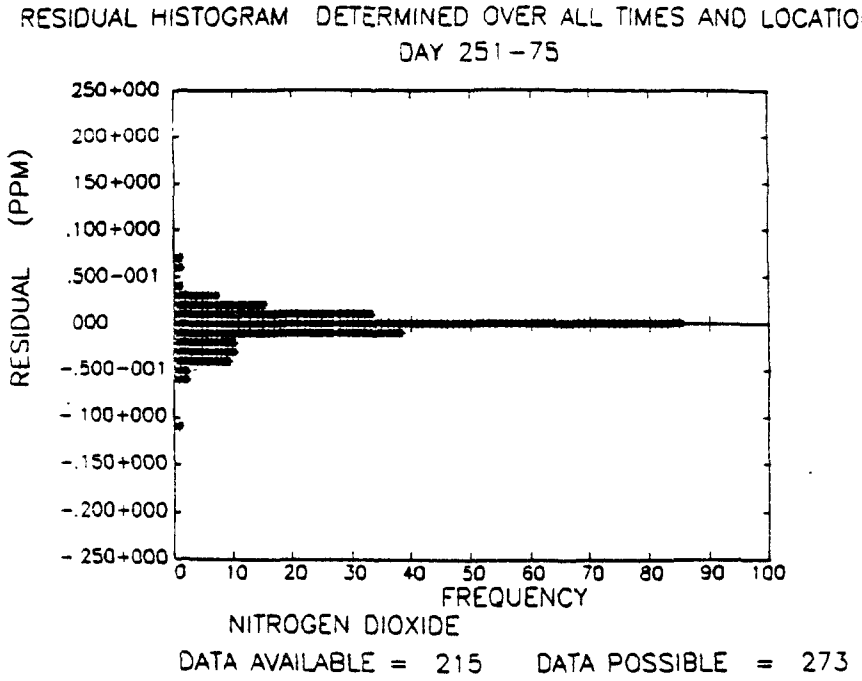

Figure D-26a. Residual histogram for NO_2 from the UAM simulation results for Day 251-75.

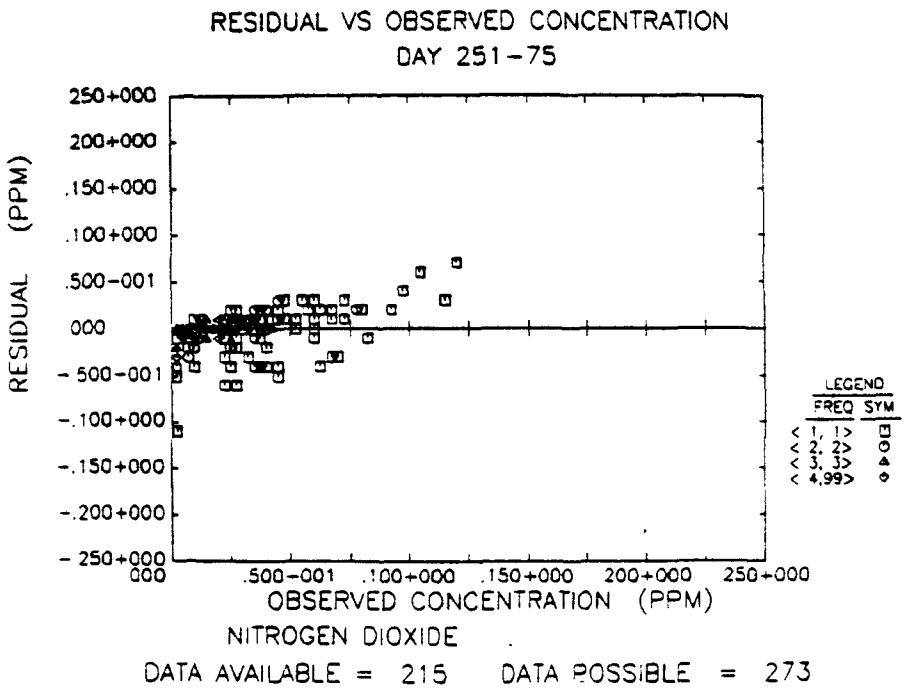

Figure D-26b. Residual vs. observed plot for NO_2 from the UAM simulation results for Day 251-75.

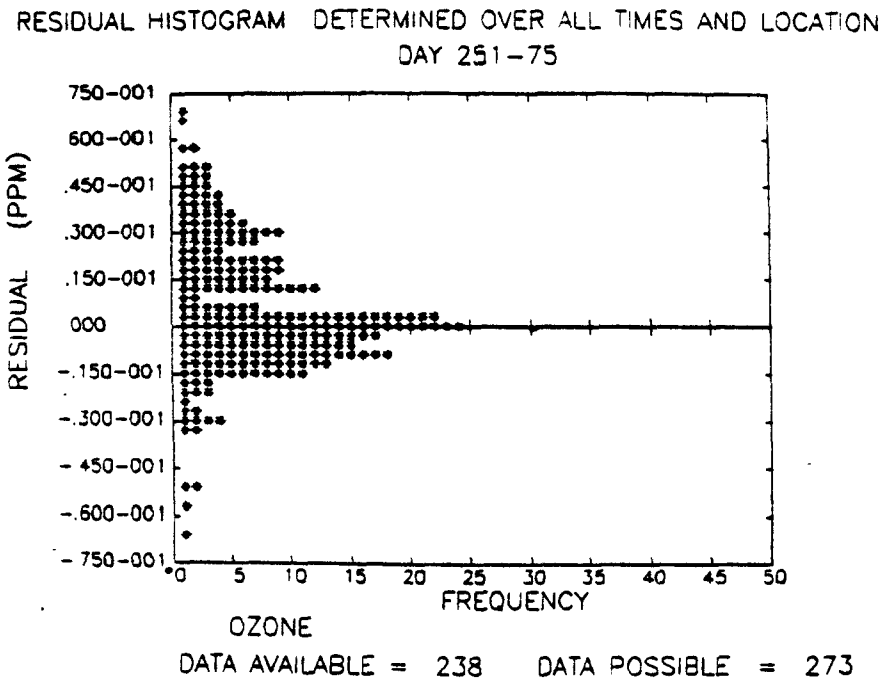

Figure D-27a. Residual histogram for O_3 from the UAM simulation results for Day 251-75.

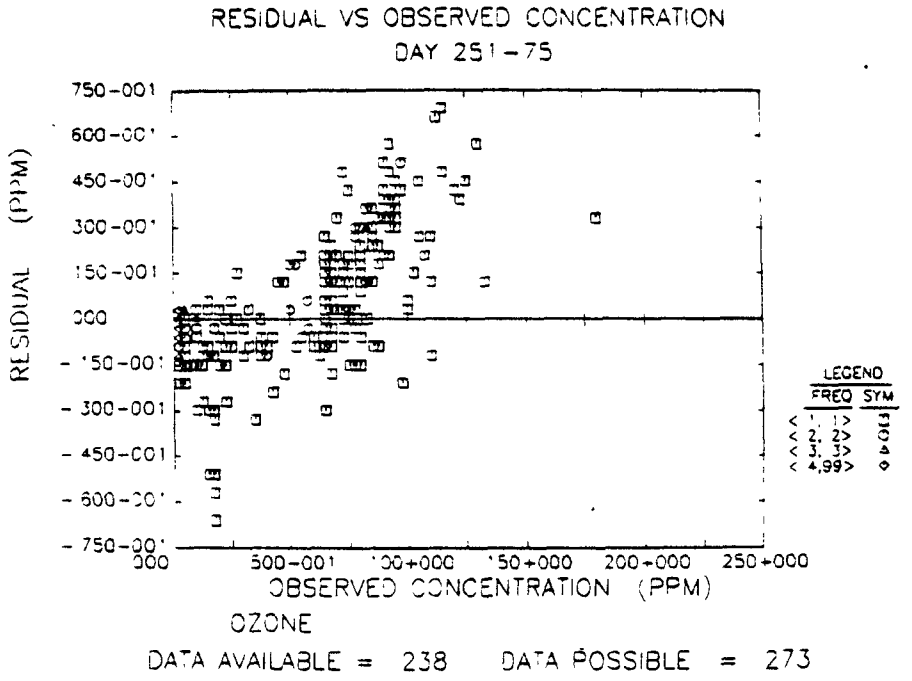

Figure D-27b. Residual vs. observed plot for O_3 from the UAM simulation results for Day 251-75.

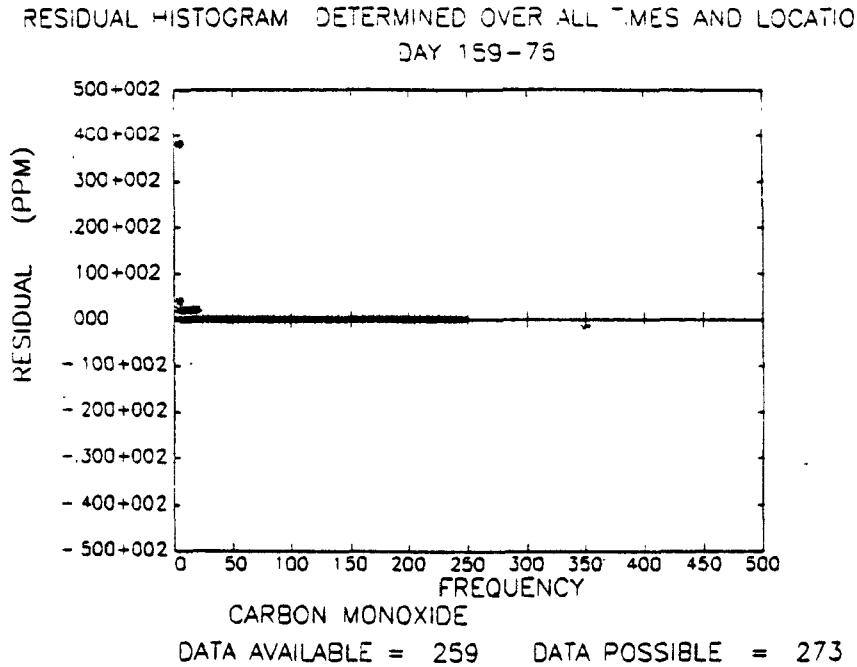

Figure D-28a. Residual histogram for CO from the UAM simulation results for Day 159-76.

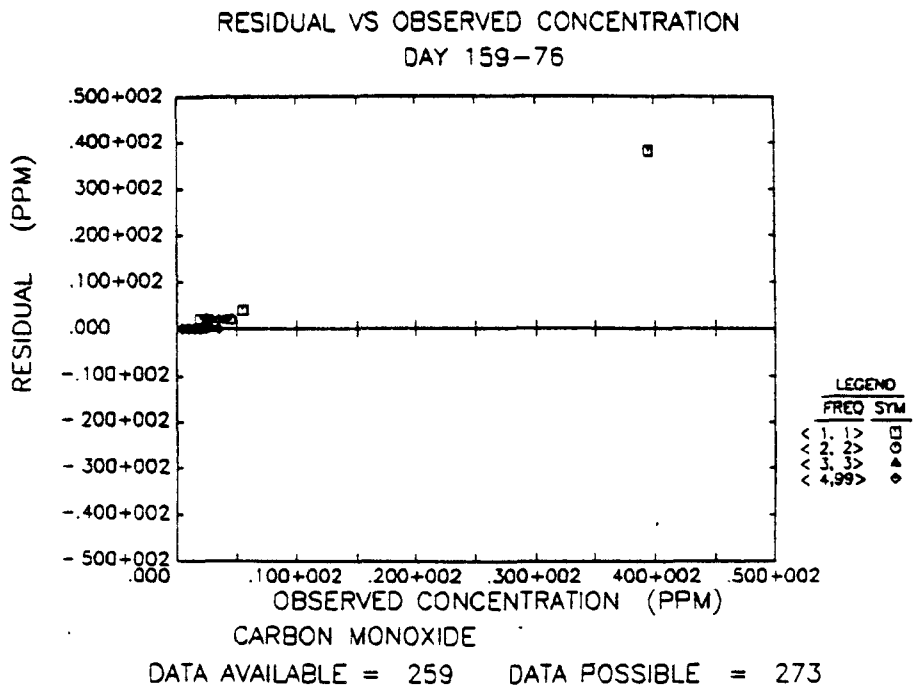

Figure D-28b. Residual vs. observed plot for CO from the UAM simulation results for Day 159-76.

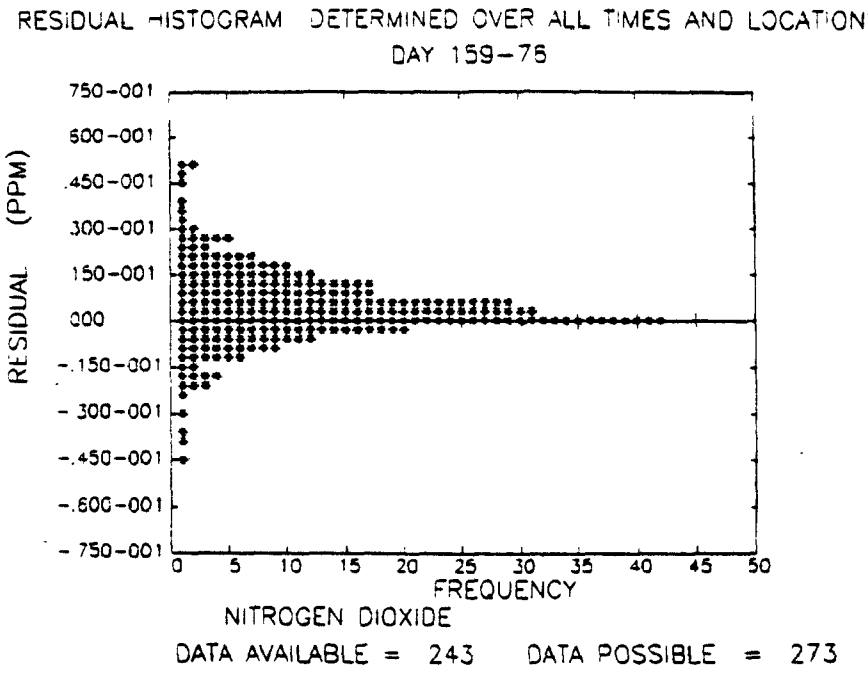

Figure D-29a. Residual histogram for NO_2 from the UAM simulation results for Day 159-76.

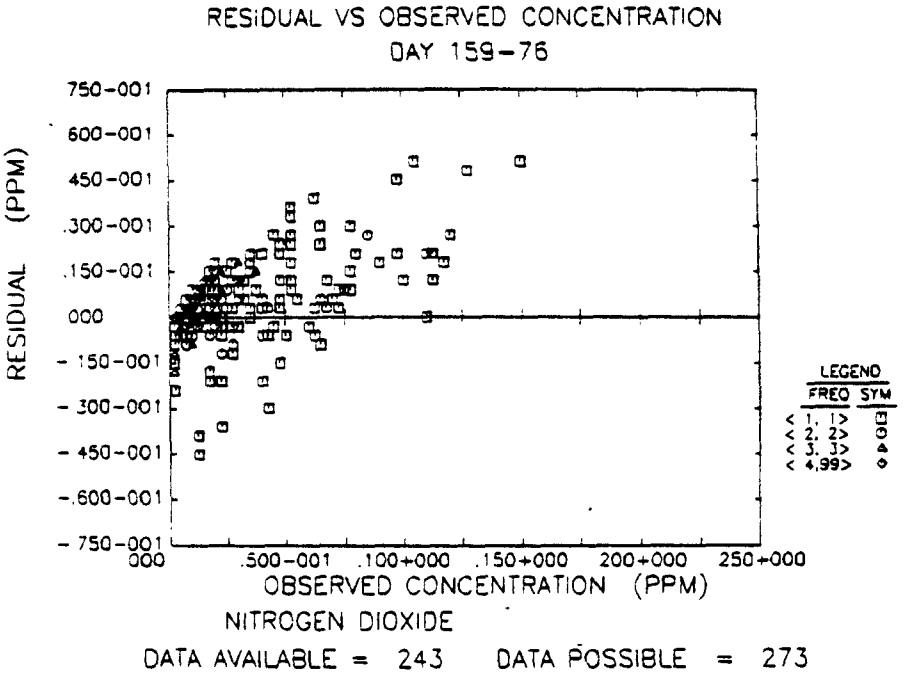

Figure D-29b. Residual vs. observed plot for NO_2 from the UAM simulation results for Day 159-76.

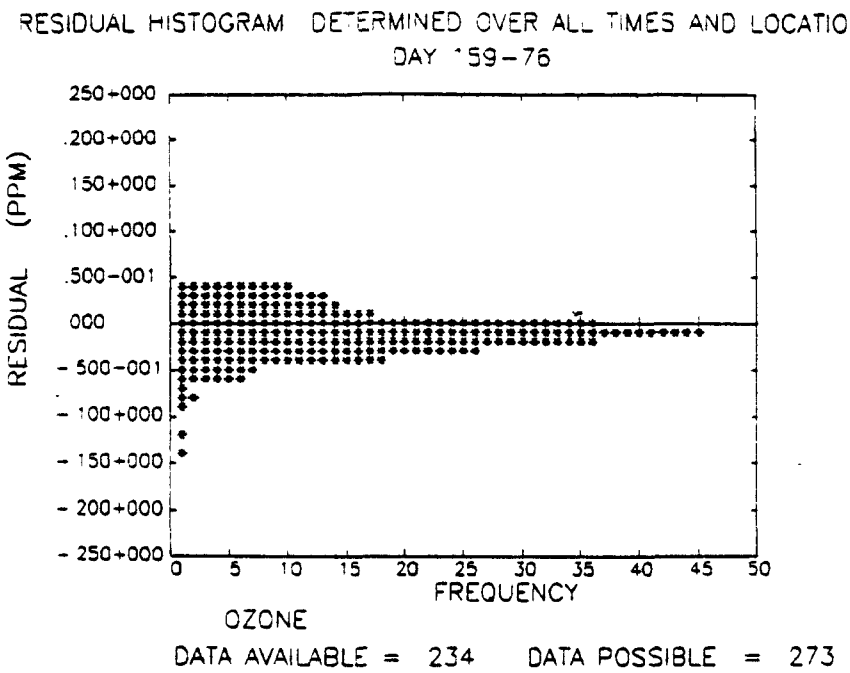

Figure D-30a. Residual histogram for O_3 from the UAM simulation results for Day 159-76.

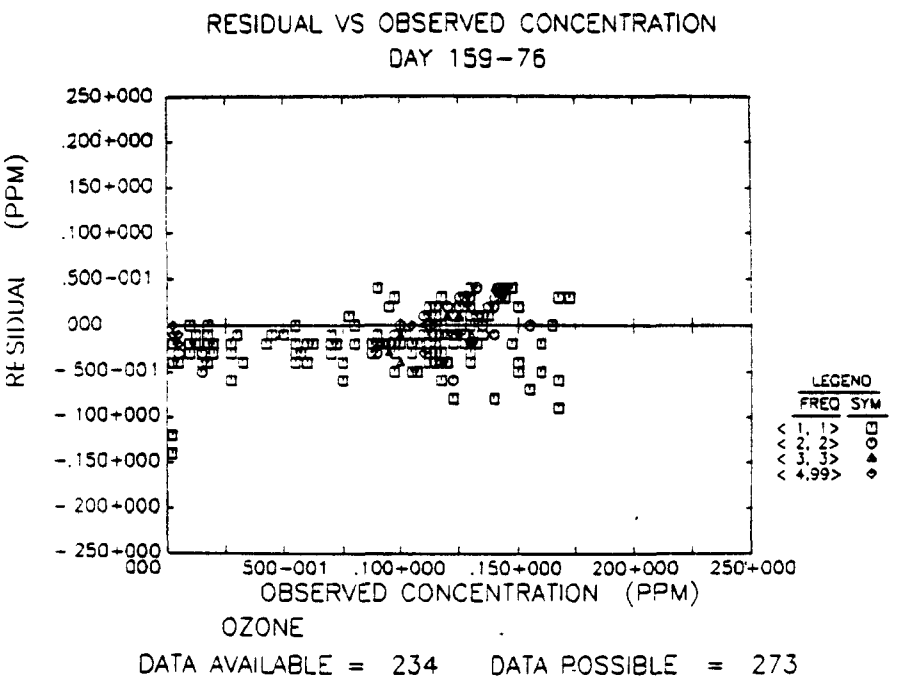

Figure D-30b. Residual vs. observed plot for O_3 from the UAM simulation results for Day 159-76.

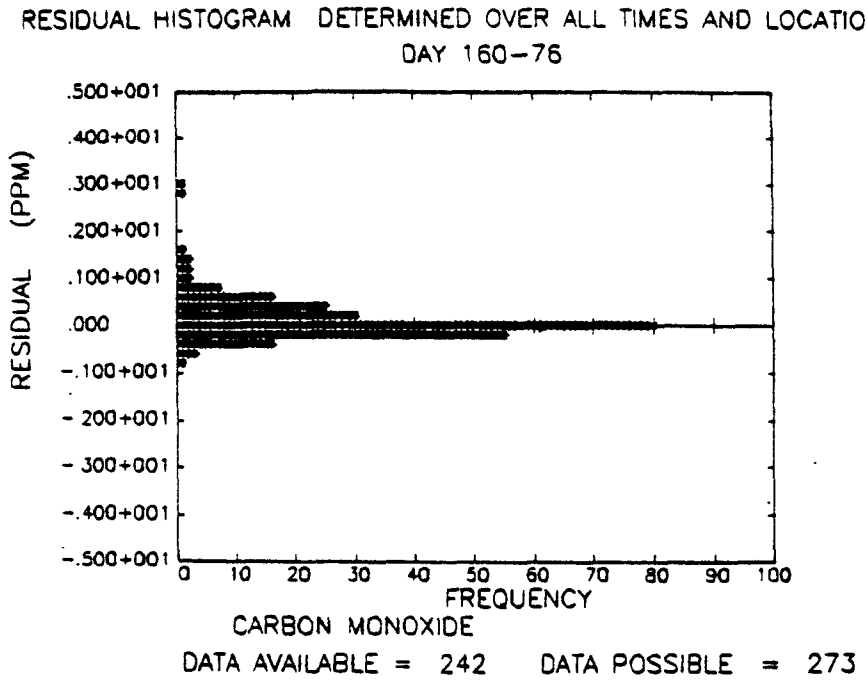

Figure D-31a. Residual histogram for CO from the UAM simulation results for Day 160-76.

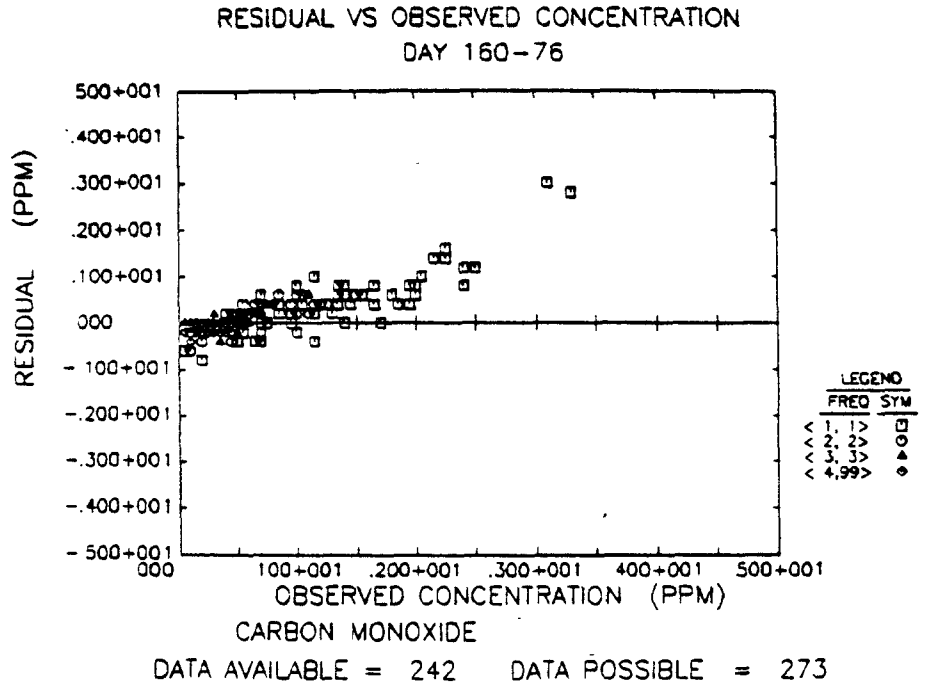

Figure D-31b. Residual vs. observed plot for CO from the UAM simulation results for Day 160-76.

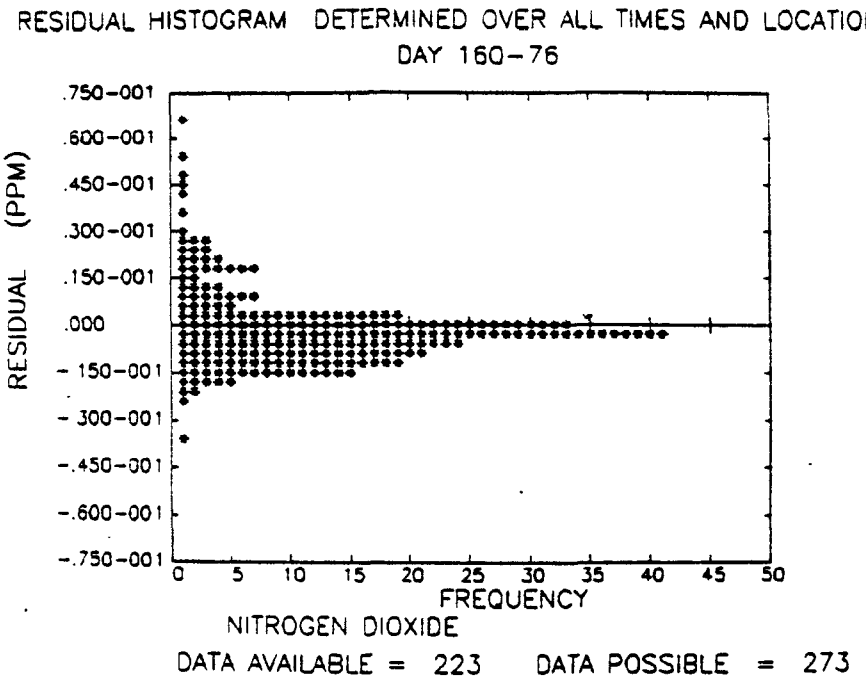

Figure D-32a. Residual histogram for NO_2 from the UAM simulation results for Day 160-76.

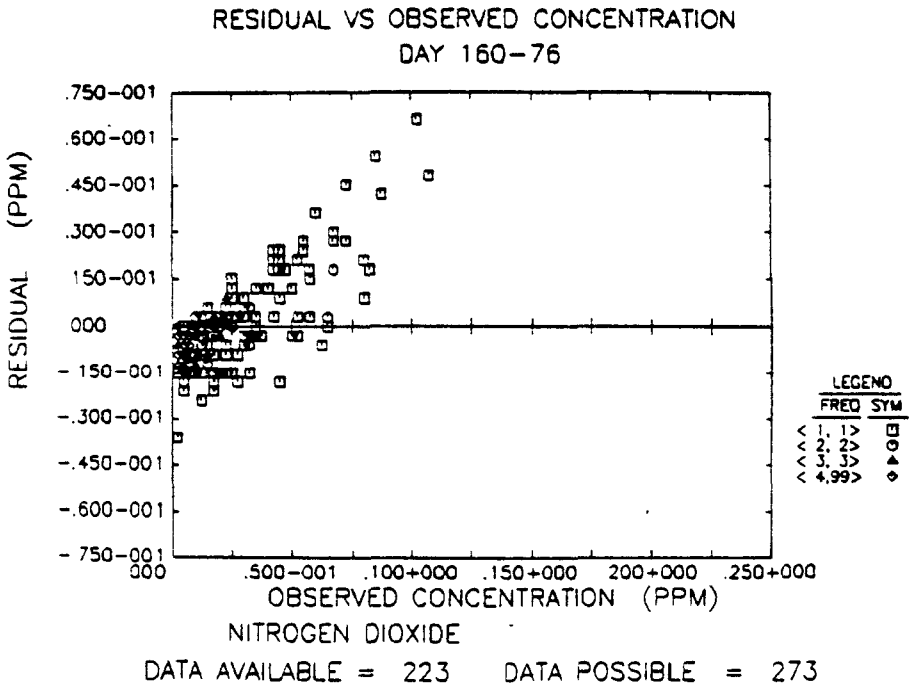

Figure D-32b. Residual vs. observed plot for NO_2 from the UAM simulation results for Day 160-76.

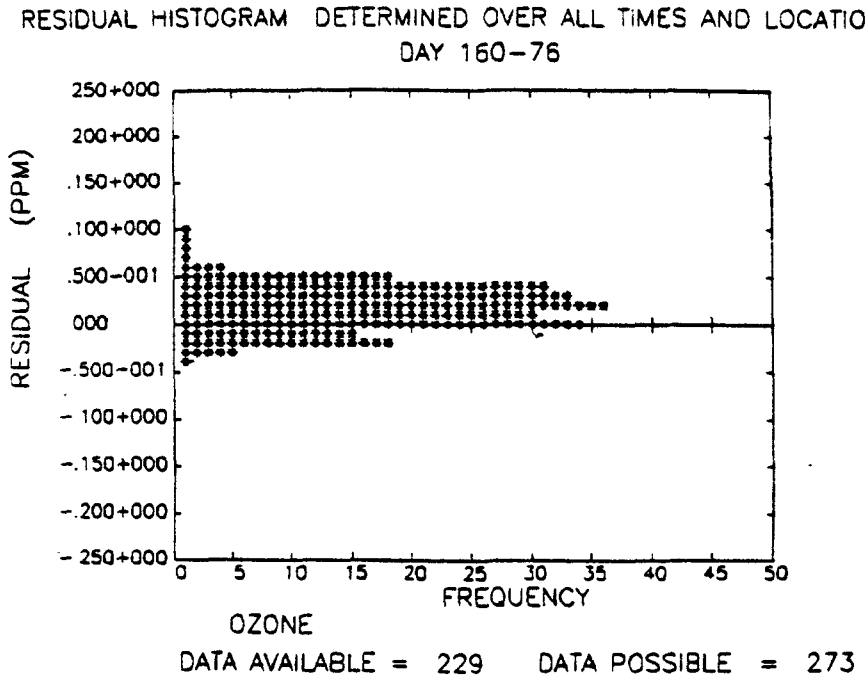

Figure D-33a. Residual histogram for O_3 from the UAM simulation results for Day 160-76.

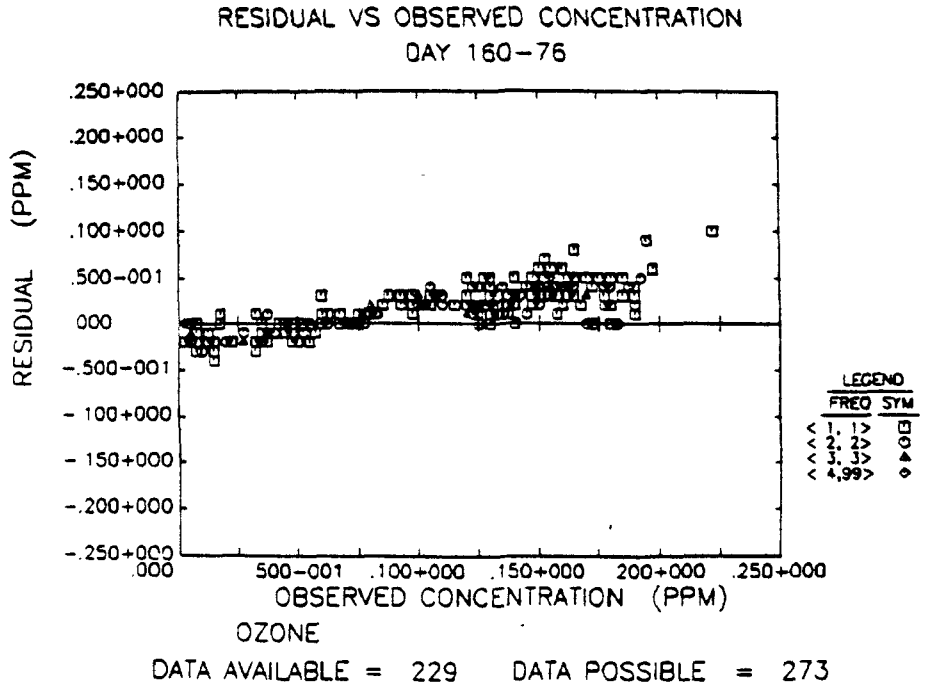

Figure D-33b. Residual vs. observed plot for O_3 from the UAM simulation results for Day 160-76.

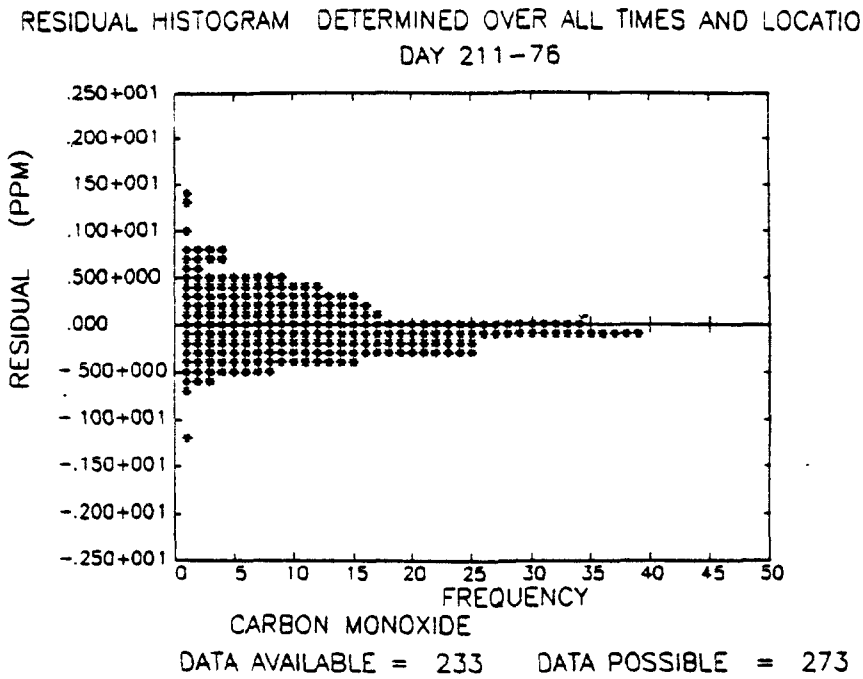

Figure D-34a. Residual histogram for CO from the UAM simulation results for Day 211-76.

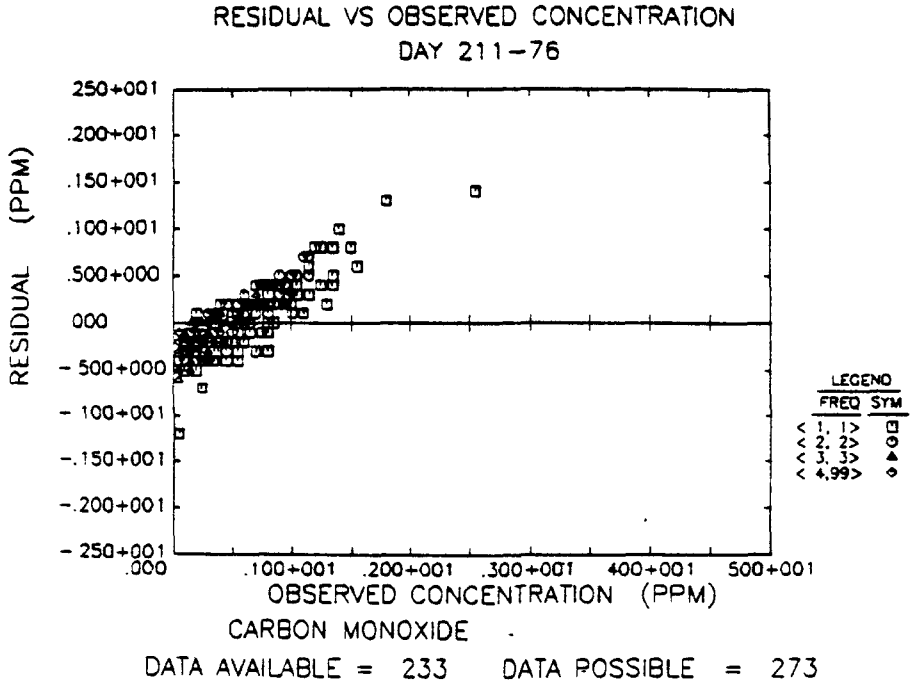

Figure D-34b. Residual vs. observed plot for CO from the UAM simulation results for Day 211-76.

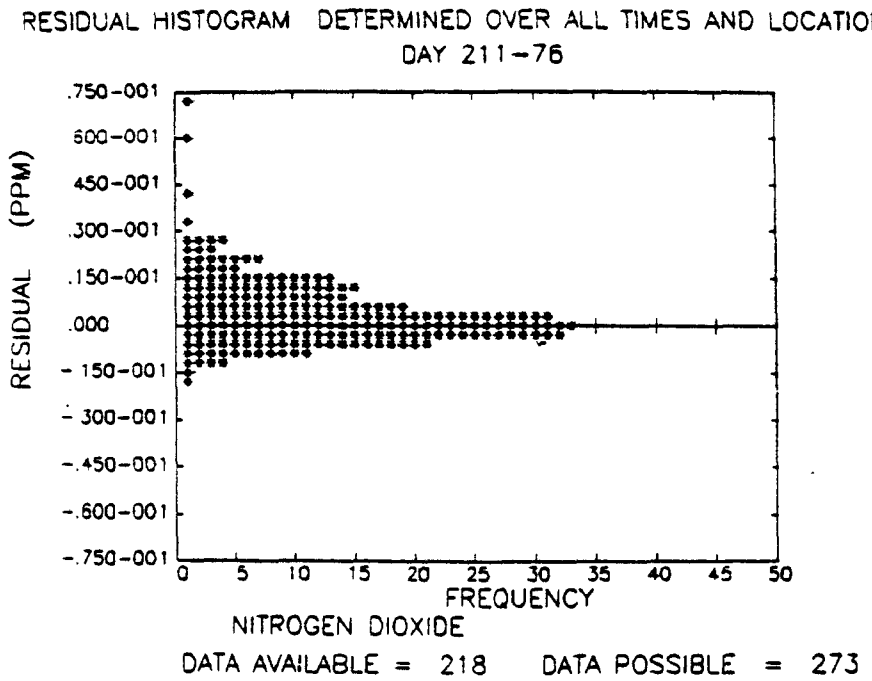

Figure D-35a. Residual histogram for NO_2 from the UAM simulation results for Day 211-76.

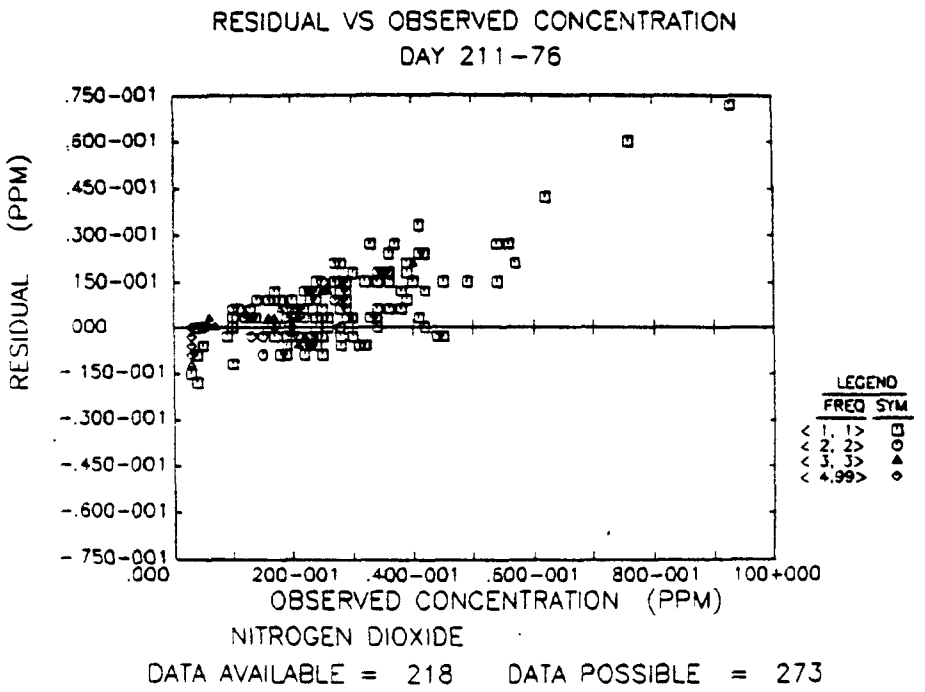

Figure D-35b. Residual vs. observed plot for NO_2 from the UAM simulation results for Day 211-76.

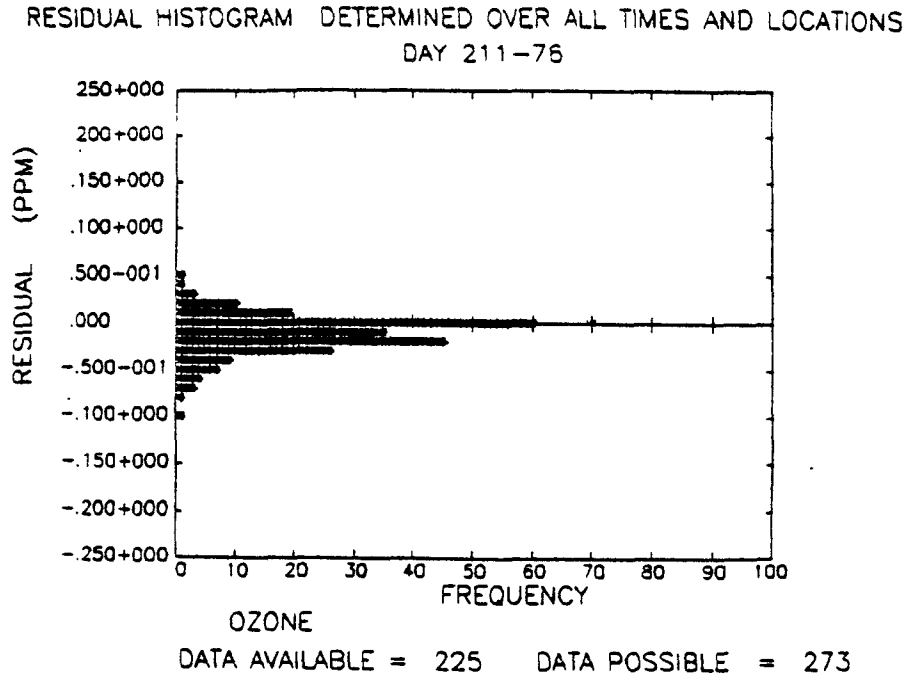

Figure D-36a. Residual histogram for O_3 from the UAM simulation results for Day 211-76.

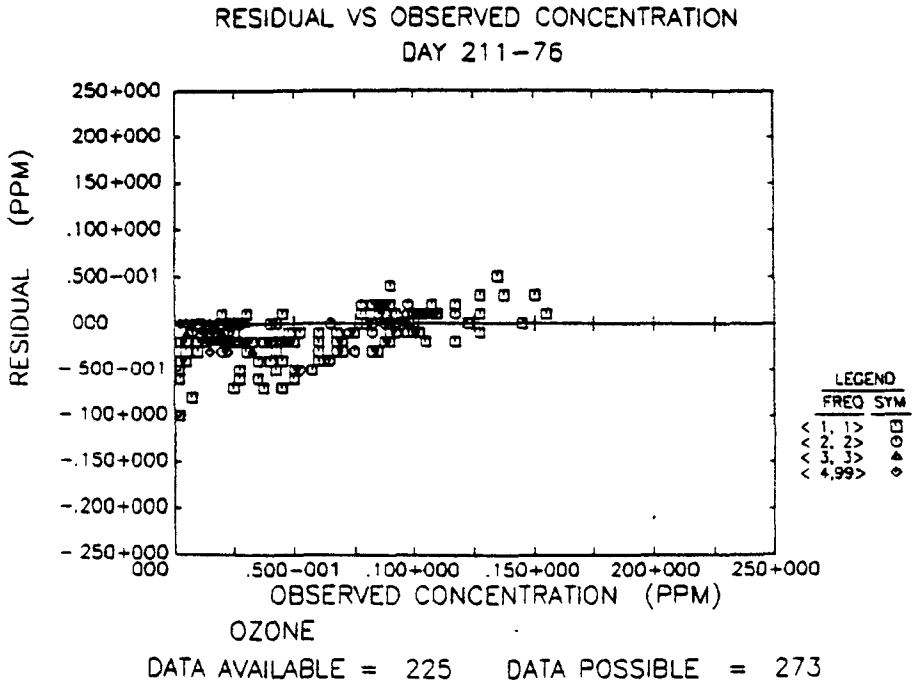

Figure D-36b. Residual vs. observed plot for O_3 from the UAM simulation results for Day 211-76.

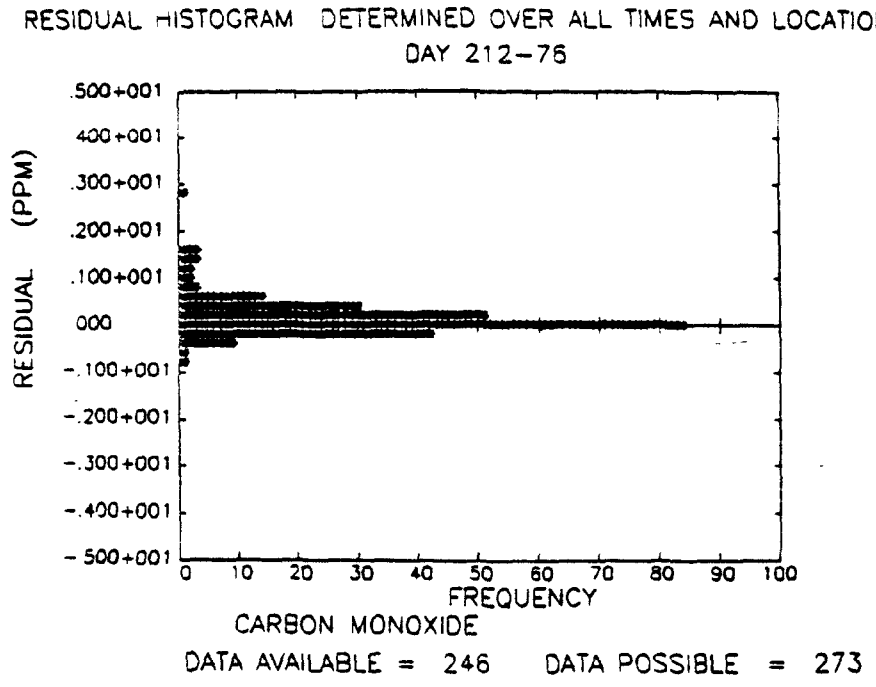

Figure D-37a. Residual histogram for CO from the UAM simulation results for Day 212-76.

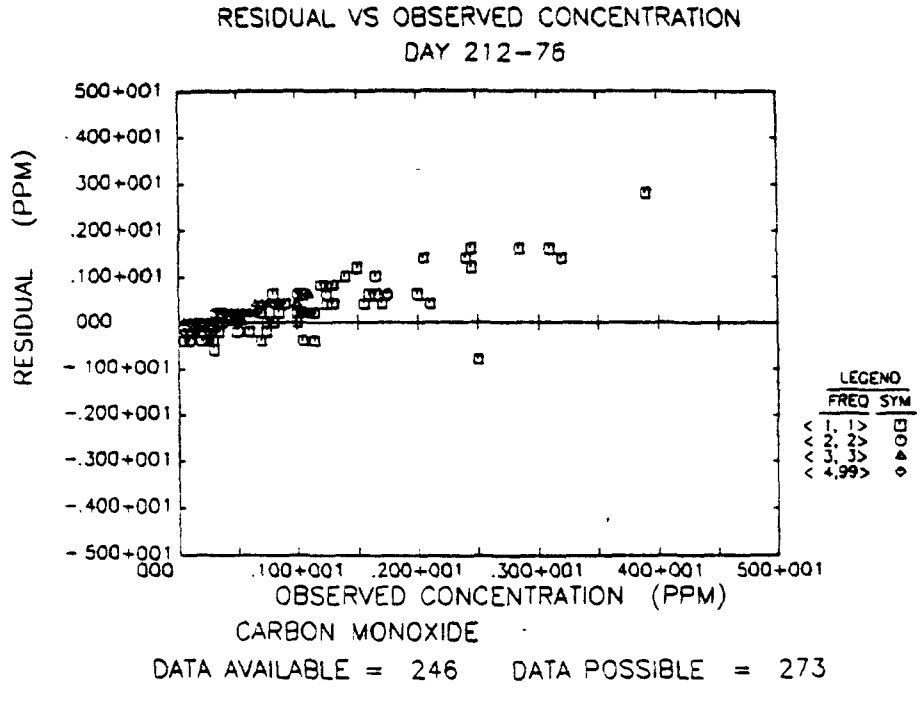

Figure D-37b. Residual vs. observed plot for CO from the UAM simulation results for Day 212-76.

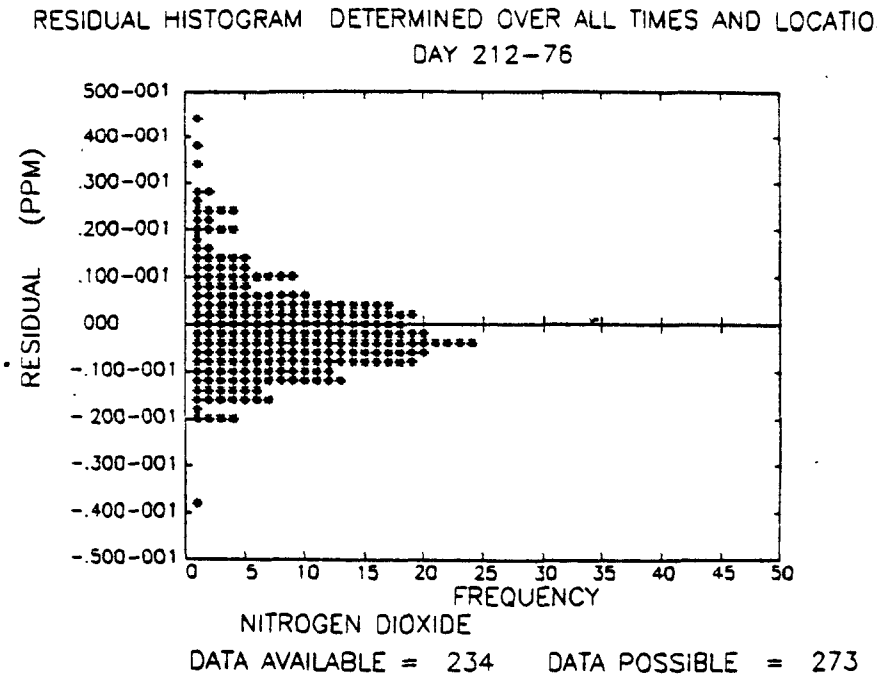

Figure D-38a. Residual histogram for NO_2 from the UAM simulation results for Day 212-76.

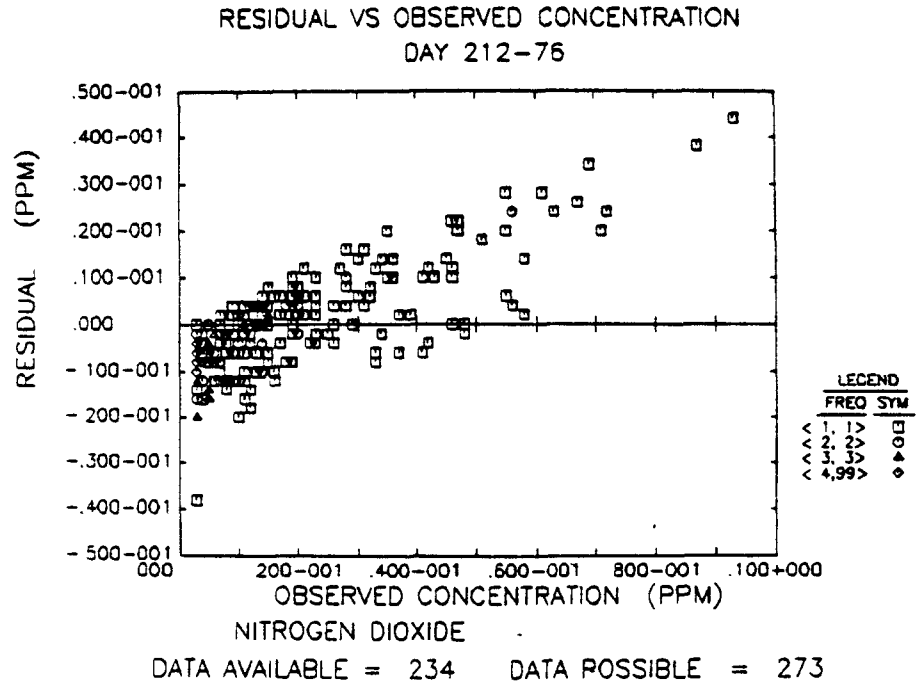

Figure D-38b. Residual vs. observed plot for NO_2 from the UAM simulation results for Day 212-76.

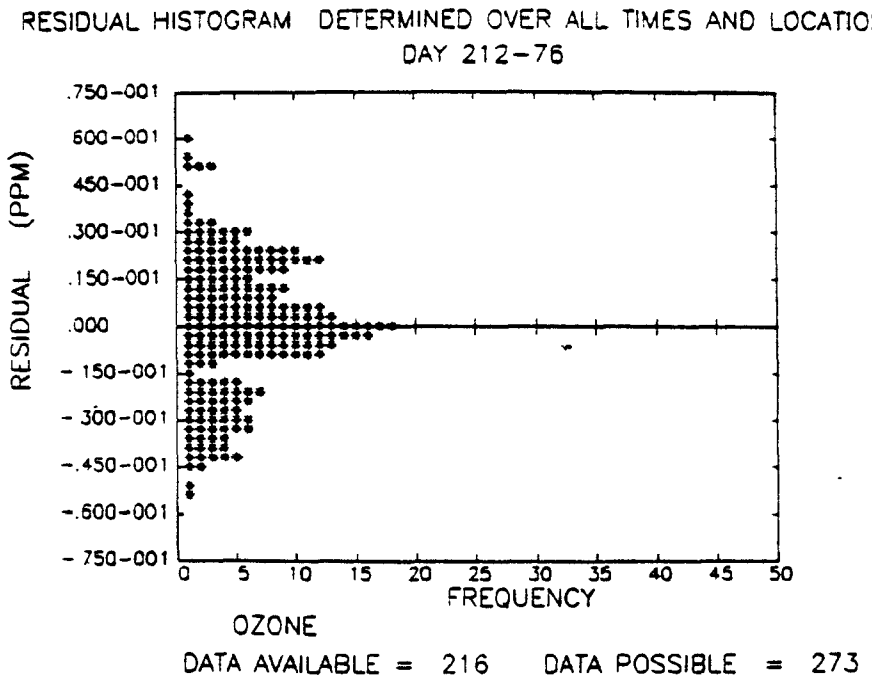

Figure D-39a. Residual histogram for O_3 from the UAM simulation results for Day 212-76.

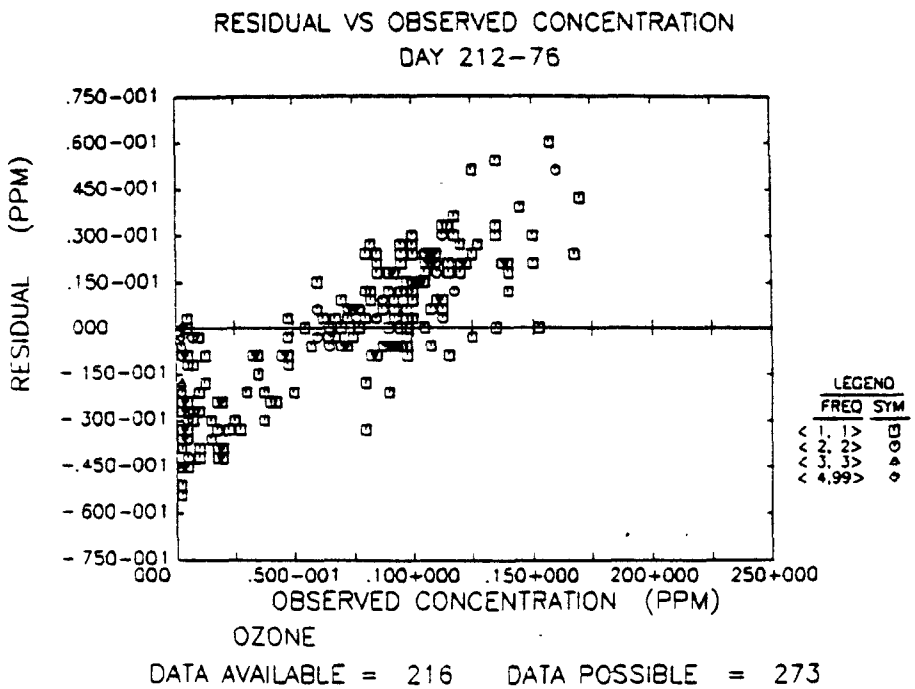

Figure D-39b. Residual vs. observed plot for O_3 from the UAM simulation results for Day 212-76.

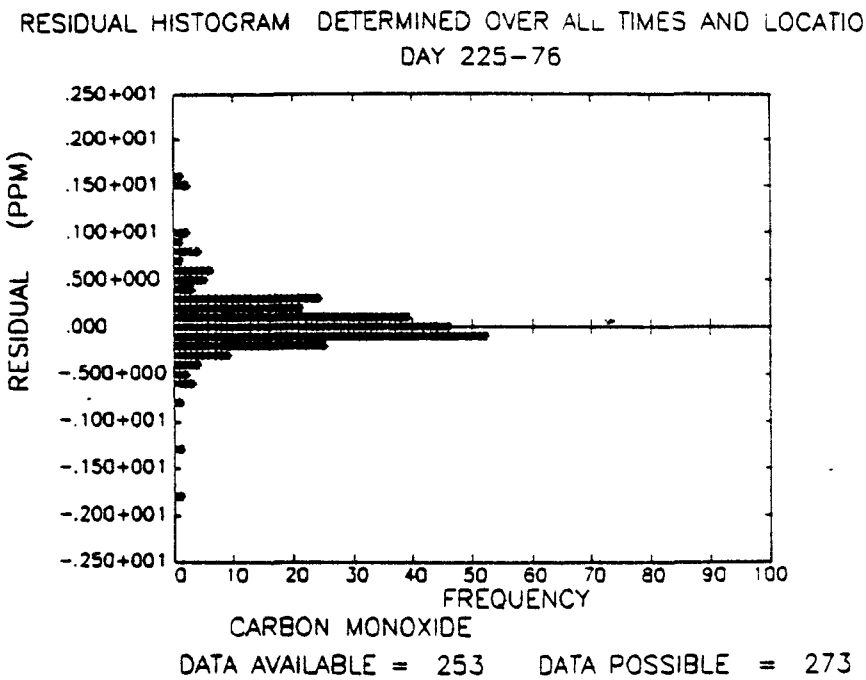

Figure D-40a. Residual histogram for CO from the UAM simulation results for Day 225-76.

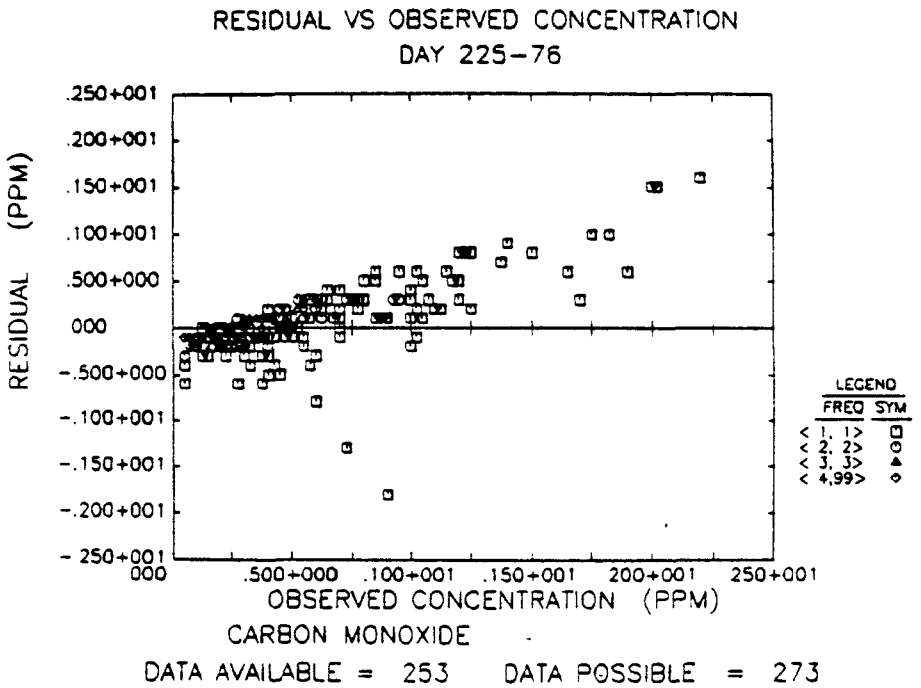

Figure D-40b. Residual vs. observed plot for CO from the UAM simulation results for Day 225-76.

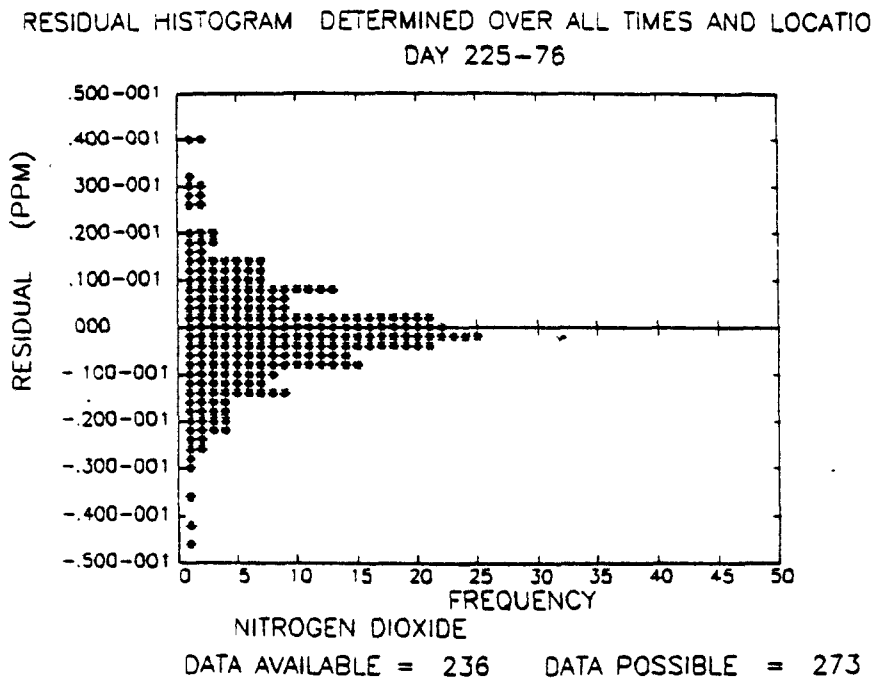

Figure D-41a. Residual histogram for NO_2 from the UAM simulation results for Day 225-76.

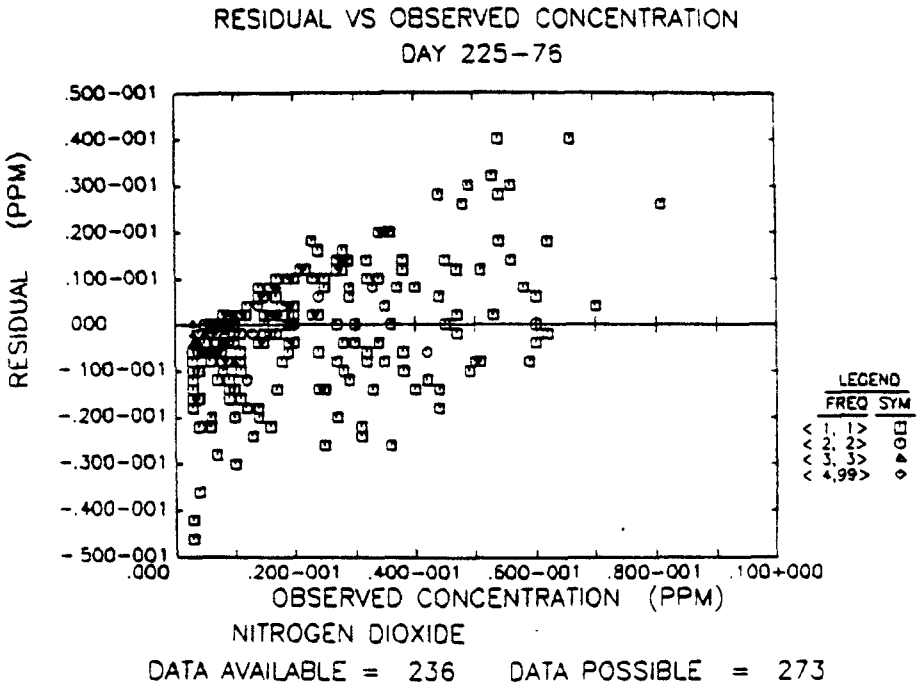

Figure D-41b. Residual vs. observed plot for NO_2 from the UAM simulation results for Day 225-76.

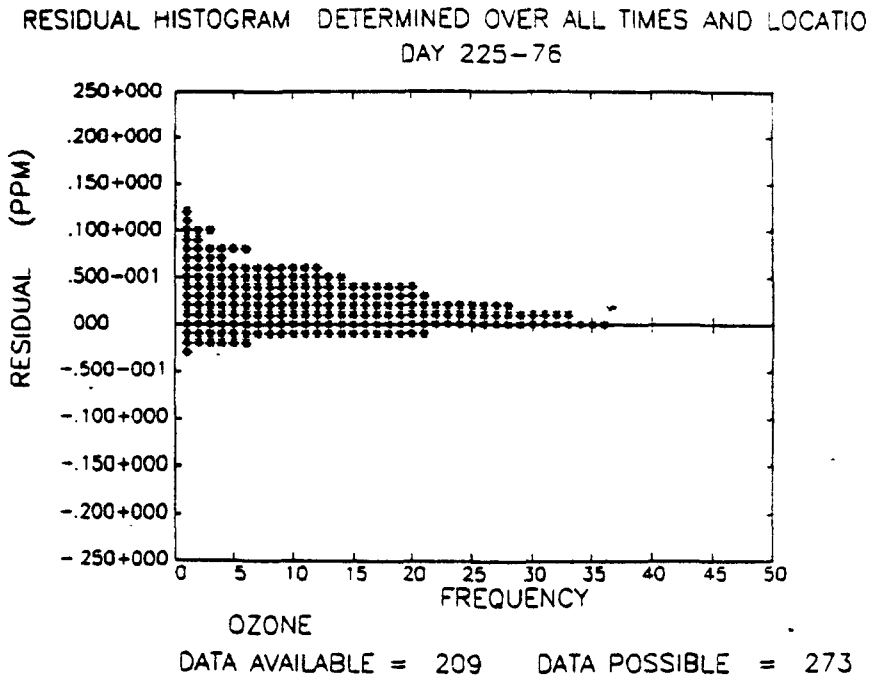

Figure D-42a. Residual histogram for O_3 from the UAM simulation results for Day 225-76.

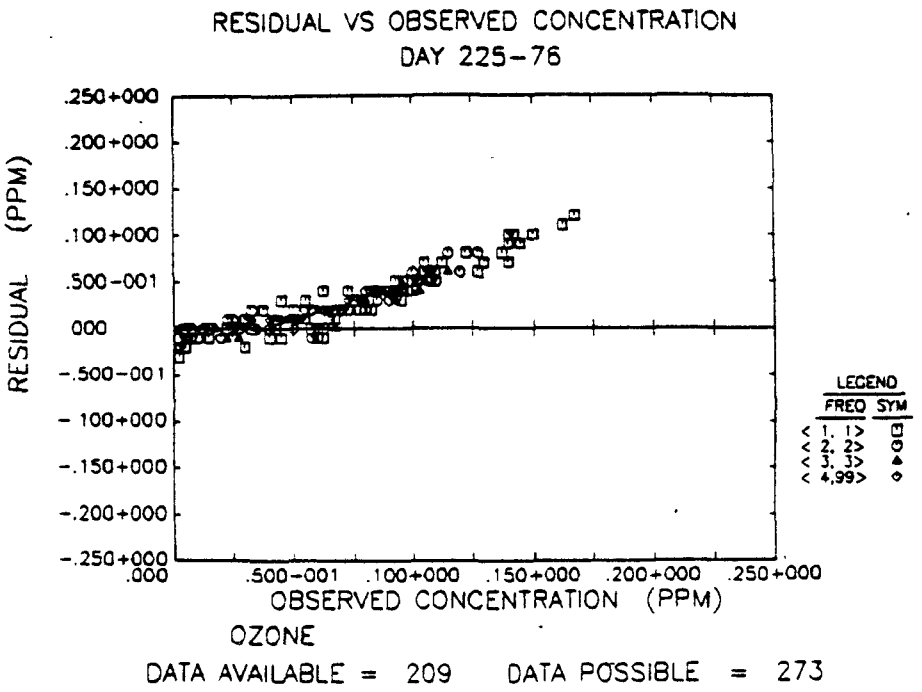

Figure D-42b. Residual vs. observed plot for O_3 from the UAM simulation results for Day 225-76.

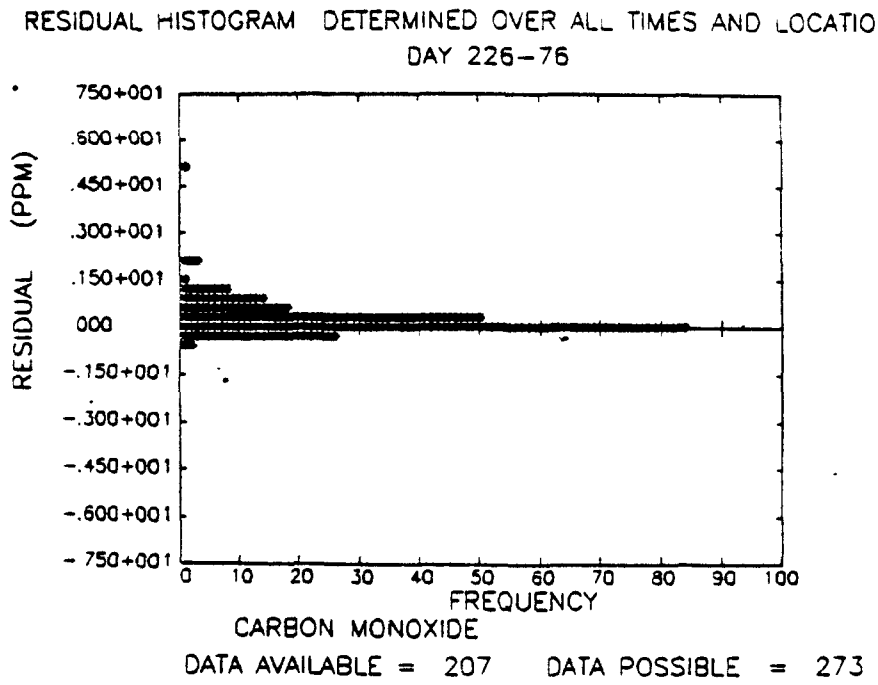

Figure D-43a. Residual histogram for CO from the UAM simulation results for Day 226-76.

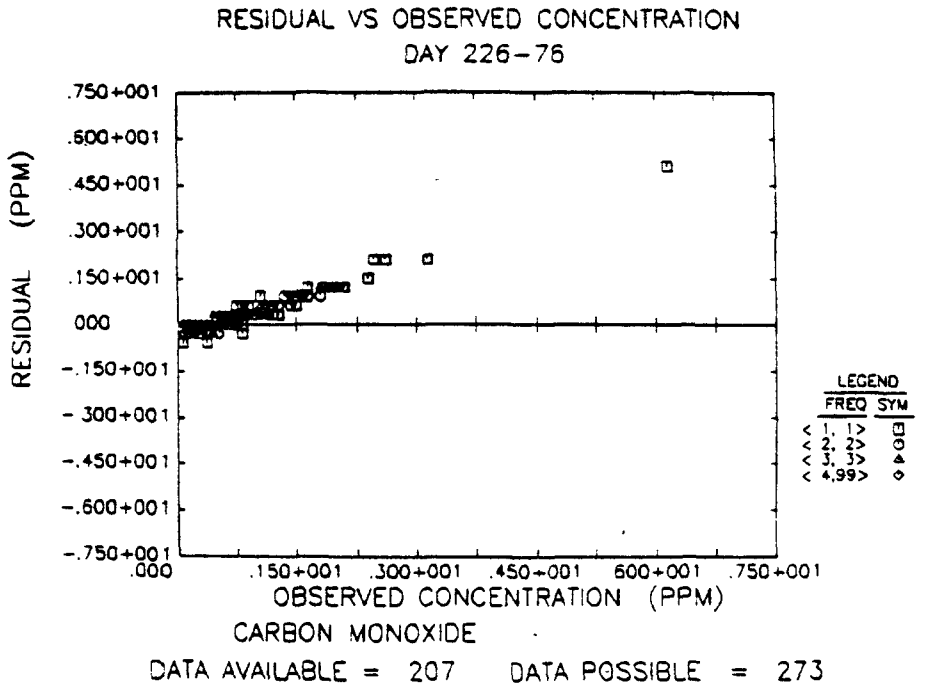

Figure D-43b. Residual vs. observed plot for CO from the UAM simulation results for Day 226-76.

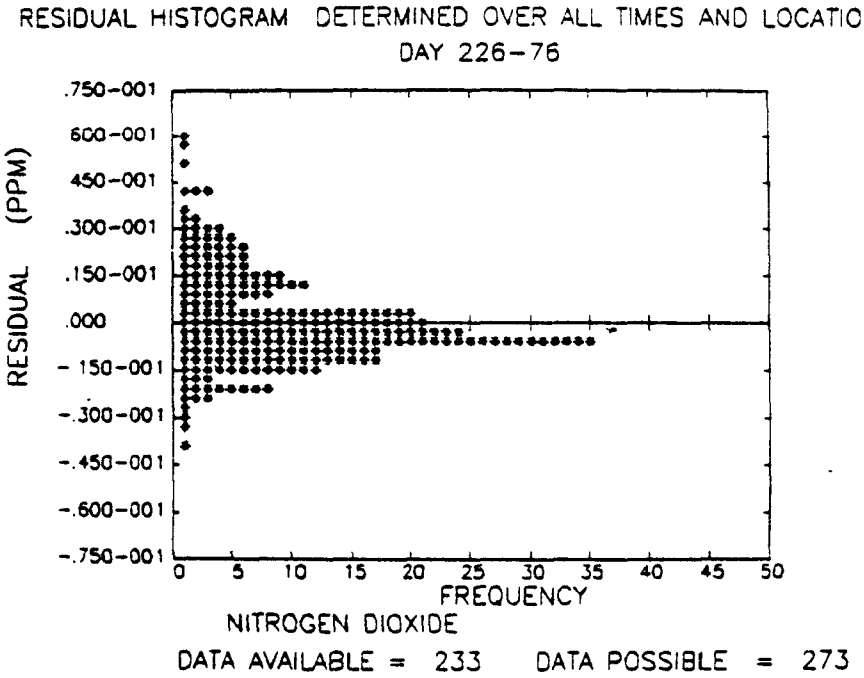

Figure D-44a. Residual histogram for NO_2 from the UAM simulation results for Day 226-76.

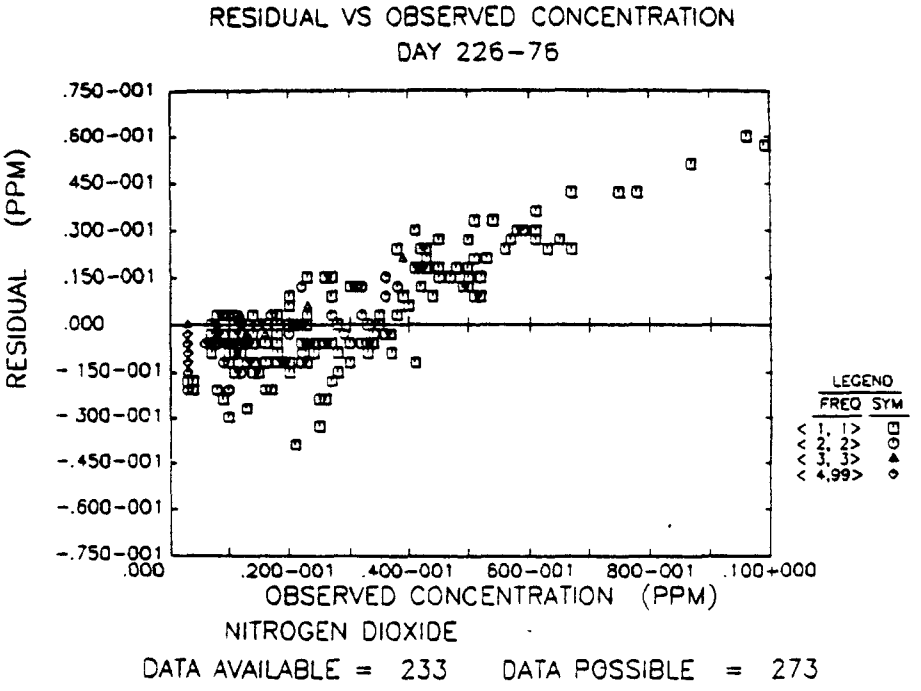

Figure D-44b. Residual vs. observed plot for NO_2 from the UAM simulation results for Day 226-76.

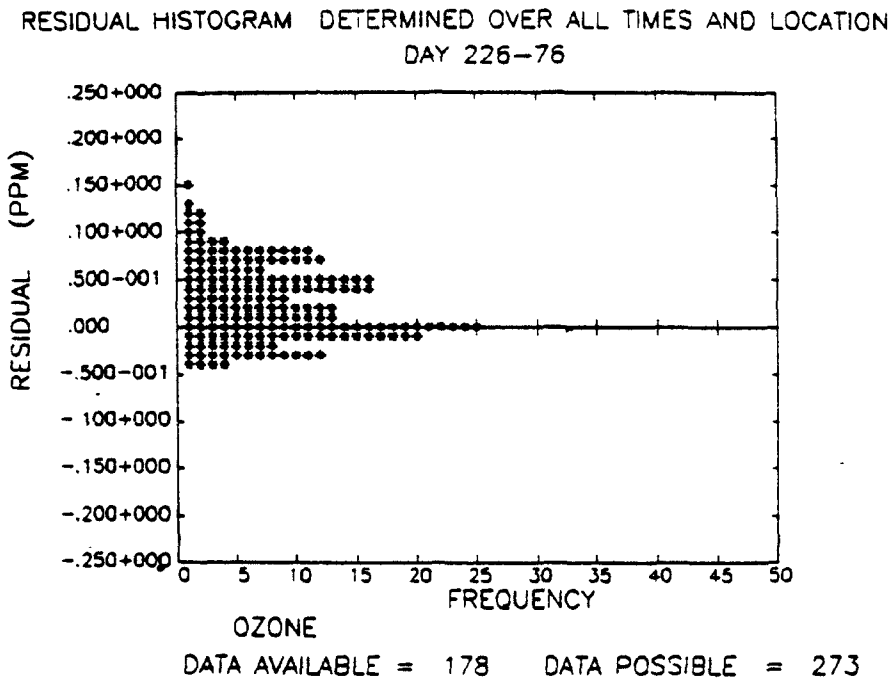

Figure D-45a. Residual histogram for O_3 from the UAM simulation results for Day 226-76.

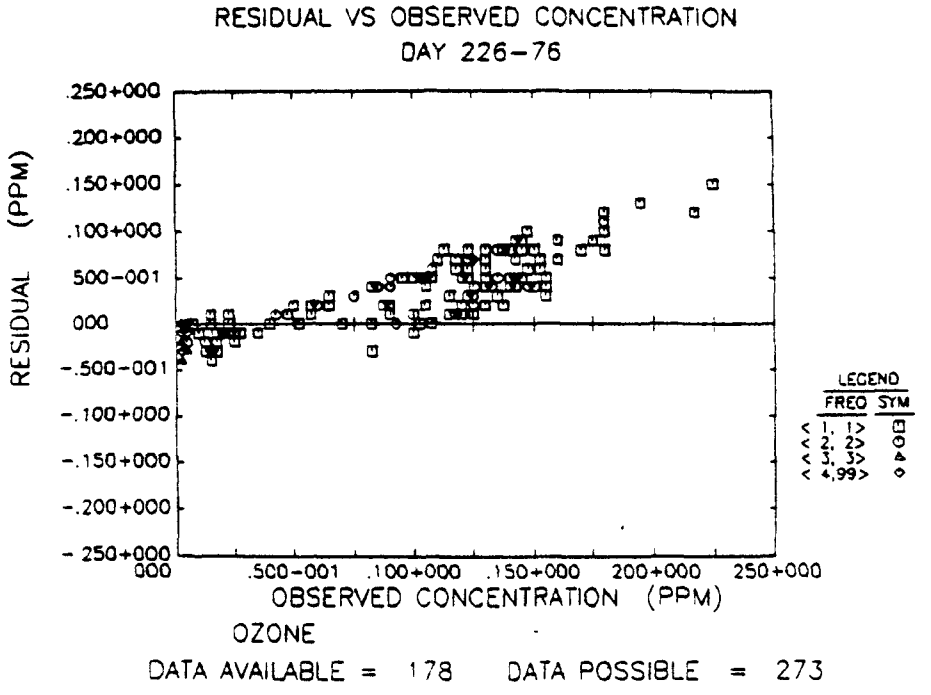

Figure D-45b. Residual vs. observed plot for O_3 from the UAM simulation results for Day 226-76.

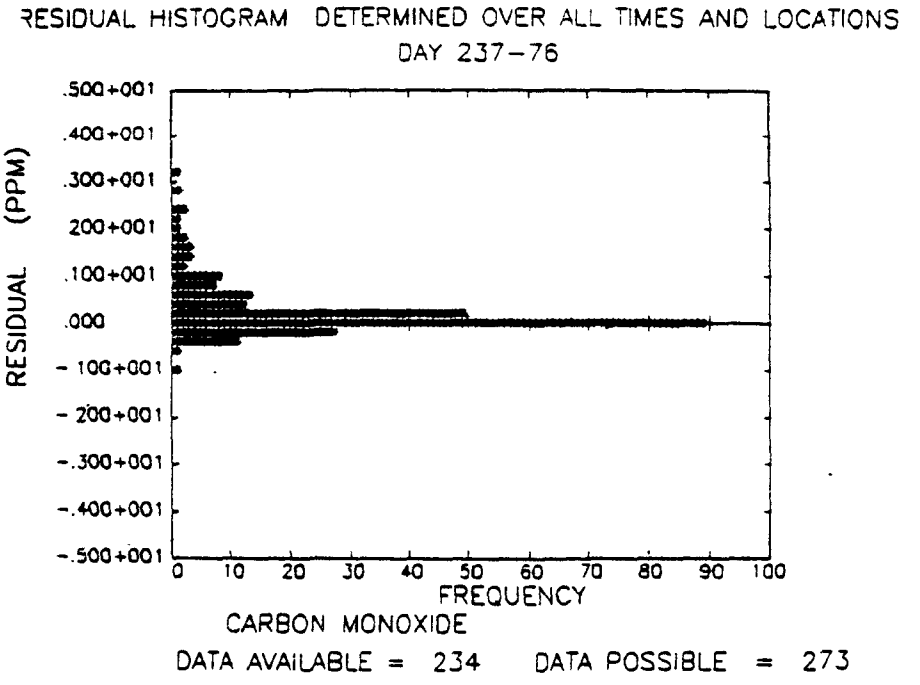

Figure D-46a. Residual histogram for CO from the UAM simulation results for Day 237-76.

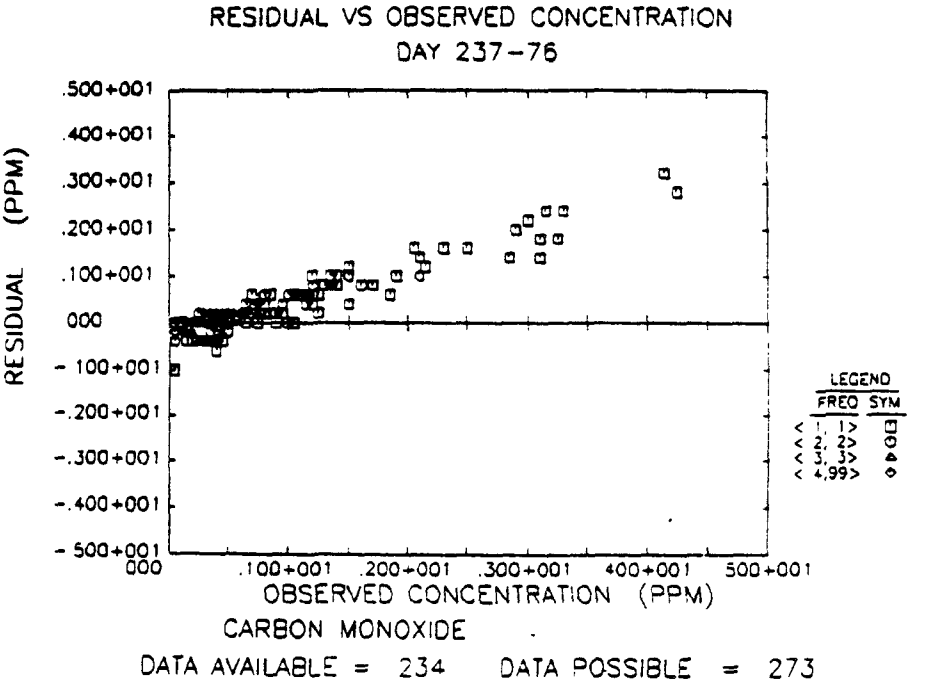

Figure D-46b. Residual vs. observed plot for CO from the UAM simulation results for Day 237-76.

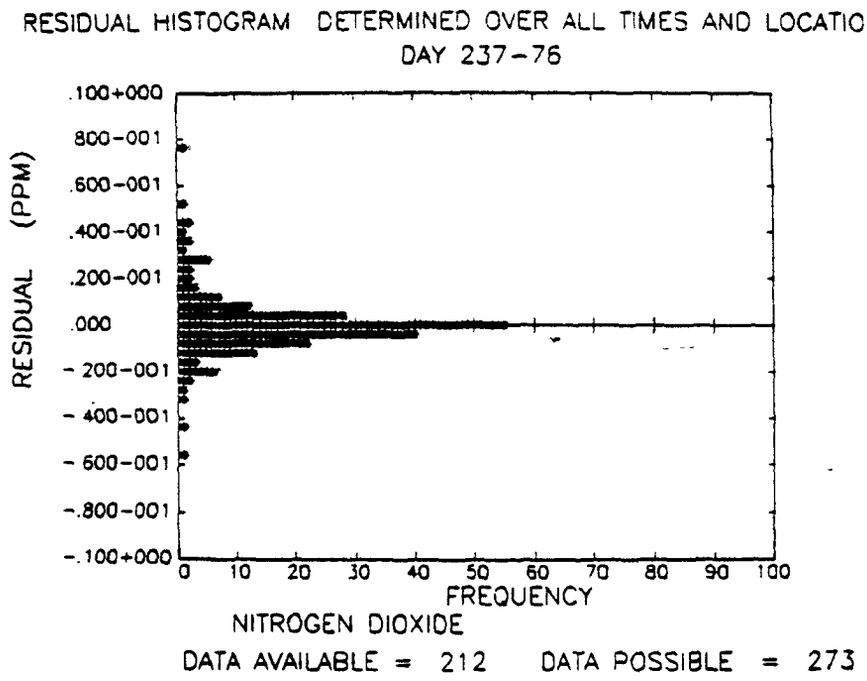

Figure D-47a. Residual histogram for NO_2 from the UAM simulation results for Day 237-76.

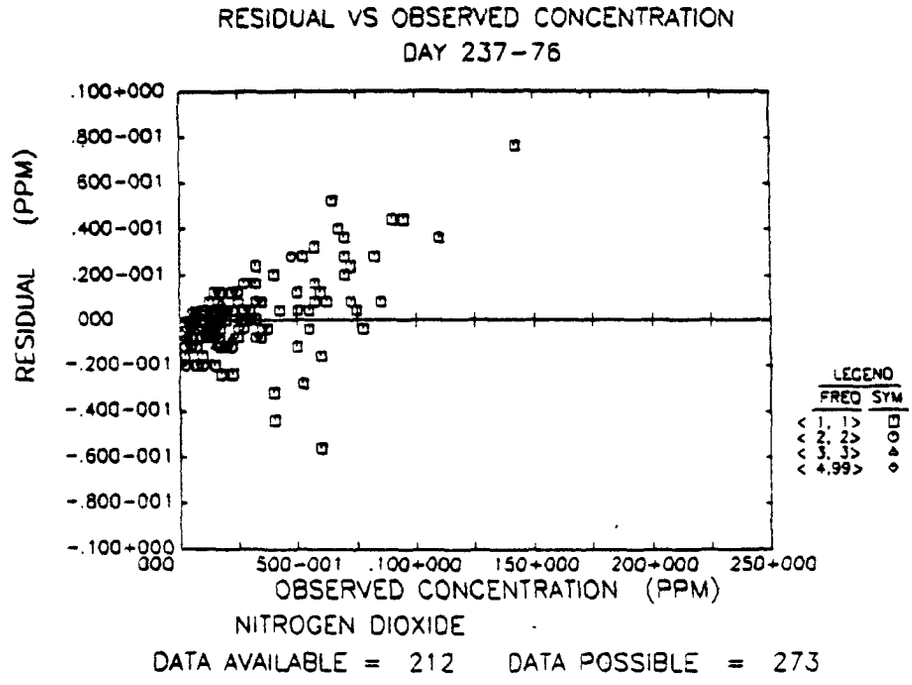

Figure D-47b. Residual vs. observed plot for NO_2 from the UAM simulation results for Day 237-76.

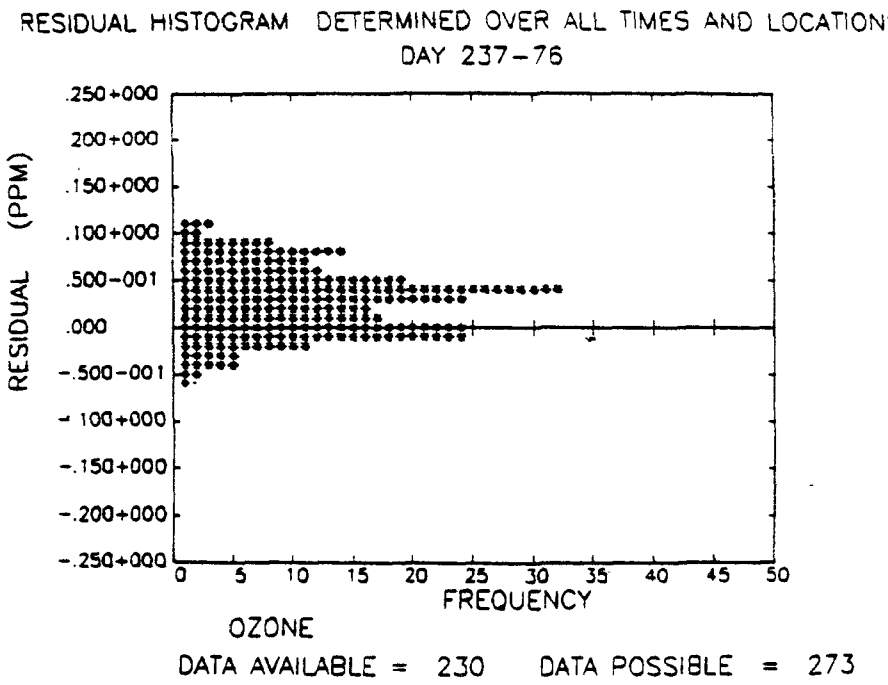

Figure D-48a. Residual histogram for O_3 from the UAM simulation results for Day 237-76.

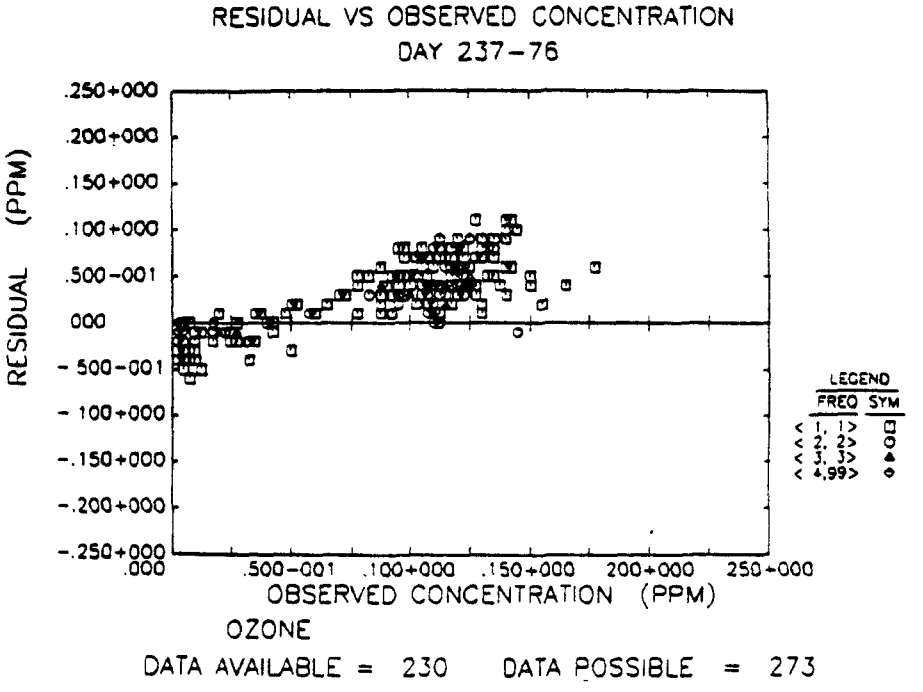

Figure D-48b. Residual vs. observed plot for O_3 from the UAM simulation results for Day 237-76.

APPENDIX E

UAM - CONTOUR PLOTS FOR REMAINING TEST DAYS

The contour plots of predicted and observed O_3 concentrations for the hour of the observed concentration maximum are presented here for all test days not specifically discussed within the body of this report. The Julian day numbers are listed in Appendix D.

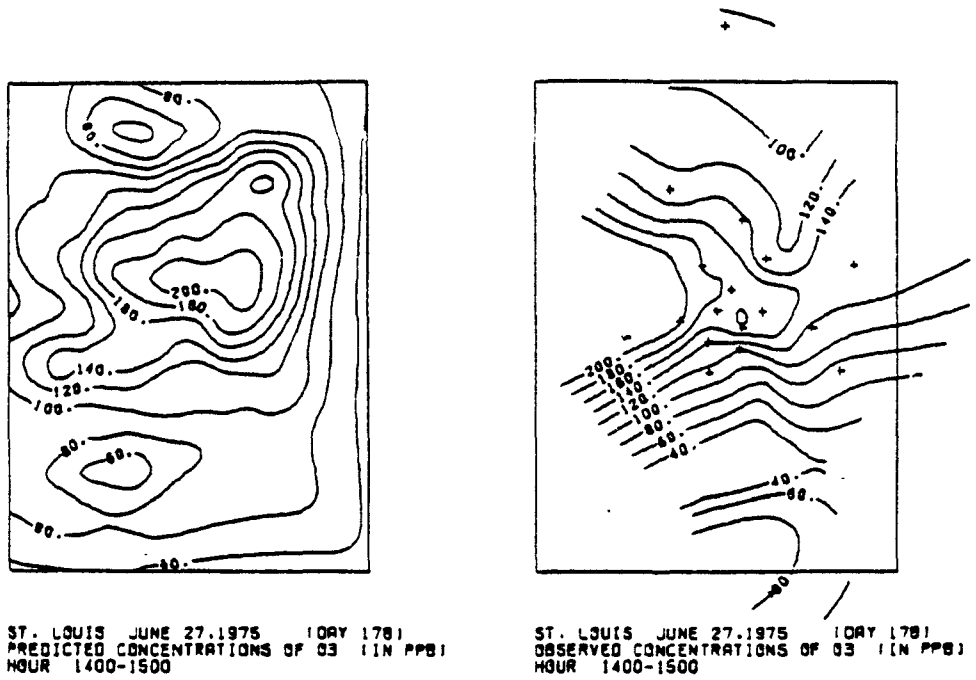

(a) (b)

Figure E-1. Contours of (a) predicted and (b) observed fields of O_3 at hour of observed maximum on Day 178-75.

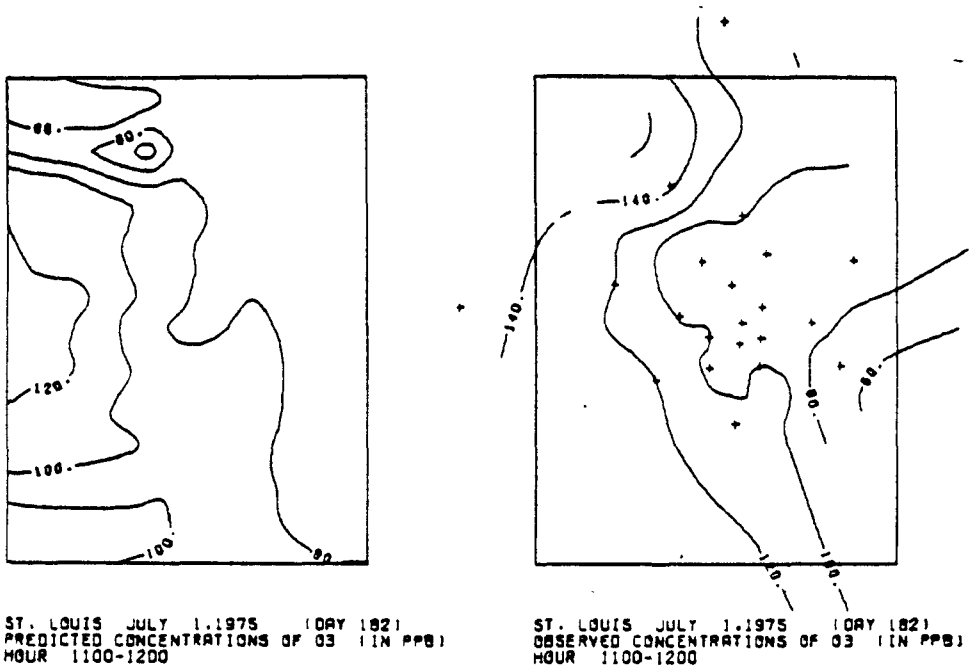

(a) (b)

Figure E-2. Contours of (a) predicted and (b) observed fields of O_3 at hour of observed maximum on Day 182-75.

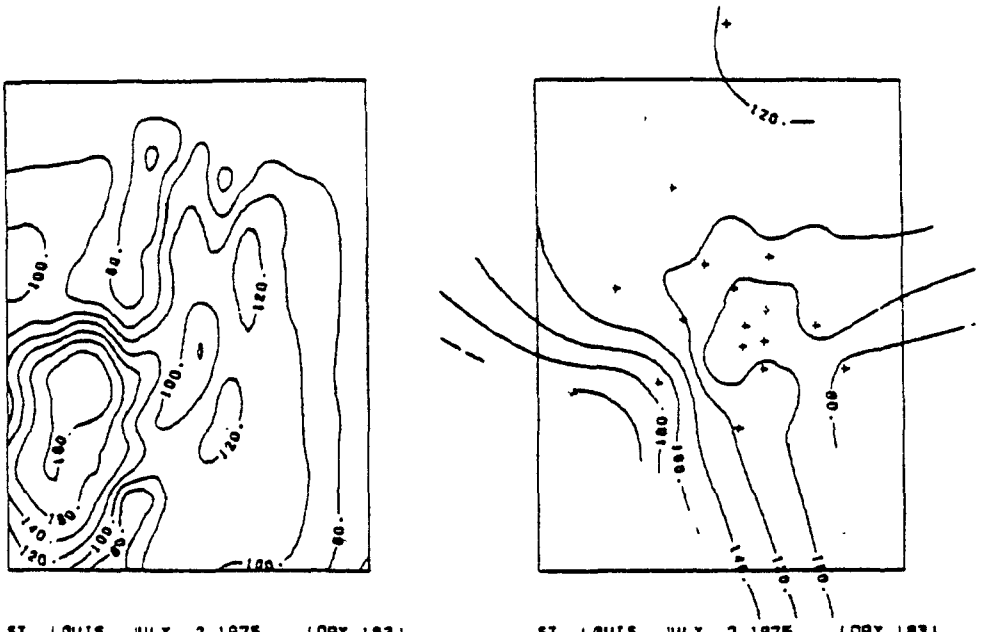

(a) (b)

Figure E-3. Contours of (a) predicted and (b) observed fields of O_3 at hour of observed maximum on Day 183-75.

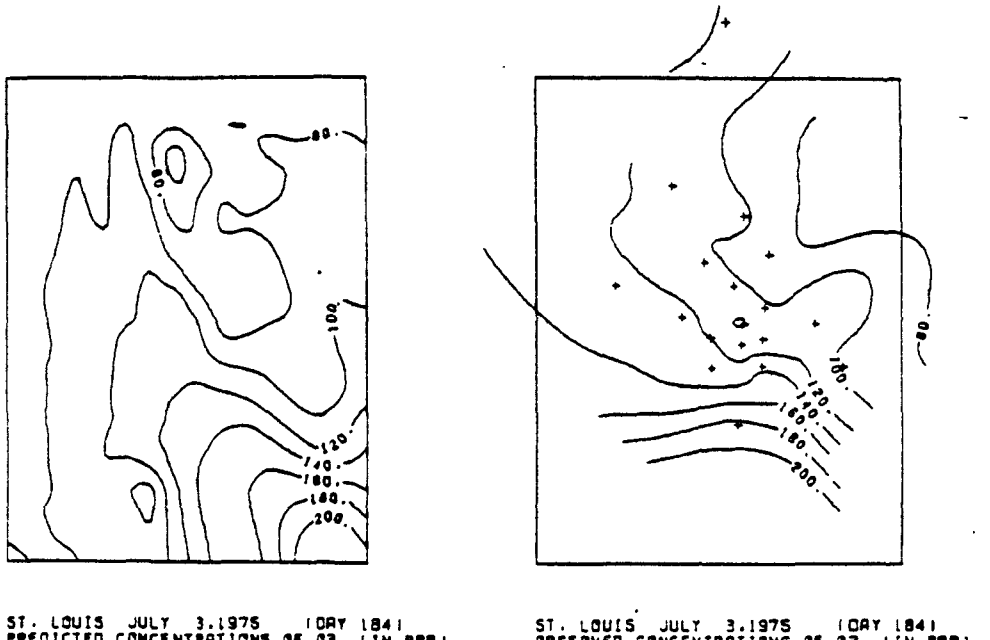

(a) (b)

Figure E-4. Contours of (a) predicted and (b) observed fields of O_3 at hour of observed maximum on Day 184-75.

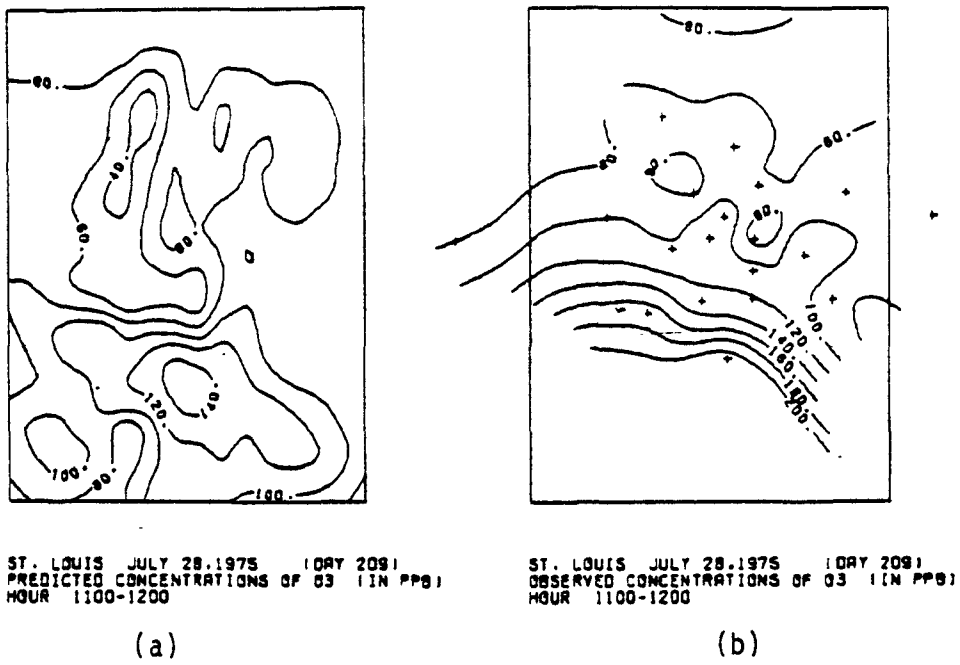

(a) (b)

Figure E-5. Contours of (a) predicted and (b) observed fields of O_3 at hour of observed maximum on Day 209-75.

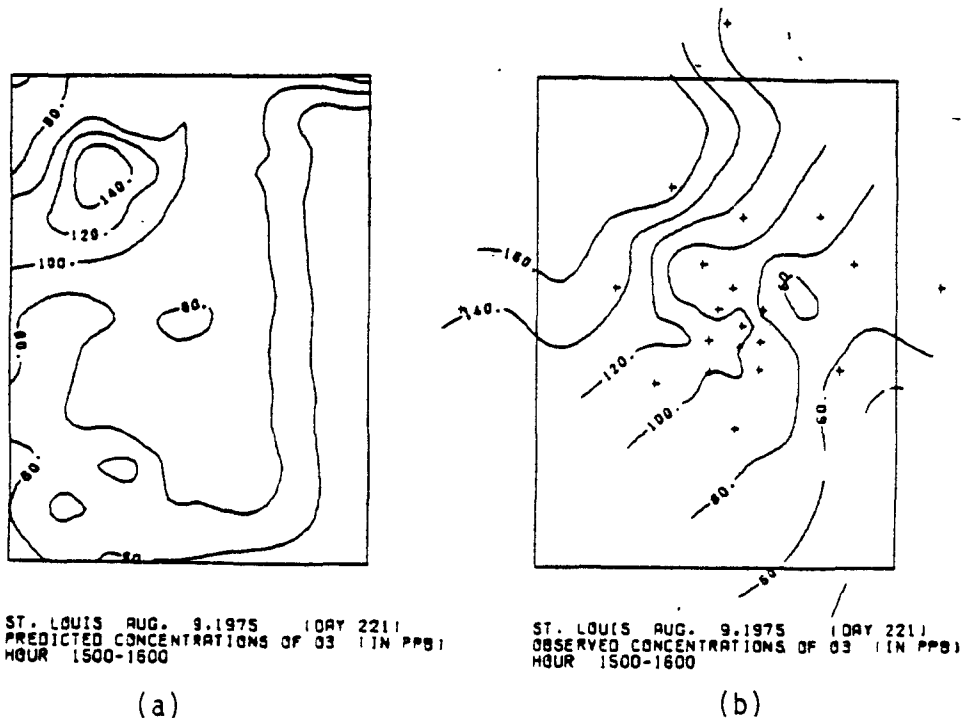

(a) (b)

Figure E-6. Contours of (a) predicted and (b) observed fields of O_3 at hour of observed maximum on Day 221-75.

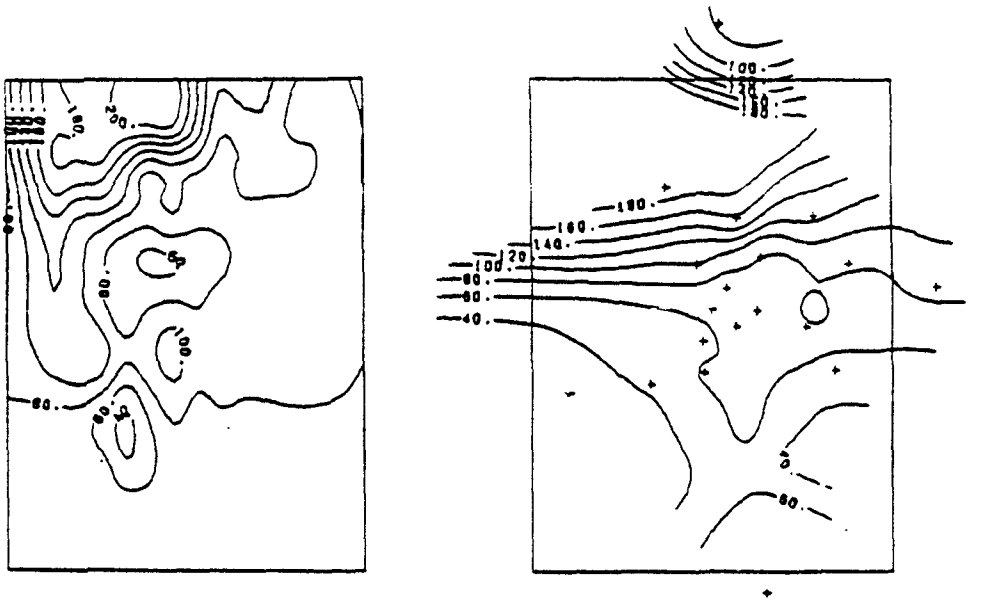

(a) (b)

Figure E-7. Contours of (a) predicted and (b) observed fields of O_3 at hour of observed maximum on Day 230-75.

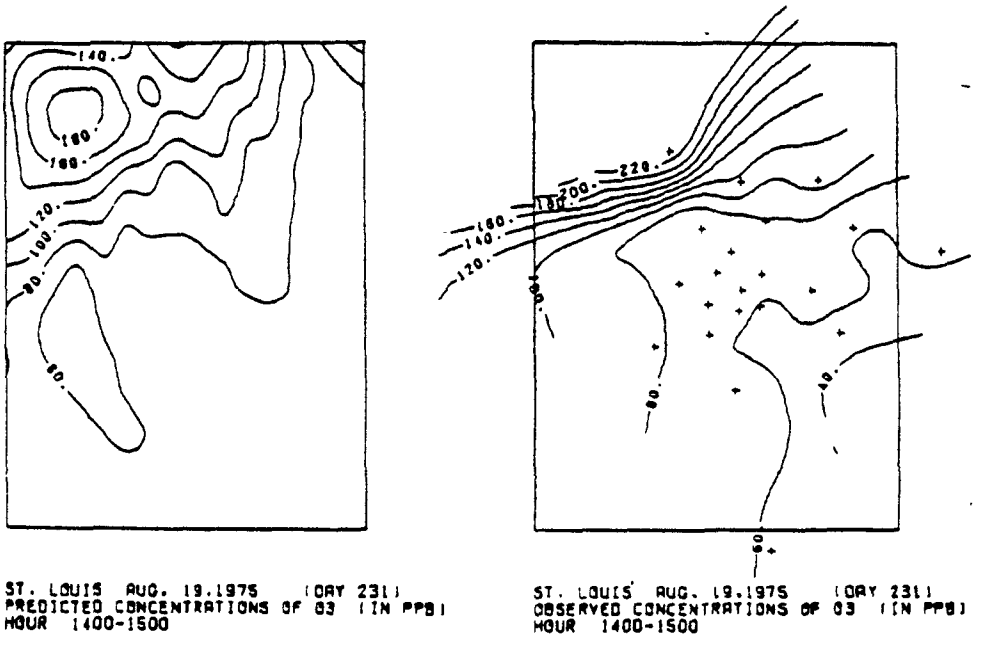

(a) (b)

Figure E-8. Contours of (a) predicted and (b) observed fields of O_3 at hour of observed maximum on Day 231-75.

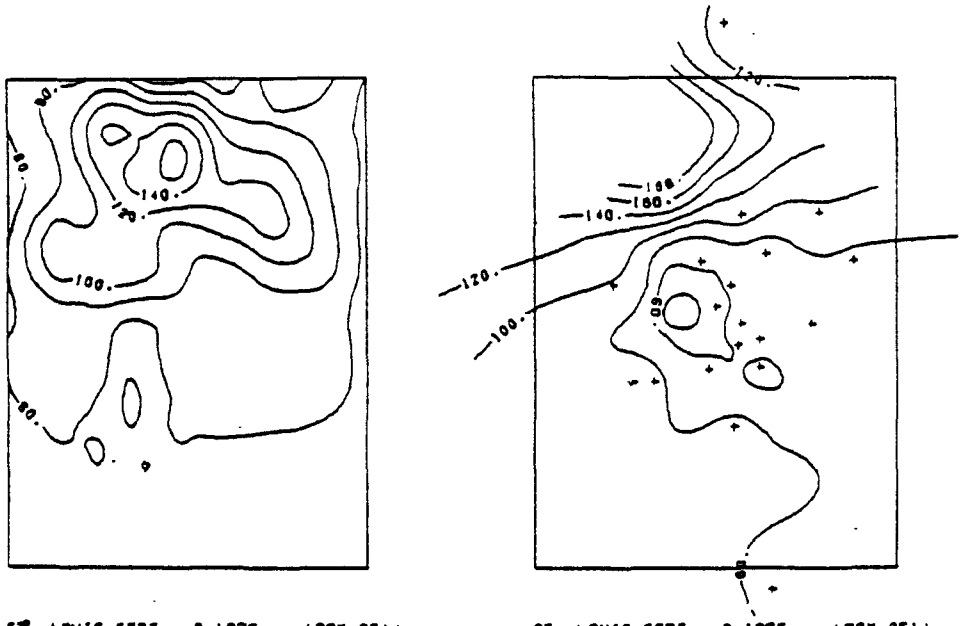

(a) (b)

Figure E-9. Contours of (a) predicted and (b) observed fields of O_3 at hour of observed maximum on Day 251-75.

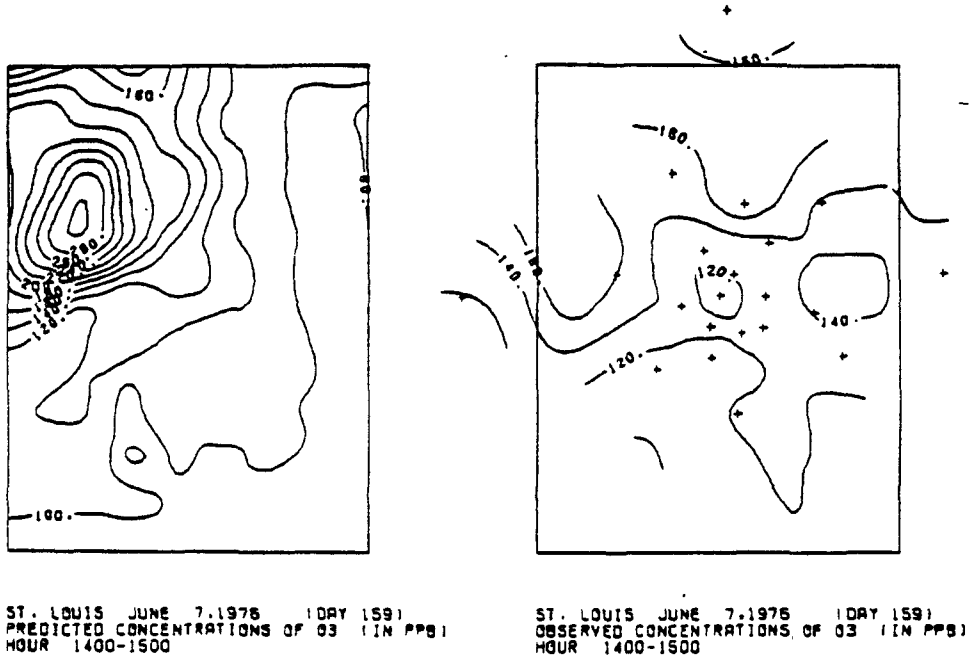

(a) (b)

Figure E-10. Contours of (a) predicted and (b) observed fields of O_3 at hour of observed maximum on Day 159-76.

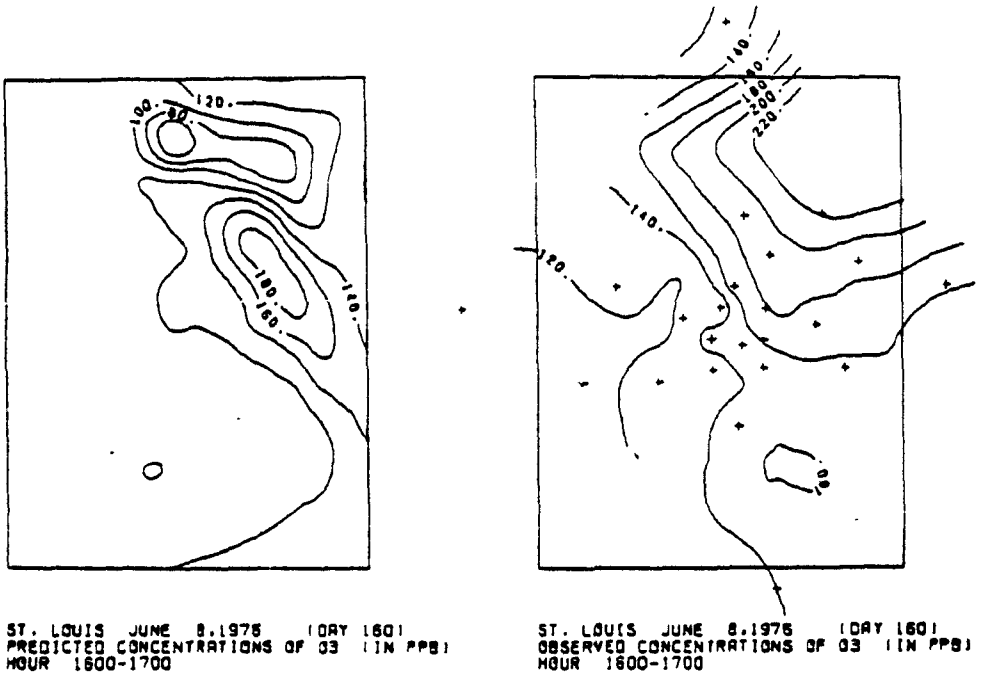

(a) (b)

Figure E-11. Contours of (a) predicted and (b) observed fields of O_3 at hour of observed maximum on Day 160-76.

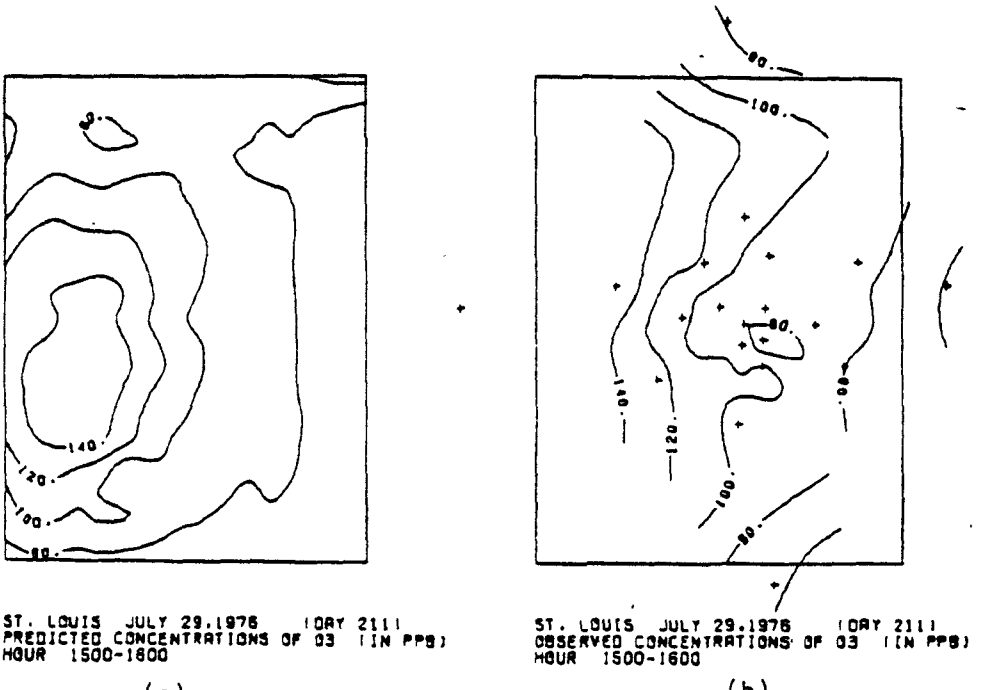

(a) (b)

Figure E-12. Contours of (a) predicted and (b) observed fields of O_3 at hour of observed maximum on Day 211-76.

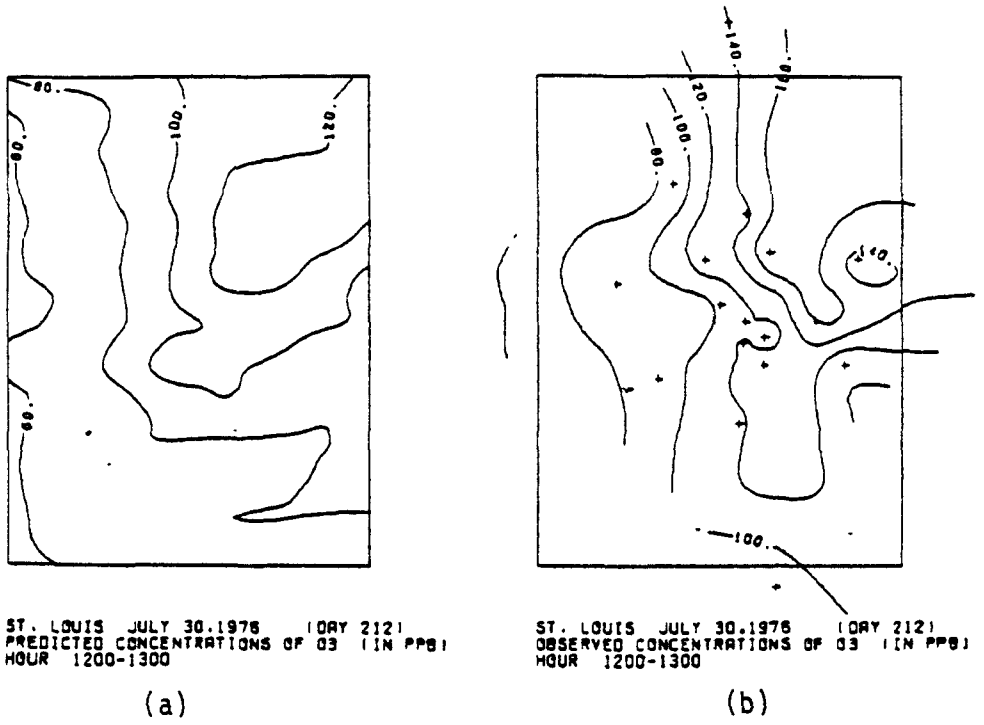

Figure E-13. Contours of (a) predicted and (b) observed fields of O_3 at hour of observed maximum on Day 212-76.

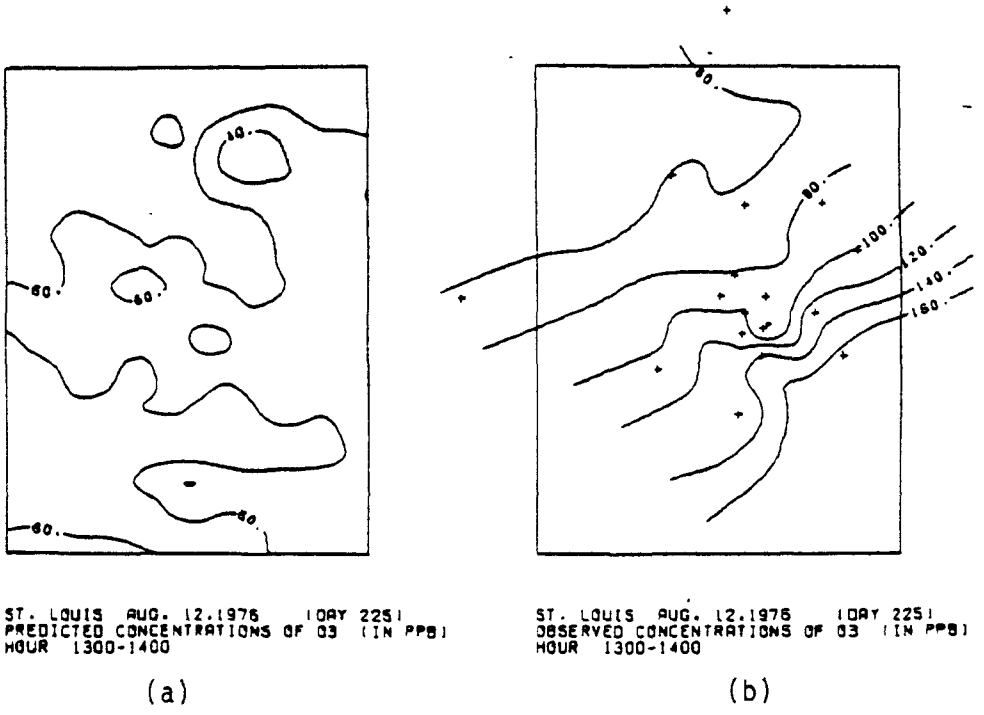

Figure E-14. Contours of (a) predicted and (b) observed fields of O_3 at hour of observed maximum on Day 225-76.

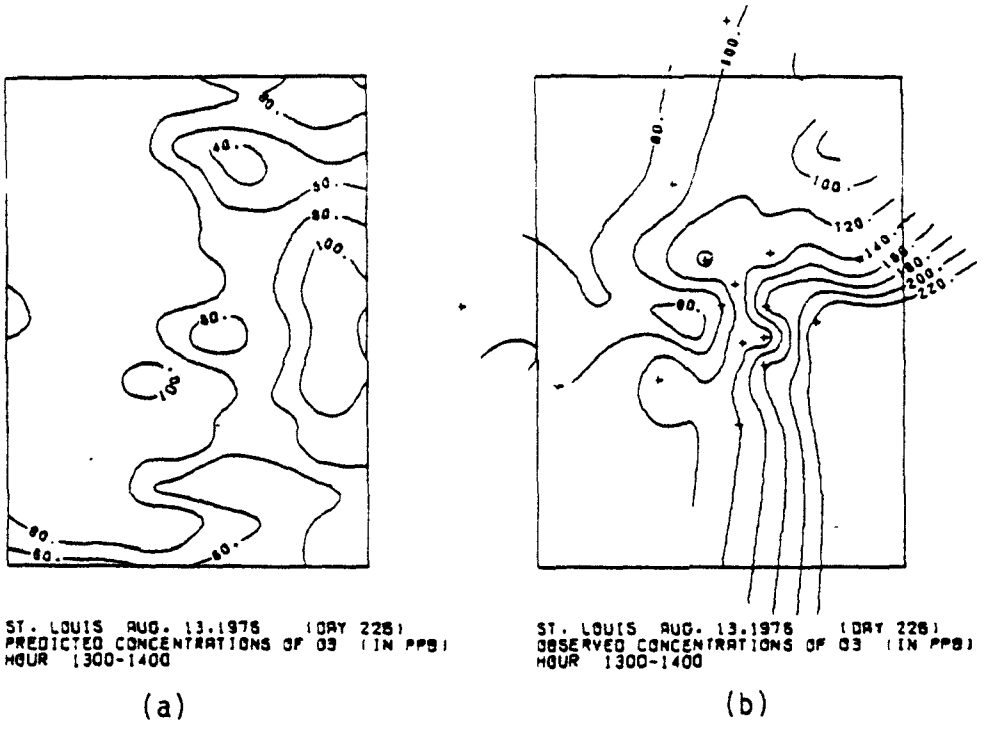

(a) (b)

Figure E-15. Contours of (a) predicted and (b) observed fields of O_3 at hour of observed maximum on Day 226-76.

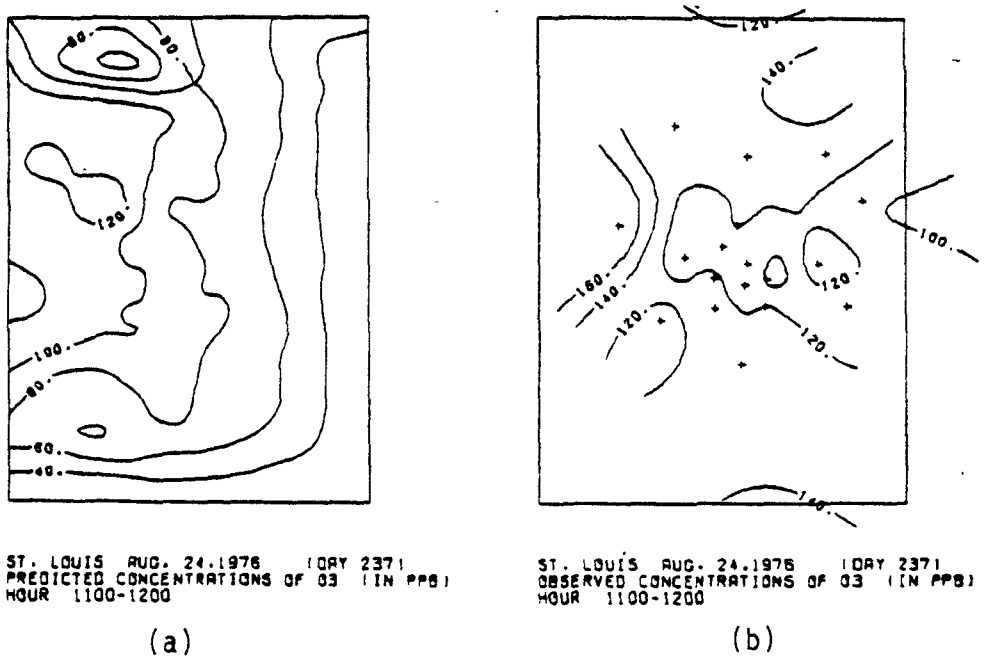

(a) (b)

Figure E-16. Contours of (a) predicted and (b) observed fields of O_3 at hour of observed maximum on Day 237-76.

APPENDIX F

UAM - SUMMARY OF STATISTICAL RESULTS

Three tables are presented in this appendix. Table F-1 summarizes the statistics for the mean quantities on each of the 20 days for the species NO, NO_2, O_3, OLE, NMHC and CO. Note that the observed OLE (olefin) value was obtained by a temporally and spatially constant splitting factor from NMHC. This factor was based on an analysis of the composite of volatile organic emissions over the entire St. Louis area.

Table F-2 summarizes the analysis of trends data for the species NO_2, O_3 and CO, and Table F-3 presents concentration maxima data for the same species. The statistical parameters included in the 3 tables are the same as those defined in Appendix B, except for the following:

(1) in addition to an overall correlation coefficient there are also the following:

(a) average spatial correlation (average over correlation coefficients for each hour of simulation calculated separately), and

(b) average temporal correlation (average over correlation coefficients for each location calculated separately);

(2) for concentration maxima data the following descriptions apply:

(a) peak observed concentration (along with the location and time of occurrence), and

(b) peak predicted concentration (at same location as peak observed concentration, along with the time of occurrence).

TABLE F-1. SUMMARY OF MODEL PERFORMANCE STATISTICS FOR MEAN CONCENTRATIONS FROM THE UAM.

Julian date	Species	Mean observed concentration (ppm)	Mean predicted concentration (ppm)	Mean residual (ppm)	RMS error (ppm)	Mean residual / Mean obs. conc. (%)	Error band[a] (%)
142-75	NO	0.0086	0.0064	0.0022	0.0094	25.6	19.7
	NO_2	0.0134	0.0181	-0.0047	0.0111	-35.1	30.8
	O_3	0.0635	0.0779	-0.0145	0.0317	-22.8	42.1
	OLE	0.0080	0.0044	0.0036	0.0093	45.0	17.0
	NMHC	0.183	0.258	-0.0754	0.202	-41.2	25.0
	CO	0.481	0.479	0.0016	0.416	0.3	33.9
178-75	NO	0.0088	0.0070	0.0018	0.0116	20.5	15.0
	NO_2	0.0212	0.0259	-0.0047	0.0168	-22.2	28.6
	O_3	0.0920	0.0850	0.0070	0.0314	7.6	46.3
	OLE	0.0147	0.0062	0.0085	0.0113	57.8	13.2
	NMHC	0.334	0.384	-0.0494	0.265	-14.5	22.5
	CO	0.809	0.723	0.0860	0.537	10.6	31.9
182-75	NO	0.0082	0.0029	0.0052	0.0105	63.4	11.0
	NO_2	0.0172	0.0128	0.0045	0.0113	26.2	28.6
	O_3	0.0737	0.0777	-0.0040	0.0186	-5.4	69.5
	OLE	0.0118	0.0041	0.0077	0.0100	65.3	87.0
	NMHC	0.269	0.202	0.0669	0.208	24.9	22.5
	CO	0.517	0.307	0.210	0.521	40.6	27.1
183-75	NO	0.0105	0.0055	0.0051	0.0144	48.6	17.5
	NO_2	0.0227	0.0224	0.0004	0.0162	1.8	32.1
	O_3	0.0809	0.0855	-0.0046	0.0248	0.3	54.0
	OLE	0.0126	0.0059	0.0067	0.0112	53.1	7.8
	NMHC	0.285	0.298	-0.0126	0.239	-4.4	28.7
	CO	0.655	0.466	0.189	0.559	28.9	24.4

TABLE F-1. (Continued)

SUMMARY OF MODEL PERFORMANCE STATISTICS FOR MEAN CONCENTRATIONS FROM THE UAM.

Julian date	Species	Mean observed concentration (ppm)	Mean predicted concentration (ppm)	Mean residual (ppm)	RMS error (ppm)	Mean residual / Mean obs. conc. (%)	Error band[a] (%)
184-75	NO	0.0118	0.0044	0.0074	0.0179	62.7	16.5
	NO_2	0.0254	0.0212	0.0042	0.0220	16.5	28.9
	O_3	0.0814	0.0806	0.0008	0.0319	1.0	48.9
	OLE	0.0253	0.0131	0.0122	0.0208	48.2	13.6
	NMHC	0.575	0.470	0.106	0.412	18.4	24.5
	CO	0.859	0.612	0.247	0.671	28.8	25.6
207-75	NO	0.0070	0.0060	0.0010	0.0077	14.3	24.2
	NO_2	0.0134	0.0182	-0.0048	0.0079	-35.8	29.9
	O_3	0.0802	0.0656	0.0146	0.0209	18.2	51.9
	OLE	0.0113	0.0063	0.0050	0.0149	44.2	17.9
	NMHC	0.258	0.233	0.0246	0.341	9.5	24.4
	CO	0.378	0.377	0.0002	0.331	0.1	35.4
209-75	NO	0.0077	0.0070	0.0006	0.0104	7.8	14.7
	NO_2	0.0149	0.0190	-0.0042	0.0095	-28.2	31.6
	O_3	0.0698	0.0616	0.0082	0.0265	11.7	50.9
	OLE	0.0095	0.0056	0.0040	0.0090	42.1	21.4
	NMHC	0.216	0.289	-0.0736	0.242	-34.1	17.6
	CO	0.486	0.442	0.0440	0.986	9.1	39.6
221-75	NO	0.0097	0.0073	0.0024	0.0153	24.7	15.9
	NO_2	0.0191	0.0185	0.0006	0.0127	3.1	30.6
	O_3	0.0703	0.0523	0.0180	0.0274	25.6	38.5
	OLE	0.0138	0.0063	0.0075	0.0128	54.3	10.5
	NMHC	0.303	0.221	0.0919	0.294	30.3	21.6
	CO	0.755	0.476	0.279	0.831	37.0	30.2

TABLE F-1. (Continued)

SUMMARY OF MODEL PERFORMANCE STATISTICS FOR MEAN CONCENTRATIONS FROM THE UAM.

Julian date	Species	Mean observed concentration (ppm)	Mean predicted concentration (ppm)	Mean residual (ppm)	RMS error (ppm)	Mean residual / Mean obs. conc. (%)	Error band[a] (%)
230-75	NO	0.0130	0.0100	0.0030	0.0165	23.1	18.3
	NO_2	0.0188	0.0215	-0.0026	0.0091	-13.8	38.5
	O_3	0.0449	0.0534	-0.0086	0.0209	-19.2	29.9
	OLE	0.0146	0.0065	0.0081	0.0117	55.5	17.5
	NMHC	0.332	0.317	0.0148	0.243	4.5	25.9
	CO	0.550	0.468	0.0821	0.420	14.9	32.4
231-75	NO	0.0084	0.0089	-0.0004	0.0095	-4.8	16.0
	NO_2	0.0165	0.0194	-0.0029	0.0087	-17.6	37.1
	O_3	0.0518	0.0530	-0.0012	0.0221	-2.3	45.5
	OLE	0.0125	0.0061	0.0064	0.0101	51.2	14.0
	NMHC	0.284	0.337	-0.0535	0.209	-18.8	15.4
	CO	0.437	0.456	-0.0190	0.355	-4.3	33.7
251-75	NO	0.0198	0.0141	0.0058	0.0307	29.3	19.0
	NO_2	0.0253	0.0279	-0.0026	0.0190	-10.3	39.1
	O_3	0.0507	0.0447	0.0061	0.0214	12.0	38.2
	OLE	0.0193	0.0087	0.0106	0.0166	54.9	13.3
	NMHC	0.438	0.449	-0.0111	0.349	-2.5	22.2
	CO	0.806	0.648	0.158	0.777	19.6	27.9
159-76	NO	0.0163	0.0084	0.0079	0.0215	48.5	17.5
	NO_2	0.0275	0.0230	0.0045	0.0130	16.4	35.8
	O_3	0.0880	0.0996	-0.0116	0.0270	-13.2	53.0
	OLE	0.0182	0.0095	0.0088	0.0149	48.4	15.2
	NMHC	0.414	0.401	0.0128	0.303	3.1	31.5
	CO	0.968	0.693	0.275	2.46	28.4	35.1

TABLE F-1. (Continued)

SUMMARY OF MODEL PERFORMANCE STATISTICS FOR MEAN CONCENTRATIONS FROM THE UAM.

Julian date	Species	Mean observed concentration (ppm)	Mean predicted concentration (ppm)	Mean residual (ppm)	RMS error (ppm)	Mean residual / Mean obs. conc. (%)	Error band[a] (%)
160-76	NO	0.0091	0.0063	0.0028	0.0147	30.8	15.3
	NO_2	0.0198	0.0207	-0.0009	0.0132	-4.5	28.7
	O_3	0.107	0.0890	0.0176	0.0237	16.4	59.0
	OLE	0.0130	0.0065	0.0066	0.0126	50.8	14.7
	NMHC	0.297	0.325	-0.0286	0.276	-9.6	22.6
	CO	0.606	0.504	0.102	0.440	16.8	30.2
195-76	NO	0.0042	0.0038	0.0005	0.0041	11.9	18.0
	NO_2	0.0159	0.0154	0.0005	0.0105	3.1	41.1
	O_3	0.0827	0.0738	0.0089	0.0179	10.8	75.0
	OLE	0.0093	0.0033	0.0061	0.0086	65.6	13.7
	NMHC	0.212	0.237	-0.0251	0.179	-11.8	31.1
	CO	0.360	0.396	-0.0357	0.400	-9.9	27.1
211-76	NO	0.0074	0.0034	0.0040	0.0090	54.1	11.6
	NO_2	0.0208	0.0166	0.0043	0.0112	20.7	38.1
	O_3	0.0462	0.0584	-0.0122	0.0214	-26.4	38.7
	OLE	0.0127	0.0061	0.0066	0.0118	52.0	14.3
	NMHC	0.288	0.313	-0.0252	0.245	-8.8	30.2
	CO	0.472	0.473	-0.0019	0.342	-0.4	24.5
212-76	NO	0.0102	0.0045	0.0057	0.0137	55.9	17.6
	NO_2	0.0181	0.0186	-0.0005	0.0109	-2.8	31.2
	O_3	0.0664	0.0665	-0.0001	0.0219	-0.2	56.9
	OLE	0.0155	0.0062	0.0093	0.0129	60.0	13.1
	NMHC	0.352	0.295	0.0573	0.283	16.3	30.4
	CO	0.572	0.429	0.143	0.397	25.0	27.6

TABLE F-1. (Continued)

SUMMARY OF MODEL PERFORMANCE STATISTICS FOR MEAN CONCENTRATIONS FROM THE UAM.

Julian date	Species	Mean observed concentration (ppm)	Mean predicted concentration (ppm)	Mean residual (ppm)	RMS error (ppm)	Mean residual / Mean obs. conc. (%)	Error band[a] (%)
225-76	NO	0.0065	0.0044	0.0021	0.0076	32.3	22.4
	NO_2	0.0208	0.0221	-0.0013	0.0124	-6.3	35.2
	O_3	0.0625	0.0391	0.0235	0.0280	37.6	26.8
	OLE	0.0116	0.0058	0.0058	0.0110	50.0	18.9
	NMHC	0.264	0.267	-0.0030	0.257	-1.1	23.7
	CO	0.479	0.427	0.0521	0.343	10.9	32.4
226-76	NO	0.0088	0.0056	0.0031	0.0144	35.2	18.5
	NO_2	0.0236	0.0227	0.0010	0.0155	4.2	27.9
	O_3	0.0806	0.0545	0.0261	0.0397	32.4	20.2
	OLE	0.0147	0.0051	0.0096	0.0142	65.3	15.4
	NMHC	0.324	0.272	0.0527	0.285	16.3	33.5
	CO	0.693	0.450	0.244	0.570	35.2	25.1
237-76	NO	0.0115	0.0052	0.0064	0.0170	55.7	14.6
	NO_2	0.0192	0.0189	0.0003	0.0140	1.6	30.2
	O_3	0.0813	0.0538	0.0275	0.0355	33.8	20.4
	OLE	0.0225	0.0068	0.0157	0.0212	69.8	7.8
	NMHC	0.511	0.284	0.226	0.448	44.2	24.0
	CO	0.649	0.414	0.236	0.562	36.4	32.1
275-76	NO	0.0364	0.0264	0.0100	0.0432	27.5	13.5
	NO_2	0.0507	0.0519	-0.0012	0.0319	-2.4	35.1
	O_3	0.0782	0.0878	-0.0096	0.0392	-12.2	36.7
	OLE	0.0304	0.0152	0.0152	0.0197	50.0	11.8
	NMHC	0.691	0.892	-0.201	0.394	-29.1	25.1
	CO	1.74	1.44	0.295	1.35	17.0	27.2

[a]Percent of predictions within 25% of observations.

TABLE F-2. SUMMARY OF MODEL PERFORMANCE STATISTICS FOR ANALYSIS OF TRENDS DATA FROM THE UAM

Julian date	Species	Correlation coefficient	Average spatial correlation	Average temporal correlation	Slope	Intercept (ppm)	Sum of squared error (ppm^2)
142-75	NO_2	0.621	0.689	0.489	0.665	0.0014	0.0183
	O_3	0.805	0.174	0.850	0.887	-0.0057	0.186
	CO	0.488	0.633	0.374	0.246	0.119	5.330
178-75	NO_2	0.478	0.598	0.388	0.447	0.0096	0.0498
	O_3	0.864	0.357	0.913	0.867	0.0183	0.186
	CO	0.581	0.735	0.299	0.275	0.610	60.4
182-75	NO_2	0.771	0.518	0.779	0.523	0.0105	0.0380
	O_3	0.875	0.571	0.897	0.610	0.0263	0.142
	CO	0.559	0.395	0.432	0.172	0.464	75.4
183-75	NO_2	0.685	0.466	0.559	0.574	0.0099	0.0601
	O_3	0.864	0.435	0.879	0.614	0.0284	0.193
	CO	0.685	0.527	0.479	0.326	0.503	94.1
184-75	NO_2	0.683	0.549	0.521	0.397	0.0170	0.157
	O_3	0.726	0.444	0.696	0.470	0.0436	0.317
	CO	0.770	0.583	0.435	0.403	0.612	154.
207-75	NO_2	0.791	0.734	0.682	0.751	-0.0002	0.0139
	O_3	0.927	0.461	0.959	0.654	0.0373	0.173
	CO	0.669	0.533	0.528	0.340	0.249	35.8
209-75	NO_2	0.741	0.536	0.682	1.01	-0.0044	0.0209
	O_3	0.759	0.411	0.670	0.570	0.0347	0.192
	CO	0.185	0.524	0.650	0.063	0.458	224.
221-75	NO_2	0.675	0.612	0.615	0.493	0.0100	0.0419
	O_3	0.795	0.395	0.818	0.516	0.0433	0.268
	CO	0.415	0.321	0.308	0.145	0.686	177.

TABLE F-2. (Continued)

SUMMARY OF MODEL PERFORMANCE STATISTICS FOR ANALYSIS OF TRENDS DATA FROM THE UAM

Julian date	Species	Correlation coefficient	Average spatial correlation	Average temporal correlation	Slope	Intercept (ppm)	Sum of squared error (ppm^2)
230-75	NO_2	0.824	0.804	0.606	0.774	0.0022	0.0188
	O_3	0.819	0.361	0.885	0.729	0.0059	0.0950
	CO	0.764	0.694	0.698	0.419	0.354	58.6
231-75	NO_2	0.772	0.706	0.552	0.790	0.0012	0.0165
	O_3	0.814	0.436	0.804	0.645	0.0176	0.152
	CO	0.685	0.694	0.719	0.483	0.217	31.5
251-75	NO_2	0.600	0.410	0.576	0.585	0.0090	0.0635
	O_3	0.821	0.451	0.864	0.618	0.0232	0.150
	CO	0.630	0.616	0.571	0.359	0.574	159.
159-76	NO_2	0.887	0.676	0.732	0.740	0.0105	0.0546
	O_3	0.859	0.392	0.929	0.862	0.0021	0.158
	CO	0.294	0.556	0.652	0.064	0.923	1700.
160-76	NO_2	0.796	0.747	0.637	0.535	0.0088	0.0565
	O_3	0.937	0.592	0.961	0.676	0.0464	0.247
	CO	0.628	0.368	0.529	0.340	0.435	61.5
195-76	NO_2	0.660	0.654	0.321	0.457	0.0089	0.0335
	O_3	0.947	0.495	0.964	0.720	0.0296	0.112
	CO	0.286	0.485	0.282	0.113	0.315	40.4
211-76	NO_2	0.621	0.685	0.373	0.415	0.0140	0.0322
	O_3	0.833	0.421	0.715	0.773	0.0010	0.104
	CO	0.511	0.519	0.304	0.274	0.342	32.1
212-76	NO_2	0.798	0.642	0.538	0.503	0.0088	0.0424
	O_3	0.912	0.614	0.742	0.632	0.0244	0.189
	CO	0.759	0.639	0.546	0.439	0.383	57.8

TABLE F-2. (Continued)

SUMMARY OF MODEL PERFORMANCE STATISTICS FOR ANALYSIS OF TRENDS DATA FROM THE UAM

Julian date	Species	Correlation coefficient	Average spatial correlation	Average temporal correlation	Slope	Intercept (ppm)	Sum of squared error (ppm^2)
225-76	NO_2	0.704	0.657	0.578	0.657	0.0063	0.0333
	O_3	0.753	0.377	0.780	0.310	0.0504	0.247
	CO	0.540	0.573	0.588	0.396	0.310	30.8
226-76	NO_2	0.561	0.688	0.368	0.331	0.0161	0.0670
	O_3	0.796	0.110	0.605	0.426	0.0574	0.445
	CO	0.607	0.707	0.516	0.170	0.617	86.0
237-76	NO_2	0.799	0.793	0.648	0.669	0.0065	0.0476
	O_3	0.687	0.354	0.759	0.432	0.0581	0.383
	CO	0.734	0.561	0.640	0.279	0.534	108.
275-76	NO_2	0.597	0.761	0.329	0.604	0.0193	0.183
	O_3	0.844	0.239	0.916	0.896	-0.0004	0.340
	CO	0.533	0.622	0.410	0.219	1.42	572.

TABLE F-3. SUMMARY OF MODEL PERFORMANCE STATISTICS FOR CONCENTRATION MAXIMA FROM THE UAM

Julian date	Species	Observed Peak Concentration Value (ppm)	Location (RAPS site)	Time (CST)	Predicted Peak Concentration[a] Value (ppm)	Time (CST)	Residual (ppm)	Residual / Obs. conc. (%)
142-75	NO_2	0.0458	102	1300	0.0654	1300	-0.0196	-42.8
	O_3	0.195	101	1200	0.149	1400	0.0460	23.6
	CO	4.03	121	1700	0.667	1500	3.36	83.4
178-75	NO_2	0.0701	103	0700	0.0517	0900	0.0184	26.2
	O_3	0.202	112	1400	0.162	1500	0.0400	19.8
	CO	4.04	107	0600	1.22	1400	2.82	69.8
182-75	NO_2	0.0867	106	0800	0.0659	0600	0.0208	24.0
	O_3	0.142	121	1100	0.103	1400	0.0390	27.5
	CO	4.19	115	1400	0.196	1700	3.99	95.2
183-75	NO_2	0.106	106	0700	0.0955	0800	0.0105	9.9
	O_3	0.171	119	1000	0.154	1000	0.0170	9.9
	CO	3.81	112	0700	1.39	0700	2.42	63.5
184-75	NO_2	0.180	104	0700	0.0795	0600	0.101	56.1
	O_3	0.184	118	1300	0.133	1400	0.0510	27.7
	CO	5.26	104	0700	2.05	0500	3.21	61.0
207-75	NO_2	0.0621	106	0600	0.0530	0600	0.0091	14.7
	O_3	0.185	113	1400	0.141	1400	0.0440	23.8
	CO	4.26	104	0500	1.63	0500	2.63	61.7
209-75	NO_2	0.0501	110	0800	0.0589	0900	-0.0088	-17.6
	O_3	0.209	118	1100	0.128	1100	0.0810	38.8
	CO	14.4	117	1700	1.23	0800	13.2	91.7
221-75	NO_2	0.0726	102	0800	0.0478	0500	0.0248	34.2
	O_3	0.166	121	1500	0.144	1400	0.0220	13.3
	CO	5.55	107	0700	1.44	0500	4.11	74.1